VOLUME 110 NUMBER 2

THE ASTROPHYSICAL JOURNAL

AN INTERNATIONAL REVIEW OF SPECTROSCOPY AND ASTRONOMICAL PHYSICS

SEPTEMBER 1949

SPECTRA OF THE BRIGHTER VARIABLES IN GLOBULAR CLUSTERS *Alfred H. Joy* 105
INTERSTELLAR CALCIUM LINES IN THE SPECTRA OF STARS IN OPEN CLUSTERS *Roscoe F. Sanford* 117
MAGNETIC INTENSIFICATION OF STELLAR ABSORPTION LINES *Horace W. Babcock* 126
THE SPECTRUM OF R CORONAE BOREALIS AT THE 1948–1949 MINIMUM *George H. Herbig* 143
SPECTROSCOPIC OBSERVATIONS OF THE SHORT-PERIOD VARIABLE AI VELORUM *George H. Herbig* 156
THE SPECTROSCOPIC BINARY VV ORIONIS (HD 36695) *O. Struve and W. J. Luyten* 160
A PHOTOMETRIC STUDY OF THE SPECTRUM OF PLEIONE *Anne B. Underhill* 166
LUMINOSITY DISTRIBUTION AND PROPER MOTIONS OF TENTH-MAGNITUDE K STARS *F. K. Edmondson, A. N. Vyssotsky, and Edith M. Janssen* 182
COLOR EXCESS, TOTAL PHOTOGRAPHIC ABSORPTION, AND THE DISTANCE OF THE DARK CLOUD IN THE AQUILA REGION OF THE MILKY WAY *Harold F. Weaver* 190
THE URSA MAJOR GROUP *Nancy Grace Roman* 205
THE FREQUENCY AND POSITIONS OF FLARES WITHIN THREE ACTIVE SUN-SPOT AREAS *Helen W. Dodson and E. Ruth Hedeman* 242
THE DYNAMICS OF STAR STREAMING *P. Stehle* 250
REGIONS WITH VARYING MEAN MOLECULAR WEIGHT (WHITE DWARFS WITH COMPLEX STRUCTURES) *Evry Schatzman* 261
THE RADIATIVE EQUILIBRIUM OF A SPHERICAL PLANETARY NEBULA *Hari K. Sen* 276
THE TRANSFER OF RADIATION IN A SPHERICAL ATMOSPHERE OF ELECTRONS *Marshal H. Wrubel* 288
STRUCTURE OF THE CAMERON BANDS OF CARBON MONOXIDE *K. Narahari Rao* 304
NOTES
A NOTE ON THE SPECTROGRAPHIC ORBITS OF HD 193576 *E. S. Keeping* 312
THE RADIAL VELOCITY OF ALPHA VIRGINIS *Shu-Kee Kao and O. Struve* 312
SODIUM D IN THE SPECTRUM OF METEORS *F. E. Roach* 314
REVIEWS 315

THE UNIVERSITY OF CHICAGO PRESS
CHICAGO, ILLINOIS, U.S.A.

September 1949 Vol. 110, No. 2

THE ASTROPHYSICAL JOURNAL

AN INTERNATIONAL REVIEW OF SPECTROSCOPY AND ASTRONOMICAL PHYSICS

Edited by

W. W. MORGAN
Managing Editor
Yerkes Observatory of the University of Chicago

S. CHANDRASEKHAR

PAUL W. MERRILL
Mount Wilson Observatory of the Carnegie Institution of Washington

HARLOW SHAPLEY
Harvard College Observatory
Cambridge, Massachusetts

N. U. MAYALL
Lick Observatory
University of California

With the Collaboration of the American Astronomical Society

Collaborating Editors:

1947-49	1948-50	1949-51
LYMAN SPITZER, JR. Princeton University Observatory	CECILIA H. PAYNE-GAPOSCHKIN Harvard College Observatory	W. BAADE Mount Wilson Observatory
A. N. VYSSOTSKY Leander McCormick Observatory	H. N. RUSSELL Princeton University	LEO GOLDBERG Observatory of the University of Michigan
ALBERT E. WHITFORD Washburn Observatory	ANDREW McKELLAR Dominion Astrophysical Observatory, Victoria	O. HERZBERG National Research Council, Ottawa

The Astrophysical Journal is published bimonthly by the University of Chicago at the University of Chicago Press, 5750 Ellis Avenue, Chicago, Illinois, during July, September, November, January, March, and May. ¶The subscription price is $12.00 a year; the price of single copies is $3.00. Orders for service of less than a full year will be charged at the single-copy rate. ¶Postage is prepaid by the publishers on all orders from the United States and its possessions, Argentina, Bolivia, Brazil, Chile, Colombia, Costa Rica, Cuba, Dominican Republic, Ecuador, Guatemala, Haiti, Republic of Honduras, Mexico, Morocco (Spanish Zone), Nicaragua, Panama, Paraguay, Peru, Rio de Oro, El Salvador, Spain (including Balearic Islands, Canary Islands, and the Spanish Offices in Northern Africa; Andorra), Spanish Guinea, Uruguay, and Venezuela. ¶Postage is charged extra as follows: for Canada and Newfoundland, 42 cents on annual subscriptions (total $12.42); on single copies, 7 cents (total $3.07); for all other countries in the Postal Union, 96 cents on annual subscriptions (total $12.96), on single copies 16 cents (total $3.16). ¶Patrons are requested to make all remittances payable to The University of Chicago Press, in United States currency or its equivalent by postal or express money orders or bank drafts.

The following is an authorized agent:

For the British Empire, except North America and Australasia: The Cambridge University Press, Bentley House, 200 Euston Road, London, N.W. 1, England. Prices of yearly subscriptions and of single copies may be had on application.

Claims for missing numbers should be made within the month following the regular month of publication. The publishers expect to supply missing numbers free only when losses have been sustained in transit, and when the reserve stock will permit.

Business correspondence should be addressed to The University of Chicago Press, Chicago 37, Illinois.

Communications for the editors and manuscripts should be addressed to: W. W. Morgan, Editor of THE ASTROPHYSICAL JOURNAL, Yerkes Observatory, Williams Bay, Wisconsin.

Line drawings and photographs should be made by the author, and all marginal notes such as co-ordinates, wave lengths, etc., should be included in the cuts. It will not be possible to set up such material in type.

One copy of the corrected galley proof should be returned as soon as possible to the editor, Yerkes Observatory, Williams Bay, Wisconsin. Authors should take notice that the manuscript will not be sent to them with the proof.

The cable address is "Observatory, Williamsbay, Wisconsin."

The articles in this journal are indexed in the *International Index to Periodicals*, New York, N.Y.

Applications for permission to quote from this journal should be addressed to The University of Chicago Press, and will be freely granted.

Entered as second-class matter, July 31, 1940, at the Post-Office at Chicago, Ill., under the Act of March 3, 1879.
Acceptance for mailing at special rate of postage provided for in United States Postal Act of October 3, 1917, Section 1103, amended February 28, 1925.

[PRINTED IN U.S.A.]

THE ASTROPHYSICAL JOURNAL

AN INTERNATIONAL REVIEW OF SPECTROSCOPY AND ASTRONOMICAL PHYSICS

VOLUME 110 SEPTEMBER 1949 NUMBER 2

SPECTRA OF THE BRIGHTER VARIABLES IN GLOBULAR CLUSTERS

ALFRED H. JOY
Mount Wilson and Palomar Observatories
Received May 19, 1949

ABSTRACT

Spectrograms of 35 variables of high luminosity in 14 globular clusters were obtained at Mount Wilson with low dispersion. Membership in the clusters was tested by measures of radial velocity, which were compared with the velocities obtained at the Lick Observatory from the integrated light of the clusters.

A tabulation of the stars according to period and physical characteristics indicates that the globular clusters contain, in addition to the RR Lyrae stars, several variables of four definite groups: short period (1–2 days), W Virginis, RV Tauri (with high luminosity), and irregular or semiregular variables (period 60–110 days). Cepheids, Mira stars, and semiregular variables (types M4–M6) are rare or absent. In general, the variables found in the clusters correspond to those of population II.

The results of the spectroscopic observation[1] of Barnard's variable in Messier 3 led to the observation of other variable stars in globular clusters for the purpose of making more extended tests of the relationship between the variables in the clusters and the high-velocity stars of the RR Lyrae, W Virginis, RV Tauri, and Mira classes, well scattered throughout the galactic system. With the 100-inch telescope and dispersion of 110 A/mm at $H\gamma$, spectrograms of most of the brighter variables were readily obtained in good seeing with exposures less than 4 hours. For some of the fainter stars in more distant clusters a dispersion of 220 A/mm was necessary.

On account of the low luminosity and the rapid changes in light and velocity of the variables with periods less than a day, satisfactory observations of such stars with available equipment were not feasible. These stars, which, to avoid confusion, may be called "RR Lyrae variables" rather than "cluster variables," are by far the most numerous of the variable stars in clusters.

The known variables in the globular clusters number about 1300[2] in 60 different clusters. Among these variables, 67, because of their high luminosity and slow light-changes, evidently do not belong to the RR Lyrae class. About ten years ago spectroscopic observation of these brighter variables was begun at Mount Wilson. The program included all for which periods had been determined except 19, whose southern declinations are greater than $-40°$. A few bright variable stars whose periods are unknown were added.

[1] A. H. Joy, *Mt. W. Contr.*, No. 637; *Ap. J.*, **92**, 396, 1940.

[2] H. B. Sawyer, *Pub. Dunlap Obs.*, **1**, 127, 1939; 383, 1947.

Spectrograms were eventually obtained for 35 variables in 14 clusters. While the observations are few and the quality not all that could be desired, the radial velocities assist in identifying the variables with the clusters, and the spectral characteristics usually define the type of variation.

The data pertaining to the observations, together with the estimated spectral types and measured radial velocities, appear in Table 1. Plates taken with the lower dispersion of 220 A/mm are starred, and their measurement is subject to larger accidental errors. The relative intensity of the hydrogen emission lines on different spectrograms is indicated by a number (scale 1–5) following the letter *e* of the spectral type. The weights depend to a large extent on the definition of the lines of the plate as well as on the dispersion of the spectrograms. The elements for the phases and references to their source are in the notes following the table.

If the velocities define a curve, the γ-velocity of the curve was taken to be the mean velocity of the star; but for the remaining stars, whose velocities are scattering because of poor measurement, irregular velocity changes, or inaccurate elements, the weighted mean of the measured velocities was computed.

In Figure 1 the light-curves and velocity-curves of NGC 6205 (M13) var 2, 6254 (10) var 2, 7089 (2) var 11, and 5272 (3) var 95 (periods 5, 19, 67, and 103 days) are shown to illustrate the behavior of different classes of variables in clusters. The accuracy of the measurements does not warrant drawing conclusions based on details of the curves, but the characteristic velocity changes correspond to those observed in similar variables distributed throughout the galactic system.

Table 2 is a summary of the measured radial velocities of the several variables. The weighted mean velocities for 14 clusters were derived and compared with the values determined from integrated light of the clusters by N. U. Mayall[3] at the Lick Observatory. Except for one cluster, NGC 6218 (M12), for which the difference is 78 km/sec, the agreement of the velocities is satisfactory for observations with low dispersion. The positive and negative differences are equal in number, and no certain systematic differences can be detected. The Lick values were obtained, for the most part, with a dispersion of 430 A/mm.

The velocities for individual stars are clearly of insufficient precision to justify any conclusions as to peculiar motions or rotation effects.

In order to study the distribution of the brighter variables of the clusters among the different classes, the observed stars were arranged, as far as possible, in order of period in Table 3. The position in the table of the five variables for which no periods are known was determined largely from consideration of their spectra. The spectral distinctions between W Virginis, RV Tauri, and semiregular variables are not clearly evident at those phases at which the spectral types overlap; but, if the observations are distributed throughout the cycle of variation, the class may be assigned with considerable confidence.

The median photographic absolute magnitudes of the seventh column of Table 3 are computed by assuming a value of 0.0 for the median absolute magnitude of the RR Lyrae variables in the same cluster. The relative intensity of the greatest observed strength of hydrogen emission in different stars is shown in the last column of the table. In several stars the maximum strength of emission has probably not been observed. The high intensities found in the W Virginis group are especially noteworthy.

The data of Table 3 represent the physical characteristics of 33 variables. Since they comprise nearly all the variables in globular clusters observable at Mount Wilson which have periods greater than 1 day, we may conclude that they are fairly representative of such stars. Inspection of the table reveals several significant facts in regard to the variables which are members of globular clusters.

[3] *Ap. J.*, **104**, 290, 1946.

TABLE 1

SPECTROSCOPIC OBSERVATIONS OF VARIABLES IN CLUSTERS

NGC (M)	Var. No.	Plate	JD	Phase (Days)	Spectrum	Velocity (Km/Sec)	Wt.
5139 (ω Cen)	1	E 2162	2423024.77	.....	F6	+176	0.5
5272 (3)	95	C 6772	2427998.76	26.93	M2e2	−168	0.3
		7168	9027.95	24.22	K1	−156	0.3
		7274	9364.95	51.65	G5e2	−155	1.0
		7290	9392.83	79.53	G8e1	−163	0.3
		7303	9410.81	97.51	M0	.....	.....
		7346	9452.73	36.24	G8e3	−153	0.3
		E 152	2430149.77	10.95	M2e2	.....	.....
		201	0207.71	68.89	G5e1	−176	1.0
		430	0445.96	100.76	M1	−146	0.5
		463	0501.80	53.40	G5e4	−156	0.5
		475	0515.73	67.34	G4e3	−173	0.5
		498	0533.77	85.38	G8	−162	0.3
		1363	1550.84	70.55	K1	−166	0.3
		1411	1599.78	16.30	M2	−156	1.0
		1674	1892.93	103.07	M1	−142	0.5
		1715	1979.76	86.71	M1	−161	1.0
	.....	.....	.....	.....	.....	−159	7.8
5272 (3)	154	(15)	.....	.....	.....	−153	14.0
5904 (5)	42	E 174	2430179.68	12.35	G3	+ 33	1.0
		472	0514.66	12.73	G3	+ 59	1.0
		502	0534.73	7.06	F8	+ 46	1.0
		512	0546.68	19.01	G2	+ 47	0.5
		538	0575.67	22.26	G2e1	+ 87	0.5
		880	0917.68	3.94	F8	+ 64	1.0
		1434	1636.69	2.29	F6	+ 42	1.0
		1686	1921.81	4.29	F6	+ 67	1.0
		1976	2637.95	25.50	F4	+ 56	1.0
	.....	.....	.....	.....	.....	+ 54	8.0
5904 (5)	50	E 1383	2431564.95	.....	M1	+ 42	0.5
		1435	1636.80	.....	M0	+ 35	0.5
		1692*	1923.88	.....	K0	+ 72	0.3
		1977*	2638.00	.....	G4	+ 65	0.3
	.....	.....	.....	.....	.....	+ 50	1.6
5904 (5)	84	E 175	2430179.74	20.7	G0	+ 65	1.0
		473	0514.79	11.3	G2	+ 47	1.0
		493	0531.74	1.7	F7e1	+ 51	0.5
		501	0534.69	4.7	F5	+ 34	1.0
		505	0544.67	14.7	G5	+ 55	1.0
		527	0563.68	7.2	G1	+ 34	1.0
		851	0894.84	20.3	G5	+ 55	1.0
		1386	1564.90	1.4	F5e1	+ 61	0.5
		1992	2669.82	19.8	G0e2	+ 67	1.0
	.....	.....	.....	.....	.....	+ 50	8.0
6093 (80)	1	E 1431	2431635.76	15.26	F6e5	+ 15	0.5
		1859*	2377.76	3.66	G0	+ 6	0.3
		2050*	2747.72	12.52	G0e2	.....	.....
	.....	.....	.....	.....	.....	+ 20	0.8

* Dispersion 220 A/mm at $H\gamma$.

TABLE 1—*Continued*

NGC (M)	Var. No.	Plate	JD	Phase (Days)	Spectrum	Velocity (Km/Sec)	Wt.
6121 (4)	4	E 508	2430545.71	.....	G2	+ 61	0.5
		523	0562.69	.....	G4	+ 53	1.0
		535	0574.67	.....	G8	+ 43	1.0
		1387	1564.96	.....	G6	+ 52	1.0
		2015	2698.89	.....	G3	+ 69	1.0
	.....	.....	.....	.....	.....	+ 55	4.5
6121 (4)	13	E 509	2430545.77	.....	G8	+ 80	0.7
		1391	1565.95	.....	K0	+ 77	1.0
		1461	1665.71	.....	G6	+ 94	0.5
		2014*	2698.83	.....	G3	+ 22	0.3
	.....	.....	.....	.....	.....	+ 75	2.5
6205 (13)	1	E 1717*	2432007.757	1.057	F2	−245	0.5
		1719*	2008.722	0.564	A2	−261	0.3
		1721*	2009.733	0.115	A8	−246	0.3
	.....	.....	.....	.....	.....	−245	1.1
6205 (13)	2	E 176	2430179.840	4.246	F5	−242	1.0
		205	0208.722	2.467	G0	−246	1.0
		207	0209.736	3.481	G2	−217	0.5
		561	0604.674	4.946	F2	−249	1.0
		856	0896.715	0.606	F0	−263	1.0
		1855	2375.771	2.863	G2	−244	1.0
		2012*	2397.965	4.618	G3	−251	0.3
		2056*	2749.691	3.751	G0	−216	0.3
		2061*	2750.691	4.751	F5	−239	0.5
	.....	.....	.....	.....	.....	−244	6.6
6205 (13)	6	E 835*	2430857.833	1.717	F5	−237	0.3
		1150	1308.785	0.519	F2	−256	0.3
	.....	.....	.....	.....	.....	−245	0.6
6205 (13)	10	E 528	2430562.795	.....	G5	−281	0.3
		532	0573.733	.....	G6	−248	1.0
		1724*	2010.726	.....	K0	−257	0.5
		1738	2054.682	.....	G8	−241	0.5
		1837	2344.759	.....	G2	−248	1.0
		2010*	2697.838	.....	G5	−257	0.5
		2023*	2716.793	.....	G8	−272	0.5
		2058*	2749.774	.....	G2	−237	0.5
	.....	.....	.....	.....	.....	−252	4.8
6205 (13)	11	E 513	2430546.809	.....	G8	−251	1.0
		855	0895.922	.....	G5	−260	1.0
		899	0945.715	.....	G5	−266	1.0
		1418	1601.924	.....	K0	−241	1.0
		1841	2346.729	.....	G5	−234	1.0
		2011*	2697.903	.....	G8	−290	0.5
		2024*	2716.851	.....	G5	−270	0.5
		2057*	2749.736	.....	G2	−246	0.3
	.....	.....	.....	.....	.....	−255	6.3

TABLE 1—*Continued*

NGC (M)	Var. No.	Plate	JD	Phase (Days)	Spectrum	Velocity (Km/Sec)	Wt.
6218 (12).....	1	C 7301	2429409.938	9.649	G5	− 39	0.3
		7347	9452.851	6.039	G0	− 32	0.3
		7500	9805.826	2.330	F8	− 40	1.0
		7508	9807.715	4.219	F8	− 58	1.0
		E 476	2430515.868	14.512	G0e2	.....	.....
		831	0855.928	13.396	G2	− 34	1.0
		1439	1638.722	5.282	G0	− 29	1.0
		1853	2374.747	12.431	G0	− 50	1.0
	.....	.....	.....	.....	.....	− 42	5.6
6254 (10).....	1	E 1436	2431637.748	.....	G4	+ 78	1.0
		1842	2346.883	.....	G0	+ 86	0.5
	.....	.....	.....	.....	.....	+ 81	1.5
6254 (10).....	2	C 7271	2429363.995	18.199	F8e2	+ 25	1.0
		7321	9439.842	0.276	G0e1	+ 38	1.0
		E 145	2430147.891	14.427	F5e3	+ 57	1.0
		172	0178.781	7.809	G2	+ 78	1.0
		1437	1637.878	4.094	G0	+ 70	1.0
		1456	1663.733	11.185	F8e5	+109	1.0
		1687	1921.933	6.839	G0	+ 94	1.0
	.....	.....	.....	.....	.....	+ 67	7.0
6402 (14).....	1	E 1857*	2432376.865	.....	G2	−101	0.2
		2046*	2746.721	.....	G0	−120	0.5
	.....	.....	.....	.....	.....	−115	0.7
6402 (14).....	2	E 2053*	2432748.742	.....	F8	−129	0.2
	7	1882*	2453.684	.....	F5	−124	0.3
		2047*	2746.826	.....	G2e3	−153	0.2
	.....	.....	.....	.....	.....	−136	0.5
6402 (14).....	17	E 2020*	2432715.833	.....	F8	+ 9	0.3
		2051*	2747.828	.....	G2	− 18	0.2
	.....	.....	.....	.....	.....	− 4	0.5
6626 (28).....	4	E 1887*	2432454.650	.....	G3	− 25	0.3
		2054*	2748.849	.....	G4	+ 32	0.3
	.....	.....	.....	.....	.....	+ 4	0.6
6656 (22).....	5	E 524	2430562.749	.....	G0	−149	0.3
		879	0916.838	.....	G2e1	−122	0.5
		1412	1599.941	.....	G2	−144	1.0
		1454	1662.837	.....	G5e1	−105	1.0
		1468	1667.736	.....	G6e2	−139	1.0
	.....	.....	.....	.....	.....	−130	3.8
6656 (22).....	8	E 1709	2431976.866	59.	G2	−134	0.5
		1764	2083.715	44.	G5e1	−215	0.5
	.....	.....	.....	.....	.....	−174	1.0

TABLE 1—*Continued*

NGC (M)	Var. No.	Plate	JD	Phase (Days)	Spectrum	Velocity (Km/Sec)	Wt.
6656 (22)	9	E 1710	2431976.951	41.62	G5	−158	0.3
		1760	2082.675	59.64	G2	−157	0.5
		2089*	2790.739	66.02	G5	−146	0.5
						−153	1.3
6656 (22)	11	E 1713	2431977.936	0.198	A8	−149	1.0
		1714	1978.931	1.192	F2	−147	0.3
		1716	1979.930	0.501	F0	−144	1.0
						−147	2.3
6656 (22)	14	E 1440*	2431638.84	64.8	M5e5	+ 58	0.3
		1722	2009.87	35.5	M3.5e4	+ 57	0.5
						+ 57	0.8
6779 (56)	1	E 1784*	2432111.688	1.340	A6	−178	0.5
		2055*	2748.899	1.340	A8	−166	0.3
						−174	0.8
6779 (56)	3	E 533	2430573.865	16.31	G3	−121	0.5
		1466*	1666.868	92.62	G5	−157	0.5
		1720*	2008.940	29.68	G2	−147	0.5
		1742*	2055.790	74.86	F8	−201	0.3
		2026*	2716.934	24.34	G2	−160	0.3
		2049*	2746.962	54.34	G0	−168	0.5
						−158	2.6
6779 (56)	6	E 173	2430178.920	6.22	G4e5	−135	1.0
		202	0207.851	35.15	G2	−123	1.0
		252	0249.779	77.08	F6	−133	1.0
		507	0344.920	82.20	G0e3	−129	0.5
		562	0604.771	71.99	F8	−154	0.3
		852	0894.948	2.09	G2	−128	1.0
		1460	1664.892	51.87	G0	−118	1.0
		1856	2375.941	42.76	F8	−137	1.0
		2025*	2716.910	23.65	G0	−125	0.3
		2048*	2746.908	53.65	G0e4	−155	0.3
		2090*	2790.785	7.50	G2	−127	0.3
						−132	7.7
7078 (15)	1	E 1761*	2432082.794	0.816	F0	−138	0.5
		1765*	2083.688	0.271	A8	−162	0.5
						−153	1.0
7078 (15)	Neb.	E 1117*	2431284.951			−115	0.5
		2060*	2749.957			−129	0.5
						−122	1.0
7089 (2)	1	E 1794	2426607.800	10.984	G0e1		
		1879	2432452.802	8.240	G2		
		1883*	2453.757	9.194	G2e1	− 42	0.2
		1906*	2496.717	5.260	F8	− 10	0.3
						− 23	0.5

TABLE 1—*Continued*

NGC (M)	Var. No.	Plate	JD	Phase (Days)	Spectrum	Velocity (Km/Sec)	Wt.
7089 (2)	5	E 1862*	2432408.977	4.803	F6	+ 7	0.3
		1884*	2453.806	14.523	G0e5	− 11	0.5
	.....	.....	.....	.....	.....	− 8	0.8
7089 (2)	6	E 1880*	2432452.865	2.450	F6	− 6	0.5
		2087*	2789.861	11.329	G2	+ 36	0.5
	.....	.....	.....	.....	.....	+ 13	1.0
7089 (2)	11	C 6977	2428466.688	24.499	F6	− 14	0.5
		7087	8731.946	21.414	F8	− 9	0.5
		γ 21219	8793.792	16.174	G0	− 17	1.0
		C 7153	8850.676	5.972	G0e1	+ 4	0.5
		7187	9143.701	30.653	G3	− 4	0.5
		E 282	2430268.747	15.237	G0	− 14	1.0
		306	0296.722	43.212	F5	− 24	1.0
		317	0298.747	45.237	F5	− 27	0.2
		340	0324.667	4.071	G3e2	+ 7	0.5
		511	0545.958	24.104	F8	− 15	1.0
		534	0573.951	52.097	F8	0	0.5
		γ 24423	0602.828	13.888	G0	− 28	1.0
		E 599	0633.724	44.784	G2	− 15	1.0
		609	0635.767	46.827	F8	− 15	0.5
		630	0654.729	65.789	G0	+ 16	0.5
		857	0896.962	39.678	F6	− 3	1.0
		1854	2374.920	41.744	F5	− 8	1.0
		1861	2377.938	44.762	F6	− 18	1.0
		1888	2454.834	54.572	F6	− 27	1.0
		1901	2494.684	27.336	G0	+ 4	1.0
		1905	2496.648	29.300	F8	− 2	0.5
		2091*	2790.895	55.203	G0	+ 15	0.3
	.....	.....	.....	.....	.....	− 4	10.8

NOTES TO TABLE 1

5272 (3) Var. 95. Min. = JD 2427249.5 + 103^{d}19*E*. J. L. Greenstein, *Harvard Bull.*, No. 901, 1935. A spectrogram by D. M. Popper (*Ap. J.*, **105**, 208, 1947) showed an M-type spectrum 16 days after minimum, but no emission lines. The first observation of the table was made by R. F. Sanford, who previously (*Pop. Astr.*, **27**, 99, 1919) in 1918 had obtained low-dispersion spectrograms of this star on April 9–10, showing bright *H*γ and *H*δ, and on May 13–14, showing no emission lines.

5272 (3) Var. 154. Barnard's variable for which results from 15 spectrograms have been published by Joy (*Mt. W. Contr.*, No. 637; *Ap. J.*, **92**, 396, 1940). The spectral type varied between F5 and G3e, and the velocity range was 56 km/sec.

5904 (5) Var. 42. Max. = JD 2427567.8 + 25^{d}738*E*. P. Oosterhoff, *Leiden Obs. Ann.*, **17**, Part IV, **18**, 1941.

5904 (5) Var. 50. Probably irregular. Mrs. Helen Sawyer Hogg writes that the period of 106 days suggested by S. I. Bailey does not hold at present.

5904 (5) Var. 84. Max. = JD 2415027.5 + 26^{d}5*E*. S. I. Bailey, *Harvard Ann.*, **78**, 158, 1917. The period can probably be improved.

6093 (80) Var. 1. Max. = JD 2429406.8 + 15^{d}70*E*. H. B. Sawyer, letter of July 21, 1948. Light-curve of W Virginis type.

6121 (4) Var. 4. Irregular, with cycles of variation between 50 and 80 days, resembling UU Her in spectrum and light-fluctuations. H. B. Sawyer, *J.R.A.S. Canada*, **36**, 213, 1942.

6121 (4) Var. 13. No period known. Probably irregular or RV Tauri class.

6205 (13) Var. 1. Max. = JD 2427685.763 + 1^{d}45899*E*. H. B. Sawyer, *Pub. Dunlap Obs.*, **1**, 233, 1942.

6205 (13) Var. 2. Max. = JD 2427308.868 + 5^{d}11003*E*. H. B. Sawyer, *Pub. Dunlap Obs.*, **1**, 233, 1942.

6205 (13) Var. 6. Max. = JD 2427274.867 + 2^{d}11283*E*. H. B. Sawyer, *Pub. Dunlap Obs.*, **1**, 233, 1942. The near-by south preceding companion star gives a velocity of −244 km/sec on one plate.

6205 (13) Var. 10. Irregular or RV Tauri class.

6205 (13) Var. 11. Irregular or RV Tauri class. A spectrogram, spectral type K0 *Ib* at maximum, was obtained by D. M. Popper (*Ap. J.*, **105**, 209, 1947). Color index at minimum, +1.8 mag.
6218 (12) Var. 1. Max. = JD 2427306.708 + 15^{d}508*E*. H. B. Sawyer, *Pub. Dunlap Obs.*, **1**, 61, 1938. The variable star is the preceding and usually the brighter star of the close pair. Both stars fall on the slit. The radial velocity of the following star, spectral type cK0, from four plates is −47 km/sec.
6254 (10) Var. 1. Small magnitude range and comparatively low absolute magnitude place this star in the irregular or RV Tauri group.
6254 (10) Var. 2. Max. = JD 2426607.712 + 18^{d}754*E*. H. B. Sawyer, *Pub. Dunlap Obs.*, **1**, 65, 1938.
6402 (14) Var. 1. Per. = 18.75 days. H. B. Sawyer, *Pub. Dom. Ap. Obs. Victoria*, **7**, 126, 1938.
6402 (14) Var. 2. Per. = 2.7952 days. H. B. Sawyer, *Pub. Dom. Ap. Obs. Victoria*, **7**, 126, 1938.
6402 (14) Var. 7. Per. = 13.59 days. H. B. Sawyer, *Pub. Dom. Ap. Obs. Victoria*, **7**, 126, 1938.
6402 (14) Var. 17. Spectral lines few and poor. The velocity measures are unsatisfactory and have been omitted from the mean for the cluster. The type of variation is uncertain. Membership in the cluster may be questioned because of distance from the center and poor agreement of the radial velocities.
6626 (28) Var. 4. Per. = 12–15 days. H. B. Sawyer, letter of July 21, 1948. Although the spectrograms are very poor, they seem to indicate irregular or RV Tauri variability.
6656 (22) Var. 5. No period. Irregular or RV Tauri class.
6656 (22) Var. 8. Max. = JD 2413373.6 + 61^d*E*. H. B. Sawyer, *Pub. Dunlap Obs.*, **1**, 300, 1944.
6656 (22) Var. 9. Max. = JD 2416761.5 + 87^{d}71*E*. H. B. Sawyer, *Pub. Dunlap Obs.*, **1**, 300, 1944.
6656 (22) Var. 11. Max. = JD 2429436.917 + 1^{d}69050*E*. H. B. Sawyer, *Pub. Dunlap Obs.*, **1**, 300, 1944.
6656 (22) Var. 14. Max. = JD 2418160.6 + 200^{d}2*E*. H. B. Sawyer, *Pub. Dunlap Obs.*, **1**, 300, 1944. The large positive velocity indicates that this Mira variable is not a member of the cluster.
6779 (56) Var. 1. Max. = JD 2428688.733 + 1^{d}50998*E*. H. B. Sawyer, letter of October 24, 1946.
6779 (56) Var. 3. Min. = JD 2428015.8 + 101^{d}67*E*. H. B. Sawyer, letter of February 26, 1948.
6779 (56) Var. 6. Min. = JD 2430172.7 + 90^{d}02*E*. *J.R.A.S. Canada*, **43**, 38, 1949.
7078 (15) Var. 1. Max. = JD 2415021.990 + 1^{d}437478*E*. M. J. Levy, *Harvard Bull.*, No. 893, p. 29, 1933.
7078 (15) Nebula. Planetary nebula discovered by F. G. Pease, *Pub. A.S.P.*, **40**, 342, 1928. Plate E 1117 was obtained by R. Minkowski. The bright lines of hydrogen and 4471 *He* I, 3726 [*O* II], 3728 [*O* II], 3868 [*Ne* III], 4363 [*O* III], 4958 [*O* III], and 5006 [*O* III] were measured. The line 4686 *He* II is very weak, if present. The close agreement of the radial velocity with that of the cluster indicates that the nebula is, without doubt, a member of the cluster. No variation of light has been suspected.
7089 (2) Var. 1. Max. = JD 2426607.800 + 15^{d}5647*E*. H. B. Sawyer, *Pub. Dom. Ap. Obs. Victoria*, **6**, 278, 1935.
7089 (2) Var. 5. Max. = JD 2426628.644 + 17^{d}5548*E*. H. B. Sawyer, *Pub. Dom. Ap. Obs. Victoria*, **6**, 278, 1935.
7089 (2) Var. 6. Max. = JD 2422162.928 + 19^{d}3010*E*. H. B. Sawyer, *Pub. Dom. Ap. Obs. Victoria*, **6**, 278, 1935.
7089 (2) Var. 11. Min. = JD 2431259.8 + 67^{d}086*E*. H. B. Sawyer, *J.R.A.S. Canada*, **43**, 38, 1949. Chèvremont's well-known variable. The star is among the most luminous variables in the clusters.

The stars almost exclusively fall in certain groups. Period and spectral type define the groups, within each of which the magnitude range and luminosity are conspicuously limited.

The RR Lyrae stars preponderate among the variables in clusters but do not appear in the table because they have not been observed spectroscopically. The stars of Group 1 (Table 3) with periods from 1.4 to 2.8 days are well separated from the other groups in period, absolute magnitude, and spectral type. Although a distinct gap in period separates this group from the RR Lyrae stars and the absolute magnitudes are definitely brighter, the periodic range in spectral type is much the same as in those of the shorter-period variables. Since cepheids with periods greater than 2 days are practically nonexistent in clusters, it seems reasonable to conclude that Group 1 is more closely related to, or perhaps an offshoot of, the populous RR Lyrae group. Two noncluster variables, SW Tau (Per. = 1.6 days, A7–F2) and XX Vir (Per. = 1.3 days, A2–F0), with early spectral type and high galactic latitude, may belong to this isolated group. The remaining 43 noncluster variables with periods between 1.0 and 3.0 days are fairly concentrated toward the galactic plane and for the most part probably fall in the cepheid category. All those known to be cepheids, such as SU Cas (1.9 days, F5–F7), TU Cas (2.1 days, F5–G2), and DT Cyg (2.5 days, F5–F7), have spectral types somewhat later than SW Tau, XX Vir, and the stars of Group 1.

In Group 2 only one cepheid, NGC 6205 (M13) var 2, was observed at Mount Wilson,

although another variable—5139 (ω Cen) var 48 (Per. = 4.5 days, M = −1.1)—may be a member of this class. The conspicuous lack of cepheids in the clusters is the outstanding fact of the distribution of the variable stars and shows beyond question that the population of the clusters is on a basis quite different from that of the galactic system as a whole.

The stars of Group 3, period 13–19 days, constitute a relatively large group, whose characteristics differ materially from those of the other groups. Their spectroscopic behavior closely duplicates that of W Virginis. When they are compared with galactic cepheids of like period, their spectral types are considerably earlier, especially at minimum light, and the G band (*CH*) is not seen. Their absolute magnitudes, determined by comparing their apparent magnitudes with those of the RR Lyrae stars, are fainter than those of the cepheids of like periods. This conclusion is also supported by the lesser strength of the lines of ionized atoms in the stars of the clusters. The emission lines of hydrogen reach great intensity during increasing light in the variables of the clusters but have not been detected in the cepheids. The light-curves of some of these variables show distinct resemblance to that of W Virginis, but further photometric observations are

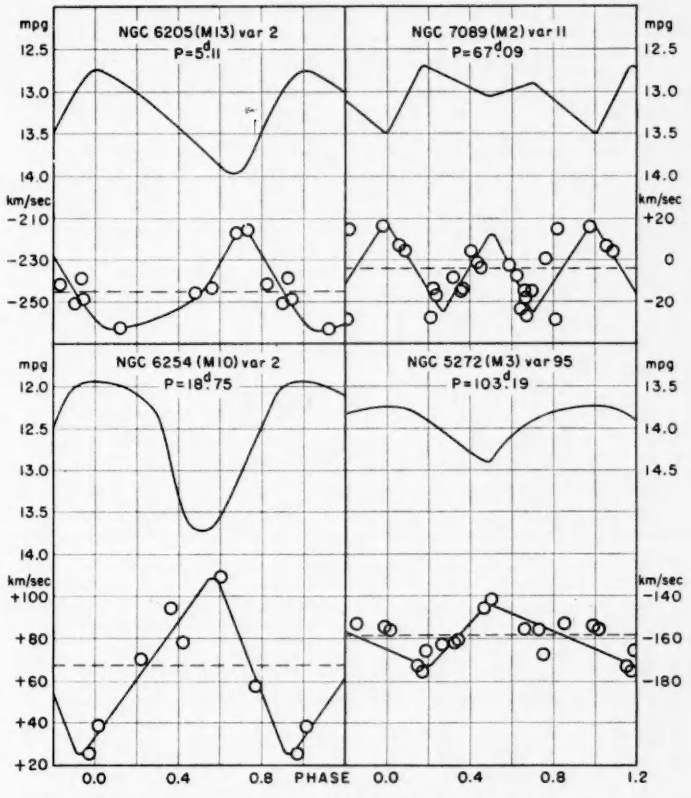

FIG. 1.—Light- and velocity-curves of four variable stars in globular clusters. The sources of the light-curves are found in the notes to Table 1.

TABLE 2

SUMMARY OF RADIAL VELOCITIES

CLUSTER NGC (M)	VAR. NO.	NO. PLATES	VELOCITIES			
			Mt. W.		Lick (Km/Sec)	Mt. W. − Lick (Km/Sec)
			Km/Sec	Wt.		
5139 (ω Cen)	1	1	+176	1	.....	.....
5272 (3)	95	14	−159	8	.....	.....
	154	15	−153	14	.....	.....
	.....	.....	−155	22	−161	+ 6
5904 (5)	42	9	+ 54	8	.....	.....
	50	4	+ 50	2	.....	.....
	84	9	+ 50	8	.....	.....
	.....	.....	+ 52	18	+ 58	− 6
6093 (80)	1	3	+ 20	1	+ 15	+ 5
6121 (4)	4	5	+ 55	4	.....	.....
	13	4	+ 75	2	.....	.....
	.....	.....	+ 62	6	.....	.....
6205 (13)	1	3	−245	1	.....	.....
	2	9	−244	7	.....	.....
	6	2	−245	1	.....	.....
	10	8	−252	5	.....	.....
	11	8	−255	6	.....	.....
	.....	.....	−249	20	−225	−24
6218 (12)	1	8	− 42	6	+ 36	−78
6254 (10)	1	2	+ 81	2	.....	.....
	2	7	+ 67	7	.....	.....
	.....	.....	+ 70	9	+ 65	+ 5
6402 (14)	1	2	−115	1	.....	.....
	2	1	−129	0	.....	.....
	7	2	−136	1	.....	.....
	.....	.....	−126	2	−121	− 5
6626 (28)	4	2	+ 4	1	− 3	+ 7
6656 (22)	5	5	−130	4	.....	.....
	8	2	−174	1	.....	.....
	9	3	−153	1	.....	.....
	11	3	−147	2	.....	.....
	.....	.....	−143	8	−162	+19
6779 (56)	1	2	−174	1	.....	.....
	3	6	−158	3	.....	.....
	6	11	−132	8	.....	.....
	.....	.....	−142	12	−182	+41
7078 (15)	1	2	−153	1	.....	.....
	Neb.	2	−122	1	.....	.....
	.....	.....	−138	2	−118	−20
7089 (2)	1	2	− 23	1	.....	.....
	5	2	− 8	1	.....	.....
	6	2	+ 13	1	.....	.....
	11	22	− 4	11	.....	.....
	.....	.....	− 4	14	+ 14	− 18

TABLE 3

VARIABLES IN CLUSTERS

NGC	(M)	VARIABLE	PERIOD (DAYS)	m_{pg}	MAG. RANGE	MEDIAN M_{pg}	NO. PLATES	SPECTRUM RANGE	MAX. EMISSION INT.
				Group 1. Period 1–2 Days					
6205	(13)	Var. 1	1.4	13.2–15.0	1.8	−0.9	3	A2–F2	.....
7078	(15)	Var. 1	1.4	14.4–15.5	1.1	−0.6	2	A8–F0	.....
6779	(56)	Var. 1	1.5	15.1–16.2	1.1	−0.8	2	A6–A8	.....
6656	(22)	Var. 11	1.7	12.9–13.8	0.9	−0.7	3	A8–F2	.....
6205	(13)	Var. 6	2.1	13.5–14.8	1.3	−1.0	2	F2–F5	.....
6402	(14)	Var. 2	2.8	15.4–16.3	0.9	−1.0	1	–F8	.....
	.....	.....	.....	.....	1.2	−0.8	.....	.....	.....
				Group 2. Period 5 Days (Cepheid)					
6205	(13)	Var. 2	5.1	12.6–14.1	1.5	−1.8	9	F0–G3	.....
				Group 3. Period 13–19 Days (W Virginis)					
6626	(28)	Var. 4	13:	13.9–14.9	1.0	.....	2	G3–G4	.....
6402	(14)	Var. 7	13.6	14.9–16.2	1.3	−1.3	2	F5–G2	e3
5272	(3)	Var. 154	15.3	12.9–14.0	1.1	−2.1	15	F5–G3	e4
6218	(12)	Var. 1	15.5	11.9–13.2	1.3	.....	8	F8–G5	e2
7089	(2)	Var. 1	15.6	13.2–14.8	1.6	−2.1	4	F8–G2	e1
6093	(80)	Var. 1	16.0	13.1–14.5	1.4	−2.2	3	F6–G0	e5
7089	(2)	Var. 5	17.6	13.2–14.9	1.7	−2.1	2	F6–G0	e5
6254	(10)	Var. 2	18.8	11.9–13.7	1.8	−1.9	7	F5–G2	e5
6402	(14)	Var. 1	18.8	14.3–16.0	1.7	−1.7	2	G0–G2	.....
7089	(2)	Var. 6	19.3	13.2–14.9	1.7	−2.1	2	F6–G2	.....
	.....	.....	.....	.....	1.5	−1.9	.....	.....	.....
				Group 4. Period 25–90 Days (RV Tauri)					
5904	(5)	Var. 42	25.7	11.2–12.2	1.0	−3.4	9	F4–G3	e1
5904	(5)	Var. 84	26.5	11.5–12.6	1.1	−3.1	9	F5–G5	e2
5139	(ω)	Var. 1	58.7	10.7–12.6	1.9	−3.0	2	F6–	.....
7089	(2)	Var. 11	67.1	12.5–13.7	1.2	−3.0	22	F5–G3	e2
6779	(56)	Var. 6	90.0	13.1–14.8	1.7	−2.5	11	F6–G4	e5
	.....	.....	.....	.....	1.4	−3.0	.....	.....	.....
				Group 5. Period 65–106 Days (Semiregular)					
6254	(10)	Var. 1	.....	13.2–13.8	0.6	−1.2	2	G0–G4	.....
6656	(22)	Var. 5	.....	12.0–12.8	0.8	−1.7	5	G0–G6	e2
6121	(4)	Var. 4	65±	11.4–12.2	0.8	−2.1	5	G2–G8	.....
6656	(22)	Var. 8	67±	12.0–12.7	0.7	−1.7	2	G2–G5	e1
6656	(22)	Var. 9	88	12.7–13.3	0.6	−1.1	3	G2–G5	.....
6205	(13)	Var. 10	.....	13.1–14.0	0.9	−1.6	8	G2–K0	.....
6205	(13)	Var. 11	.....	12.9–13.8	0.9	−1.8	8	G2–K0	.....
6121	(4)	Var. 13	.....	12.4–13.1	0.7	−1.2	4	G3–K0	.....
6779	(56)	Var. 3	102	14.4–15.2	0.8	−1.6	6	F8–G5	.....
5272	(3)	Var. 95	103	13.7–14.4	0.7	−1.5	16	G4–M2	e4
5904	(5)	Var. 50	106	13.0–14.2	1.2	−1.5	4	G4–M0	.....
	.....	.....	.....	.....	0.8	−1.5	.....	.....	.....

needed for others. Few noncluster variables of this class are known, and the prototype W Virginis is the only one bright enough to be easily observed.

Group 4 is anomalous, and the relation of the 5 stars included in it to other variables either in or outside the clusters is uncertain. Spectroscopically they are like AC Her, but the spectral range is much less. The spectra differ little from those of Group 3, except that the bright lines do not attain such great intensity. The luminosity is much higher than that of stars of any other group. H. B. Sawyer[4] has recently shown that two of the stars—7089 (2) var 11 and 6779 (56) var 6—have light-changes characteristic of the RV Tauri class. The period of 7089 (2) var 11 is double that previously recognized; possibly further observation will show that the periods of 5904 (5) var 42 and 5904 (5) var 84 also should be doubled. Although the high luminosity of the stars of the group corresponds to that of the cepheids with period of 30 days, they can hardly be normal cepheids because their spectral types, especially at minimum light, are too early and between minimum and maximum they show hydrogen emission lines which do not appear in cepheids. Their velocities seem to be irregular, with comparatively small range. Doubtless, 5139 (ω Cen) var 1, whose period (58.7 days) also was doubled when it was recognized as an RV Tauri variable, is properly included in this group, although only one plate is available.

The stars of Group 5 have slow light-changes and are irregular or semiregular. The range of variation is less than in the other groups and the spectral type definitely later.

The luminosities are comparatively low and do not increase with their longer periods. Although the physical characteristics of the different stars of this group agree reasonably well among themselves, different classes of variation may be represented. For example, the light-curve[5] and spectrum of 6121 (4) var 4 are similar to those of UU Her, which may be related to the variables of the RV Tauri class. Further observations will probably make it possible to identify some of the other variables as members of the RV Tauri class. The last two stars of the list show faint titanium oxide bands at minimum, but in other respects their spectra do not resemble those of Mira variables, and their luminosities are too bright.

The long-period variables in 5139 (ω Cen) and 104 (47 Tuc) are likewise too bright as compared with galactic long-period Me variables. We may conclude that Me variables as well as cepheids are either very rare or entirely absent in the globular clusters.

The variable stars found most frequently in the globular clusters are those of the RR Lyrae, W Virginis, RV Tauri, and irregular classes. Such noncluster stars have long been known[6] to have large peculiar motions and to be widely scattered in galactic latitude. However, the Me variables[7] and the less regular M-type variables,[8] many of which have high velocities, have not yet been certainly identified in the clusters. The presence of the high-velocity stars in large numbers and the paucity of cepheids in the clusters definitely indicate that population II largely predominates in these systems.

The occurrence of large numbers of RR Lyrae variables in systems where cepheids are practically nonexistent shows that the two classes of variables are not so closely related as has hitherto been assumed.

In this study of the high-luminosity variable stars in the globular clusters I am deeply indebted to Mrs. Helen Sawyer Hogg for supplying firsthand many of the data concerning the periods and magnitudes used in this discussion. Without her untiring interest in the problems of the clusters and her kind co-operation, my observations would have little significance.

[4] *J.R.A.S. Canada*, **43**, 38, 1949.

[5] *Ibid.*, **36**, 213, 1942.

[6] A. H. Joy, *Pub. A.S.P.*, **37**, 157, 1925; **44**, 240, 1932.

[7] P. W. Merrill, *Mt. W. Contr.*, No. 649; *Ap. J.*, **94**, 171, 1941.

[8] A. H. Joy, *Mt. W. Contr.*, No. 668; *Ap. J.*, **96**, 344, 1942.

INTERSTELLAR CALCIUM LINES IN THE SPECTRA OF STARS IN OPEN CLUSTERS

ROSCOE F. SANFORD
Mount Wilson and Palomar Observatories
Received June 1, 1949

ABSTRACT

Distances of 31 open star clusters have been derived from the equivalent widths of the interstellar lines in the early-type stars.

Velocities which have been obtained from both the interstellar and the stellar lines accord with differential galactic rotation.

The distances have been derived by means of both stellar and interstellar velocities. Although the correlation of these distances with the corresponding equivalent widths is not especially good, it seems to be considerably better than the correlation of Trumpler's distances with equivalent width. The equivalent widths and both the stellar and the interstellar velocities seem, therefore, to provide a useful means of obtaining the distances of open clusters.

Large systematic and accidental errors in the interstellar velocities of open clusters derived by Miss Phyllis Hayford probably explain why her observations were unsuited to a solution for galactic rotation.

The stellar and interstellar velocities of 14 stars (Table 3) provide good evidence that they belong to the h and χ Persei clusters.

A series of papers published during the interval 1937–1939[1] dealt with the equivalent widths and radial velocities of the interstellar lines in distant and consequently relatively faint stars. It was shown that the equivalent width of these lines increases with distance and that the radial velocities conform to the simple theory of differential galactic rotation, i.e., a complete cycle in 180° of galactic longitude has an amplitude roughly equal to half that given by the stellar velocities from the same stars. In other words, the effective source of interstellar lines is midway between observer and star.

Those results may now be supplemented by the observations of nearly all the stars with interstellar *Ca* II lines in the open star clusters which can be reached from Mount Wilson. Observations have been made both at the 60-inch and at the 100-inch reflectors, with the dispersions given in the accompanying tabulation. Several of the stars were observed with two or three of these dispersions.

Designation	Dispersion	Stars	Weight
D 10	10 A/mm	Brighter than 7.5 mag.	4
D 25	25 A/mm	7.6–8.5 mag.	2
D 50	50 A/mm	Fainter than 8.5 mag.	1

THE EQUIVALENT WIDTHS

The equivalent widths (E.W.) were determined by reference either to spectral calibrations or, in a few instances, to sensitometer spots, and they are expressed in angstroms of

[1] P. W. Merrill and R. F. Sanford, *Mt. W. Contr.*, No. 564; *Ap. J.*, **85**, 73, 1937; O. C. Wilson and P. W. Merrill, *Mt. W. Contr.*, No. 570; *Ap. J.*, **86**, 44, 1937; R. F. Sanford, *Mt. W. Contr.*, No. 573; *Ap. J.*, **86**, 136, 1937; P. W. Merrill, R. F. Sanford, O. C. Wilson, and Cora G. Burwell, *Mt. W. Contr.*, No. 576; *Ap. J.*, **86**, 274, 1937; P. W. Merrill and O. C. Wilson, *Mt. W. Contr.*, No. 582; *Ap. J.*, **87**, 9, 1938; P. W. Merrill and R. F. Sanford, *Mt. W. Contr.*, No. 585; *Ap. J.*, **87**, 118, 1938; R. F. Sanford and O. C. Wilson, *Mt. W. Contr.*, No. 613; *Ap. J.*, **90**, 235, 1939; O. C. Wilson, *Mt. W. Contr.*, No. 614; *Ap. J.*, **90**, 244, 1939.

total absorption. Since $H\epsilon$ often rendered it difficult or impossible to measure the E.W. of H, the equivalent width of K only is considered in what follows.

Since E.W.'s previously determined at Mount Wilson depended largely upon D 25 spectrograms, it seemed best to reduce all the E.W.'s to that dispersion. The intercomparison of the three dispersions showed the following E.W. relations in angstrom units:

$$\text{D } 25 = \text{D } 50 - 0.056\text{A};$$

$$\text{D } 25 = 1.25\,\text{D } 10 \qquad (\text{E.W.} \leq 0.40\text{A});$$

$$\text{D } 25 = \text{D } 10 + 0.10\text{A} \qquad (\text{E.W.} > 0.40\text{A}).$$

The correction for D 50 can be accepted as constant, since it applies only to faint stars with large measured E.W.'s, except for a few stars in NGC 1502, 1960, and 6531, for which no systematic corrections were used. The measures of E.W. are given in the fifth column of Table 1. The weight for each star is the sum of the weights of the plates used.

Table 1 indicates that stars in the same group and presumably at the same distance have interstellar *Ca* II lines with essentially the same E.W.'s. This is to be expected, inasmuch as all stars in a cluster have practically an identical interstellar path with nearly the same *Ca* II content. This similarity among the individual stars of a cluster ought to provide mean E.W.'s of considerable weight for each cluster. These mean E.W.'s are collected in the fourth column of Table 2. The distances given in the seventh column depend upon the relation of equivalent width to distance already found by the writer.[2] The weights are the sums of weights of the individual plates involved.

THE RADIAL VELOCITIES

Radial velocities have been derived from the interstellar *Ca* II lines and from all suitable stellar lines. All interstellar velocities were reduced to D 10 by corrections obtained from stars photographed with more than one dispersion. It was found necessary to increase interstellar velocities from D 25 by +1.8 km/sec and those from D 50 by +2.7 km/sec to correct them to the D 10 velocities. The interstellar *Ca* II velocities thus corrected and the stellar velocities for the individual stars are given in Table 1. The number following an interstellar velocity sums the weights for the plates involved.

Mean interstellar and stellar velocities are collected in the ninth and eleventh columns of Table 2. The interstellar velocity for a cluster and its probable error are derived from a weighted mean of the interstellar velocities for the stars involved. The stellar velocity for a cluster is a mean of the velocities of the separate stars, weights being assigned on the basis of the number of spectrograms per star. The tenth and twelfth columns are the velocities of the ninth and eleventh columns, respectively, corrected for solar motion (+20 km/sec and apex α 271°, $\delta + 28°$) and then reduced to a distance of 1 kpc by division by the corresponding E.W. distance in kiloparsecs from the seventh column.

Figure 1, *A*, has the reduced interstellar velocities of the tenth column plotted against galactic longitude. Figure 1, *B*, shows how the stellar velocities, when they are freed from solar motion and reduced to a distance of 1 kpc (twelfth column), progress with galactic longitude. The curve in Figure 1, *A*, is for differential galactic rotation about a center at $l = 325°$ with a semiamplitude of 8.9 km/sec[3] appropriate to a distance of 0.5 kpc. The curve in Figure 1, *B*, has the semiamplitude 17.7 km/sec, that of differential galactic rotation for 1 kpc. Velocities of low weight are represented by open circles. There is good evidence of differential galactic rotation.

[2] *Mt. W. Contr.*, No. 573; *Ap. J.*, **86**, 136, 1937.

[3] R. E. Wilson, *Mt. W. Contr.*, No. 631; *Ap. J.*, **92**, 185, 1940.

TABLE 1

STARS IN OPEN CLUSTERS: VELOCITIES AND EQUIVALENT WIDTHS

CLUSTER	STAR DESIG.	MAG.	SP. CL.	E.W. OF K		VELOCITIES (KM/SEC)				
						Mount Wilson			Other Observatories	
				A	Wt.	*Ca* II and Wt.		Stellar	*Ca* II	Stellar
NGC 457R*	No. 3	9.7	B1	0.65	3	−23.8	4	−53: e		
	No. 4	9.8	B3e	.74	2	−22.7	4	−32 e		
	No. 5	9.9	B3	.61	2	−22.0	3	−48 e		
	No. 7	10.0	B3	.63	1	−24.3	2	−50 e		
NGC 581	No. 119	10.1	B3	.58	3	−14.4	3	−30.8 d		
	No. 146	9.2	B3	.61	2	−10.9	3	−51.6 d		
	HD 9311	7.3	B5					−39.7 d		−38.1 V
NGC 663	BD+60°339	8.8	B5					−30.5 d		
	BD+60°343	9.1	B3	.62	2	−24.3	3	−32.6 d		
NGC 869	HD 12856	8.4	B2ea			−23.5	3			
884	13051	8.0	B0ea			−24.1	3			
	13402	8.2	B0			−12.6	4	−40 e		
	13745	8.0	B0			−16.8	4	−29.5 c		
	13841	7.2	B1	.65	4	−23.8	4	−38.7 a	−28.2	−35.5 V
	13854	6.4	B0	.74	2	−23.1	4	−41.4 b	−26.0	−38.0 V
	13866	7.7	B2p			−22.4	4	−47.0 c		
	13969	8.8	B2			−20.2	1	−48 e		
	14053	8.7	B2			−27.7	2	−44.5 d		
	14134	6.7	B3ea	.65	2			−42.9 c	−31.4	−44.5 V
	14143	6.7	B1	.72	4	−22.2	1	−33.9 d	−25.5	−47.6 V
	14357	8.9	B3			−24.1	3	−41.1 b		
	14422	9.4	Bp			−16.8	2			
	14434	8.5	B0			−21.9	2	−20.1 d		
	14443	8.6	B2			−10.8	2	−39.5 c		
	14818	6.2	B1ea	.68	2	−18.9	2	−45.9 b	−24.4	−46.7 V
	14956	7.3	B1	.59	2			−21.1 c	−20.5	−30.3 V
	15642	8.0	B2			−21.2	1	−28 d		
	15690	7.7	B3			−22.1	5	−35.3 c		
IC 1805	HD 15558	8.5	O8	.47	2	− 9.0	3	−59: e		
	15570	8.8	O5e	.58	2	−22.1	2	−24 e		
	15629	8.4	B3			−16.5	3	−57 e		
	No. 5	9.0	B3	.59	3	−10.1	3			
	No. 7	9.8	O9	.49	1	−14.6	2	−47 e		
NGC 1444	HD 23675	6.8	B0	.28	4	− 5.5	6	+ 6 e	− 0.1	− 1.9 V
NGC 1502	HD 25638	7.0	B1	.24	2	− 3.7	4	−23: e	− 7.4	+11.0 V
	25639	7.1	B0	.28	2	+ 4.8	3	−19: e	− 8.2	−13 V
										−18.7 LN
	No. 4	9.8	B3	.36	2	+ 1.3	3	−15: e		
	No. 5	10.0	B3	.32	1	+ 1.7	1	−19 e		
	No. 7	10.1	B3	.26	2	+ 3.0	2	−30 e		
	No. 8	10.3	B3	.35	1	+ 1.6	1	−25 e		
NGC 1960	No. 120	9.8	B3	.21	1	+ 0.3	2	− 8.9 d		
	No. 208a	8.5	B3	.23	4	+ 5.1	5	−19 e		
	No. 238	9.5	B3	.21	1	+13.2	2	+ 5.6 d		
	No. 249	9.4	B3	.19	1	+ 3.3	2	+40: e		
	No. 250	9.2	B2	.24	1	+ 8.2	2	− 9: e		
	No. 258	8.6	B3	.29	4	+ 2.2	6	+ 0.4 d		
	No. 313	8.8	B3	.31	4	+ 8.4	9	−23.2 c		
	No. 350	8.7	B3	.26	4	+ 7.6	4	− 3 e		
	No. 365	9.0	B2e	.33	4	+ 4.8	6			
NGC 1981	HD 37016	6.3	B3	.19	4	+27.5	16		+25.9	+31 V
	37017	6.5	B3	.14	8	+30.3	4			+29 V
	37040	6.3	B3	.24	4	+27.6	8			+30 V
	37129	7.0	B5					+36 e	+18.5	+25.5 V
NGC 2129	BD+23°1148	8.3	B1	.37	4	+14.6	6	+18.0 d		
	BD+23°1149	7.4	B1	.38	4	+14.7	14	+16.3 b		
	No. 3	10.1	B3	.54	3	+23.6	3	+ 8.0 d		
NGC 2169	HD 41909	8.7	B3	.21	6	+17.3	4	+38.2 d		
	41943br	7.0	B1	.21	3	+18.3	9	+17.8 d		+ 5.2 V
	41943ft	8.5	B1	.20	8	+16.7	4	+19.8 d		
	No. 16	8.9	B3			+14.2	1	+ 8 e		
NGC 2244	HD 46056	8.2	B3	.32	2	+28.0	3			+45 V
	46106	7.7	B3	.38	6	+25.8	4	−20: e		+26.9 V
	46149	7.6	O8	.30	6	+19.3	4	+43.4 d	+17.5	+38.9 V
	46150	6.9	O5	.32	10	+22.2	12	+37.1 d	+24.0	+35.9 V
	46202	8.1	B0	.45	2	+25.6	3	+33.7 d		
	46223	7.1	O8	.36	8	+22.6	4	+48.6 d	+16.0	+42.2 V
	No. 8	8.5	B2	.31	4	+16.5	6	+12 e		
	No. 13	9.7	B3	.38	1	+14.4	2	+35.1 d		
	No. 15	10.4	B3	0.37	1	+30.4	2	+32.6 d		

* "R" calls attention to notes at the end of the table.

TABLE 1—*Continued*

Cluster	Star Desig.	Mag.	Sp. Cl.	E.W. of K		Velocities (Km/Sec)			
						Mount Wilson		Other Observatories	
				A	Wt.	*Ca* II and Wt.	Stellar	*Ca* II	Stellar
NGC 2264.....	HD 47839	4.8	B0	0.17	4	+16.8 4	.....	+16.2	+33.4 V
									+31.7 Y
	47961	7.3	B3	.22	4	+16.9 4	+ 0 e	.....	+27 V
NGC 2353.....	HD 55879	6.0	O9	.13	12	+27.1 8	+30.9 d	+30.2	+31.9 V
								+33	+33.7 LN
	55901	8.4	B5	.....	.....	.....	+11.6 d	.....	.....
NGC 2362.....	HD 57061	4.4	O9	.18	4	+28.4 24	.....	+26.9	+37.3 V
									+40.4 Y
	57192	6.8	B3	.09	8	+23.6 8	(+34:) e	.....	.....
	No. 3	8.1	B2	.15	4	+26.4 4	(+54) e	.....	.....
NGC 6231.....	HD 152233	6.4	O8	.42	1	− 7.5 2	−17 e	− 5.2	−15.6 McD
	152234	5.3	B0	.50	2	− 6.4 2	− 2.3 e	−13.0	− 2.2 McD
									−13 L
	152248	7.3	B	.56	2	− 8.6 2	.....	−11.8	−35.0 McD
	152249	6.8	B0	.48	2	−10.5 2	−19 e	− 6.4	−25.2 McD
									−22 L
Anon 24.....	HD 152405	7.3	B0	.45	2	− 5.4 2	+19 e	.....	.....
	152408	6.0	O7e	.47	2	− 9.6 2	.....	.....	.....
	152667	6.4	O9	.53	2	− 5.6 2	+51 e	.....	.....
	152723	7.2	O8	.49	2	− 8.2 2	+14 e	.....	.....
NGC 6383.....	HD 159176	5.7	O6	.28	8	− 4.9 12	+13 e	−29.0	− 4 L
NGC 6530R.....	HD 164794	5.9	O5	.25	2	− 7.5 16	+ 3.6 a	.....	+15.3 V
									− 8 L
	164906	7.5	B0ne	.23	4	−10.2 8	.....	.....	.....
	165052	6.8	O6	.29	8	− 7.0 8	− 1 e	.....	+ 3 V
	No. 5	8.3	B2	.27	4	−10.5 6	+95: e	.....	.....
	No. 6	8.5	B2	.23	1	−20.0 3	− 3 e	.....	.....
	No. 12	9.3	B3	.....	.....	− 2.6 2	−11: e	.....	.....
NGC 6531.....	HD 164844	8.2	B3	.33	3	−10.4 6	− 2 e	.....	−16.9 LN
	164883	7.1	B1	.12	5	− 3.2 5	− 5 e	−16	−11.2 LN
	No. 4	8.6	B3	.26	2	− 8.7 4	+ 3: e	.....	.....
	No. 6	9.1	B3	.29	1	....	−16: e	.....	.....
	No. 7	9.5	B2	.20	1	− 8.9 2	− 6.9 d	.....	.....
NGC 6604.....	HD 167971	7.0	O9	.50	8	− 1.3 8	.....	−19	− 4.1 LN
NGC 6611.....	HD 168075	8.9	O8	.71	2	+ 2.6 3	+37: e	.....	.....
	168076	8.6	O6ea	.60	7	+ 4.4 7	− 6: e	.....	.....
	168137	9.2	O9	.90	2	− 7.8 2	+19.0 d	.....	.....
	No. 4	9.6	O9	.78	1	− 3.8 4	+ 9.1 d	.....	.....
NGC 6613R.....	HD 168352	9.4	B3	.69	1	−18.4 1	− 8 e	−29	−16 P
								−30	−27.8 LN
	168368	10.1	B3	.64	1	− 5.6 2	−14.0 d	.....	− 1.3 LN
	No. 9	10.2	B3	.36	2	+ 0.6 2	− 9 e	.....	.....
NGC 6871R.....	HD 190918	7.0	O9	.50	2	−13.4 148	−21.8 a	−16.7	−13.4 V
	190919	7.2	B1	.56	6	−11.6 4	− 9.2 c	−13.0	−22 V
	227634	7.6	B1	.60	4	−14.7 6	−15.1 d	.....	.....
	BD+35°3955	8.0	B0	.45	4	−12.1 4	− 1 e	−14.0	−8.8 V
	BD+35°3956	8.9	B1	.52	6	−11.6 16	−36 e	.....	.....
IC 4996.....	HD 193007	8.4	O9	.36	6	−13.5 8	(+16::)e	.....	.....
	No. 20	10.5	B1	.42	2	−15.5 3	− 3 e	.....	.....
	No. 37	9.5	B0	.58	2	−16.4 5	−47:: e	.....	.....
NGC 6883.....	ADS 13486AB	9.3	B3	.32	4	+ 0.5 2	−10.0 d	.....	.....
	ADS 13486D	9.2	B3	.42	2	− 6.2 3	− 3.2 d	.....	.....
NGC 6910R.....	HD 194279	7.0	B0	.82	4	−11.2 7	−29.4 b	−12.8	−30.2 V
	No. 4	9.4	O8	.74	2	− 8.8 9	−38:: d	.....	.....
	No. 6x	10.4	B1	.70	3	−12.8 5	−14:: e	.....	.....
NGC 6913R.....	No. 2	9.7	B0	.38	5	−10.2 7	−34 e	.....	.....
	No. 3	9.9	B0	.59	2	−10.2 2	+20 e	.....	.....
	No. 4	9.9	B0	.41	2	−12.4 2	−15: e	.....	.....
	No. 6	10.2	Be	.46	2	− 9.8 3	−21 e	.....	.....
	No. 7	10.2	B0	.52	2	−10.9 8	−14 e	.....	.....
	No. 10x	10.8	B0	.48	2	− 6.7 3	−19.6 d	.....	.....
NGC 7160.....	HD 208392	7.1	B1	.40	2	−12.2 5	−60 e	−15.7	−26.2 V
	No. 3	9.5	B3	.50	2	− 3.4 3	−25 e	.....	.....
	No. 4	10.0	B3	.37	2	−12.7 5	−46 d	.....	.....
NGC 7380.....	HD 215835	8.9	B1	.69	3	−19.4 4	.....	.....	.....
	No. 4	10.4	B0	0.52	4	−19.2 5	−37.9 d	.....	.....

NOTES TO TABLE 1

The sources for the velocities in the last two columns of Table 1 are as follows:

V = Victoria, *Pub. Dom. Ap. Obs. Victoria*, **5**, 13, 98, 1935.
McD = McDonald Obs., *Ap. J.*, **100**, 189, 1944.
Y = Yerkes.
L = Lick Obs., *Pub. Lick Obs.*, Vol. **18**, 1932.
LN = Neubauer at Lick, *Ap. J.*, **97**, 300, 1943.
P = Popper at McDonald, *Ap. J.*, **100**, 94, 1944.

A letter attached to each mean stellar velocity has the following estimated significance:

	Probable Error (Km/Sec)
a	≤0.7
b	0.8–1.5
c	1.6–2.5
d	2.5–8.0
e	>8.0

A colon following a stellar velocity signifies a mean of individual velocities that are very discordant. Two colons occur when it appears certain that the star is a spectroscopic binary.

NGC 457. Stars without numbers from well-known catalogues can be identified by reference to Miss Phyllis Hayford's Table II, *Lick Obs. Bull.*, **16**, 62–66, 1932.
NGC 6530. No. 5 has four stellar velocities, −11, +112, +131, and +148 km/sec.
NGC 6613. Star No. 9 follows 4[a] and is 1′ south of HD 168368.
NGC 6871, HD 190918. The absorption-line velocity is that obtained for the systemic velocity of this spectroscopic binary from 74 spectrograms (O. C. Wilson, *Mt. W. Contr.*, No. 755; *Ap. J.*, **109**, 76, 1949). Dr. Wilson has permitted me to use his measures of the interstellar velocities on these same 74 spectrograms.
NGC 6910. Star No. 4 is a spectroscopic binary, showing lines of both components. Both HD 194279 and star No. 4 show a weak component of interstellar K, whose measured velocity is about −53 km/sec.
NGC 6913. All the signs of the differential co-ordinates for the stars in this cluster given by Miss Hayford need to be reversed.

A comparison of Figure 1, *A* and *B*, shows that interstellar velocities of stars at a distance of 1 kpc have a differential galactic rotation-curve with about half the amplitude given by the stellar velocities. This merely confirms the results of various earlier studies.

EQUIVALENT WIDTHS AND GALACTIC ROTATION

Since Figure 1, *A* and *B*, have shown differential galactic rotation fairly well, it seemed possible that the velocities of the clusters might serve to determine the distances of the clusters. In testing this possibility, it seemed best to omit the clusters with velocities of low weight near the null points of differential galactic rotation by excluding those for which $\sin 2(l - 325°)$ is numerically less than 0.500 and also to omit the three clusters with the highest galactic latitudes. This left fifteen clusters with interstellar velocities and thirteen with stellar velocities. These velocities, when freed from solar motion, were divided by their respective values of $\sin 2(l - 325°)$. It was assumed that the resulting velocities would be the semiamplitudes of differential galactic rotation appropriate to the distances of the respective stars.

The mean equivalent widths for the fifteen clusters are plotted against these values of the semiamplitudes from the interstellar lines in Figure 2, *A*. Figure 2, *B*, is a similar treatment of the stellar velocities. The correlation of equivalent width with velocity is apparent in both figures but is, of course, far from perfect. The abscissae for Figure 2, *B*, are twice those of Figure 2, *A;* their ordinates are the same. Since the freehand curve through the points in *A* is much like that through the points in *B*, it is once again demonstrated that the semiamplitude of differential galactic rotation for the interstellar velocities is half that for the stellar lines for the same stars, at least statistically.

RELATION OF EQUIVALENT WIDTHS TO DISTANCE

The sixth column of Table 2 contains the distances which Trumpler[4] has derived for these clusters, with the exception of the distance for the h and χ Persei clusters, for which the value obtained by W. P. Bidelman[5] was substituted. The E.W.'s of the fourth

[4] *Lick Obs. Bull.*, **14**, 154, 1930.

[5] *Ap. J.*, **98**, 61, 1943.

column of Table 2 are plotted against these distances in Figure 3, *A*. The E.W.'s are seen to increase statistically with distance, but the scatter is very large.

It has been assumed that each interstellar velocity used in Figure 2, *A*, will give a value of the distance of the cluster to which it belongs if divided by 8.9 km/sec, the semiamplitude of interstellar velocity variation for stars at a distance of 1 kpc. Likewise, the velocities in Figure 2, *B*, are assumed to provide distances if divided by 17.7 km/sec, the semiamplitude of stellar-velocity variation at 1 kpc. Mean values of these distances from stellar and interstellar velocities are in the eighth column of Table 2. These are plotted against E.W.'s in Figure 3, *B*. The same stars are distinguished in Figure 3, *A*, by triangles, and it is evident that the correlation in 3, *B*, though far from perfect, is much better than for the triangles representing the same stars in 3, *A*. Hence it is concluded

TABLE 2

OPEN CLUSTERS: MEAN VELOCITIES AND EQUIVALENT WIDTHS

Cluster	Galactic		E.W. of K		Distance (Kpc)			Interstellar Ca II Velocities (Km/Sec)		Stellar Velocities (Km/Sec)	
	l	b	A	Wt.	Trumpler	By E.W.	By Vel.	Meas.	1 Kpc Res. Vel.	Meas.	1 Kpc Res. Vel.
NGC 457	94°	− 4°	0.66	8	1.48	2.28	2.2	−23.1±0.7	− 7.9	−46.7±3.1	−18.3
581	96	− 1	.59	5	1.96	1.87	1.4	−12.7±1.2	− 3.8	−40.4±3.5	−18.7
663	97	0	.62	2	2.17	2.00	1.8	−24.3±2.4	− 9.8	−31.6±0.7	−13.4
869–884R*	102	− 3	.68	16	1.92*	2.16	2.0	−21.3±0.9	− 8.8	−37.2±1.5	−16.1
IC 1805	102	+ 2	.54	8	1.81	1.70	2.0	−13.8±1.5	− 6.2	−54.0±4.2	−29.8
NGC 1444	116	0	.28	4	3.34	0.76	0.5	− 2.8±1.8	− 5.4		
1502	111	+ 8	.30	10	1.45	0.79	.....	+ 1.0±0.5	+ 3.3	−21.2±1.3	−23.5
1960	142	+ 2	.28	24	0.98	0.74	.....	+ 5.9±0.7	− 4.3	− 2.3±4.9	−15.4
1981R	176	−18	.18	16	0.49	0.45	.....	+28.0±0.6	+22.2	+30.5±1.5	−27.8
2129	154	+ 2	.42	11	1.77	1.22	.....	+15.9±1.4	+ 2.8	+14.7±1.9	+ 1.8
2169	163	− 1	.20	17	1.95	0.52	0.6	+17.5±0.4	+ 5.2	+22.9±4.0	+15.6
2244	174	− 1	.34	40	1.34	0.92	1.0	+22.2±0.6	+ 6.3	+33.7±2.5	+18.8
2264R	171	+ 4	.20	8	0.45	0.50	0.6	+16.9±0.0	+ 3.0	+30	+29.3
2353R	192	+ 2	.13	12	0.76	0.30	0.7	+27.1±0.3	+29.6	+25.1±3.7	+23.0
2362R	206	− 4	.13	16	1.25	0.30	1.2	+27.1±1.0	+26.0	+40.4	+70.4
6231R	311	0	.50	7	0.98	1.50	.....	− 7.9±0.6	− 1.3	−16.8±2.3	− 7.2
Anon 24	312	0	.48	8	0.58	1.44	.....	− 7.2±0.7	− 0.7		
NGC 6383R	323	− 1	.28	8	2.13	0.76	.....	− 4.9±0.9	+ 5.7	− 4	+ 6.8
6530	334	− 3	.27	19	1.09	0.73	.....	− 9.4±1.1	+ 3.7	− 1.3±2.1	+14.8
6531	335	− 2	.22	12	0.98	0.51	.....	− 7.6±1.2	+ 9.2	− 4.9±2.0	+14.5
6604	346	0	.50	8	3.68	1.50	2.4	− 1.3±1.2	+ 9.3		
6611	345	− 1	.68	12	2.05	2.43	2.4	0.0±1.0	+ 6.1	+11.6±5.0	+10.9
6613	342	− 2	.51	4	1.78	1.53	1.0	− 5.5±3.4	+ 5.6	−11.4±1.2	+ 1.7
6871	40	+ 1	.53	22	1.34	1.60	.....	−13.2±0.2	+ 3.0	−20.3±2.2	− 1.4
IC 4996	43	0	.41	10	1.84	1.20	.....	−14.6±0.6	+ 2.6		
NGC 6883	41	0	.35	6	1.81	0.98	.....	− 1.7±2.1	+16.4	− 6.6±2.3	+11.4
6910	46	+ 1	.54	9	2.09	1.68	.....	−11.0±0.7	+ 3.8	−26.9±2.5	− 5.7
6913	45	0	.46	15	2.10	1.36	.....	−10.0±0.5	+ 5.4	−16.7±4.3	+ 0.5
7160	72	+ 6	.42	6	1.03	1.23	.....	−10.4±1.4	+ 1.9	−42.5±5.6	−24.2
7380	75	− 1	0.62	7	1.84	1.56	1.4	−19.3±0.0	− 4.4	− 5.2	.....

*"R" calls attention to notes at end of table.

NOTES TO TABLE 2

NGC 869 and 884. The interstellar velocity for the cluster is the simple mean of all individual values derived from two or more spectrograms.
NGC 1981. Mean stellar velocity for the cluster is derived from one Mount Wilson and four Victoria velocities.
NGC 2264. Stellar velocity for this cluster is the mean of the two velocities from Victoria.
NGC 2353. Mean stellar velocity is the mean of two Mount Wilson, the Victoria, and the Neubauer velocities.
NGC 2362. The velocity of this cluster has been assumed to be +40.4 km/sec, the systemic velocity derived for the orbit of HD 57061, 30 τ CMa, a member of this cluster (Struve and Pogo, *Ap. J.*, **68**, 335, 1928).
NGC 6231. The stellar velocity for this cluster is the mean of the Lick, McDonald, and Mount Wilson velocities.
NGC 6383. The velocity of this cluster has been assumed to be −4 km/sec, the systemic velocity derived for the spectroscopic binary HD 159176 (Trumpler, *Pub. A.S.P.*, **42**, 342, 1930).

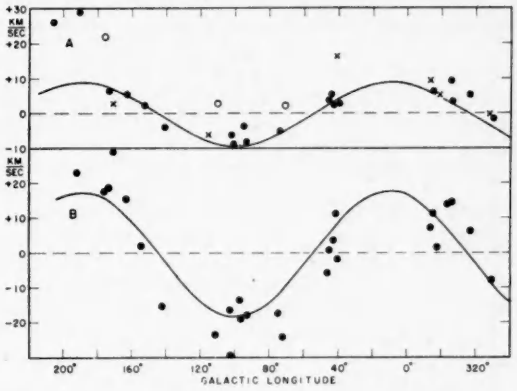

FIG. 1.—*A*, Measured interstellar velocities of clusters after correction for solar motion and to 1 kiloparsec by distances derived from equivalent widths are plotted against galactic longitude. Curve is for differential galactic rotation at ½ kpc. *B*, Measured stellar velocities similarly reduced and plotted. Curve is that for differential galactic rotation at 1 kpc.

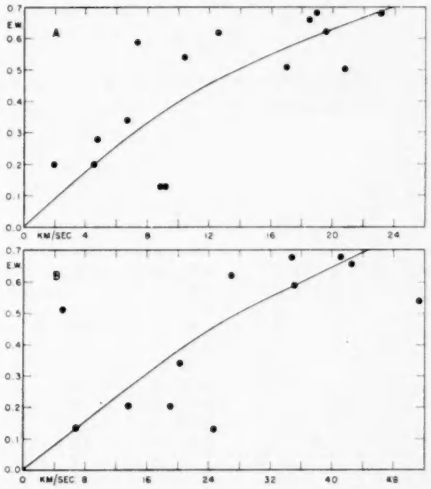

FIG. 2.—*A*, Measured interstellar velocities for clusters with sin 2 $(l - 325°) \geq 0.500$ numerically, freed of solar motion and divided by sin 2 $(l - 325°)$, are plotted against equivalent widths. *B*, Same for measured stellar velocities of clusters. Curves are drawn freehand.

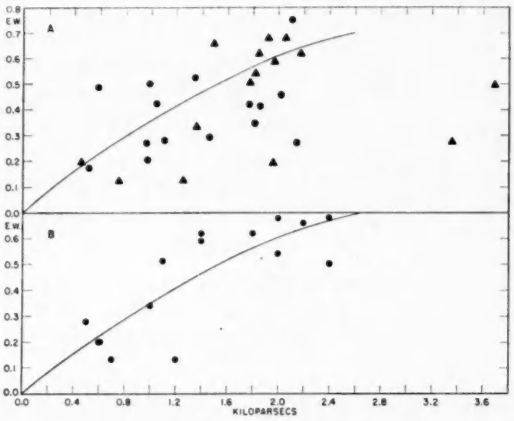

FIG. 3.—*A*, Equivalent widths are plotted against Trumpler's distances. Curve is that of *Mt. W. Contr.*, No. 573; *Ap. J.*, **86**, 141, 1937. *B*, Equivalent widths are plotted against distances derived from the velocities. Triangles identify the stars in 3,*A*, that are also in 3,*B*. Curve is freehand.

TABLE 3

VELOCITIES OF 14 STARS NEAR THE h AND χ PERSEI CLUSTERS

DESIGNATION	SP CL.	MAG.	1900		VELOCITY (KM/SEC)			
			R.A.	Decl.	Interstellar	No. Pl.	Stellar	No. Pl.
HD 12981	B3	9.5	$2^h\ 2^m0$	+55°36′	+15.8 c	2	−31.6 c	2
12993	B3	8.6	2.1	+57 27	−19.4 c	2	−78.0 d	2
13716	B1	8.5	8.6	+57 18	−17 e	1	−50.0 d	6
13831	B0	8.6	9.7	+56 17	−19.8 d	2	−43.5 d	4
13970	B3	8.6	10.8	+56 11	−24 e	1	−23:: e	6
14162	B	9.4	12.4	+56 41	−16 e	2	−37.3 d	2
14302	B2	8.8	13.6	+55 52	−19 e	2	−42.8 d	2
14501	B3	9.5	15.4	+57 42	− 8 e	2	−52.1 e	1
14605	B0	9.7	16.5	+56 8	−21.1 c	2	−17 e	1
14707	B	9.9	17.3	+57 53	−18.4 c	3	−30.0 c	2
15325	B3e	8.5	22.9	+56 48	−19 e	1	−33.1 d	2
15450	B0eβ	8.7	24.2	+56 27	−19.8 c	2	.....	.....
15571	B	8.0	25.2	+56 59	−16.6 c	3	−41.7 c	3
15752	B0	8.8	26.8	+57 58	−27 e	1	−44 e	1

that both E.W.'s and velocities of open clusters provide criteria of their distances that merit their use at least for clusters of low galactic latitudes and those away from null points.

It will be noted that there are eight clusters for which the distance by E.W. is less than half that given by Trumpler, and only one cluster for which the criterion of E.W. would more than double the distance. In practically all instances radical changes in distance determined by E.W.'s have been reductions. The over-all mean derived from Trumpler's distances of the clusters in Table 2 is about 1600 parsecs, and the mean distance from E.W.'s is 1200 parsecs.

The mean difference between the interstellar velocities in Table 2 and those which Miss Phyllis Hayford[6] derived is $+8.9 \pm 9.0$ km/sec, showing large systematic and accidental errors. This probably explains why she found her interstellar velocities unsuited to a determination of differential galactic rotation.

Fourteen stars adjacent to, but not previously identified with, the h and χ Persei clusters are listed in Table 3. Since their interstellar, as well as their stellar, velocities agree with those of the cluster stars, they are probably outlying cluster members.

[6] *Lick Obs. Bull.*, **16**, 53, 1932.

MAGNETIC INTENSIFICATION OF STELLAR ABSORPTION LINES

HORACE W. BABCOCK
Mount Wilson and Palomar Observatories
Received May 5, 1949

ABSTRACT

The total intensity of a saturated absorption line may be increased several fold in a magnetic field of a few kilogauss because the Zeeman pattern may be considerably wider than the thermal Doppler profile. The effect should be particularly marked for lines having wide, anomalous Zeeman patterns of many components; it is enhanced for elements of high atomic weight at reduced temperatures and in the absence of turbulence. An upper limit to the intensification factor is half the number of components in the Zeeman pattern of the line.

A method is developed for computing the magnetic intensification, W_s/W_0, for a saturated line of given pattern in integrated light of a star viewed from the direction of the pole ($i = 0°$) or viewed from the plane of the star's equator ($i = 90°$). For the line *Fe* I λ 4260, having a triplet pattern ($Z = 1.60$), $W_s/W_0 = 1.25$ for a field of 8 kilogauss and a temperature of 10,000°. The intensification factor appears to be essentially independent of i; it may approach 7 for an exceptional line like *Eu* II λ 4205, which has 21 widespread components. If equivalent widths can be measured, it should be possible in principle to estimate stellar magnetic field strengths by detailed comparisons of lines selectively intensified by Zeeman splitting, even if pronounced rotational broadening is present.

In a number of the peculiar stars of type A, magnetic fields ranging up to several kilogauss have been measured with the polarizing analyzer; the conclusion is practically inescapable that magnetic intensification must contribute to the abnormal line intensities in the spectra of some of these stars. For about fifty lines in the spectrum of α^2 CVn, for which intensity estimates at three phases of the spectral variation have been published by Struve and Swings, the degree of observed intensity variation is compared with the magnetic intensification factor predicted from the Zeeman patterns; a satisfactory correspondence is found.

I. INTRODUCTION

In the spectrum of a star having a general magnetic field of several kilogauss intensity, the Zeeman patterns of many of the absorption lines must be considerably wider than the thermal Doppler profiles. This is easily shown by a simple calculation. For absorption lines that are strongly saturated (i.e., on the nearly horizontal part of the curve of growth), pronounced Zeeman broadening may therefore lead to a marked increase in total absorption. The intensification should be selective, affecting particularly those lines having wide anomalous Zeeman patterns of many components. It will also depend on the strength and direction of the magnetic field over the surface of the star; in this respect the problem is more complicated than in sunspots, for in a spot near the center of the sun's disk it may often be assumed that the lines of force are parallel to the line of sight so that one deals only with the longitudinal Zeeman effect. Curves of growth for lines in the spectra of sunspots and the center of the sun have been compared by P. ten Bruggencate and H. von Kluber,[1] who obtained a relation for the broadening action of the Zeeman effect for the spot lines by treating it as a pseudo-Doppler effect. The increase of line intensities by the Zeeman effect in spot spectra has been emphasized by H. D. Babcock and C. E. Moore.[2]

The probable importance of magnetic intensification in certain stellar spectra is suggested by the fact that strong general magnetic fields have recently been found in several of the "peculiar" stars of type A, including the spectrum variables; it is in spectra of stars of this group that puzzling anomalies in line intensity have been recognized for many years. The great diversity in spectra of stars of this type, with the tendency for

[1] *Zs. f. Ap.*, **18**, 284, 1939.

[2] "The Solar Spectrum, λ 6600 to λ 13495," *Pub. Carnegie Inst. Washington*, No. 579, p. 9, 1947.

the enhancement of lines of certain elements or groups of elements (*Eu* II and other rare earths, *Cr*, *Mn*, *Sr* II, etc.), has never been explained. Therefore, it is of particular interest to investigate to what extent the normal spectral characteristics of A-type stars are modified by Zeeman broadening of saturated absorption lines when a magnetic field is present and whether such factors as actual differences in relative abundance from one star to another have to be considered. The concentration or stratification of certain elements in a stellar atmosphere through magnetic, electric, and rotational effects is another possibility. The supposition that the peculiarities are due simply to actual differences in abundance from star to star receives little favor, since many of the peculiar stars are spectrum variables in which some of the lines undergo large intensity variations in periods of a few days.

The problems of the A-type stars have been ably discussed by O. Struve and P. Swings,[3] who have emphasized the failure of ionization theory to account for the abnormalities and who have suggested an explanation based on departures from thermodynamic equilibrium caused by the shape of the energy-curves. Previously, W. W. Morgan summarized the problem in these words: "It seems safe to conclude that there is some physical factor other than temperature and surface gravity concerned in the production of the spectra of the A stars. . . ."[4] The inference now is strong that Morgan's unknown physical factor is the magnetic field. This inference is strengthened by the fact that the observations, as far as they go, show a general correspondence between the degree of peculiarity of the spectrum and the strength of the magnetic field, which in one spectrum variable star, HD 125248, attains a maximum of about +7800 gauss.[5] Almost without exception, evidence of a magnetic field has been found in the brighter peculiar A stars that have sufficiently sharp spectral lines to permit a test with the double polarizing analyzer and that are within the range of declination accessible to the coudé spectrograph of the 100-inch telescope. The well-known spectrum variable α^2 Canum Venaticorum is now included in the group in which a magnetic field has been found. In contrast, spectra of normal A-type stars, such as Sirius, taken with the same apparatus, show no evidence of the Zeeman effect.

In the present article the electromagnetic effects on the motions of ions and on the equilibrium of the stellar atmosphere will largely be neglected; only the results of Zeeman broadening of spectral lines will be considered. As in previous papers,[6] the magnetic field intensity quoted is that at the pole of the star computed on the assumptions that the field is dipolar, that the star is spherical, that the number of effective atoms of a given kind per unit area is the same at all points on the surface, and that the coefficient of limb darkening is 0.45.

II. THE UPPER LIMIT OF MAGNETIC INTENSIFICATION

A line of moderate intensity in a star having no magnetic field is represented by a point at C on the nearly horizontal part of the curve of growth (Fig. 1). An absorption line on this transition portion of the curve is strongly saturated, and its actual width is determined mainly by thermal Doppler broadening, with some small contribution from damping. Turbulence may also be a general contributing factor, but it is left out of consideration for the present. The line has an equivalent width, W_0, and the number of atoms effective in forming it is represented here by N_0. Now let the star acquire a mag-

[3] *Observatory*, **64**, 291, 1942; Struve, *Proc. Amer. Phil. Soc.*, **85**, 349, 1942.

[4] *Pub. Yerkes Obs.*, **7**, Part III, 118, 1935. *Note added in proof:* Morgan's original suggestion that the additional factor is effective abundance of the elements is not contradicted but is supplemented by the new evidence for the strong magnetic field, which may well be more fundamental.

[5] H. W. Babcock, *Pub. A.S.P.*, **59**, 260, 1947; *Phys. Rev.*, **74**, 498, 1948.

[6] H. W. Babcock, *Mt. W. Contr.*, No. 727; *Ap. J.*, **105**, 105, 1947; *Mt. W. Contr.*, No. 748; *Ap. J.*, **108**, 191, 1948.

netic field of several kilogauss. The line is split into a pattern of Zeeman components, specified, through the Landé g formula, by the spectroscopic terms of the two levels involved. If the splitting is comparable to, or greater than, the Doppler broadening, the n components of the pattern tend to separate (we are dealing now with light from an elementary area on the surface of the star as observed with an ideal spectroscope). In each of the n components of the pattern there will be roughly $1/n$ times as many atoms effective as acted originally, the actual distribution being specified by the "intensity" rules for the direct Zeeman effect in emission. Since initially the line was strongly saturated, each component would now have nearly the same total absorption, W_0, as the original unaffected line, were it not for the fact that the atoms are polarized by the magnetic field, so that each resolved component can absorb, at most, half the radiation from the continuous spectrum, the remaining radiation being transmitted. The total absorption or equivalent width, W_0, of such a line may be multiplied by a factor approaching as an

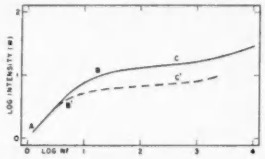

FIG. 1.—Schematic curve of growth

upper limit half the total number of components in its Zeeman pattern, if the applied field is of sufficient strength. For the upper limit of magnetic intensification we may write

$$\left(\frac{W_z}{W_0}\right)_{\max} \rightarrow \frac{n}{2}. \tag{1}$$

This limit can never be fully attained, however, because, for regions of the stellar surface where the line of sight is parallel to the magnetic field, the π components of the Zeeman pattern are absent.

The residual central intensity of a saturated absorption line will necessarily increase as the Zeeman components begin to be resolved in an increasing magnetic field; if resolution is complete, the minimum intensity in the absorption pattern must be greater than 50 per cent, owing to the polarization effect mentioned above.

The half-width (total breadth at half-intensity), $2\Delta'\lambda$, of an absorption line affected only by thermal motion of the atoms is

$$2\Delta'\lambda = 7.16 \times 10^{-7}\, \lambda \sqrt{\frac{T}{\mu}}, \tag{2}$$

where T is the temperature and μ is the atomic weight. The formula and notation are those of A. Unsöld,[7] where $2\Delta'\lambda$ is related to the "Doppler breadth," $\Delta\lambda_D$, by the formula $2\Delta'\lambda = 1.665\ \Delta\lambda_D$. Resolution of Zeeman patterns will therefore be approached more readily for low temperature and high atomic weight. As an example, consider *Eu* II λ 4205, which in HD 125248 at the phase of maximum positive field intensity is the strongest line in the photographic region of the spectrum, with the exception of the *H* lines. For this line of *Eu* II ($\mu = 152$) at a temperature of 10,000° the half-width is 0.023 A, while for a magnetic field of 8 kilogauss and a Zeeman pattern 2.75 times as wide as a normal triplet the pattern width becomes 0.36 A. The computed pattern of this line has twenty-one equally spaced components, an unusually large number. A com-

[7] *Physik der Sternatmosphären* (Berlin: Julius Springer, 1938), p. 158.

parison of the half-width with the pattern width shows that the line is widened by a factor of about 15 in the field of 8 kilogauss; this, however, is insufficient for complete resolution, so that the intensification will fall considerably short of the upper limit, $21/2 = 10.5$. The field strength required to separate the components by the amount $2\Delta'\lambda$ is about 11,000 gauss, and even with this there would be considerable overlapping of the wings.

There is a large range in the complexity of the patterns and in the separation of the components for astrophysically interesting lines. Some of the "anomalous" patterns, particularly those arising from levels of high multiplicity with large J values, like *Eu* II λ 4205, have twenty or more components, with an over-all spread up to about three times that of a normal Zeeman triplet. Most lines have simpler patterns of a few components, some are triplets, and a very few, such as arise from $^5D_0 - {}^5F_1$ transitions, are unaffected by the magnetic field. The sensitivity of an absorption line to magnetic intensification should then depend in a predictable way upon its Zeeman pattern.

In Figures 2 and 3 are plotted Zeeman patterns for a few typical lines of *Eu* II, *Fe* I, and *Cr* I. The relative intensities of the components have been computed by the usual rules. The spread of each pattern is indicated in terms of the normal triplet and also in angstroms for a field of 8 kilogauss. This field strength is used because it corresponds approximately to the maximum polar field of HD 125248. The half-width, $2\Delta'\lambda$, is also indicated for each line, the assumed temperature being 10,000° K. For *Eu* II λ 4129 and λ 4205 are plotted the patterns observed in the laboratory with a field of 87,850 gauss by Russell, Albertson, and Davis.[8] Because of the much stronger field, the scale of these two laboratory patterns is not directly comparable with the others; they are shown because they do not agree in detail with the computed patterns in either spacing or intensity. The differences are presumably due to breakdown of L-S coupling.

An effect related to magnetic intensification may occur in lines that in the absence of a field are very weak and that fall on the proportional part of the curve of growth between A and B (Fig. 1). If split into Zeeman components by a magnetic field, a weak line becomes broader and shallower, so that its visibility may decrease, although its total absorption cannot change.

As a third case we may consider a line initially strong enough to possess wings due to radiation damping, so that it falls on the right-hand portion of the curve of growth where the equivalent width is proportional to the square root of the number of effective atoms. In general, the width of the Zeeman pattern, even for a field of 8 kilogauss, will be narrower than the over-all width of such a strong line. The intensification of the core of the line due to magnetic splitting will be less marked than for a line initially on the flat part of the curve but may still be of importance. Again, the magnitude of the effect should be predictable from the initial position of the line on the curve of growth, the nature of the Zeeman pattern, and the field intensity. Very weak lines and very strong "winged" lines, however, will not be further considered in this paper.

Small-scale turbulence (along a given emergent ray) will, of course, broaden the line profile with an increase in total absorption and, if sufficiently strong, may diminish, or perhaps entirely mask, the effect of magnetic broadening. The two effects should be distinguishable, however, as turbulence will affect all lines of a given element similarly and may result in profiles with quite low central intensities. In many of the peculiar A stars, particularly those like γ Equulei, β Coronae Borealis, and HD 188041, turbulence is certainly not obvious and is probably quite small. Spectrograms at 2.9 A/mm of γ Equ have metallic lines of unusual sharpness, apparently limited by the resolution of the instrument. The equivalent slit-width is 0.1 A. This star, so far as observations have shown, has an essentially constant magnetic field with $H_p = 1900$ gauss.[9] There are no

[8] *Phys. Rev.*, **60**, 641, 1941.

[9] H. W. Babcock, *Mt. W. Contr.*, No. 748; *Ap. J.*, **108**, 191, 1948.

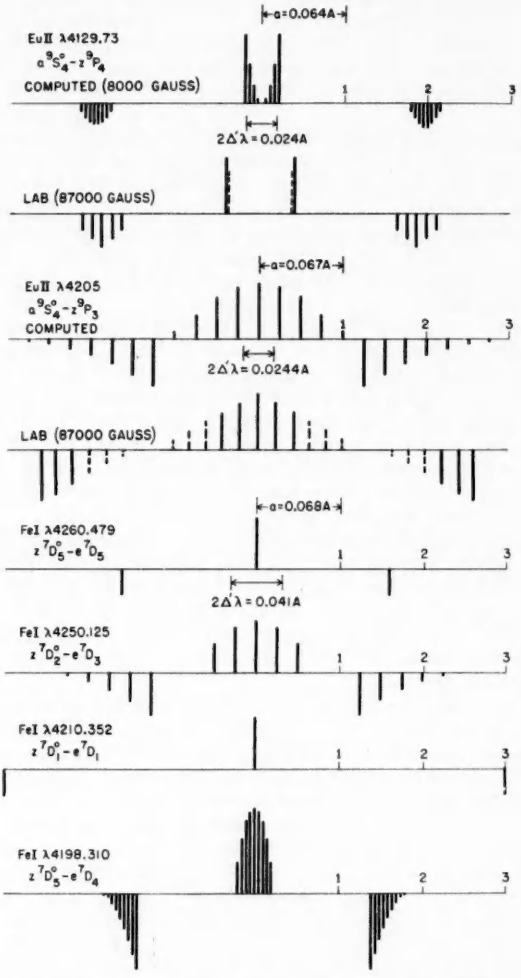

FIG. 2.—Calculated Zeeman patterns for typical lines of *Eu* II and *Fe* I, showing the variety in number and spacing of components. Heights represent relative intensities. The unit of pattern width is the normal triplet; this unit is also indicated in terms of angstroms for a magnetic field of 8 kilogauss. The half-width is also indicated for each pattern. Note the much smaller half-width of *Eu* as compared to *Fe*. For the two *Eu* II lines, patterns observed in the laboratory by Russell, Albertson, and Davis are given (to a different scale) for comparison with the computed patterns.

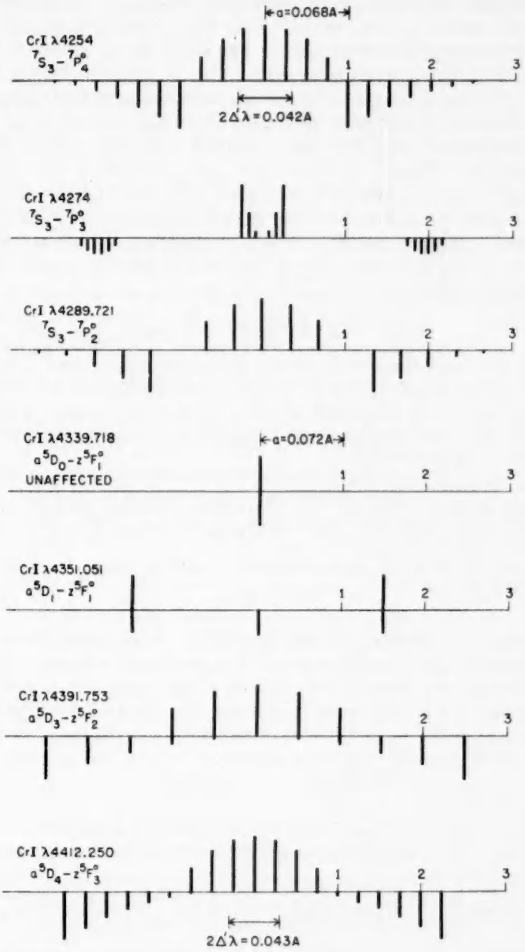

FIG. 3.—Computed Zeeman patterns for typical lines of *Cr* I. Two multiplets are represented. Note the variety of patterns within a multiplet; this may lead to marked selective effects on line intensities.

certain changes either in line intensity or in radial velocity. Any reduction of turbulence will increase the degree of saturation of absorption lines and will lower the level part of the curve of growth (as from B, C, to B', C', in Fig. 1), thus increasing the number of lines susceptible to magnetic intensification. The mechanical effects of a magnetic field on a moving mass of gas have been discussed by T. G. Cowling[10] with particular reference to the solar surface close to sunspots, where the field is about 1000 gauss. He concludes that any mass motion of the gas must be nearly along the lines of force. It is not clear to what extent this conclusion may be applicable to the problem of turbulence in the atmosphere of a star like γ Equ.

It is evident that magnetic intensification should be most pronounced in stars having a strong magnetic field but not excessively high temperature and for lines arising from terms having a multiplicity of magnetic levels in elements of high atomic weight. These specifications fit so closely in most respects the peculiar stars of type A that a more exact study of the effect is desirable.

III. THE INTEGRATED EFFECT

In the absence of a field the line in question is assumed to have the same equivalent width, W_0, at all points on the disk of the star. Limb darkening is left out of consideration. The curve of growth is idealized, so that W is proportional to N, the number of atoms, up to a point at which saturation takes place abruptly; further increase in N is supposed to make no change in W.

As an example, consider the line λ 4260.479 of *Fe* I ($z^7D^0_5 - e^7D_5$), for which $2\Delta'\lambda = 0.041$ A at a temperature of 10,000°. The theoretical Zeeman pattern may be computed from the Landé g-values, which for the two terms in question are

$$g = 1 + \frac{J(J+1) + S(S+1) - L(L+1)}{2J(J+1)} = 1.60. \tag{3}$$

In this simple case, the predicted pattern is $\pm$ (0.00), 1.60, where the π component is in parentheses and the σ components follow. For a normal triplet, $\pm$ (0.00), 1.00, the shift of the σ components from the unshifted π component is $\Delta\nu = 4.67 \times 10^{-5} H$ cm^{-1}; hence, for *Fe* I λ 4260 the shift is 0.109 A in a field of 8000 gauss; but this applies only at the pole of the star. The field intensity at the surface of a uniformly magnetized sphere is

$$H = \tfrac{1}{2} H_p (1 + 3 \sin^2 \phi)^{1/2}, \tag{4}$$

where H_p is 8000 gauss and ϕ is latitude on the surface of the star.

The components of H parallel to the three co-ordinate axes are conveniently represented by

$$H_x = \tfrac{3}{2} x z H_p, \qquad H_y = \tfrac{3}{2} y z H_p, \qquad H_z = \{ z^2 - \tfrac{1}{2}(x^2 + y^2) \} H_p, \tag{5}$$

where the z-axis is the polar axis of the star and x and y are rectangular co-ordinates in the equatorial plane.

It is also necessary to know the relative numbers of atoms effective in the components of the patterns for any surface element on the star as a function of the angle between the field and the line of sight. Here we shall assume that the field is strong enough to produce essentially complete resolution of the components. The quantities N_v, N_m, and N_r correspond to the intensities of the triplet components as observed in the direct Zeeman effect (in emission) without an analyzer. They may be found with the aid of the Lorentz model of the atom used in the classical explanation of the Zeeman effect. Starting with an assemblage of electrons moving in orbits oriented at random in space, it may be

[10] *Proc. R. Soc. London, A*, **183**, 453, 1945.

shown, by resolving the vibrations into components along the three axes, that the results will be represented by the following fictional model when a magnetic field is applied. One-third of the electrons move with unchanged frequency as linear oscillators along the z-axis, parallel to the field; one-third move with counterclockwise circular motion normal to z with frequency $\nu_0 + \Delta\nu$; one-third move with clockwise circular motion normal to z with frequency $\nu_0 - \Delta\nu$. If the amplitude of the linear oscillators along the z-axis is a and if the radii of the circular orbits is b, it may be shown that $a = \sqrt{2}\, b$. This follows from the fact that the intensity of light emitted is independent of direction. The effective amplitude of each type of vibration will be the component of vibration perpendicular to the line of sight. Hence, if γ is the angle between the line of sight and the z-axis, the intensities of the components are

$$N_r = N_v = \tfrac{1}{4}\,(1 + \cos^2\gamma)\,; \qquad N_m = \tfrac{1}{2}\sin^2\gamma\,. \tag{6}$$

These equations apply when no polarizing analyzer is used. For completeness, the corresponding expressions, if an analyzer for circularly polarized light is used, are given also, from the work of F. H. Seares:[11]

$$N_v = \tfrac{1}{4}\,(1 \pm \cos\gamma)^2 \qquad N_m = \tfrac{1}{2}\sin^2\gamma\,; \qquad N_r = \tfrac{1}{4}\,(1 \mp \cos\gamma)^2\,. \tag{7}$$

Since equations (6) and (7) specify the relative intensities of the components in emission, we may expect that they also specify the relative intensities of weak, unsaturated absorption lines in the inverse Zeeman effect; as the total number of atoms is increased, first the stronger components and then the weaker ones reach a condition of saturation. At saturation each component will have a central intensity of about 50 per cent and a total absorption of $\frac{1}{2}W_0$. It is important to note that the total absorption of the component—not the number of atoms effective in it—is reduced to one-half by the polarization.

The foregoing elementary theory applies when the components are well separated by the field. Complications arise when this restriction is discarded. The effects that occur when the components partially overlap are closely related to the Faraday effect and to magnetic double refraction; they were treated by W. Voigt[12] and by H. A. Lorentz,[13] and the results were discussed by P. Zeeman in 1913.[14] For the present one can do no better than apply the elementary theory as a first approximation, although it must be recognized that this is inaccurate for most anomalous patterns encountered in the investigation of stellar magnetic fields, as a reference to Figures 2 and 3 shows that the Doppler widths of components are often nearly equal to their separations. For some triplets, however, practically complete resolution is attained in fields of several kilogauss; for these lines the elementary theory should suffice. To take account of the variation in strength and direction of H over the surface of the visible hemisphere, and of the changes in the equivalent width, W, for the components of the pattern as interpreted through the curve of growth, recourse is had to a graphical method. Two conditions will be considered in turn: Case I, in which the axis of the star is directed toward the observer ($i = 0°$), and Case II, in which the axis of the star is at right angles to the line of sight ($i = 90°$).

Case I ($i = 0°$).—In Figure 4, *a*, is a schematic profile for the line *Fe* I λ 4260, assumed to be saturated, in the absence of a magnetic field. N_0 atoms are effective. The half-width is 0.04 A, and the total absorption is W_0. For the present purpose we may suppose that W_0 is also equal to 0.04 A, since this simplifies the graph; and it will be

[11] *Mt W. Contr.*, No. 72; *Ap. J.*, **38**, 99, 1913.

[12] *Ann. d. Phys.*, **1**, 389, 1900.

[13] *Proc. Amsterdam Acad.*, **12**, 321, 1909.

[14] *Researches in Magneto-optics* (London: MacMillan & Co., Ltd., 1913), chap. ix.

seen in what follows that the percentage increase in W is independent of its initial value. In actual fact, W_0 for a line on the flat portion of the curve of growth is usually about two to three times the total width at half-intensity.

Figure 4, *b*, shows the separation of the components of the triplet, λ 4260, $Z = 1.60$, as a function of latitude on the star when a dipole field exists with $H_p = 8000$ gauss. The splitting is half as great at the equator as at the pole. The states of polarization are also indicated; in a zone corresponding to $\phi = 35°.6$ the components are plane-polarized because the Zeeman effect is transverse. The field strength here is $0.71\ H_p$. The latitude scale of ordinates is compressed at top and bottom, so that the relative contributions of

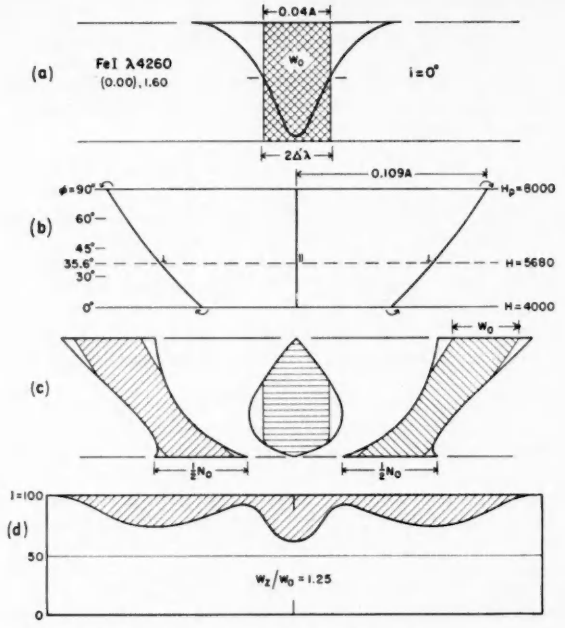

FIG. 4.—Graphical computation of increase in total absorption due to a stellar magnetic field of 8 kilogauss when the line of sight is parallel to the stellar axis. (*a*) Line profile and total absorption with no magnetic field. (*b*) Separation of components of a Zeeman triplet as a function of stellar latitude when $H_p = 8$ kilogauss. (*c*) In any elementary zone of latitude, the intercepts of the outer patterns represent the number of effective absorbing atoms, N. Saturation limits the absorption of any elementary components to the value W_0. The total absorption in integrated light is found by summing the cross-hatched areas and dividing by 2 to allow for polarization of the components. $W_z/W_0 = 1.25$ for the small degree of saturation assumed here. (*d*) Profile of the affected line.

the elementary latitude zones are properly represented in integrated light. The contribution of each zone is proportional to $\sin\phi\cos\phi$. Therefore, the ordinate for a given ϕ is proportional to $\int \sin\phi\cos\phi d\phi = \frac{1}{2}\sin^2\phi$.

Figure 4, *c*, is based upon *b*, but the effective number of atoms, N, as a function of latitude is now indicated by the over-all width of each component. The relative widths are obtained from equations (5) and (6); the scale of these pattern widths is proportional to N_0 and is arbitrarily adjusted with respect to the width, W_0, to correspond to a condition slightly beyond the saturation point. The relative intensities of the components

would be represented by the over-all widths, were it not for this saturation, which sets a limit when N attains a value corresponding to W_0 for any component at any latitude. A width equal to W_0 is therefore indicated on the pattern of each component. It is only those areas that are common to the N outline and the W_0 width that are effective in absorption. These areas are cross-hatched in the figure.[15] The total absorption of the magnetically affected line, W_z, is now found by integrating the cross-hatched areas of all components and dividing by 2, because of the polarization already mentioned, which dilutes the absorption of each component by 50 per cent. In the present example a comparison of areas with a planimeter gave the ratio $W_z/W_0 = 1.25$.

The profile of the magnetically broadened line, as inferred from the distribution of absorption in the pattern, is shown in Figure 4, *d*. Chief characteristics are the shallowness and the tendency toward tripling.

Up to this point the analysis has been made on the assumption that the axis of the star is directed toward the observer. If there is a small angle of obliquity, i, between the line of sight and the polar axis of the star, the effects of rotational broadening on the line profiles may be noticed. This broadening will be most pronounced for low latitudes on the star; while it will affect the profiles, it will not alter the equivalent widths, at least as long as i is small, and we can neglect the change in the angle γ between the line of sight and the field direction for a surface element on the star.

Case II ($i = 90°$).—Rotational broadening of stellar absorption lines when i is large has been treated by a number of authors. It is well known that such broadening results in a characteristic dish-shaped profile. The connection between magnetization and rotation in stars is not yet clear, but it is plausible that many of the rapidly rotating stars have strong fields. Some of the A-type stars are known to have equatorial velocities of axial rotation as great as 250 km/sec; this is sufficient, if a star is viewed at right angles to its axis, to broaden the line profiles in the photographic region to widths of about 6 A —many times the width due to Zeeman splitting. Such extreme broadening precludes the measurement of equivalent widths for all except a few of the strongest lines because of the shallow profiles and blending, even though the total absorption is not altered by the Doppler broadening due to rotation. It is nevertheless instructive to examine the effect of a magnetic field on the equivalent width of a line where i, the inclination of the axis of the star, is 90°.

The graphical development of the equivalent width for the triplet *Fe* λ 4260 is shown in Figure 5. Here, as in the preceding example, the separation of the three components is considered as a function of stellar latitude, in order to allow for the variation of H with ϕ. It is also convenient to refer to Figure 6, where one quadrant of the stellar disk is represented. On the meridian, at $\phi = 35°.6$, the line of sight is parallel to the field. Around the limb and along the equator it is perpendicular to the field, while for all other parts γ lies between 0° and 90°. The contributions of the elementary zones of latitude are proportional to their projected areas, as limb darkening is again neglected. The ordinate for a given latitude ϕ is therefore proportional to $\int \cos^2\phi \, d\phi = \frac{1}{2}\phi + \frac{1}{4} \sin 2\phi$ in Figure 5. At the pole and at the equator, where $\gamma = 90°$, the Zeeman effect is transverse, and the relative N's for the components have the ratios $\frac{1}{4}$, $\frac{1}{2}$, $\frac{1}{4}$; the widths of the components are so plotted in Figure 5. For intermediate values of γ the relative N's for the three components are obtained from equations (6); in this way the pattern of Figure 5 is built up. For each elementary zone of latitude, γ is assumed constant, and its value is taken to be that for the middle of the projected zone in Figure 6; i.e., it is the γ for a stellar longitude 30° from the central meridian on the star. In order to compute γ for a zone, the horizontal and vertical components of the angle, $\gamma_h = 30°$ and γ_v are

[15] As a separate example, N_0 might be made much smaller, avoiding any saturation. W_0, corresponding to the onset of saturation, would remain as before, but the widths of the patterns determined by N would be much narrower and would fall entirely within the limits of W_0. Thus the total absorption would be proportional to N_0, and no magnetic intensification would occur.

first found. Here γ_v is the angle on a meridional plane between the field vector, H, and the horizontal; it can be found with the aid of equation (5). Finally, the desired angle can be obtained through the relation

$$\cos \bar{\gamma} = \cos \gamma_v \cos \gamma_h \,. \tag{8}$$

Once this so-called "mean γ" is known for a given zone of latitude, the N's can be computed for the components of the pattern in Figure 5. As in Case I, the outer borders of each component represent the respective N's, while the equivalent width at saturation limits the effective absorption of the wider portions of each part of the pattern to the value W_0. As before, the dilution of one-half arising from polarization must be taken into account. The total absorption of the affected line, W_z, is therefore half the sum of the areas of the central parts of the components in the diagram of Figure 3, and this is to be compared to the W_0 of the original unaffected line, plotted to the same scale of wave length and total intensity. With the planimeter it is found that, for $i = 90°$, $W_z/W_0 = 1.26$.

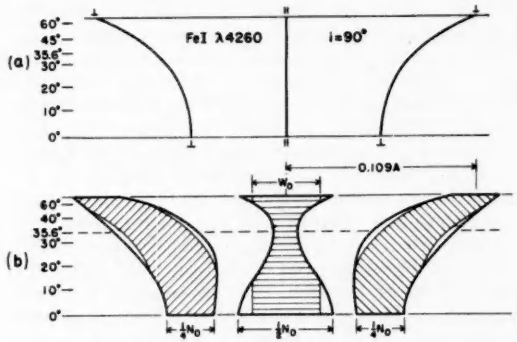

FIG. 5.—Total absorption, W_z, when the line of sight is at right angles to the stellar axis. $H_p = 8$ kilogauss. (*a*) Separation of components as a function of latitude. (*b*) Outer boundaries represent number of atoms; cross-hatched areas are saturation-limited absorptions. $W_z/W_0 = 1.26$.

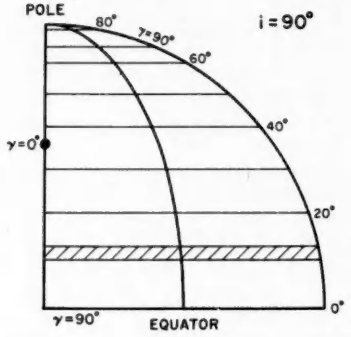

FIG. 6.—Quadrant of stellar disk. The angle γ is computed for the middle of each zone of latitude

A similar graphical integration has been carried out for a normal Zeeman triplet (0.00), 1.00. Since it was assumed that $H_p = 8000$ gauss and that the wave length is about 4250 A, the displacement of the components at the pole is 0.068 A. The Doppler half-width, $2\Delta'\lambda$, was taken to be 0.036 A; this corresponds to *Fe* at 8000° K. Here the number of atoms, N_0, is the same as before, but the degree of saturation is greater because of the smaller Doppler width. The magnetic intensification obtained for $i = 0°$ and $i = 90°$, respectively, was 1.30 and 1.32.

An increase in the degree of saturation of the absorption line, due to lowering of the temperature, a reduction of turbulence, increase in atomic weight, or increase in the effective number of atoms in the appropriate state (N_0), will increase the magnetic intensification toward the upper limit, $n/2$ or 1.5 for triplets. A relatively small increase in N_0 will quickly raise the ratio above 1.4 in the present examples. Here the magnetic field is strong enough for nearly complete resolution of the components, since Figures 4 and 5 show that any overlapping of the wings of profiles represented by the equivalent widths of the patterns generally occurs for opposite states of polarization. Therefore, the absorptions are almost purely additive. (This will not be the case for a number of overlapping components characterized by the same type of polarization in an anomalous pattern.) An appreciable reduction in H_p would, however, result in a corresponding decrease in W_z/W_0.

It is highly significant that W_z/W_0 is identical, within the computational limit of error, for $i = 0°$ and $i = 90°$; no example with intermediate i has been carried through, but it seems safe to conclude that magnetic intensification is essentially independent of the obliquity of the axis of the star to the line of sight. This conclusion is valid, at best, only on the basis of the assumptions employed here. It may require revision if limb darkening, oblateness of figure, and distortion of the field are taken into account. The change in total intensity of a supersaturated absorption line in proceeding from a condition of no field to a field of several kilogauss is then a measure of the field intensity, H_p, with little dependence upon i. While W_z/W_0 may be appreciable in a strong stellar field for a line like *Fe* I λ 4260, having a rather ordinary triplet pattern, it will be greater for many saturated lines with more numerous Zeeman components. This leads to the suggestion that the intensity of stellar magnetic fields can be measured by detailed study of relative effects on line intensities in instances where these can be reliably measured, even though the rotational broadening may be large because of the obliquity of the stellar axis.[16] (The measurement of line displacements with the polarizing analyzer is, of necessity, limited to spectra in which the rotational broadening is quite small or negligible.) The method would probably be most applicable to lines within a given multiplet, where the relative Nf values in the absence of a magnetic field are available, yet for which a variety of Zeeman patterns resulting in differing degrees of magnetic intensification may occur. In the same star in which H_p may be inferred from measurements of W_z, the projected component of equatorial velocity, $V_e \sin i$, may be found from the width of rotationally broadened profiles. This is a method, possible at least in principle, for observing in many stars magnetic fields inaccessible to the polarizing analyzer and of determining a component of the equatorial velocity of rotation in the same star—a type of observation of interest in the study of a possible relationship between magnetization and rate of rotation.

IV. DISCUSSION

Precise spectrophotometric data are not yet at hand to provide a definitive comparison of theory and observation, but a preliminary comparison can be made with published eye-estimates of changes in line intensity in the spectrum of one peculiar A-type star, α^2 CVn. Before proceeding with this, it can be said that examination of spectra of several stars having strong magnetic fields suggests that magnetic intensification is actually an

[16] This suggestion has been independently made in a private communication by Dr. A. J. Deutsch.

important contributor to some abnormally strong lines, particularly those of *Eu* II and of *Cr* I and *Cr* II. These lines tend to be rectangular in profile, with moderate central intensities. If the strength of the magnetic field in the reversing layer varies periodically, either as a function of time or as a function of position on the surface of a rotating star, the intensities of the sensitive lines should vary correspondingly, regardless of the stage of ionization. It is here that the ionization theory has proved inadequate, for in some stars, *Cr* I and *Cr* II increase and decrease together in intensity. The ionization theory further fails to explain why, in typical peculiar stars, lines of *Eu* II may vary enormously, while lines of *Sr* II and *Ca* II vary comparatively little. (The lines in question are ultimate lines, and the ionization potentials of the three elements are nearly the same—11.0, 11.8, and 11.2 volts, respectively.) The true reason apparently lies in the magnetic field and in differences in the Zeeman patterns, which for three outstanding lines are:

Eu II λ 4205 $^9S_4-{}^9P_3$ (**0.00** 0.25 0.50 0.75) **1.25** 1.50 1.75 2.00 2.25 2.50 2.75
Sr II λ 4215 $^2S_{1/2}-{}^2P_{1/2}$ (0.67) 1.33
Ca II λ 3933 $^2S_{1/2}-{}^2P_{3/2}$ (0.33) **1.00** 1.67

The differences in atomic weight—152, 88, and 40, respectively—also contribute to the comparatively greater changes in *Eu* II.

While Zeeman broadening seems to offer an explanation of many of the changes in line intensity in the spectrum variables of type A, the reason for the out-of-phase intensity variations of different groups of elements in the spectra of some of these stars remains obscure. In HD 125248, lines of *Eu* II attain maximum intensity when the field reaches its maximum positive value (about +7800 gauss), while lines of *Cr* I and *Cr* II vary out of phase with *Eu* II, reaching maximum intensity when the observed field has reversed and attained a maximum strength of opposite polarity (about −6500 gauss). A further study of line profiles, polarization, and differential radial velocities of the elements in the spectrum of this star is in progress, with the aim of finding an explanation of these out-of-phase variations, which are linked with the regular reversal of the observed magnetic field in a 9-day period. A model of a spectrum variable star, consistent with all the observations, may eventually emerge.

Another well-known spectrum variable star, rather similar to HD 125248, is α^2 CVn. Magnetic observations of it are few as yet, but they show that it has a varying magnetic field that must reach a maximum of several kilogauss. The field is strong when the lines of *Eu* II are most intense. For many years it has been known that the two groups of lines characterized by *Eu* II (with other rare earths) and by *Cr* II vary out of phase in a period of 5.5 days. Recently, P. Swings has shown that the intensity variations of lines of *Eu* in the first and second stages of ionization occur in phase.[17] A detailed study of the spectrum of α^2 CVn has been published by O. Struve and P. Swings,[18] who, from measures of high-dispersion plates, have given a large number of line identifications, together with data on velocities for various elements. They have also given, as a secondary result, visual estimates of line intensity for a limited number of lines at three phases. In the absence of more precise data on line-intensity variations, it is possible to make an interesting preliminary comparison between the intensity estimates of Struve and Swings and predictions based on the Zeeman patterns of the lines.

Struve and Swings, following Belopolsky, divide the elements into three groups, those that vary with *Eu* II (group A), those like *Cr* II (group B) that vary out of phase with group A, and those like *Si* II and *Mg* II (group C) that do not change appreciably in intensity. In Table 10 of their paper they give intensity estimates on an arbitrary scale for lines at phases 3.530, 4.520, and 5.430 days, the last phase corresponding very nearly to the maximum intensity of lines of *Eu* II. In my Table 1 are listed the lines from

[17] *Mt. W. Contr.*, No. 695; *Ap. J.*, **100**, 132, 1944.

[18] *Ap. J.*, **98**, 361, 1943.

TABLE 1

LINE-INTENSITY VARIATIONS COMPARED WITH MAGNETIC INTENSIFICATION FACTOR

ELEMENT	λ	INTENSITY	ZEEMAN PATTERN	W_s/W_o
			Lines Showing Little or No Change with Phase	
Mg II	4481.129 4481.327	Const.	(0.17 0.51 **0.86**) 0.34 0.69 **1.03** 1.37 1.71 *or* (**0.03** 0.09 0.14) **1.00** 1.06 1.11 1.17 1.23 1.28	2
Si II	4128.0	6-6-6	(**0.03** 0.09) 0.77 0.83 0.89 **0.94**	1½
Ti II	4171.9	4-4-5	(**0.03** 0.09) 0.77 0.83 0.89 0.94	1½
	4314.9	2-3-3	(1.33) 1.33	2
	4395.8	2-3-3	(**0.03** 0.09 0.14) **1.00** 1.06 1.11 1.17 1.23 1.28	1¾
	4468.5	2-3-3	(**0.02** 0.05 0.08 0.11) **1.00** 1.03 1.06 1.10 1.13 1.16 1.20	1¾
	4501.3	2-3-3	(**0.02** 0.05 0.08) 0.81 0.84 0.87 0.90 0.94 **0.97**	1½
Cr II	4269.3	3-3-2	(0.40 **1.20**) 0.00 **0.80** 1.50	3
Mn II	4259.3	2-3-3	(0.15 0.30 0.45 **0.60**) 0.90 1.05 1.20 **1.35** **1.50** 1.65 1.80 1.95	2½
Fe I	4271.8	2-3-3	(**0.00** 0.05 0.10 0.15 0.20) **1.00** 1.05 1.10 1.15 1.20 1.25 1.30 1.35 1.40	2¼
	4307.9	2-3-3	(**0.00** 0.03 0.07 0.10) **0.95** 0.98 1.02 1.05 1.08 1.12 1.15	2
Fe II	4057.5	3-3-3	(0.00) 0.89	1½
	4061.8	3-4-4	(0.11 0.34 0.51) 0.86 1.09 1.31 1.54 1.77 **2.00**	3½
	4122.6	4-4-3	(0.29 0.86 **1.43**) 0.17 0.74 **1.31** 1.89 2.46	4
			Lines Showing Moderate Change with Phase	
Ti II	4163.6	1-4-4	(**0.03** 0.09 0.14) **1.00** 1.06 1.11 1.17 1.23 1.28	1¾
	4312.8	2-3-4	(0.11 0.34 0.57) 1.03 1.26 **1.48** 1.72 1.94	2½
	4386.8	2-4-5	(**0.02** 0.05 0.08) 0.81 0.84 0.87 0.90 0.94 **0.97**	1½
	4395.0	2-4-5	(**0.03** 0.09 0.14) **1.00** 1.06 1.11 1.17 1.23 1.28	1¾
	4488.3	1-3-3	(**0.03** 0.09 0.14) **1.00** 1.06 1.11 1.17 1.23 1.28	1¾
Cr II	4070.9	2-3-1	(**0.02** 0.05 0.08 0.11) **1.00** 1.03 1.06 1.10 1.13 1.16 1.19 1.22	1¾
	4076.9	5-6-3	(0.33 **1.00**) 0.87 **1.53** 2.20	4
	4195.4	3-3-1	(0.20 0.60 **1.00**) 0.60 1.00 **1.40** 1.80 2.20	4
	4242.4	5-5-3	(**0.05** 0.14 0.24 0.33) **1.00** 1.10 1.19 1.29 1.38 1.48 1.57 1.67	2½
Fe I	4260.5	1-3-2	(0.00) 1.50	1½
	4404.8	4-5-6	(**0.00** 0.07 0.13 0.20) 0.95 1.02 1.08 1.15 1.22 1.28 **1.35**	2¼
Fe II	4233.2	8-6-5	(**0.09** 0.26 0.43) **1.00** 1.17 1.34 1.56 1.68 1.86	2½
	4385.4	5-4-3	(1.33) 1.33	2
	4489.2	5-6-4	(**0.10** 0.31 0.52) 0.72 0.92 1.13 1.34 1.55 **1.76**	3
Sr II	4077.7	3-6-5	(0.33) **1.00** 1.67	2¾
Ce II	4117.0	1-3-3	(**0.01** 0.03 0.05 0.07 0.09) **1.00** 1.02 1.04 . . . 1.18	2
	4186.6	0-2-1	(**0.02** 0.05 0.08 0.11 0.14 0.17 0.20) **1.00** 1.03 1.06 . . . 1.40	2½
	4255.8	1-3-1	(0.08 0.24 0.40 0.57 **0.73**) 0.61 0.77 0.93 1.09 **1.25** 1.42 1.58 1.74 1.90	4
	4418.8	1-3-2	(0.00) 1.23	1½
	4486.9	0-2-1	(0.12 0.36 0.61 0.85 **1.00**) −0.12 +0.12 0.36 0.61 **0.85** 1.09 1.33 1.58 1.82	5
Eu II	4129.7	(0-8-10)	(0.05 0.10 0.15 **0.20**) 1.80 1.85 1.90 1.95 **2.00** **2.05** 2.10 2.15	2½
	4435.6	2-5-6	(**0.00** 0.05 0.10 0.15) **1.80** 1.85 1.90 1.95 2.00 2.05 2.10	2¼
Gd II	4241.3	0-2-3	(0.06 0.18 0.30 0.42 **0.54**) 1.15 1.27 1.39 1.51 **1.64** 1.76 1.88 2.00 2.12	4½
	4467.2	0-2-3	(0.27 **0.80**) 1.60 **2.13** 2.67	4

TABLE 1—*Continued*

Element	λ	Intensity	Zeeman Pattern	W_s/W_o
	Lines Showing Large Change with Phase			
Ti II	4300.0	0-4-5	(**0.09** 0.26 0.43) **1.00** 1.17 1.34 1.52 1.68 1.86	3
	4301.9	0-3-4	(0.73) **0.47** 1.93	$2\frac{1}{2}$
Cr II	4052.0	5-3-0	(**0.11** 0.34 0.57) **0.86** 1.08 1.31 1.54 1.77 2.00	$3\frac{1}{2}$
Ni I	4401.6	0-3-5	(**0.00** 0.10 0.20 0.30 0.40) **1.00** 1.10 1.20 1.30 1.40 1.50 1.60 1.70 1.80	3
Ce II	4289.9(bl?)	0-5-6	(0.00) 0.89	$1\frac{1}{2}$
	4461.1	1-3-4	(0.08 0.25 0.42 0.59 0.76 **0.92**) 0.17 0.34 0.50 0.67 0.84 **1.01** 1.17 1.34 1.51 1.68 1.85	6
Eu II	4085.4	0-3-3	(**0.00** 0.42 0.83) **1.42** 1.83 2.25 2.67 3.08	6
	4205.0	0-4-10	(**0.00** 0.25 0.50 0.75) **1.25** 1.50 1.75 2.00 2.25 2.50 2.75	7
	4355.1	0-3-6	(**0.00** 0.20 0.40 0.60 0.80) **1.00** 1.20 1.40 1.60 1.80 2.00 2.20 2.40 2.60	6
Gd II	4037.3	1-5-3	(**0.10** 0.28 0.48 0.66) 1.43 1.62 1.81 **2.00** 2.19 2.38 2.57	$4\frac{1}{2}$
	4184.2	1-3-4	(**0.01** 0.03 0.05 0.07 0.09) **1.59** 1.61 1.63 1.65 1.67 1.69 1.70 1.72 1.74 1.77	$2\frac{1}{4}$
	4212.0	0-5-5	(**0.02** 0.07 0.13 0.18) **1.58** 1.62 1.69 1.74 1.78 1.83 1.89 1.93	$2\frac{3}{4}$
	4215.0	1-3-4	(**0.12** 0.36 0.60 0.85) **0.92** 1.15 1.40 1.64 1.88 2.12 2.36 2.60	6
	4217.2	1-3-4	(**0.10** 0.30 0.50 0.70 0.90) **0.78** 0.97 1.17 1.38 1.58 1.78 1.98 2.18 2.38 2.58	6
	4251.7	1-3-5	(**0.08** 0.22 0.38) **1.53** 1.68 1.83 1.98 2.13 2.28	$3\frac{1}{2}$
	4483.3	0-3-5	(**0.07** 0.21 0.35 0.49 0.64) **1.00** 1.14 1.28 1.42 1.57 1.71 1.85 1.99 2.13 2.27	5

Struve and Swings, their intensity estimates at the three phases being given in the third column. A number of lines of the rare earths had to be omitted because term analyses are incomplete. In the fourth column is the Zeeman pattern for the line. This is followed by a figure intended to represent the maximum magnetic intensification factor for the line in a field of 8 kilogauss. The field strength here is entirely arbitrary, but only the relative effect is of interest. This intensification factor is an estimate based on the number of components in the pattern and on their spacing in the π and σ groups in relation to the half-width of the Doppler profile. The table is divided into three sections, corresponding to (1) lines showing little or no change in intensity with phase, (2) lines showing a moderate change with phase, and (3) lines showing a large intensity-dependence upon phase. No distinction is made as to whether a line showing a change falls into group A or B, as this is not an attempt to explain the phase relationships; the aim is rather to see whether lines showing large variations have large magnetic intensification factors. No pronounced change should occur for a line having a small intensification factor unless ionization or some other effect than the one in question is responsible. It must be borne in mind that in a rich spectrum like that of α^2 CVn, even with high dispersion, the possibility of disturbing blends is often present; this is well illustrated by an examination of the extensive lists of line identifications given by Struve and Swings.

A comparison of the three sections of Table 1 shows a satisfactory degree of consistency between the observed change of intensity with phase and the estimated intensification factor. The average intensification factor estimated from the Zeeman pattern is 2.2, 2.6, and 4.3, respectively, for the three groups of lines showing little or no change, moderate change, or large change of intensity with phase. It is particularly significant

that *Eu* II λ 4205, the line with the largest intensification factor (7), is one of the two listed by Struve and Swings as having a very large change in intensity—from 0 to 10. According to their estimates, *Eu* II λ 4129 has a similar change, but my own plates of α^2 CVn and other peculiar stars showing the lines of *Eu* II in great strength invariably show λ 4129 weaker than λ 4205. A case in point is HD 125248, in which λ 4205 at maximum is the strongest line in the photographic region of the spectrum, with the exception of the *H* lines, and in which λ 4129 appears only about half as strong as λ 4205. I have preferred, therefore, to list *Eu* II λ 4129 as a line showing a moderate change with phase. Practically the only seriously discordant line is *Ce* II λ 4289.9, (0.00) 0.89, which showed a large change, although its intensification factor is only 1½. According to Table 3 of Struve and Swings, this line may be blended with *Gd* II and *Ti* II, but I have nevertheless included it in taking the average. A few others, notably *Fe* II λ 4122, have moderately large intensification factors, yet show little change; this behavior may be related to the presumed nonuniform distribution of elements in the atmosphere. Other lines listed by A. J. Deutsch[19] as showing pronounced changes in α^2 CVn are:

Eu II λ 3930	(0.08 0.17 **0.25**) 1.75 1.83 **1.92 2.00** 2.08 2.17	2¾
Ca II λ3933	(0.33) **1.00** 1.67	2½
Cr II λ 4078	(**0.25** 0.74) **0.63** 1.12 1.62 2.11	4½

I have added the notation for the Zeeman patterns and the intensification factors, which are adequate to account for considerable variation. The conclusion seems justified that magnetic intensification is probably an important factor contributing to the abnormal line intensities in the spectrum of α^2 CVn and similar stars. There is also a strong suggestion that particular elements are concentrated in certain regions of the atmosphere.

Although somewhat apart from the main topic of this paper, it may be appropriate here to mention one or two practical consequences that result from the polarization of stellar absorption lines in the Zeeman effect. Stellar spectrographs employing prisms are usually rather efficient plane-polarizers, owing to the oblique incidence of the light on the surfaces of the prism or prisms. Furthermore, when prism spectrographs are used at the Cassegrain or coudé foci of reflecting telescopes, oblique reflections from mirrors may be involved. Under certain circumstances such oblique reflections may introduce appreciable phase shifts between the vibrations in the plane of incidence and the perpendicular plane, resulting in a change in the ellipticity of any elliptically or circularly polarized light that may be present in the beam. In an extreme case (not likely to be encountered in practice) the phase shift may approach 90°, so that the reflection from the mirror may have the same effect as a quarter-wave plate, converting circularly polarized light into plane-polarized light. Provided that the azimuth of the resulting plane polarization (or the principal azimuth of the elliptically polarized beam) is suitably related to the azimuth of the prisms in the spectrograph, the combination may perform as a fairly efficient analyzer for circularly polarized light, rejecting any circular vibrations of one sign that may be present in the light of the star. In the case of a star with a strong magnetic field in whose light the longitudinal Zeeman effect is predominant, this analyzing effect of the telescope and prism spectrograph could conceivably result in actual displacements of the lines, in a manner dependent upon the Zeeman patterns and intensities. While in practice the analyzing effect can be only partial, it might be observable; in which case its magnitude would depend upon the obliquity of the reflections and, for a coudé prism spectrograph, upon the hour-angle of the object.

It is possible that in certain stars in which the magnetic axis is greatly inclined to the line of sight, the transverse Zeeman effect may predominate, particularly if limb darkening is severe. If so and if rotational broadening is not so extreme as to preclude study of line profiles, the plane-polarizing effect of a prism spectrograph alone may alter line pro-

[19] *Ap. J.*, **105**, 283, 1947.

files by suppressing either the π or the σ components, depending upon the azimuth of the plane of vibration and of the prism. This effect, tending toward either a doubling or a sharpening of the lines, may occur even if no oblique reflections are involved.

Some gratings exhibit pronounced plane polarization, while others do not; this behavior may easily be checked with a Nicol prism. With the coudé grating spectrograph of the 100-inch telescope there are no appreciable polarizing effects. For the observation of the Zeeman effect in stars of northerly declination an adjustable phase-shifter is now in use. It compensates for the phase-shift introduced by the flat mirror, in such a way that elliptical polarization of starlight entering the telescope is effectively preserved until it reaches the double polarizing analyzer directly in front of the slit of the spectrograph. The compensator rotates with the telescope and coudé flat; it has been so calibrated that the phase-shift introduced into the beam can be adjusted as a function of declination.

I am grateful to Messrs. I. S. Bowen, J. L. Greenstein, and R. Minkowski for reading the manuscript and making valuable suggestions.

THE SPECTRUM OF R CORONAE BOREALIS AT THE 1948–1949 MINIMUM*

GEORGE H. HERBIG†
Yerkes and McDonald Observatories
Received June 13, 1949

ABSTRACT

The spectrum of R Coronae Borealis was observed at the McDonald Observatory on the descent to the 1948–1949 minimum and for some time after it had reached minimum brightness. No change was noted in the spectrum until the star had fallen to magnitude 10.0, when emission cores appeared in the H and K lines. As the variable continued to fade, these emission lines strengthened, and others appeared. In addition, a curious "veiling" of the absorption spectrum was observed. Near minimum light, the strongest emission lines were the D lines of *Na* I, followed by H and K of *Ca* II, and a line near λ 3888 which may be due to *He* I. Most of the other emission lines were due to *Sc* II, *Ti* II, *Sr* II, and *Ca* I, but λλ 3726–3729 of [*O* II] was also present. There was no sign of hydrogen emission, and *Fe* II appeared only weakly. The fact that lines of low excitation were strong indicated that a low excitation temperature was at least partly responsible for the character of the emission spectrum. No marked change was seen in the C_1 or C_2 absorption features as the star faded. Likewise, no change in radial velocity was observed during the first 4.8 mag. of the descent to minimum, the only period for which spectrograms of adequate dispersion were available. The emission lines showed an apparently constant shortward displacement of about 12 km/sec with respect to the absorption spectrum. Spectrophotometry of the H and K emission lines showed that their *relative* intensities (with respect to the underlying continuum) increased during the star's fall to minimum but that the *absolute* intensities seemed to pass through a maximum when the star was at about magnitude 11. The reality of this decrease at fainter magnitudes, however, depends crucially on the assumption of constant color temperature during the variations. O'Keefe's proposed explanation for the variations of R CrB, in terms of an obscuring cloud thrown off by the star, is discussed only briefly. The lack of marked reddening of the variable at minimum requires, if the O'Keefe picture is correct, that the effective temperature of the obscuring cloud be less than 1400° or 1500°.

The absorption spectrum of the irregular variable star R Coronae Borealis[1] was investigated in 1935 by Louis Berman[2] on the basis of the best spectroscopic material available up to that time. The work of Berman refers, however, essentially to the spectrum at or very near maximum light. The only published spectroscopic observations of R CrB when it was faint (or, for that matter, of any R CrB-type variable near minimum light) are those of A. H. Joy and M. L. Humason,[3] made during the 1923 minimum, at which the star fell to magnitude 12.5. They found bright lines of *Ca* II, *Ti* II, *Sc* II, and *Sr* II when the star was faint, but the emission lines vanished when the star again rose to within 4 mag. of maximum brightness.

In late November, 1948, R CrB began to fade from maximum brightness, which it had maintained since April, 1947, when it had recovered from the last minimum. It was at this time very nearly in conjunction with the sun, however, and spectroscopic observations were not begun at the McDonald Observatory until December 20, when it was accessible in the early-morning sky. From that time until the writer's departure from Mount Locke, in late February, 1949, spectrographic observations were made as

* *Contributions from the McDonald Observatory, University of Texas*, No. 174.

† National Research Fellow.

[1] $\alpha(1900) = 15^h44^m4$; $\delta(1900) = +28°28'$; the total visual range is from magnitude 5.8 to fainter than magnitude 14. The star remains near maximum brightness for a majority of the time; the minima have occurred at intervals of from somewhat less than a year to about 9 years. A light-curve up to 1923 is given by H. Shapley and L. Campbell in *Harvard Circ.*, No. 247, 1923.

[2] *Ap. J.*, **81**, 369, 1935.

[3] *Pub. A.S.P.*, **35**, 325, 1923.

often as the very unfavorable observing conditions would permit. I am indebted to Mr. A. D. Code for obtaining an additional spectrogram of R CrB in April. The spectrograms are listed in Table 1, together with other pertinent information. The radial velocities given in Table 1 are to be discussed later.

Through the courtesy of Mr. Leon Campbell, of the Harvard College Observatory, it is possible to reproduce in Figure 1 a plot of the AAVSO observations of R CrB from September, 1948, until May, 1949. The times when spectrograms were obtained are marked by vertical lines under the curve. The visual magnitudes of the variable, as estimated by the writer with either the 82-inch telescope or its finders at the time that the spectrographic exposures were made, are listed in Table 1. Although these were made by

TABLE 1

SPECTROGRAMS OF R CORONAE BOREALIS

Plate*	Date U.T.	Estimated m_{vis}	V_{abs} (Km/Sec)	V_{em} (Km/Sec)	No. Emission Lines	Remarks
	1948					
G *f*/2 10500	Mar. 29.4	6.0:	+28	.....	.....	Plate by W. P. Bidelman
G *f*/2 10554	Apr. 3.4	6.0:	+23	.....	.....	Plate by W. P. Bidelman
G *f*/2 11544	Dec. 20.49	8.5: †	+25	.....	.....	
G *f*/2 11545	Dec. 20.52	8.5: †	.....	.....	.....	
G *f*/2 11553	Dec. 28.50	8.6†	+25	.....	.....	
	1949					
G *f*/2 11592	Jan. 15.52	10.0	+32	+18:	2	
G *f*/2 11609	Jan. 21.52	10.8	+25	−10	3	
G *f*/1 11647	Jan. 30.52	13.1	.....	+22	13	
Q *f*/2 11677	Feb. 2.50	13.5	.....	+25	5	
G *f*/1 11703	Feb. 4.44	13.3	.....	+16	18	
G *f*/2 11711	Feb. 5.42	13.3	.....	.....	.....	Visual region
G *f*/1 11739	Feb. 8.49	13.7	.....	+23	17	
G *f*/1 11752	Feb. 10.48	13.8	.....	+16	17	
G *f*/2 11765	Feb. 14.43	13.9	.....	.....	.....	Visual region
G *f*/1 11787	Feb. 16.41	14.0	.....	+10	6	
Q *f*/1 11811	Feb. 18.46	14.0	.....	.....	.....	
Q *f*/1 11819	Feb. 19.48	13.9	.....	.....	.....	
G *f*/1 11908	Apr. 6.46	13.8	.....	− 6:	2	Plate by A. D. Code
Weighted means	.....	.....	+27	+15	.....	

* The dispersions of the various prism-camera combinations at $H\gamma$ are: G *f*/2, 75 A/mm; G *f*/1, 148 A/mm; Q *f*/2, 169 A/mm; Q *f*/1, 332 A/mm. At λ 3600 the dispersions of the quartz-prism combinations are: Q *f*/2, 88 A/mm; Q *f*/1, 176 A/mm.
† Read from the AAVSO light-curve.

use of the same comparison-star magnitudes employed by the AAVSO observers, there are a few instances of apparent disagreement with the AAVSO estimates. The original estimates are reproduced here not because they deserve more weight than any others but because these are the magnitudes that had best be used in a discussion of these particular spectrograms, on account of the possibility of rapid fluctuations in the light of R CrB.

The spectrum of R CrB at maximum light is most nearly matched, among stars of normal spectra, by supergiants of type F5 or F8. There are, however, certain striking and significant differences: the hydrogen absorption lines in R CrB are abnormally weak, the strongest band heads of the Swan system of C_2 as well as high-excitation C I lines are present, and many of the weaker absorption features differ in relative strength from their appearance in normal supergiants.[2,4]

[4] W. P. Bidelman, *Ap. J.*, **107**, 413, 1948.

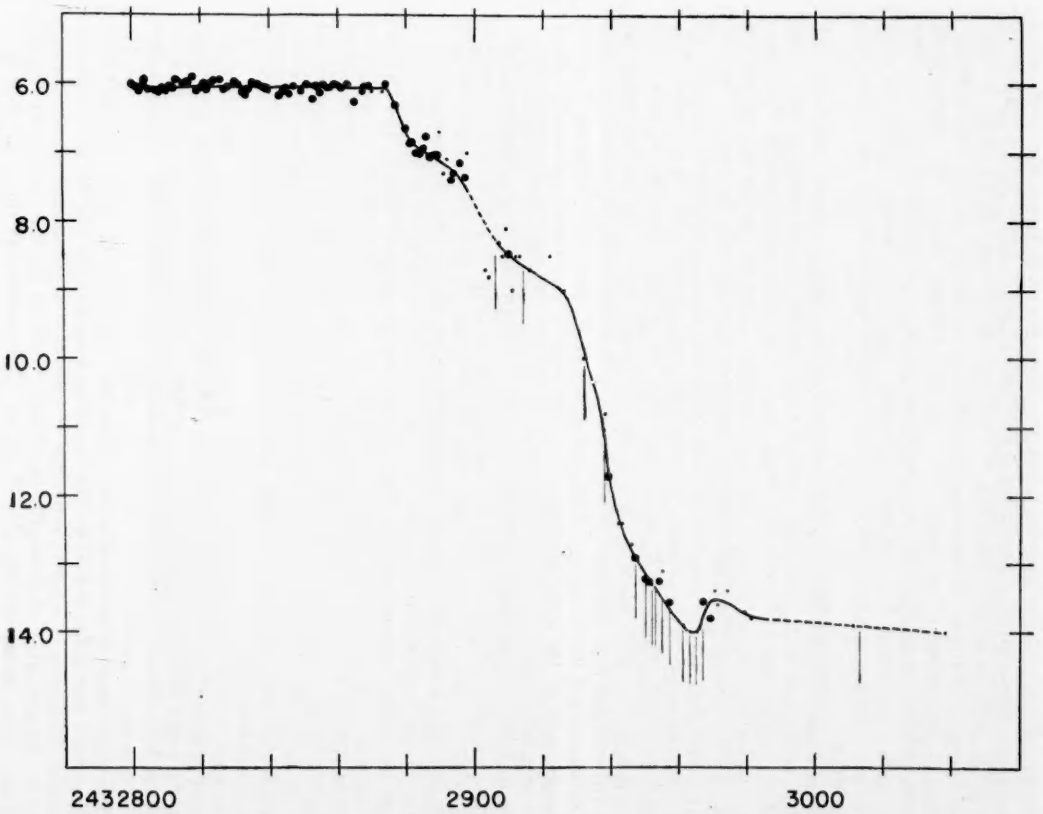

FIG. 1.—The AAVSO visual light-curve of R Coronae Borealis from September, 1948, to May, 1949. The large points represent means of two or more observations, while the small points represent a single estimate. The vertical lines indicate the times when spectrograms were obtained.

Comparison of the four spectrograms exposed as the variable faded from about magnitude 8.5 to 10.0 with films taken at maximum light (about mag. 6.0) showed no perceptible change in the absorption spectrum; but on the negative taken at magnitude 10.0, weak, narrow emission cores had appeared in the H and K lines of *Ca* II. The next spectrogram was taken 6 days later, when R CrB had fallen to magnitude 10.8. A remarkable change had come over the spectrum: the absorption lines appeared shallow and diffuse as though veiled; only the stronger absorption features could be seen with any distinctness. Strong emission lines were present in H and K and near λ 3888. These lines were not sharp but were quite diffuse; their total half-width corresponded to a velocity of 170 km/sec, uncorrected for instrumental broadening. A considerably weaker emission line had appeared at the position of *Sc* II λ 4246, obliterating the strong absorption line at that position.

The next spectrogram was obtained 9 days later, by which time the variable had faded to magnitude 13.1. This plate and most of those to follow were necessarily obtained with a dispersion of 150 A/mm, half that of the earlier spectrograms. The spectrum appeared almost continuous: only vague depressions in the continuum marked the positions of the strongest individual lines or groups of lines. The emission lines in H and K and at λ 3888 had become very intense, and many more weaker emission lines had appeared. The stronger of these were *Sc* II λλ 4246, 4314, 4320, 4374, and 4400; *Ti* II λλ 3913, 4300, 4314, 4395, 4399, 4443, 4468, 4501, 4533, 4549, and 4571; *Ca* I λ 4226; and *Sr* II λ 4077, λ 4215. Most of these lines were noted also by Joy and Humason[3] in 1923. All emission lines observed to longward of λ 3900 are listed in Table 3, together with intensities and identifications. The strong lines H, K, and λ 3888 retained their diffuse appearance on the lower dispersion, but the weaker lines looked reasonably sharp on all negatives.

The remaining G *f*/1 plates were exposed as R CrB faded further to magnitude 14.0, and then recovered slightly. There was little change in the spectrum during this period. More emission lines were visible than on the spectrogram taken at magnitude 13.1, but the absorption spectrum still appeared as though heavily veiled. This suppression did not seem to be due in general to the presence of emission lines filling in the absorption. Although the sudden weakening of the whole absorption spectrum at magnitude 10.8 coincided approximately with the appearance of line emission, when the star dropped to minimum and the emission spectrum developed much further, there was still no sign of any line emission in many absorption lines. One feature in the emission spectrum seemed to respond individually to the brightness of the variable: *Ca* I λ 4226 was slightly stronger with respect to the other lines when the star was fainter than magnitude 13.5 than when it was brighter.

Two spectrograms are available of the visual region when R CrB was near minimum. The only emission line seen in the region $\lambda > 5000$ was a very intense feature, the strongest in the entire observed spectral range, at λ 5893. This feature is without doubt the D lines of *Na* I. There was no trace of *Hα* in emission. No Balmer lines in emission were seen on any spectrogram.

Three negatives were obtained of the ultraviolet region with the quartz prisms; emission lines were seen as far as λ 3236. The measured wave lengths (on two Q *f*/1 plates of dispersion 176 A/mm at λ 3600), estimated intensities, and identifications are given in Table 2. The tabulated wave lengths have been corrected for the earth's motion, slit curvature, and a stellar velocity of +15 km/sec. The weakness of the continuous spectrum makes the numerous emission lines below λ 3900 appear more prominent than those in the photographic region. For this reason it is not possible to guarantee identity of the intensity scales of Tables 2 and 3, although an effort has been made to keep them reasonably similar. The strongest lines with $\lambda < 3888$ are *Sc* II λλ 3572, 3613, 3630, 3642; *Ti* II λλ 3341, 3349, 3361, 3372, 3383, 3685, 3759–3761; and a markedly diffuse emission line

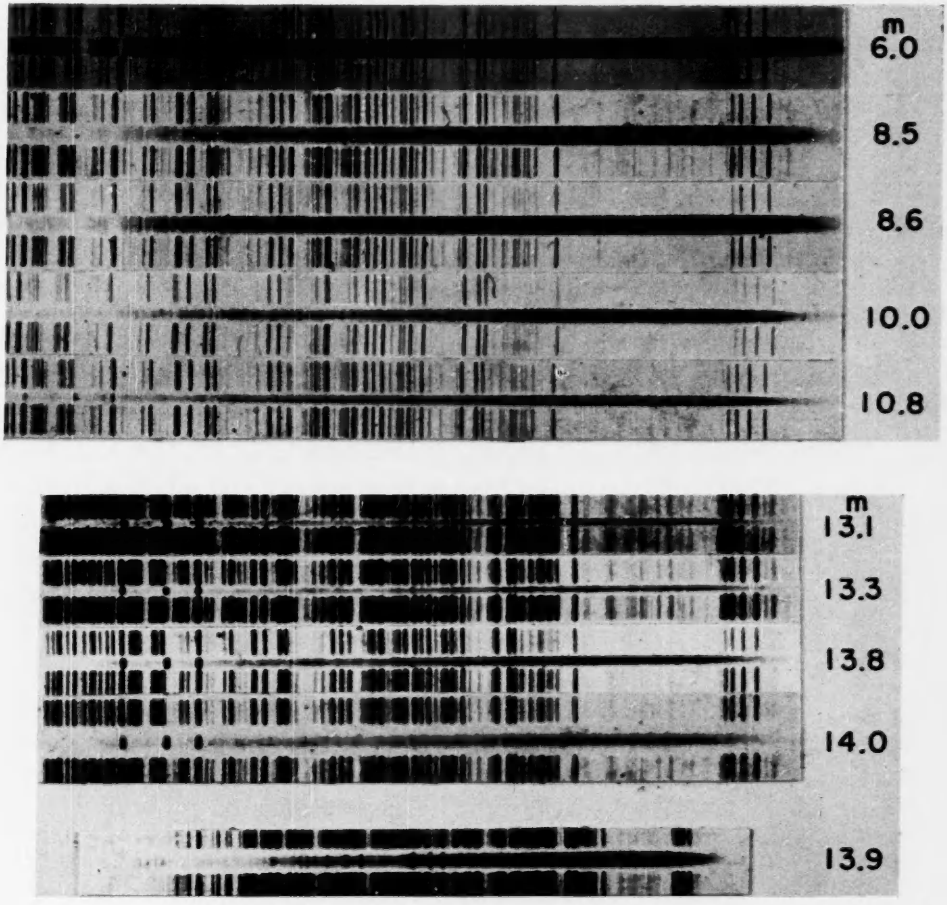

FIG. 2.—Slit spectrograms of R Coronae Borealis. The visual magnitudes of the variable when the negatives were taken are indicated. The spectrograms reproduced are, from top to bottom, G *f*/2 10500, 11544, 11553, 11592, 11609; G *f*/1 11647, 11703, 11752, 11787; Q *f*/1 11819.

TABLE 2

EMISSION LINES IN R CORONAE BOREALIS, λλ 3234–3888

Measured λ	Estimated Intensity	Identification	Measured λ	Estimated Intensity	Identification
3236.5	1:	*Ti* II 34.52 (2), 36.57 (2)	3511.2	0.5	*Ti* II 10.84 (88)
3240.3	1:	*Ti* II 39.04 (2), 41.98 (2)	3558.4	1	*Sc* II 58.54 (3)
3252.8	1:	*Ti* II 52.91 (2), 51.91 (2), 54.25 (2)	3572.6	2.5	*Sc* II 72.52 (3)
			3576.8	1	*Sc* II 76.34 (3)
3323.2	0.5	*Ti* II 22.94 (7)	3582.2	1.5	*Sc* II 80.93 [+*Y* II 84.53 (9)?]
3329.2	1	*Ti* II 29.46 (7)			
3335.7	1	*Ti* II 35.19 (7)	3590.1	1	*Sc* II 89.64, 90.48 (3)
3341.5	2.5	*Ti* II 41.88 (16) [+*Ti* II 40.34 (7)?]	3596.3	1	*Ti* II 96.05 (15)
			3600.7	1	*Y* II 00.74 (9)?
3349.0	4	*Ti* II 49.40 (1), 49.04 (16)	3614.3	4*n*	*Sc* II 13.84 (2)
3354.2	0	*Sc* II 53.73 (12)	3626.7:	1	?
3360.8	4	*Ti* II 61.21 (1)	3630.8	3	*Sc* II 30.74 (2)
3373.0	3.5	*Ti* II 72.80 (1) [+*Sc* II 72.15 (4)?]	3642.8	4	*Sc* II 42.78, 45.31 (2) [+*Ti* II 41.33 (52)?]
3380.4	1	*Ti* II 80.28 (1)	3674.2:	1*n*	?
3384.0	4	*Ti* II 83.76 (1)	3685.2	6	*Ti* II 85.19 (14)
3388.7	1	*Ti* II 87.83 (1)	3693.4	1.5	?
3394.5	2	*Ti* II 94.57 (1)	3709.7	0.5	*Y* II 10.30 (7)
3409.9	0.5	*Cr* II 08.76 (3)? [+*Ti* II 09.81 (1)?]	3721:	1.5*n*	*Ti* II 21.63 (13)?, *Fe* I 19.94 (5) ?
3416.9	0	?	3727.4	4*n*	[O II] 26.16, 28.91 (1F)
3423.3	0.5	*Cr* II 22.74 (3)	3760.5	8	*Ti* II 59.29, 61.32 (13)
3430–3445.	Broad, faint	*Ti* II 44.31 (6) +?	3773.3	1*n*	*Y* II 74.33 (7) ?
			3782.6	1.5*n*	?
3461.8	1.5	*Ti* II 61.50 (6)	3801–3825.	Broad, faint	?
3477.0	1	*Ti* II 77.18 (6)			
3491.5:	1.5	*Ti* II 91.05 (6) +?	3860–3882.	Broad	*CN* ?
3503.8	0.5	*Ti* II 04.89 (88)?	3888.4	30	*He* I 88.65 (2)?

TABLE 3

EMISSION LINES IN R CORONAE BOREALIS, λλ 3900–5893

Laboratory λ	Estimated Intensity	Identification*	Laboratory λ	Estimated Intensity	Identification*
3900.55	0.5	*Ti* II (34)	4337.92	1	*Ti* II (20)
3913.46	2	*Ti* II (34)	4367:	0	?
3933.66	35:	*Ca* II (1)	4374.46	1.5	*Sc* II (14)
3968.47	30:	*Ca* II (1)	4395.03	4*n*	*Ti* II (19)
4077.14	1	*Sr* II (1)	4399.77	1.5	*Ti* II (51)
4215.52	1	*Sr* II (1)	4400.36		*Sc* II (14)
4226.73	2 var	*Ca* I (2)	4415.56	0.5	*Sc* II (14)
4233.17	0	*Fe* II (27)	4417.72		*Ti* II (40)
4246.83	5	*Sc* II (7)	4443.80	2	*Ti* II (19)
4290.22	0.5	*Ti* II (41)	4450.49	1	*Ti* II (19)
4294.10	1	*Ti* II (20)	4468.49	2.5	*Ti* II (31)
4300.05	2	*Ti* II (41)	4501.27	3	*Ti* II (31)
4307.90	0.5	*Ti* II (41)	4533.97	2.5	*Ti* II (50)
4312.86	2.5	*Ti* II (41)	4549.62	3	*Ti* II (82)
4314.08		*Sc* II (15)	4563.76	3	*Ti* II (50)
4314.98		*Ti* II (41)	4571.97	3.5	*Ti* II (82)
4320.74	1	*Sc* II (15)	5889.95	50:	*Na* I (1)
4325.01	1	*Sc* II (15)	5895.92		*Na* I (1)

* The numbers in parentheses are the multiplet numbers of the *Revised Multiplet Table.*

at λ 3727.4, which must be [*O* II] λ 3726, λ 3729. Its hazy appearance is probably due to its duplicity.

Of considerable interest is a broad emission feature which seems, on the Q $f/1$ plates, where it appears most strongly, to run with diminishing intensity shortward from the strong emission line at λ 3888. The G $f/1$ negatives show that the feature does not actually merge with the emission line but comes to a fairly abrupt end about 6 A to the shortward. The wave length of this discontinuity has been measured on five G $f/1$ negatives. If it participates in the velocity of the rest of the emission lines, the mean wave length is λ 3882.2, with a probable error of about ±0.3 A. The emission can be traced to about λ 3860 in the opposite direction, where it fades out gradually. There seems to be a secondary maximum in the intensity distribution at λ 3878 ± 1. The well-known $\Delta v = 0$ sequence of the bands of the *CN* violet system has heads at λ 3883, λ 3871, etc., and degrade to shortward. It is tempting to associate them with this feature in R CrB. These bands occur in emission in the solar chromosphere,[5] but they have not been observed in emission in any stellar spectrum.

TABLE 4

THEORETICAL RELATIVE PEAK INTENSITIES OF *CN* BANDS

v', v''	λ	RELATIVE INTENSITIES			
		$T = 2000°$	$T = 3000°$	$T = 4000°$	$T = 5000°$
1, 0	3590	5.	8.	10.	12.
2, 1	3585	2.	5.	9.	12.
0, 0	3883	100.	100.	100.	100.
1, 1	3871	19.	31.	41.	47.
0, 1	4216	4.	4.	4.	4.
1, 2	4197	2.	2.	3.	4.
0, 2	4606	0.2	0.2	0.2	0.2

There are two obvious objections to a *CN* identification: the measured wave length of the "head" in R CrB is not in satisfactory agreement with the laboratory value, λ 3883.4. Furthermore, no sign is seen of bands of the other *CN* sequences at λ 3590 and λ 4215. Consider the latter difficulty. These transitions are expected to be weaker than those of the $\Delta v = 0$ sequence, since the Franck-Condon parabola of the violet system of *CN* is a very narrow one. It is possible to calculate relative intensities of the violet *CN* bands in emission as a function of temperature if a Boltzmann distribution of molecules among the excited states can be assumed. Relative values of the vibrational transition probabilities, freed of their frequency dependence, are available for the $\Delta v = +1, 0, -1$, and -2 sequences from the laboratory measurements of L. S. Ornstein and H. Brinkman.[6] Theoretical peak intensities of the stronger bands obtained in this way are shown in Table 4.

The data of Table 4 demonstrate that, after $\Delta v = 0$, the $\Delta v = +1$ sequence (λ 3590, etc.) is the most intense. This region is adequately exposed on the two Q $f/1$ spectrograms, which also show the broad feature shortward of λ 3882 in moderate strength. Although there is a number of emission lines which confuse the vicinity of λ 3590, there is no indication of the presence of the band. Likewise, nothing can be seen of the (0, 1) head

[5] *Pub. Lick Obs.*, Vol. **17**, Pl. I, 1931.

[6] *Proc. Kon. Akad. Amsterdam*, **34**, 33, Table III, 1931.

at λ 4215, although the *Sr* II line at that wave length would mask a weak head. In an effort to determine whether the absence of λ 3590 is consistent with the theoretical intensities of Table 4 and the observed intensity of the λ 3882 feature, on the assumption that the latter is actually λ 3883 of *CN*, a tracing of Q*f*/1 11819 was reduced, using the mean calibration-curve for this series of spectrograms. The plate-plus-instrument sensitivity function at λ 3590, in terms of that at λ 3880, was determined by assuming a black-body distribution in the continuum with a color temperature of 6700°, as determined by Berman for the λλ 3500–4500 region when the star was at maximum. The result was that, if the ratio of I (λ 3880)/I (λ 3590) = 10, the peak intensity to be expected of λ 3590 might be barely detectable on the spectrograms in question; but, if this ratio was 20, the band would not be observed. If a temperature of 3000° or less is admitted, the absence of λ 3590 is therefore not inconsistent with the *CN* identification for the λ 3882 feature. A low temperature would account also for the absence of the λ 3871 head. No attempt has been made to determine whether the rotational intensity distribution to be expected of the *CN* bands at such a temperature is consistent with the observed profile.

If *CN* is not responsible for the bandlike feature in R CrB, one must find for it identifications among atomic lines whose occurrence is reasonable in view of the character of the rest of the spectrum and whose blending would produce a structure with the profile observed. Despite the fact that the writer has not been able to find such identifications, it is felt that the molecular identification should not be regarded as more than an interesting possibility until the serious discrepancy of about 1 A in the position of the "head" in R CrB can be explained.

The most obvious identification of the very intense emission line at λ 3888 is with the well-known $2^3S - 3^3P^\circ$ transition in *He* I. An assignment to $H\zeta$ seems much less likely because of a wave-length difference of over 0.6 A, an amount too large to be dismissed as observational error. If the *He* I assignment is correct, the line is displaced to shortward by 0.23 ± 0.06 (p.e.) A from its laboratory wave length with respect to the rest of the emission spectrum; this corresponds to a wave length of λ 3888.42. No other at all plausible identification is possible with any line listed in the *Revised Multiplet Table*. Other difficulties appear, however, if the line is due to *He* I. No other helium lines have been found in the spectrum; unfortunately, there are no accessible lines arising from the same upper level. Furthermore, the level of excitation represented by *He* I λ 3888 is much greater than that suggested by the rest of the emission spectrum: 3^3P° in *He* I has an excitation potential of 22.91 volts, while the other emission lines in the spectrum of R CrB have low upper-excitation potentials of from 2 to 6 volts.

The usual means of explaining such an apparent anomaly as this is a nonequilibrium process which can populate selectively the upper level of the transition in question. Any fluorescent process operating by line coincidence could not be a direct one, since the ground state of *He* I is 1^1S, and the transition to 3^3P° is strongly forbidden. Direct excitation from the metastable term 2^3S would, of course, demand an exciting feature at very nearly the wave length of λ 3888 itself. A process populating 3^3P° from 2^3S via excitation and subsequent cascade from upper levels would have to involve two such upper levels because of the parity restriction, and it seems unlikely that two such overpopulated levels could fail to produce some other observable emission lines. Furthermore, such a process would not be very efficient. If a collisional explanation is invoked, with the colliding particle possessing very nearly the precise amount of internal energy required to excite 3^3P° from some lower, well-populated state, it would be necessary both to identify the particle and to explain the great selectivity of the energy-transfer process, since the upper levels of λ 5875 and λ 5015 lie only 0.06 and 0.08 volts higher, respectively, than 3^3P°. Neither of these lines appears in emission in R CrB. The selectivity of such collisional processes does not seem to be so high as to permit this hypothetical one to be highly efficient for 3^3P° and still fall off in efficiency by a large factor for an energy difference of

less than 0.1 volt. It is known that λ 3888 appears strongly in helium excited collisionally by electrons of energies greater than the ionization potential of *He* I; but, for energies up to about 40 volts, other lines (such as λ 5875 and λ 5015) should appear somewhat less strongly but of the same order of intensity.[7] At higher energies, λ 5015 would be stronger than λ 3888. In view of such difficulties and the small wave-length discrepancy, an identification of λ 3888 with *He* I should be regarded cautiously and the possibility that it is due to some unknown line kept in mind.

In view of the hypotheses proposed as to the cause of the variation of R CrB, it is of interest to see whether any change takes place in the strength of the blend involving the C_2 band head at λ 4737 or in the group of *C* I lines near λ 4770 as the star varies. The G*f*/2 negatives obtained between magnitudes 8.5 and 10.0 show no essential difference in these features, with respect to neighboring absorption lines, from their strength at maximum light. A decision is more difficult with regard to the later spectrograms, on which the features are seen only indistinctly, because of the general weakness of the absorption spectrum and the poorer definition in that region on the negatives of lower dispersion. It is safe to say, however, that there cannot have been any considerable increase in the equivalent widths of the C_2 and *C* I features. Any explanation of the variation of R CrB in terms of a vast increase in the strength of the Swan bands is thus definitely ruled out.

No indication is seen on any of the negatives of any marked change in the energy distribution in the continuous spectrum during the descent to minimum; but, since the dispersion was changed after the star fell below magnitude 10.8, this statement does not have the weight for the fainter magnitudes that it does for those brighter than that value. Photoelectric observations of the color of R CrB as it varies would be of considerable interest and importance. If such observations were made, the spectral regions λλ 3888–3968 and λ 5893 should be avoided because of the presence of intense emission lines.

Because the absorption spectrum of R CrB differs in many ways from those of ordinary F- and G-type giants and dwarfs, a dispersion table for the G*f*/2 (75 A/mm) negatives of that star was constructed directly from measurements of spectrograms of the same dispersion of the F- and G-type supergiants ε Leonis, γ Cygni, δ Canis Majoris, the peculiar star[4] HD 25878, and two negatives of R CrB itself at or near maximum light.[8] The latter negatives were reduced on the basis of a radial velocity of +25.0 km/sec, very nearly the mean of Berman's three-prism velocities of R CrB.[2] The other spectrograms were reduced with the velocities given in Moore's *Catalogue*.[9] This mean dispersion table was based on only eight spectrograms, but it was found to be much more satisfactory in practice than one containing blended wave lengths built up from the wave lengths of individual lines. Twenty-eight lines were chosen for measurement in the region λλ 4005–4501. They were selected by inspection of a CG plate (dispersion 26 A/mm) of R CrB on the basis of symmetry and freedom from disturbing features which might prove troublesome on exposures of different densities. The "V_{abs}" values in Table 1 result from measures of at least twenty of these lines on each plate. The absorption spectrum was measurable on the descending branch of the light-curve only as far as magnitude 10.8. Below that magnitude the absorption lines were generally too weak to measure.

The emission-line velocities are based entirely on laboratory wave lengths; neither blended emissions nor the line at λ 3888 was used in determining the velocities. In order to give some idea of the degree of confidence to be placed in these values, the number of lines upon which each "V_{em}" is based is also shown. The measured emission-line velocities are not regarded as indicating any real change in the velocity. The emission lines

[7] R. Bernard, *The Emission Spectra of the Night Sky and Aurorae* (1948), p. 93; J. H. Lees, *Proc. R. Soc. London, A*, **137**, 173, 1932.

[8] I am indebted to Dr. W. P. Bidelman for the loan of his negatives of γ Cyg, δ CMa, R CrB at maximum, and HD 25878, as well as a CG film of R CrB.

[9] *Pub. Lick Obs.*, Vol. **18**, 1932.

are, however, definitely displaced to shortward with respect to the absorption spectrum by about 12 km/sec in the mean. This is in agreement with the result of Joy and Humason, who found a relative displacement of "about 20 km/sec" in the same direction. It should be remembered that this velocity difference has been obtained from absorption lines measurable only when the star was 10.8 mag. or brighter, and emission lines seen only when the star was 10.0 mag. or fainter. There is no assurance that the velocity from the absorption spectrum measured when the variable is bright is the same as that later when the emission lines are well seen (although there is no evidence to the contrary), and the value of 12 km/sec for the relative displacement is hypothetical to that extent. The evidence of the two plates showing both emission and absorption lines demonstrates, however, that the displacement between magnitudes 10.0 and 10.8 agrees in sign and roughly in magnitude with the mean value found from all material.

The agreement of the absorption velocities in Table 1 is deceptively good, since the internal probable error of the velocity from one plate is, on the average, ± 1.6 km/sec and the actual probable error is somewhat larger. There is nothing in the G $f/2$ velocities to suggest any real variation in radial velocity on the descending branch of the light-curve. This fact cannot be considered, however, as evidence ruling out the possibility that the light-variations of R CrB are due to a change in radius, for the following reasons. If the effective temperature is constant during the decline from magnitude 6.0 to 10.8, an assumption which is supported by the observed lack of change of color temperature, the change in radial velocity due to a contraction of the star can be readily computed. This velocity change depends on the radius of the star at maximum light and hence on the maximum visual absolute magnitude. If one carries out the computation for $M_v = -1$ and -4, the corresponding velocity changes while the variable faded from 10.0 to 10.8 mag. would be $+0.9$ and $+3.6$ km/sec, respectively.[10] The accuracy of the individual G $f/2$ velocities is insufficient to enable them to be considered as evidence either for or against velocity changes of this size.

The apparent suppression of the continuous spectrum and the emergence of the emission lines as R CrB becomes fainter raise the interesting question of whether the emission spectrum may not always be present in substantially constant strength but is simply masked by the strength of the continuum when the variable is bright. This question was approached by measurement of the intensities of the emission H and K lines of *Ca* II. When three of the stellar spectrograms were taken, sensitometer spots were impressed on a piece of film taken from the same box, and the pair of films were then developed together. The sensitometer was provided with a violet filter, which caused the effective wave length of the light reaching the emulsion to lie near λ 4100. A calibration-curve was constructed from tracings of each of the sensitometer exposures and used in the photometric reduction of the corresponding spectrogram. For those negatives not calibrated, the curve used was a mean one formed from these three curves. Since the processing procedure for the entire series of spectrograms was kept as uniform as possible, it is believed that no serious error can have been committed by this improvisation.

The spectrograms were traced in the Yerkes microphotometer with magnifications of 100 for the G $f/2$ films and 200 for the G $f/1$ negatives. The continuum was drawn in over the regions of H and K in a manner as consistent as possible on all the tracings, with a tracing of the spectrum at maximum light serving as a guide. The tracing deflections were converted to intensities, and the integrated intensities of the lines were obtained. This procedure evaluates the energy of only that portion of the emission line lying above the drawn-in continuum and does not include the energy required to "fill in" the *Ca* II absorption lines in the underlying star spectrum. Unfortunately, no photometrically cali-

[10] The first value of M_v is obtained from Berman's analysis of the atmosphere of R CrB, the assumption of black-body radiation, and the mass-luminosity relation. The second is derived from spectroscopic luminosity criteria.

brated spectrograms of R CrB at maximum light were available for the determination of the undisturbed profiles. However, several excellent calibrated spectrograms of γ Cygni, a supergiant of quite similar spectral type of R CrB, were available. The *Ca* II lines were of nearly equal strength in the two stars, although the presence of $H\epsilon$ in γ Cygni might be expected to disturb H slightly. The profiles of H and K in γ Cygni were determined, after approximate allowance for $H\epsilon$, and were then used to determine the energy required to fill in those lines to the level of the continuum in the case of R CrB.

All the spectrograms of R CrB studied in this way were taken with the glass prisms, so the density of the continuous spectrum was dropping off rather rapidly to shortward in the region of H and K. Accordingly, the location of the continuum is usually more uncertain at K than at H, and the intensities of K therefore deserve lower weight.

The assumption made here—that the true continua upon which the emission lines are superimposed are actually the absorption lines observed near maximum light—seems to be a fairly reasonable one. The tracings show, on adequately exposed films, absorption wings on either side of the strong H and K emission lines. These cannot be a photo-

TABLE 5

INTENSITIES OF EMISSION H AND K IN R CORONAE BOREALIS

PLATE	m_v	H λ 3968				K λ 3933			
		Emission Intensity	Corr.	Total Rel. Int.	Total Abs. Int.	Emission Intensity	Corr.	Total Rel. Int.	Total Abs. Int.
G*f*/2 11592...	10.0	.....	.....	2.5	0.49	.....	.....	.....	.....
G*f*/2 11609...	10.8	5.8	4.7	10.5	1.00	9.1	5.5	14.6	1.00
G*f*/1 11647...	13.1	44.3	8.5	53.	0.60	57.8	8.3	66.	0.79
G*f*/1 11703...	13.3	38.2	7.5	46.	0.43	47.5	7.3	55.	0.54
G*f*/1 11739...	13.7	43.6	7.6	51.	0.34	68.2	8.2	76.	0.52
G*f*/1 11752...	13.8	47.6	6.8	54.	0.32	(46)	7.3	(53)	(0.33)
G*f*/1 11787...	14.0	37.5	7.2	45.	0.22	49.2	7.4	57.	0.30

graphic effect, which might be expected on low dispersion at the edges of such intense lines, since the equally strong λ 3888 shows no such wings. It does not seem that line emission causes the weakening of the entire absorption spectrum, and it may not be solely responsible in the cases of H and K. If the absorption lines have been "filled in" by some other agency, the emission-line intensities have been overcorrected and are therefore too large. The correction is large, percentagewise, only for the early plates where the emission is weak; when the star is very faint and the emission lines strong, the correction is not so important. For comparison purposes, the intensity above the drawn-in continuum and the additional energy required to fill in the absorption line are given separately in Table 5, as well as their sum.

The unit of the total relative intensities of Table 5 is the energy in a 1 A strip of the continuum at the wave length of the center of each line, as drawn in between the undisturbed continuous spectrum on either side. The relative intensities have been converted into absolute intensities, in units of the intensity of the line on G*f*/2 11609, by correction for a change of intensity in the underlying continuum which is given by the change in visual magnitude. This correction involved the fundamental assumption that there is no change in the color temperature in the magnitude range 10.0–14.0. These absolute intensities of H and K are given in the sixth and tenth columns of Table 5.

The data of Table 5 show that the relative intensities of emission H and K increase

as the star fades to at least magnitude 13.1, but beyond that point any systematic change is concealed by the large scatter. The absolute intensities, on the other hand, seem to show the unexpected feature (see Fig. 3) of passing through a maximum in the region of magnitude 11. The reality of the decrease toward brighter magnitudes does not rest solely on the point at magnitude 10.0; it is supported by the negative evidence of the three spectrograms obtained at about magnitude 8.5, on which emission lines of the absolute intensity of H and K at magnitude 10.8 should be seen easily. This decrease must mean that the emission lines are somehow linked with the mechanism responsible for the decrease in light and that they are not permanent features which appear simply because of the great weakening of the stellar continuum. It should not be too difficult to confirm this by observations at maximum light. If permanent emissions exist in H and K with absolute intensities equal to the largest observed here and if the strengthening of the

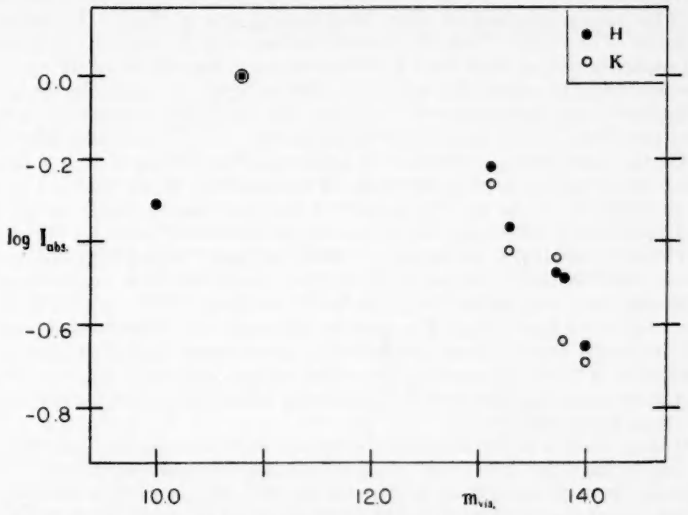

FIG. 3.—Absolute intensity of the H and K emission lines of *Ca* II in R Coronae Borealis plotted against the visual magnitude of the variable. The units are the intensities of the respective emission lines on the plate exposed at magnitude 10.8.

continuum (without change in color temperature) is the only factor to be considered between magnitudes 10.8 and 6.0, then the central intensities of the H and K absorption lines in R CrB at maximum should be raised about 4 per cent. An excess of this amount in R CrB over the central intensities in, say, γ Cygni, should be detectable and would further test the reality of the decrease toward brighter magnitudes indicated by Figure 3.

The apparent decay of absolute intensity of the emission lines toward fainter magnitudes should not be regarded as established until the question of a possible change in color has been investigated with some care, since this decay could be explained by a small reddening of the star, which would cause the correction from relative to absolute intensity, as made here, to be in error.

J. A. O'Keefe[11] has considered the hypothesis that the variations of R CrB are due to

[11] *Ap. J.*, **90**, 294, 1939. The calculations of O'Keefe were based on old vapor-pressure data for carbon which are not in good agreement with the recent work of L. Brewer, P. W. Gilles, and F. A. Jenkins (*J. Chem. Phys.*, **16**, 797, 1948).

local obscuration by material thrown off by the star. Since Berman's work suggests that carbon is abnormally abundant in the atmosphere of R CrB, O'Keefe supposes that the receding gas cloud would cool and condense, forming small carbon particles. These would be efficient absorbers, and the large apparent drop in brightness of the underlying star is consequently understandable in a qualitative way. The eventual recovery of maximum light is presumed to be due to dissipation of the cloud or shell.

The light of R CrB at minimum would, according to this hypothesis, arise from two sources: the star, seen dimly through the obscuring shell, and the shell itself. The latter, after equilibrium has been reached, would radiate with an effective temperature such that the absorbed and re-emitted energies would be equal. Since the total energy escaping from the system would be fixed because the star itself is not supposed to change, the light-variations would be due simply to a transfer of energy from the observable region to the inaccessible infrared. The observations, within their considerable uncertainty, especially at the fainter magnitudes, show no reddening near minimum. This might be explained in one of two ways. First, the thermal emission by the small particles of the shell would probably not be black body in character, and a simulation of the maximum color temperature might conceivably result in a limited spectral region. It would have to be demonstrated that this property of the absorption coefficient is consistent with the the required transferral of the bulk of the stellar energy to an inaccessible part of the spectrum. On the other hand, it seems more likely that the shell is at such a distance from the star and its effective temperature is, in consequence, so low that it makes no significant contribution in the observable part of the spectrum. A rough computation was made of the relative importance of the two sources of emission based on the assumptions of black-body radiation by both star and shell and "gray" absorbing particles. The results indicate that the shell emission would not have been detected in the photographic region if the effective temperature had been less than about 1400° or 1500° K. These values correspond to a value of $R_{\text{shell}}/R_{\text{star}}$ greater than about 12. Effective temperatures below this limit would seem to be compatible with the existence of solid particles of carbon. It is difficult, if this latter explanation is the correct one, to ascribe the apparent "veiling" of the absorption spectrum of R CrB near minimum to continuous emission by solid particles in the shell.

A very striking feature of the emission spectrum of R CrB to one familiar with stars with emission spectra is the absence of hydrogen emission, the weakness of emission *Fe* II, and the presence in such strength of *Sc* II and *Ti* II. The absence of *H* is in accordance with the weakness of that element in the absorption spectrum, an effect which has been interpreted by Berman as due to low abundance. No such abundance anomaly was found for iron, however. It seems that, to some extent at least, this latter is an excitation effect. In Table 6 are listed the ionization potentials and upper excitation potentials of the stronger permitted lines of the neutral and first ionized states of those elements most abundant in R CrB. The upper excitation potentials are separated into those corresponding to observed and unobserved lines. It will be noticed that the ions appearing in strength in emission in R CrB are those which have strong permitted lines arising from low levels, i.e., just those which would be favored by a low excitation temperature. The weakness of *Fe* II (only one faint line was seen) must be due partly to this phenomenon, since its strong lines in the photographic region arise from levels 5.5 volts high. No lines of the ultraviolet $a^4D-z^6D^\circ$ multiplet of *Fe* II were found, although the upper levels in that case are of appreciably lower energy, 4.8 volts. Likewise, none of the [*Fe* II] lines in the photographic region was observed; their upper levels have energies of about 3.0 volts.

The most striking discordance with an explanation entirely in terms of a low excitation temperature is the observation of two *Ti* II lines (λ 3504, λ 3510) and two *Cr* II lines (λ 3408, λ 3422), which originate in 5.4 and 6.1 volt levels, respectively. The identifica-

tion of λ 3504 and of λ 3408 is not entirely satisfactory, but there is no reason to suspect the other two lines. The presence of these lines demonstrates that a low excitation temperature cannot completely account for the suppression of *Fe* II in the emission spectrum.

The material available here does not enable one to determine the excitation temperature, since it would be necessary to compare the absolute intensities of lines in widely different parts of the spectrum. Rough comparison with the chromosphere would lead one to suspect a considerably lower temperature for the emission regions of R CrB. If O'Keefe's ideas are correct, the emission lines may originate in a gaseous atmosphere lying in or just outside the obscuring shell. If the emitting atoms are in temperature equi-

TABLE 6

SUMMARY OF SPECTROSCOPIC DATA FOR ELEMENTS PRESENT IN R CORONAE BOREALIS

Ion	IP	Range of Upper E.P.'s of Accessible Expected Lines		Ion	IP	Range of Upper E.P.'s of Accessible Expected Lines	
		Unobserved	Observed			Unobserved	Observed
C I	11.2	≥ 8.6	.....	*C* II	24.3	≥16.3	.....
O I	13.6	≥10.7	.....	*O* II	35.0	≥25.5*	3.3†
Mg I	7.6	2.7–5.9	.....	*Mg* II	15.0	11.6	.....
Fe I	7.9	2.8–4.6	3.3?‡	*Fe* II	16.2	4.6–5.6	5.5§
Na I	5.1	3.7	2.1	*Na* II	47.1	>36.	.....
Ca I	6.1	4.7	2.9	*Ca* II	11.8	6.4	3.1
Ni I	7.6	≥ 3.6	.....	*Ni* II	18.4	≥ 6.4	.....
Cr I	6.7	≥ 2.9	.....	*Cr* II	16.6:	≥ 6.4	6.1
Ti I	6.8	≥ 3	.....	*Ti* II	13.6:	4.6–5.0; 5.5	3.7–4.3; 5.4
V I	6.7	≥ 2.7	.....	*V* II	14.1	4.5–5.0	.....
Sc I	6.7:	≥ 3.1	.....	*Sc* II	12.8:	.....	3.2–3.5
Y I	6.5	≥ 3.0	.....	*Y* II	12.3	≥ 3.4	3.5
Zr I	6.9	≥ 3.3	.....	*Zr* II	14.0	≥ 3.6	.....
Sr I	5.7	2.7	.....	*Sr* II	11.0	.....	2.9–3.0

* For permitted lines.
† Forbidden line.
‡ λ 3719, identification uncertain.
§ Only one line, λ 4233.

librium with the solid particles, a determination of the excitation temperature from the emission lines would give information as to the relative radii of star and shell. If the optical thickness of the shell is very large,

$$\frac{R_{\text{shell}}}{R_{\text{star}}} = \left(\frac{T_{\text{star}}}{T_{\text{shell}}}\right)^2,$$

where T_{star} is 5300°, the excitation temperature of R CrB at maximum light.

I am indebted to Dr. G. P. Kuiper and Dr. O. Struve for the opportunity to work at the Yerkes and McDonald observatories, to Dr. S. Chandrasekhar and Dr. W. P. Bidelman for discussions of some of the problems encountered in this investigation, and to the National Research Council for a Fellowship.

SPECTROSCOPIC OBSERVATIONS OF THE SHORT-PERIOD VARIABLE AI VELORUM*

GEORGE H. HERBIG†
Yerkes and McDonald Observatories
Received June 13, 1949

ABSTRACT

Spectroscopic observations of the short-period variable AI Velorum reveal that the deviations from normal RR Lyrae type variability found in the light-curve by Zagar and by van Hoof appear also in the spectral type and radial velocity variations. The range in the spectral type estimated from the H + $H\epsilon$ to K ratio is from A4 to F2; the velocity varies from 0 to +44 km/sec. The variable seems to resemble the RR Lyrae stars more nearly than it does any other recognized group of short-period objects.

The variability of AI Velorum[1] was discovered by E. Hertzsprung[2] on a series of plates obtained with the Franklin-Adams camera in Johannesburg. He derived from this material the following expression for the times of maximum light:

$$\text{Maximum} = \text{JD } 2426142.210 + 0^d.111574E\,. \qquad (1)$$

Despite Hertzsprung's lack of confidence in these elements, they served to predict fairly well the times of earliest spectral type and of minimum radial velocity found from the spectroscopic observations to be described here. The exposure time of the plates used by Hertzsprung was about one-fifth the total period of AI Velorum, so that some of the details of the light-curve were undoubtedly averaged out. Two new series of plates of short exposure were discussed by F. Zagar[3] and by A. van Hoof.[4] These workers demonstrated that the shape of the light-curve, which often resembles that of an RR Lyrae type star with rise more rapid than decline, is subject to large variations. Successive maxima may differ in brightness by half the total amplitude. On one occasion the light-variations almost subsided, and the star showed only slight fluctuations about a brightness intermediate between maximum and minimum. Such extreme departures from the fairly regular variation to be expected of an RR Lyrae type star raise the question of whether this may not be an object of a quite different sort. It was to investigate this possibility that the spectroscopic observations were undertaken.

The comparison star used by both Zagar and van Hoof in their observations of AI Velorum was HD 70506, of type A0. The best magnitude available for this star is apparently a visual determination of 7.08 made with a wedge photometer and quoted in the Boss *General Catalogue*. The observations of Zagar, reduced with this magnitude, then result in a photographic range of 6.2–7.4 mag. for AI Velorum, while those of van Hoof correspond to a range of 5.9–7.1 mag. If the star is actually an RR Lyrae type variable, it is therefore the brightest known in the sky.

A total of 37 spectrograms were obtained of AI Velorum in November and December, 1948, with the Cassegrain spectrograph of the 82-inch telescope, using the glass prisms and the 180-mm Schmidt camera. The dispersion of this combination is 75 A/mm at $H\gamma$. The exposure times, on Eastman II*a*-O film, varied from 8 to 23 minutes, depending

* *Contributions from the McDonald Observatory, University of Texas*, No. 173.

† National Research Fellow.

[1] $\alpha(1900) = 8^h10^m8$; $\delta(1900) = -44°16'$; = CPD $-44°2376$ (7^m8); = HD 69213 (F0).

[2] *B.A.N.*, **6**, 147, 1931.

[3] *B.A.N.*, **8**, 169, 1937.

[4] *B.A.N.*, **8**, 172, 1937.

upon the brightness of the variable and the seeing. Despite the low declination of AI Velorum, −44°, it could be followed for as much as 5 hours, or almost two periods, at a time if the telescope were reversed from one side of the pier to the other during the "run." All negatives were obtained with the spectrograph slit placed north-south. The spectrograms were obtained jointly by Dr. O. Struve and myself.

The radial velocities of AI Velorum rest, as a system, on sixteen spectrograms of three stars of constant velocity and spectral types A5 and F0 which were chosen from Moore's *Catalogue*.[5] The declinations of these stars ranged from −31° to −42°, so that they could be observed in very nearly the same telescope position and with the same instrumental adjustments as was the variable. The micrometer settings on all lines (about fifty in all) which were well measurable on these negatives in the wave-length region λλ 3835–4481 were reduced to a common system and compared for general reliability and for constancy of position with spectral type. Only twenty-nine lines survived this examination, and it is upon these lines that the radial velocities of AI Velorum are based.

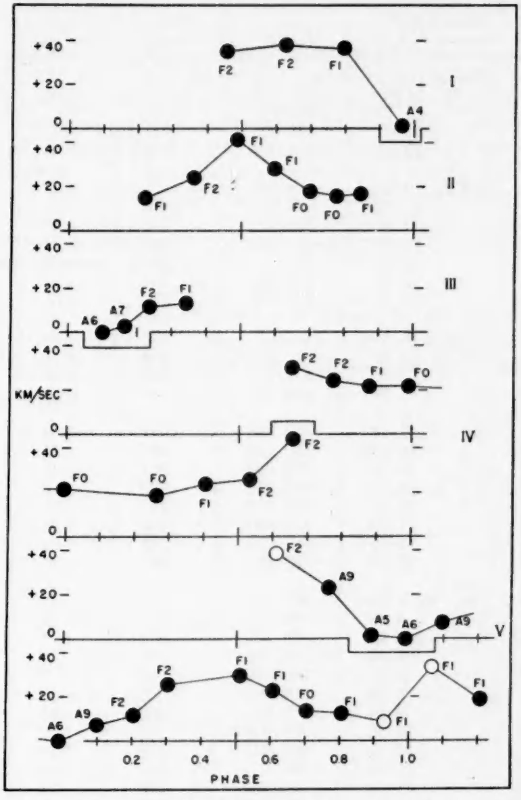

FIG. 1.—Five radial-velocity-curves of AI Velorum. Series IV and V each extend over two panels. The radii of the velocity points are equal to the probable error of the velocity from one plate. The three open points correspond to negatives of inferior definition.

[5] *Pub. Lick Obs.*, Vol. 18, 1932.

A re-reduction of the spectrograms of the standard stars using this data yielded a probable error of one plate of ± 2 km/sec from the agreement of the individual plate velocities with their mean. The velocities are actually not this reliable, however, for, although the scatter about their own mean is small, the means themselves are not in such good agreement with the *Catalogue* velocities. (As a group, the residuals of the measured standard star velocities from the *Catalogue* values, of course, sum to zero.) The source of this discrepancy is uncertain. In drawing the velocity-curves of AI Velorum (Fig. 1), the probable error of one plate has been taken as ± 3 km/sec.

The spectral type of AI Velorum was estimated on all plates by comparison with a set of spectra of standard stars kindly supplied by Dr. W. P. Bidelman. These types, given in Table 1 and marked on the velocity-curves, depend solely on the ratio of H + $H\epsilon$ to

TABLE 1

SPECTROGRAMS OF AI VELORUM

Plate G $f/2$	Time of Mid-exposure (U.T.)	JD 2432000+	Phase (Period)	Velocity (Km/Sec)	Spectral Type	Series
	1948					
11371	Nov. 18, 11^{h}12^m	873.967	0.459	+35	F2	
11372	11 40	873.986	.630	+38	F2	I
11373	12 07	874.005	.800	+37	F1	
11374	12 35	874.024	.970	+ 1	A4	
11386	Nov. 20, 10 47	875.949	.223	+15	F1	
11387	11 10	875.965	.367	+24	F2	
11388	11 30	875.979	.492	+39	F1	
11389	11 47	875.991	.600	+28	F1	II
11390	12 04	876.003	.707	+18	F0	
11391	12 16	876.011	.779	+16	F0	
11392	12 28	876.019	.851	+17	F1	
11395	Nov. 21, 10 34	876.940	.105	0	A6	
11396	10 44	876.947	.168	+ 3	A7	III
11397	10 55	876.955	.240	+12	F2	
11398	11 13	876.967	.347	+13	F1	
11431	Nov. 27, 9 58	882.915	.657	+30	F2	
11432	10 16	882.928	.774	+24	F2	
11433	10 34	882.940	.881	+22	F1	
11434	10 52	882.953	.998	+22	F0	IV
11435	11 36	882.983	.267	+18	F0	
11436	11 59	882.999	.410	+24	F1	
11437	12 19	883.013	.536	+26	F2	
11438	12 39	883.027	.661	+44	F2	
11489*	Dec. 6, 8 04	891.836	.613	+38	F2	
11490	8 28	891.853	.765	+23	A9	
11491	8 48	891.867	.891	+ 2	A5	
11492	9 04	891.878	.990	0	A6	
11493	9 21	891.890	.097	+ 7	A9	
11494	9 39	891.902	.205	+12	F2	
11495	9 55	891.913	.303	+26	F2	V
11496	10 30	891.938	.527	+29	F1	
11497	10 44	891.947	.608	+23	F1	
11498	11 00	891.958	.707	+14	F0	
11499	11 16	891.969	.805	+12	F1	
11500*	11 36	891.983	.931	+ 8	F1	
11501*	11 57	891.998	.065	+33	F1	
11502	12 20	892.014	0.208	+19	F1	

* Poor spectrogram.

K. The principal uncertainty in these estimates arises from the difficulty in comparing AI Velorum, which has quite sharp lines, with standard stars having rather diffuse lines. The error arising from this source should not exceed one-tenth of a spectral class.

The five "runs" on AI Velorum are indicated by Roman numerals in Table 1 and Figure 1. The phases were computed from the elements of equation (1). The range in spectral type is from A4 to F2. The radial-velocity range is from 0 to +44 km/sec. The velocity-curves show that the known ability of AI Velorum to remain relatively quiescent at an intermediate magnitude throughout a cycle extends to the spectral type and radial-velocity variations as well (see Ser. IV, Fig. 1). Furthermore, a velocity minimum with very low velocity and early spectral type may be followed by one during which the velocity does not fall to its minimum value and the spectral type remains like that at maximum velocity. This behavior also is matched in the light-curve. In the absence of concurrent photometric observations, it is not possible to say anything about the magnitude of the variable at the times that the spectrograms were taken. A detailed photometric study of AI Velorum from the Southern Hemisphere would be very desirable, in order to find whether any regularity exists in the deviations from normal RR Lyrae type behavior.

If the median apparent photographic magnitude of AI Velorum is 6.8 and the absolute magnitude 0.0, the distance (uncorrected for absorption) is 230 parsecs. The *General Catalogue* proper motion, corrected according to the table of Blaauw and Delhaye,[6] then corresponds to a tangential velocity of 81 km/sec. The median radial velocity, about +20 km/sec, reduces to +3 km/sec when corrected for the solar motion. AI Velorum is, therefore, a star of space velocity considerably higher than the average.

The spectroscopic material suggests that AI Velorum is more closely related to the RR Lyrae group than to any other currently recognized class of variable stars. It is unlike the β Cephei stars, the only other possible classification, in possessing a large light-range and spectral-type variation.

I am indebted to Dr. G. P. Kuiper and Dr. O. Struve for the opportunity to work at the Yerkes and McDonald observatories, to my wife for assistance with the radial-velocity reductions, and to the National Research Council for the award of a Fellowship.

[6] *B.A.N.*, **10**, 473, Table 1, 1949.

THE SPECTROSCOPIC BINARY VV ORIONIS (HD 36695)*

O. STRUVE AND W. J. LUYTEN
McDonald Observatory and University of Minnesota Observatory
Received June 4, 1949

ABSTRACT

A new set of elements has been derived for this eclipsing variable from 65 spectrograms obtained at the McDonald Observatory. The orbit is circular; $\gamma = +23.6$ km/sec, $K_1 = 138.4$ km/sec, $P = 1.485$ days. The slow variation in the velocity of the system, discovered by Daniel, has been confirmed. There are indications of the spectrum of the fainter component.

The spectrographic orbit of VV Orionis was determined in 1915 by Z. Daniel[1] from seventy spectrograms obtained at the Allegheny Observatory between November 18, 1912, and March 13, 1915. The star is also an interesting eclipsing variable, with a period of only 1.4853789 days, and a primary of class B2n, which contributes about 86 per cent of the light of the system.[2] The primary eclipse is annular, the secondary is partial. The spectrum does not appreciably change during the two eclipses. According to F. B. Wood, the ratio of the radii is nearly $k = 0.5$. From the ratio of the surface brightnesses, $\gamma = 1.9$, we infer that the spectral class of the fainter, smaller component may be about B8.

Daniel had suspected a slow variation in the velocity of the center of mass of the short-period system. "With great reserve" he gave a set of elliptical elements "as a possible explanation for the observed irregularities in the motion of the star." The period was $P = 120$ days, $e = 0.3$, and $K = 13.0$ km/sec.

At the suggestion of Professor E. Hertzsprung, VV Orionis was observed at the McDonald Observatory from November 25, 1947, until January 7, 1948. The spectrograms were obtained with the quartz spectrograph and a 500-mm UV camera, giving a linear dispersion of 40 A/mm at λ 3933. Many of the exposures were on the high-contrast Eastman Process emulsion; the rest were on Eastman 103*a*-O emulsion.

The velocity-curve of the brighter star of the system is shown in Figure 1, which was obtained by computing the phases with the help of the expression:

$$T\,(\text{eclipse}) = \text{JD } 2419835.278 + 1.4853789E\,.$$

This expression differs slightly from the one adopted in Kukarkin and Parenago's 1948 Catalogue, which is based upon observations by J. Dufay in 1947:

$$T\,(\text{eclipse}) = \text{JD } 2420095.219 + 1.48537867E\,.$$

But the probable error of the period, ±0.00000033, shows that there is no appreciable difference between the two sets.

Table 1 gives the star lines used for the measurement of the radial velocities, and Table 2 gives the resulting velocities. The data were treated in the usual manner by the Wilsing-Russell method and gave the following representation:

$$V_c = +23.3 - 138.7 \sin\theta + 1.4 \cos\theta\,.$$
$$\pm 1.7 \quad \pm 2.3 \quad \pm 2.3$$

* *Contributions from the McDonald Observatory, University of Texas*, No. 172.

[1] *Pub. Allegheny Obs.*, **3**, 179, 1915. [2] F. B. Wood, *Contr. Princeton U. Obs.*, No. 21, p. 28, 1946.

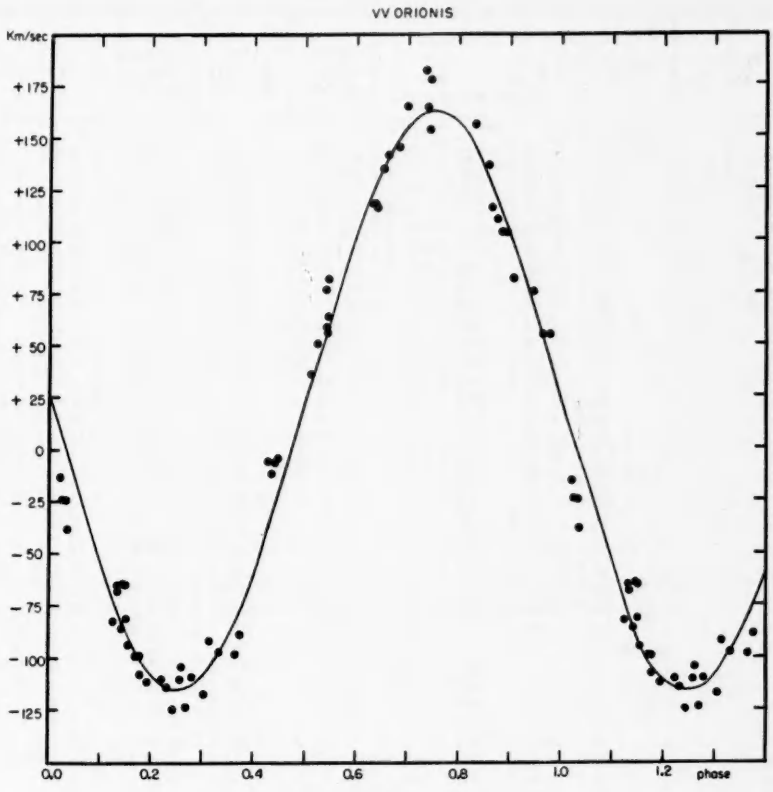

FIG. 1

TABLE 1

STAR LINES FOR VV ORIONIS

H 16 + *He* I	3704.45	*He* I	4009.27
H 13	3734.37	*He* I	4026.22
H 12	3750.15	*Hδ*	4101.74
H 11	3770.63	*He* I	4120.86
H 10	3797.90	*He* I	4143.76
He I	3819.64	*Hγ*	4340.47
H 9	3835.39	*He* I	4387.93
Hζ	3889.05	*He* I	4471.51
Ca II K	3933.67	*Mg* II	4481.23

TABLE 2

RADIAL VELOCITIES OF VV ORIONIS

PLATE CQ	DATE	U.T.	PHASE		STAR VEL. (KM/SEC)	STAR CORR. VEL. (KM/SEC)	CALCIUM VEL. (KM/SEC)	O−C1	O−C2
			P	θ°					
	1947								
6300	Nov. 25	3:50	0.127	45.6	− 82.6	− 74.3	+10.7	− 7.8	− 0.3
6301	25	4:24	.142	51.1	− 86.3	− 78.0	+ 7.7	− 2.7	+ 4.8
6302	25	4:58	.158	56.9	− 94.4	− 86.1	+ 4.5	− 2.2	+ 5.3
6303	25	5:27	.172	61.9	− 99.1	− 90.8	+13.6	− 0.7	+ 6.8
6309	25	8:57	.270	97.2	−123.9	−115.6	+16.6	− 9.4	− 1.9
6310	25	9:18	.280	100.8	−109.1	−100.8	+ 7.1	+ 4.2	+11.7
6314	25	12:22	.366	131.7	− 98.6	− 90.3	+ 9.9	−17.4	− 9.9
6315	25	12:47	.378	136.0	− 88.8	− 80.5	+37.3	−14.8	− 7.3
6323p*	26	6:13	.866	311.7	+ 67.7	+ 75.3	.....	−60.3	−52.8
6324	26	6:53	.885	318.6	+104.2	+111.8	+16.1	−12.2	− 5.2
6325	26	7:34	.904	325.5	+ 82.0	+ 89.6	+34.4	−21.2	−14.2
6329	26	9:02	.945	340.1	+ 75.9	+ 83.5	+ 6.8	+ 4.2	+11.2
6330	26	9:37	.962	346.2	+ 53.8	+ 61.4	+25.0	− 3.8	+ 3.2
6331	26	10:14	.979	352.4	+ 54.0	+ 61.6	+21.8	+11.0	+18.0
6335	26	11:58	.028	10.1	− 23.6	− 16.0	+24.8	−24.0	−17.0
6336	26	12:16	.036	13.0	− 38.1	− 30.5	+ 6.5	−35.2	−28.2
6342	27	5:16	.512	184.3	+ 36.0	+ 42.9	+22.0	+ 3.7	+10.2
6343	27	5:39	.523	188.3	+ 50.6	+ 57.5	+25.0	− 1.3	+ 5.2
6344p	27	6:14	.540	194.4	+ 54.7	+ 61.6	+12.7	− 1.8	+ 4.7
6345	27	6:32	.548	197.3	+ 63.1	+ 70.0	+21.8	− 0.2	+ 6.3
6352	27	9:40	.636	229.0	+118.2	+125.1	+12.3	− 9.2	− 2.7
6353	27	10:15	.652	234.7	+134.1	+141.0	+30.5	− 1.7	+ 4.8
6354	27	10:50	.669	238.3	+140.7	+147.6	+15.2	− 0.1	+ 6.4
6364	28	4:49	.174	62.5	− 98.8	− 92.6	+24.7	+ 0.3	+ 6.3
6365	28	5:04	.180	64.8	−108.2	−102.0	+ 6.3	− 6.6	− 0.6
6366	28	5:36	.195	70.2	−111.9	−105.7	+21.4	− 5.2	+ 0.8
6370	28	7:17	.242	87.0	−127.0	−120.8	+21.2	−11.8	− 5.8
6371	28	7:51	.259	93.2	−110.7	−104.5	+15.0	+ 4.5	+10.5
6381	29	5:16	.859	309.2	+136.7	+142.2	+27.1	+ 5.2	+10.7
6382	29	5:26	.864	311.0	+116.1	+121.6	+21.0	−13.1	− 7.6
6383	29	5:57	.879	316.5	+110.3	+115.8	+11.9	− 9.5	− 4.0
6384	29	6:28	.893	321.5	+103.9	+109.4	+20.9	− 7.3	− 1.8
6401	30	5:32	.541	194.8	+ 57.5	+ 62.1	+ 5.3	+ 0.1	+ 5.1
6402	30	5:46	.547	196.9	+ 55.8	+ 60.6	+23.6	− 6.4	− 1.4
6406	30	8:50	.633	227.8	+118.0	+122.8	+23.3	− 7.1	− 2.1
6407	30	9:08	.642	231.1	+116.2	+121.0	+23.3	−14.2	− 9.2
6419	Dec. 1	5:53	.223	80.4	−110.6	−106.5	+20.1	+ 2.5	+ 6.5
6420	1	6:15	.233	83.9	−114.4	−110.3	+20.0	0.0	+ 4.0
6421	1	6:37	.244	87.8	−125.0	−120.9	+17.0	− 9.8	− 5.8
6443	4	8:02	.303	109.1	−117.6	−115.5	+12.2	− 9.4	− 7.4
6444	4	8:32	.317	114.1	− 92.2	− 90.1	+21.3	+11.7	+13.7
6445	4	9:02	.331	119.2	− 97.4	− 95.3	+ 3.0	+ 1.0	+ 3.0
6457vp	5	10:53	.056	20.2	+ 7.5	+ 8.9	.....	+30.7	+32.2
6468	6	9:15	.683	245.9	+145.1	+145.8	+ 5.0	− 3.9	− 2.9
6469	6	9:45	.697	250.9	+164.8	+165.5	+29.4	+10.9	+11.9
6481p	7	11:59	.433	155.9	− 42.8	− 42.8	.....	− 8.4	− 8.4
6491	8	8:55	.021	7.6	− 13.0	− 13.7	+22.5	−19.4	−20.4
6492	8	9:18	.032	11.5	− 24.5	− 25.2	+22.4	−18.0	−19.0
6503	9	10:29	.738	265.6	+163.6	+162.2	+27.8	+ 2.1	+ 0.6
6504	9	10:38	.742	267.0	+153.7	+152.3	+27.8	− 8.2	− 9.7
6514	24	10:19	.832	299.5	+155.7	+144.0	+11.6	+10.9	− 1.1
6532	26	8:48	.136	49.0	− 65.1	− 78.2	+22.9	+15.2	+ 2.2
6533	26	9:22	.151	54.4	− 81.4	− 94.5	+32.0	+ 7.2	− 5.8
6542	27	6:17	0.739	266.0	+182.0	+168.2	+34.8	+20.4	+ 6.4

* "p" indicates a poor plate; "vp" indicates a very poor plate.

TABLE 2—*Continued*

Plate CQ	Date	U.T.	Phase		Star Vel. (Km/Sec)	Star Corr. Vel. (Km/Sec)	Calcium Vel. (Km/Sec)	O−C₁	O−C₂
			P	$\theta°$					
	1947								
6543	Dec. 27	6:29	0.744	267.8	+177.7	+163.9	+13.5	+15.8	+ 1.8
6553	28	7:23	.442	159.1	− 6.1	− 20.6	+28.3	+21.5	+ 7.0
6554	28	7:36	.448	161.3	− 4.7	− 19.2	+22.1	+17.7	+ 3.2
6566	29	8:03	.134	48.3	− 68.8	− 84.0	+ 9.4	+10.5	− 4.5
	1948								
6612	Jan. 3	5:32	.430	154.8	− 6.5	− 25.1	+13.3	+30.4	+11.9
6613	3	5:44	.436	157.0	− 12.0	− 30.6	+13.3	+20.1	+ 1.6
6632	4	7:03	.145	52.2	− 64.2	− 83.5	+18.9	+21.0	+ 1.5
6633	4	7:09	.148	53.3	− 64.7	− 84.0	+18.9	+22.4	+ 2.9
6661	6	8:50	.542	195.1	+ 76.3	+ 55.6	+17.8	+18.3	− 2.2
6662	6	8:59	.546	196.6	+ 81.6	+ 60.9	+17.8	+20.1	− 0.4
6679p	7	10:27	0.261	94.0	−104.0	−125.4	.....	+11.1	−10.4

The mean errors are written below the coefficients. Conjunction occurs at $\theta = +0°.58 \pm 0°.95 = 0.00161P \pm 0.00264P$. Rejecting two poor observations, we find

$$\Sigma v v = 10{,}550; \quad n = 63; \quad m = 3; \quad n - m = 60;$$

Mean error of one observation = ±13.3 km/sec .

The resulting departures are listed under (O − C₁). These values are a function of the time. Averaging, we find the values shown in the accompanying tabulation.

	$\overline{O-C_1}$		$\overline{O-C_1}$
Nov. 26.4	−6.5	Dec. 7.9	− 4.7
Nov. 29.2	−5.4	Dec. 27.2	+14.9
Dec. 2.8	−0.7	Jan. 5.3	+20.3

These values of $\overline{O - C_1}$ fit the linear relation

$$\Delta\gamma = +0.69\,(t - \text{Dec. } 7)\,.$$

This is undoubtedly Daniel's long-period variation. But our series of observations is not long enough to connect it with the Allegheny series. Nor are we justified in attempting to put a sine-curve through the values of $\overline{O - C_1}$. Qualitatively, however, our results are consistent with Daniel's, who found a range of 26 km/sec in 70 days, while we have a range of 27 km/sec in 40 days. The confirmation of a variation in γ with a period which exceeds the main period by a factor of only 80 is of major significance. But we cannot be certain that the slow variation necessarily means that the system is triple.

If the measured velocities are corrected by means of the linear formula, we obtain a new velocity-curve (Fig. 2) and a new representation:

$$V_2 = \underset{\pm 1.1}{+23.3} + \underset{}{0.69\,(t - \text{Dec. } 7)} \underset{\pm 1.6}{-138.7 \sin\theta} \underset{\pm 1.6}{+1.4 \cos\theta}\,.$$

This time we find

$$\Sigma v v = 4777; \quad n = 63; \quad m = 5; \quad n - m = 58;$$

and conjunction occurs at

$$\theta = +0°.58 \pm 0°.66 = 0.0016P \pm 0.0018P\,.$$

The corresponding departures are listed under $O - C_2$. Averaging them, we have the values in the accompanying tabulation. There is no indication of a second harmonic, and

θ	$\overline{O-C_2}$ (Km/Sec)	n	θ	$\overline{O-C_2}$ (Km/Sec)	n
10°6	−21.1	4	193°5	+ 3.4	8
52.5	+ 0.7	8	232.5	− 0.6	5
65.9	+ 3.3	4	248.5	+ 4.5	2
86.4	+ 1.9	5	266.8	− 0.2	4
97.2	− 0.3	3	299.5	− 1.1	1
114.0	+ 3.1	3	316.6	− 3.6	6
133.8	− 8.6	2	346.3	+10.8	3
157.8	+ 3.1	5			

a circular solution has been adopted as fitting the observations sufficiently well. However, the first and the last values of $\overline{O - C_2}$ clearly indicate a rotational disturbance of the velocity-curve, amounting to about ± 17 km/sec at phases $\mp 3°$ (or $0.008P$). It is reasonable, therefore, to reject these seven observations from the calculation. This

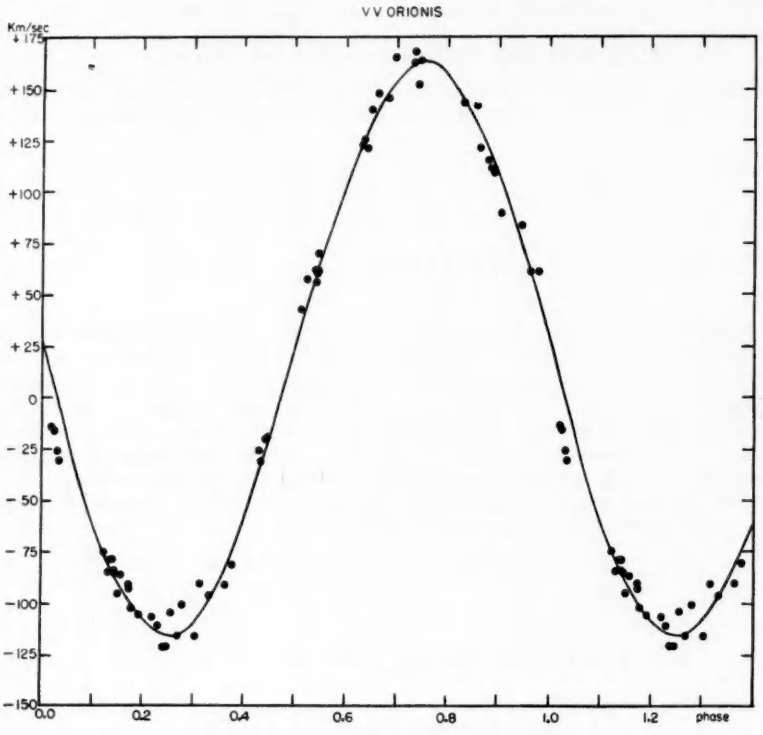

FIG. 2

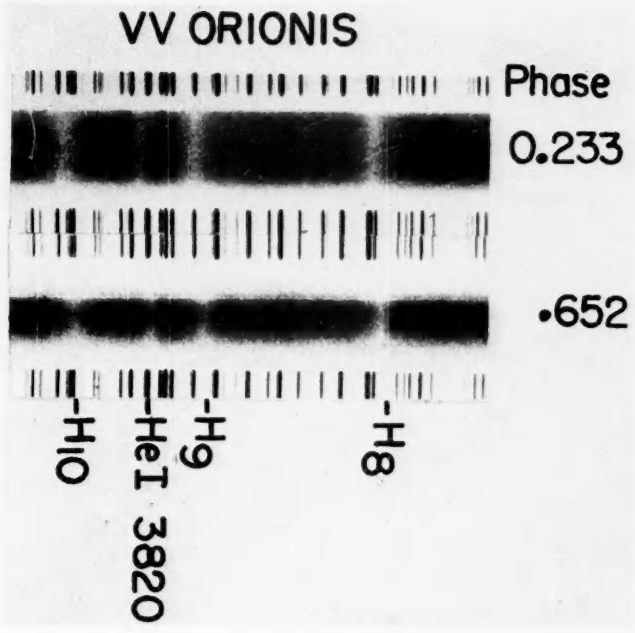
VV ORIONIS
Phase
0.233
•652
H10
HeI 3820
H9
H8

FIG. 3

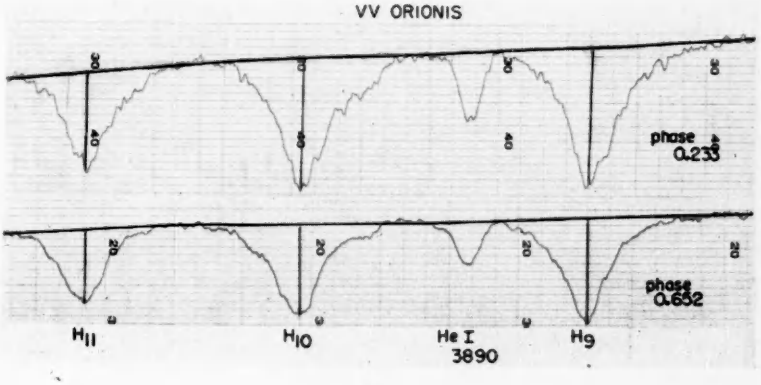
VV ORIONIS
phase 0.233
phase 0.652
H11
H10
He I 3890
H9

FIG. 4

gives, for the mean error of a single observation, $\sigma = \pm 6.8$ km/sec. Finally, we obtain the following representation:

$$V_{\text{final}} = +23.6 + 0.69\,(t - \text{Dec. } 7) - 138.2 \sin\theta + 0.9 \cos\theta\,.$$
$$\pm\ 0.9 \qquad\qquad \pm 1.3 \qquad \pm 1.3$$

The resulting $O - C_{\text{final}}$ have not been listed, because they are quite similar to the $O - C_3$. The time of conjunction now is

$$\theta = +0^{\circ}.38 \pm 0^{\circ}.55 = +0.0010P \pm 0.0015P\,.$$

The interstellar calcium lines show no variation with θ. The mean from 62 plates is $+18.4 \pm 1.1$ km/sec. The mean error of one observation is ± 8.7 km/sec. The mean Allegheny velocity from the *Ca* II lines was $+16.7$ km/sec.

The spectrum is of class B2. At the elongations we can detect on some of our best Process spectrograms clear indications of the *H* absorption lines of the fainter component. Figure 3 shows enlargements of two spectrograms, and Figure 4 gives the corresponding microphotometer tracings. We notice that at phase $0.652P$, when the primary recedes, there are faint extensions of the *H* lines on the violet sides of the stronger components. This is best shown in the case of *H*8, but it can also be seen at *H*7, *H*9, and *H*10. It is not visible in any of the *He* I lines, suggesting that the spectral type of the secondary may be late B or even A0. In Figure 4 vertical lines have been drawn to indicate the centers of the lines of the stronger component. There is a slight, but unmistakable, tendency for the violet wings to be longer at phase $0.233P$, and for the red wings to be longer at phase $0.652P$. The material, as a whole, rather strongly suggests that the fainter component is more easily seen when its velocity is negative. This is a common feature of many spectroscopic binaries of short period.

Since the fainter component is always blended with the stronger, it is possible to give only a very rough determination of its radial velocity:

Phase $0.233P$: Vel. of fainter comp. $= +141$ km/sec.

Phase $0.652P$: Vel. of fainter comp. $= -110$ km/sec.

Within the large uncertainty of these measurements the mass-ratio is $\alpha = \mathfrak{M}_1/\mathfrak{M}_2 = 1.0$. The conventional spectrographic elements are as follows:

$P = 1.4853789$ days, $\qquad K_1 = 138.4 \pm 1.3$ km/sec,

T (eclipse) $=$ Phase $0.0010P \pm 0.0018$, $\qquad K_2 = 138 \pm 10$ (?) km/sec,

$\gamma = +23.6 \pm 0.9$ km/sec, $\qquad a_1 \sin i = a_2 \sin i = 2.826 \times 10^6$ km,

$e = 0.00$, $\qquad \mathfrak{M}_1 \sin^3 i = \mathfrak{M}_2 \sin^3 i = 1.6\odot$.

Since the inclination, according to the photometric observers, is about $i = 80°$, the total masses must each be $\mathfrak{M}_1 = \mathfrak{M}_2 = 1.7\odot$. This is an unexpectedly small value, especially for the B2 primary, and it makes us suspicious of the interpretation that we have placed upon the faint extensions of the *H* lines, which we have treated as though they represented the velocities of the fainter component. The photometric results give $L_1/L_2 = 7.3$. This corresponds to a difference Δ mag. $= 2.2$ mag. The observed intensity ratios of the spectral lines agree approximately with this difference. A large error in the separation of the components is not possible. Perhaps we have here another case of an entirely abnormal secondary spectrum, violating the mass-luminosity-curve and showing changes in intensity and perhaps radial velocity. Such a secondary was previously observed in the case of HD 47129 (Plaskett's star of large mass). It is also possible that we observe the effect of absorbing streams of *H* which are not a part of the reversing layer of the fainter component.

A PHOTOMETRIC STUDY OF THE SPECTRUM OF PLEIONE*

ANNE B. UNDERHILL†
Copenhagen University Observatory
Received April 4, 1949

ABSTRACT

Two high-dispersion plates of Pleione taken in February, 1946, have been measured for radial velocity, and line profiles of all the essentially unblended lines in the region λλ 4160–4592 have been obtained. The shape of the absorption-line profiles suggests that the shell is composed of an inner part rotating with a velocity of 140 km/sec and an outer part contracting with a velocity of about 12 km/sec with respect to the inner shell. Estimates of the width of the hydrogen emission lines by Struve and Swings in 1941 showed that the inner shell was rotating with a velocity of the order of 100 km/sec. The fluctuations in the radial velocity of the shell of Pleione established by Struve and Swings in 1943 can be interpreted as alternate expansion and contraction of the outer shell. The mean shell velocity found by Struve and Swings is identical with the cluster motion of the Pleiades found by Struve and Burke Smith. The present radial-velocity measurements suggest that the B8 photosphere of Pleione is expanding with a small velocity, as well as rotating with a velocity of at least 292 km/sec.

Curves of growth are formed for the rotating shell and for the contracting shell, and an estimate of the electron pressure is obtained as a function of the temperature of the ionizing radiation. The density in the shell is estimated by means of the standard ionization equation. The electron density in the shell is of the order of 10^{12}–10^{13}, and the total density is about 7×10^{13} or about 10^{-3} that in the solar reversing layers. The shell is optically thick to radiation from a B8 star and may be in a state close to thermodynamic equilibrium at $T\sim8000°$. Consequently, the geometric dilution factor, $W = 0.061$, which is derived from the relative velocities of rotation of the shell and the B8 star on the assumption of conservation of angular momentum, has little effect on the strengths of the lines. The contracting shell has density about 0.6 that in the rotating shell. Since the shell is optically thick to radiation from a B8 star and yet we still see a B8 spectrum, we conclude that the shell is confined to an equatorial ring.

I. INTRODUCTION

The spectrum of Pleione has undergone considerable change since it was first observed. The observations up to 1941 are summarized by Struve and Swings;[1] in a second paper[2] they record the further developments of the shell spectrum. In general terms the spectral development has passed from a B8p spectrum showing high rotation and broad hydrogen emission lines before about 1905 to a typical, rapidly rotating B8 spectrum without emission lines through the years 1905 to at least 1924. Then in 1938 the *H* emission was again observed and also a shell spectrum of a large number of narrow, weak lines of *Fe* II, *Ti* II, *Sc* II, *Cr* II, *Ni* II, and perhaps *V* II. The hydrogen lines showed sharp, narrow cores typical of a shell. This shell spectrum was still present in 1946, many of the lines of *Fe* II, *Ti* II, *Sc* II, and *Cr* II being very strong. On coudé plates taken at the McDonald Observatory in 1946 the shell absorption lines on one plate vary in appearance from weak, very diffuse, essentially symmetric lines to asymmetric lines with strong, deep cores which are sharp on the red side but diffuse on the violet side.[2a] The only lines of the B8 spectrum clearly visible on these plates are *Hγ*, *Hδ*, and *Mg* II λ 4481. It is not certain whether the *Si* II doublet λ 4128, λ 4130 is present, as these lines are very diffuse and consequently hard to see on the high-dispersion plates available, particularly as these plates are not very dense in the wave-length region $\lambda < 4150$. There are no signs of the

* *Contributions from the McDonald Observatory, University of Texas*, No. 171.

† Fellow of the National Research Council.

[1] *Ap. J.*, **93**, 446, 1941. [2] *Ibid.*, **97**, 426, 1943.

[2a] Dr. Struve tells me in a private communication that W. S. Adams observed these asymmetric lines some years ago on plates taken at the Mount Wilson Observatory.

He I lines. The absence or great weakness of the *He* I lines is confirmed by microphotometer tracings which show no appreciable dip in the continuum at the position of λ 4471 and λ 4388. The *He* I lines were absent[2] in 1943 also.

Two high-dispersion plates[3] of Pleione,[4] taken by Dr. Jesse L. Greenstein at the McDonald Observatory with the coudé spectrograph, were lent to me by Dr. Greenstein for study. I measured these plates for radial velocity at the Yerkes Observatory and also made microphotometer tracings, 100× magnification, there, of the region λλ 4160–4592. The plates were calibrated for spectrophotometric work by the wedge-slit method described by Hiltner and Williams.[5]

II. THE RADIAL-VELOCITY MEASUREMENTS

The plates were measured for radial velocity, every visible line in the wave-length region λλ 4160–4592 being measured. The measurements were made in the direct and reverse directions, and the settings were reduced to wave lengths by the Hartmann formula. The lines were identified by means of the *Finding List* and *Revised Multiplet Table*.[6] Preliminary identifications were made from the study by Struve and Swings;[2] however, at a dispersion of about 3 A/mm many of the lines given multiple identifications by Struve and Swings are resolved into their several components. It was possible to identify every line measured; very few multiple identifications remain. The radial velocity was determined from all the lines (142) with single identifications. In measuring the asymmetric shell absorption lines, an attempt was made to set on the center of gravity of the feature rather than on the deepest part of the core next to the sharp red edge. The mean radial velocity from both plates is -3.48 ± 1.26 km/sec for $H\gamma$ and *Mg* II λ 4481; and $+2.43 \pm 0.18$ km/sec for the shell lines. The difference in velocity between the lines of the B8 spectrum and the lines of the shell is real, in spite of the difficulties of setting on the very diffuse lines of the B8 spectrum. If the deepest part of the shell lines had been measured, the shell velocity would have been more positive. No very clear differences of radial velocity were found between the various elements comprising the shell spectrum.

Neither of the radial velocities found here accords well with the radial velocity of $+5.2 \pm 1.0$ km/sec found by Struve and Burke Smith[7] for the Pleiades. However, Struve and Smith do show that the mean radial velocity of the rapidly rotating Pleiads is less than that of the sharp-lined members of the cluster, being $+1.17 \pm 1.41$ km/sec. Very likely the atmospheres of the rapidly rotating Pleiads are expanding with a small velocity. The shell of Pleione is known from the work of Struve and Swings[2] to have a variable radial velocity, with a range of 10 km/sec and a period of about 4 months. The mean velocity of the shell is about +5.5 km/sec, in good agreement with the cluster motion found by Struve and Burke Smith. The cluster velocity found by Struve and Smith differs somewhat from the cluster velocity of +7.86 km/sec found by J. A. Pearce from a study of plates taken at the Dominion Astrophysical Observatory (*J.R.A.S. Canada*, **40**, 143, 1946). However, since the plates studied by Struve and Swings and those studied by Struve and Smith were taken with the same instrument, the existence of a possible systematic error in the radial velocity of the Pleiades does not affect the comparison made here.

III. THE PHOTOMETRIC MEASUREMENTS

The spectra identified in the shell are *Ca* I, *Cr* I, *Cr* II, *Fe* I, *Fe* II, *Sc* II, *Sr* II, *Ti* II, and *V* II. It is uncertain whether *Mn* II and *Ni* II are present, for these spectra do not have any strong lines in the wave-length region studied and only some rather doubtful

[3] Cd 688, taken 1946, Feb. 3, at 4:11 U.T.; and Cd 700, taken 1946, Feb. 6, at 3:07 U.T.

[4] 28 Tau; α (1900) 3^h43^m2; δ (1900) $+23°50'$; mag. 5.18; B8p.

[5] *Photometric Atlas of Stellar Spectra* (Ann Arbor: University of Michigan Press, 1946), Book I.

[6] C. Moore, *Contr. Princeton U. Obs.*, No. 20, Parts I and II, 1945.

[7] *Ap. J.*, **100**, 360, 1944.

identifications could be made. The following spectra, suggested by Struve and Swings, usually as possible duplicate identifications of some of the lines in the region λλ 4160–4592, are definitely not present: *Al* II, *Ba* II, *La* II, *Mg* I, *Mo* II, *Na* I, *O* I, *S* II, *Si* II, *V* II, and *Zr* II. The spectrum in 1946 shows fewer *Fe* I lines than it did in 1941, and more *Ti* II lines.

Profiles and equivalent widths of all the essentially unblended absorption lines were derived from the microphotometer tracings by standard methods. The data from the two plates agreed well and were combined to give mean equivalent widths and mean line profiles. All the line profiles were then plotted on a uniform scale. A survey of this material showed that the shell lines had various profiles and indicated that the lines were composite. Figure 1, which gives the profiles of the five lines available from multiplet No. 38 of *Fe* II, is a small sample of the observations. The ordinate is absorption in the line expressed as percentage of the continuum, and the abscissa is in angstroms.

The lines have extensive shallow wings on both sides and an asymmetric core, which is not centrally situated on the broad wings. The asymmetries in the core are those expected for an atmosphere contracting with a velocity of the order of four times the natural half half-width of the line.[8] The broad shallow wings are typical of a rotationally distorted profile. They are too extended to be due to a contracting atmosphere. The view that part of the shell is rotating is supported by the fact that weak lines show practically no core but only the familiar dish-shaped profiles due to rotation. If the rotationally distorted profile is reconstructed (see the dotted lines in Fig. 1) and the assumption is made that the material forming the cores of the lines lies outside the material giving the rotating shell spectrum, the two parts of the shell may be separated. If we call the B8 spectrum "spectrum 1," the rotating shell spectrum "spectrum 2," and the contracting shell spectrum "spectrum 3" and if we ignore any continuous spectrum that might be produced by the shell, the continuum for spectrum 2 is spectrum 1, and the continuum for spectrum 3 is spectrum 2. It follows that the rectified profiles due to spectrum 3 are given by

$$A_3 = \frac{A' - A_2}{1 - A_2}, \tag{1}$$

where A_2 is the absorption in the rotationally disturbed profile referred to spectrum 1 as continuum and A' is the absorption in the composite profile referred to spectrum 1 as continuum. Figure 2 gives the rectified profiles for the lines of multiplet No. 38 of *Fe* II. It is evident that the line shapes of spectrum 3 are typical of a contracting atmosphere.

The instrumental profile obtained from some sharp lines of the *Fe* comparison spectrum is plotted in Figure 2 on the same scale as the shell lines. We see that the shell lines are so much wider than the instrumental profile that instrumental distortion of the profiles is not important. The instrumental profile, given in Table 1, has less extensive wings than that found by Hiltner and Williams[5] and can be well fitted by a Voigt profile[9] with parameters $\beta_1 = 0.718$, $\beta_2 = 2.66$. The data of Table 1 give the line profile magnified 100× from the plate.

From the mean extent of the wings of all the lines of spectrum 2, we find that the apparent velocity of rotation of the inner shell, v_s', is 67 km/sec. The velocity of rotation of the B8 photosphere, v_0, is 292 km/sec from the width of the *Mg* II line λ 4481. Hence, if we assume conservation of angular momentum,[10] we find that the dilution factor, W, is

$$W = \frac{1}{2}\left\{1 - \sqrt{1 - \frac{v_s'}{v_0}}\right\} = 0.061\,. \tag{2}$$

[8] *Ap. J.*, **106**, 128, 1947; compare a mirror-image of Fig. 1, *c*, with the present observations.

[9] Van de Hulst and Reesinck, *Ap. J.*, **106**, 121, 1947.

[10] Hynek and Struve, *Ap. J.*, **96**, 425, 1943.

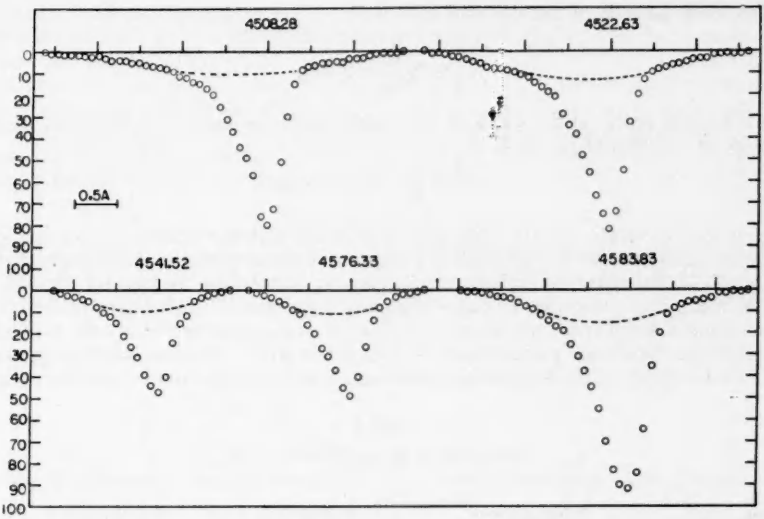

FIG. 1.—The observed profiles of the lines of multiplet No. 38 of *Fe* II. The ordinate is absorption in percentages of the continuum. Violet is on the left side; red is on the right. The size of the symbols indicates the uncertainty in the measures. Observed points are plotted.

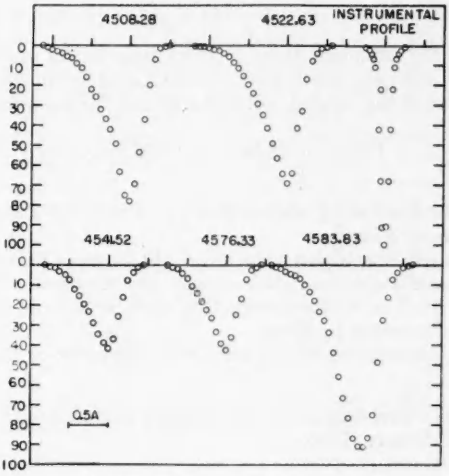

FIG. 2.—Rectified profiles of the lines of multiplet No. 38 of *Fe* II. The ordinate is absorption in percentages of the continuum. Violet is on the left side; red is on the right. Observed points are plotted.

The ratio of the radii of the star and shell is

$$\frac{R}{r} = \sqrt{\frac{v_s'}{v_0}} = 0.48, \tag{3}$$

where R is the radius of the star and r is the radius of the shell. It follows that the true velocity of rotation of the shell is

$$v_s = v_s' \frac{r}{R} = 140 \text{ km/sec}. \tag{4}$$

The velocity of rotation of the inner shell is identical with the velocity of rotation found by Hynek and Struve[10] for the shell of ζ Tauri and agrees with the rough estimate from the width of the hydrogen emission lines given by Struve and Swings[2] for Pleione.

The mean redward displacement of the lines of spectrum 3 with regard to the centers of the broad lines of spectrum 2 can be estimated on the observed composite profiles. In any one case the accuracy of such an estimate is not great; but, since we have profiles of 76 lines, the mean estimated displacement has considerable accuracy. Spectrum 3 is displaced 12 km/sec to the red of spectrum 2. This displacement is consistent with the interpretation that the source of spectrum 3 is an atmosphere contracting with a velocity of the order of four times the natural half half-width of the lines due to thermal motions of the atoms.

TABLE 1

CONTOUR OF IRON EMISSION LINE

Distance from Center on Tracing (Mm.)	Relative Intensity	Distance from Center on Tracing (Mm.)	Relative Intensity	Distance from Center on Tracing (Mm.)	Relative Intensity	Distance from Center on Tracing (Mm.)	Relative Intensity
0	100	4	22	8	2.6	14	0.57
1	91	5	11	9	1.7	16	.50
2	68	6	6.7	10	1.1	18	.44
3	42	7	4.2	12	0.72	20	0.38

The physical picture of Pleione in February, 1946, revealed by the measures so far, is the following:

1. A B8 photosphere, rotating with a velocity of about 292 km/sec and expanding with a velocity of about 8 km/sec.
2. An inner shell, rotating with a velocity of 140 km/sec. This shell may be more or less stationary. Unfortunately, my radial-velocity measurements of the shell lines do not refer clearly to this shell or to the contracting shell, so a close estimate of the radial velocity of these shells cannot be given.
3. An outer shell, contracting with a velocity of the order of 12 km/sec with respect to the rotating shell.

We shall study each part separately and attempt to estimate the physical conditions prevailing there in February, 1946.

IV. THE B8 SPECTRUM

The present material is not suitable for studying the profiles of the hydrogen lines, as the magnification is too great. ($H\gamma$ covers a distance of 4 feet on the microphotometer tracings!) The core of $H\gamma$ is deep, going to clear plate effectively, but very broad, and the

wings can be traced for at least 20 A on each side. The central part of the profile of *Mg* II λ 4481 is given in Figure 3. This profile is clearly asymmetrical and can be separated into a part from spectra 1, 2, and 3. These rectified profiles are also given in Figure 3. The equivalent width of the feature from the B8 spectrum is 0.532 equivalent angstroms. This rather great strength of λ 4481[11] and the weakness of the *He* I lines suggest that the photosphere of Pleione is not earlier than B8 and may be a little later. The effective temperature is likely of the order of 12,000°[12] rather than 17,000°, as assumed by Struve and Swings;[1] for the effective temperature of an A0 main-sequence star is close to 10,000°.[13]

V. THE ROTATING SHELL

The line-intensity data for a shell may be analyzed by curve-of-growth methods; for the simplified theory of line formation used in curve-of-growth theory[14] may be expected to give at least as close a representation of the physical conditions of line formation in a

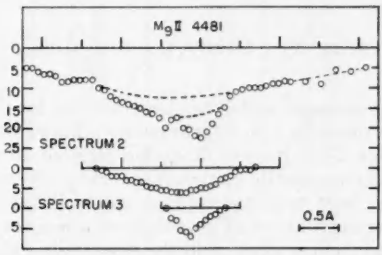

FIG. 3.—The center of the observed profile of *Mg* II λ 4481 and the rectified profiles. The ordinate is absorption in percentages of the continuum. Violet is on the left, red on the right. Observed points are plotted.

shell as it does of line formation in stellar reversing layers. Since the curve of growth relates the equivalent width of a line to the number of atoms capable of absorbing the line, the only part of the standard theory of the curve of growth that may require change is the part dealing with the relation of the number of atoms in any level to those in the ground level. If the shell is optically thick to the exciting radiation, local thermodynamic equilibrium will be set up in the shell, and the standard equations giving the degree of ionization and the number of atoms in any excited state may be used. The temperature occurring in these formulae will be the local temperature in the shell. If the shell is optically thin to the exciting radiation, the ionization may be calculated by

$$\log \frac{n_r+1}{n_r} = -\frac{5040}{T} I_r + \tfrac{5}{2} \log T - 0.48 + \log 2 \frac{u_{r+1}}{u_r} - \log \left(\frac{P_e}{W}\right); \qquad (5)$$

and the excitation by

$$\frac{n_{r,s}}{n_r} = W \frac{g_{r,s}}{u_r} e^{-\chi_{r,s}/kT}, \qquad (6)$$

where W is the dilution factor and T the temperature of the exciting radiation. The other symbols have their customary meanings.[15]

[11] Cf. the equivalent width of λ 4481 in β Ori and in ζ Dra (*Ap. J.*, **107**, 349, 1948).

[12] G. P. Kuiper, *Ap. J.*, **88**, 439, 1938. [13] *Ap. J.*, **108**, 83, 1948.

[14] Unsöld, *Physik der Sternatmosphären* (Berlin: Julius Springer, 1938), pp. 165 and 264; or Menzel, *Ap. J.*, **84**, 462, 1936.

[15] *Ibid.*, p. 64.

We shall follow in detail in the ensuing analysis the methods outlined by K. O. Wright.[16] Wright's nomenclature is based on the theory of the curve of growth by Menzel.[14] Log W/λ[17] is expressed as a function of log X_0, where X_0 is the optical depth at the center of a line. We have

$$\log X_0 = \log g_i f + \log \lambda - \frac{5040}{T}\chi_i + \log \frac{N_a}{b(T)} \frac{\pi e^2}{mc} \frac{1}{\sqrt{\pi} v} W, \tag{7}$$

where N_a is the number of atoms in the appropriate stage of ionization, $b(T)$ is the partition function, v is the most probable velocity of the atoms (which are assumed to have a Maxwellian distribution of velocities), χ_i is the excitation potential of the lower level of the line in question, and W is the dilution factor. We are assuming that the excitation is given by equation (6). However, for most lines the f-value is not known, and solar strengths must be used instead. Then the appropriate abscissa for any line is

$$\log X_* = \log X_f - 5040\chi_i \left(\frac{1}{T_*} - \frac{1}{T_\odot}\right) + C_* - C_\odot, \tag{8}$$

where X_f is the solar line strength and C has been written for the last term on the right side of equation (7). The quantity C is a constant for all lines from a given atom and includes the effect of dilution if it is present. Rotation does not affect the expected shape of the curve of growth, for it may readily be shown that rotation does not change the equivalent width of the line, at least to a first approximation. Consequently, we may use the standard methods of forming a curve of growth from the observations.

Table 2 gives the equivalent widths of all the essentially unblended lines of the shell spectrum in the region λλ 4160–4592. The lines are listed in multiplets according to wave length. The equivalent width of the combined feature is given in equivalent angstroms as well as the spectrophotometric measures $-\log W/\lambda$ for spectra 2 and 3. Solar line strengths, kindly communicated to me by Dr. K. O. Wright, are also given for most of the lines. For a few lines I derived log X_f from the equivalent width of the line in the Utrecht *Atlas*[18] and from Wright's solar curve of growth.[19] These values are given in italics and are somewhat uncertain. Greenstein[20] has recently given a list of line strengths in the F star τ UMa, which take into account the difference in opacity between an F star and the sun. However, since he does not give strengths for a number of the lines in Table 2, it is not worth while to use his line strengths in this analysis of the shell of Pleione, as the available data are then too few. The accuracy of the spectrophotometric measures, $-\log W/\lambda$, is limited; for an unknown accidental error is introduced into the separation of spectrum 2 from spectrum 3. The ordinary accidental errors of the photometry are small; for the average deviation, without regard to sign, of any one measure of the equivalent width of the combined feature from the mean value is 5.5 per cent.

The curve of growth for the rotating shell is given in Figure 4. It was formed by fitting the partial curves of growth for the various atoms to the observed curve for *Fe* II. The points are plotted for an excitation temperature of 6300°. This temperature was chosen arbitrarily, for the data are too few to determine the temperature in the ordinary way. The curve drawn is Wright's solar curve of growth, displaced to fit the data.

[16] *J.R.A.S. Canada*, **40**, 183, 1946; *Contr. Dom. Ap. Obs. Victoria*, No. 2, 1946; also *Pub. Dom. Ap. Obs. Victoria*, Vol. **8**, No. 1, 1948.

[17] The symbol W is customarily used for equivalent width and for dilution factor. However, little confusion should arise from this, for W, meaning equivalent width, is generally used in the combination "log W/λ" throughout this paper. The context will make it clear when W means the dilution factor.

[18] Minnaert, Mulders, and Houtgast, *Photometric Atlas of the Solar Spectrum* (Amsterdam, 1940).

[19] Private communication.

[20] *Ap. J.*, **107**, 151, 1948.

TABLE 2

THE SPECTROPHOTOMETRIC MEASURES, $-\log W/\lambda$

λ	Element	E.P. Lower Level	W Composite Spectrum	$-\log W/\lambda$		log X_f
				Spectrum 2	Spectrum 3	
4481.23	*Mg* II	8.83	0.616	4.82	5.25	.....
4246.83	*Sc* II	0.31	.476	4.48	4.05	+0.57
4354.61		0.60	.046	5.15	5.36	−1.34
4400.36		0.60	.176	4.85	4.53	−0.47
4305.72		0.59	.058	4.99	5.29	*−0.65*
4325.01		0.59	.282	4.61	4.36	+0.22
4294.77		0.60	.090	4.90	5.00	−1.28
4215.52	*Sr* II	0.00	.056	5.18	5.12	+1.08
4518.30	*Ti* II	1.08	.102	4.80	5.02	−1.66
4443.80		1.08	.604	4.42	3.98	+0.14
4450.49		1.08	.364	4.60	4.21	−0.49
4287.89		1.08	.219	5.01	4.46	−0.58
4294.10		1.08	.472	4.46	4.07	.....
4161.52		1.08	.150	4.85	4.62	*−0.30*
4184.33		1.08	.040	5.21	5.10	*−0.59*
4468.49		1.13	.604	4.36	4.02	+0.20
4501.27		1.11	.608	4.37	4.00	+0.07
4441.73		1.18	.115	4.77	4.98	.....
4464.46		1.16	.234	4.62	4.48	*−0.76*
4470.86		1.16	.178	4.65	4.71	*−1.43*
4290.22		1.16	.443	4.52	4.12	−0.01
4300.05		1.18	.566	4.40	4.00	+0.63
4301.93		1.16	.442	4.33	4.18	+0.13
4312.86		1.18	.378	4.55	4.19	−0.29
4563.76		1.22	.584	4.34	4.02	+0.04
4399.77		1.23	.450	4.45	4.12	−0.03
4407.68		1.22	.057	5.00	5.39	.....
4529.46		1.56	.155	4.75	4.75	−1.44
4571.97		1.56	.668	4.30	3.97	+0.14
4316.81		2.04	.094	4.86	5.12	−1.70
4386.86		2.59	.168	4.72	4.66	−1.49
4163.64		2.58	.365	4.42	4.24	−0.50
4411.08		3.08	.150	4.84	4.65	.....
4488.32		3.11	.286	4.59	4.41	−1.66
4183.44	*V* II	2.04	.052	5.12	5.21	−1.53
4205.08		2.03	.101	4.88	4.88	.....
4225.23		2.02	.042	5.30	5.24	.....
4226.73	*Ca* I	0.00	.106	4.88	4.94	+2.23
4254.35	*Cr* I	0.00	.130	4.85	4.74	+1.22
4274.80		0.00	.116	4.90	4.82	+1.03
4242.38	*Cr* II	3.85	.285	4.53	4.38	*−1.77*
4252.62		3.84	.074	4.82	4.97	*−1.71*
4261.92		3.85	.196	4.72	4.51	−1.43
4269.28		3.84	.084	4.90	5.20	*−1.63*
4275.57		3.84	.130	4.92	4.66	.....
4284.21		3.84	.144	4.75	4.69	−0.73
4565.78		4.02	.078	5.04	5.13	*−2.18*
4558.66		4.06	.604	4.35	4.00	−0.98
4588.22		4.05	.544	4.30	4.10	−1.28
4592.09		4.06	.210	4.58	4.61	−1.69
4195.41		5.30	.028	5.24	5.72	.....
4383.55	*Fe* I	1.48	.290	4.52	4.36	+2.01
4404.75		1.55	.159	4.62	4.81	+1.81
4250.79		1.55	.051	5.14	5.48	+1.28
4271.76		1.48	.225	4.45	4.68	+1.78
4325.76		1.60	0.231	4.61	4.43	+1.69

TABLE 2—*Continued*

λ	Element	E.P. Lower Level	W Composite Spectrum	$-\log W/\lambda$ Spectrum 2	$-\log W/\lambda$ Spectrum 3	$\log X_f$
4273.32	*Fe* II	2.69	0.174	4.66	4.66	.....
4303.17		2.69	.466	4.40	4.09	−0.45
4351.83		2.69	.580	4.47	3.95	.....
4385.38		2.77	.440	4.48	4.11	−0.55
4178.88		2.57	.570	4.44	3.94	−0.63
4258.16		2.69	.141	4.75	4.76	−0.85
4296.57		2.69	.280	4.57	4.37	−0.79
4369.40		2.77	.122	4.70	4.63	−1.78
4472.92		2.83	.138	4.71	4.91	−1.61
4489.18		2.82	.298	4.52	4.35	−1.34
4491.40		2.84	.393	4.38	4.27	−1.04
4515.34		2.83	.505	4.34	4.11	−0.87
4520.22		2.79	.494	4.25	4.19	−0.90
4555.89		2.82	.548	4.36	4.05	−0.83
4582.84		2.83	.296	4.58	4.35	−1.62
4508.28		2.84	.626	4.23	4.03	−0.81
4522.63		2.83	.680	4.29	4.01	−0.26
4541.52		2.84	.300	4.56	4.35	−1.58
4576.33		2.83	.308	4.50	4.37	−1.46
4583.83		2.79	0.768	4.20	3.90	−0.22

The electron pressure in the shell may be determined from the horizontal displacement between the partial curves of growth due to atoms of a given element in two stages of ionization; for

$$\Delta \log X_f''(Fe) = \log X_f''(Fe\,\text{I}) - \log X_f''(Fe\,\text{II}) = \log\left(\frac{N_{Fe\,\text{II}}}{N_{Fe\,\text{I}}}\right)_{\text{shell}} - \log\left(\frac{N_{Fe\,\text{II}}}{N_{Fe\,\text{I}}}\right)_{\odot}, \tag{9}$$

where

$$\log X_f'' = \log X_f - 5040\chi_i\left(\frac{1}{T_*} - \frac{1}{T_\odot}\right); \tag{10}$$

and, since

$$\log\left(\frac{N_{Fe\,\text{II}}}{N_{Fe\,\text{I}}}\right)_{\text{shell}} - \log\left(\frac{N_{Fe\,\text{II}}}{N_{Fe\,\text{I}}}\right)_{\odot} = -I_1(\theta_{\text{ion}} - \theta_\odot) + \tfrac{5}{2}\log\frac{T_{\text{ion}}}{T_\odot} + \log(P_e)_\odot - \log\frac{P_e}{W}, \tag{11}$$

it follows in the case of *Fe*, where the observed $\Delta \log X_f''$ is 2.90 ± 0.15, that

$$\log\left(\frac{P_e}{W}\right)_{\text{shell}} = -I_1(\theta_{\text{ion}} - \theta_\odot) + \tfrac{5}{2}\log\frac{T_{\text{ion}}}{T_\odot} + \log(P_e)_\odot - (2.90 \pm 0.15). \tag{12}$$

Here T_{ion} is the temperature of the ionizing radiation in the shell, W is the dilution factor, and θ is the temperature function, $5040/T$. We may also find $\log (P_e/W)_{\text{shell}}$ from the horizontal displacement, 1.95 ± 0.15, between the partial curves of growth for *Cr* I and *Cr* II. We shall follow Greenstein[21] and assume that, in the layers producing the solar absorption lines, $\log (P_e)_\odot = 0.80$ and $T_\odot = 5300°$.

[21] *Op. cit.*, p. 178.

From the observed value of log (P_e/W) we can find the density of the shell, for Strömgren gives tables [22] of log P, the total pressure in a stellar atmosphere in local thermodynamic equilibrium as a function of the ionization temperature and the electron pressure. The number of particles per cubic centimeter is related to the total pressure by the expression

$$n = \frac{P}{kT}. \tag{13}$$

We enter Strömgren's tables with the observed value of log (P_e/W); for, if the shell is optically thick, the observed value of log (P_e/W) is log P_e and, if the shell is optically

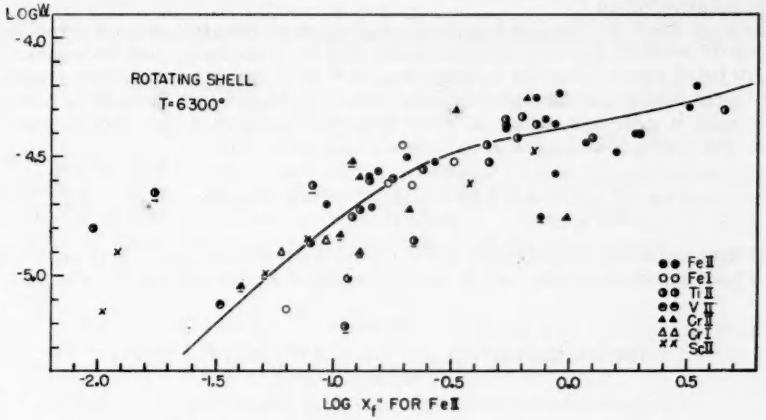

FIG. 4.—The curve of growth for the rotating shell. A dash under a symbol indicates that log X_f for that point is uncertain.

TABLE 3

THE DENSITY IN THE ROTATING SHELL

T_{ion}	12,600°	10,080°	8400°	7200°
log P_e *Fe*	3.15	2.12	1.14	0.20
Cr	3.50	2.58	1.71	0.87
Mean log P_e	3.32	2.35	1.42	0.54
n_e	1.2×10^{15}	1.6×10^{14}	2.2×10^{13}	3.5×10^{12}
log P	3.64	2.73	1.98	1.50
n	2.5×10^{15}	3.8×10^{14}	8.2×10^{13}	3.2×10^{13}

thin, the change in the ionization equation (cf. eq. [5]) requires that you enter with log (P_e/W).

Values of log P_e, n_e, log P, and n are given in Table 3 for a number of values of the ionization temperature. If the shell is not in local thermodynamic equilibrium, the tabulated values of P_e and n_e must be reduced by the dilution factor W, and the ionization temperature will be $\backsim$ 12,000°, the value for a B8 star. In 1941 Struve and Swings[1] observed the hydrogen lines to $H31$. The Teller-Inglis formula[23] gives an electron density of 1.2×10^{12} in the shell, in rough agreement with what we have found in 1946.

[22] *Pub. Copenhagen Obs.*, No. 138, pp. 47 ff.

[23] *Ap. J.*, **90**, 439, 1939.

We may compare the values of Table 3 with the corresponding values for the sun. The $\log (P_e)_\odot$ and $T_\odot$ that we have used correspond to $n_e = 8.6 \times 10^{12}$ in the upper layers of the solar atmosphere. Strömgren's model atmosphere[24] with $\log A = 3.8$ gives $n = 7 \times 10^{16}$ in these layers. The electron density at the base of the chromosphere[25] is about 4×10^{11}, and the electron density at the base of the corona[26] is 4.30×10^{8}. We see that the electron density in the rotating shell is of the order of that in the solar reversing layers but that the total density is smaller than that in the solar reversing layers by a factor of about 10^3 if T_{ion} is about 8000°. Struve and Swings[1] deduced a factor of this order from geometric considerations of the extent of the shell. The total density found is independent of the dilution factor for the reasons noted above and depends only on the ionization temperature assumed.

Since we know the density and electron pressure in the shell, we can estimate the opacity of the shell. Let us consider that the shell is composed of pure hydrogen at the density found above. Then the number of neutral hydrogen atoms per cubic centimeter is $(1 - x)n$,where x is the degree of ionization of hydrogen, and the opacity per centimeter path is $a_\nu(1-x)n$, where a_ν is the absorption coefficient per neutral hydrogen atom. The degree of ionization of hydrogen is calculated from

$$\log \frac{N_{H^+}}{N_H} = -13.54\theta + \tfrac{5}{2} \log T - 0.48 - \log P_e \qquad \left(\text{or } -\log\left[\frac{P_e}{W}\right]\right) \quad (14)$$

for several ionization temperatures and the observed value of $\log P_e$ (or of $\log [P_e/W]$). For a path length of 10^{10} cm (which is about $0.05R$, if R, the radius of the star, is about

TABLE 4

THE OPTICAL THICKNESS, τ_λ, FOR A PATH LENGTH OF 10^{10} CM IN THE ROTATING SHELL

T_{ion}	λ 763	λ 1570	λ 4500
12,600°	1.07×10^{7}	9.50×10^{2}	1.96×10^{3}
10,080°	5.45×10^{6}	44.3	55.9
8,400°	2.25×10^{6}	1.87	1.40
7,200°	1.32×10^{6}	0.103	4.72×10^{-2}

$3R_\odot$), we find the values of τ_λ given in Table 4. The wave length λ 763 corresponds approximately to the second ionization potential of *Fe*, and λ 1570 to the first ionization potential of *Fe*. The opacity at λ 4500 will tell us whether for the process of line formation the shell acts as an absorption tube, τ_λ small, or as a stellar atmosphere, τ_λ large. We see that a shell of thickness 10^{10} cm is opaque in all wave lengths to radiation of temperature greater than 10,080°. We must now estimate the thickness of the rotating shell. Since the lines in the shell are saturated, they must be formed by an atmosphere of roughly the same optical thickness as that of the sun. Since the density in the shell is 10^3 times less than that in the sun, this means that the path length in the shell must be about 10^3 times longer than in the sun. We estimate that the solar atmosphere occupies about $10^{-3} R_\odot$; hence the path length in the shell is about $R_\odot$ or 7×10^{10} cm. Consequently, we conclude that the rotating shell is opaque to the radiation from the B8 star. This means that the ionization in the shell is largely governed by a local temperature which may be of the order of 8000°. Since the shell spectrum resembles α Cygni closely in ionization and

[24] *Pub. Copenhagen Obs.*, No. 138, p. 81.

[25] Cillié and Menzel, *Harvard Circ.*, No. 410, 1935.

[26] Van de Hulst, *Ap. J.*, **105**, 471, 1947.

excitation, it seems probable that the shell is optically thick and that local thermodynamic equilibrium has been set up with a temperature of about 8000°.

The methods used in obtaining the line profiles and in separating spectrum 3 from spectrum 2 (cf. eq. [1]) imply that the shell is optically thin to the radiation of the B8 star and that the shell acts as an absorption tube producing absorption lines only and no continuous spectrum. If, however, the shell is optically thick to radiation from the B8 star, the shell will act like a stellar atmosphere and will produce a continuous spectrum as well as an absorption-line spectrum. Then, since the total flux that we receive in a frequency ν in a line is $F_c^{(1)} + F_\nu^{(2)}$ and since the total flux that we receive in the neighboring continuous spectrum is $F_c^{(1)} + F_c^{(2)}$, where $F_\nu^{(2)}$ is the flux at frequency ν produced by the shell, $F_c^{(2)}$ is the flux in the continuous spectrum produced by the shell, and $F_c^{(1)}$ is the flux produced by the B8 star, the measured absorption in the line of spectrum 2 is

$$A_2(\nu) = \frac{F_c^{(2)} - F_\nu^{(2)}}{F_c^{(1)} + F_c^{(2)}}. \tag{15}$$

We shall assume that $F_c^{(1)}$ is constant, since the B8 star does not have lines underlying most of the shell lines. The modifications necessary if $F_c^{(1)}$ is not constant are obvious. The total flux that we receive from the shell depends on the area of the shell. If $f_c^{(2)}$ is the flux in the continuous spectrum of the shell per unit area of the shell, then

$$F_c^{(2)} = f_c^{(2)} a^{(2)}, \tag{16}$$

where $a^{(2)}$ is the projected area of the shell. To a first approximation $f_c^{(2)}$ is a constant over the shell. This flux can be found by solving the equation of transfer for the shell under the appropriate boundary conditions. Similarly, we can write

$$F_\nu^{(2)} = f_\nu^{(2)} a^{(2)}, \tag{17}$$

where $f_\nu^{(2)}$ is the flux per unit area produced by the shell in frequency ν. Also we have

$$F_c^{(1)} = f_c^{(1)} a^{(1)}, \tag{18}$$

where $f_c^{(1)}$ is the flux per unit area produced by the B8 star in the continuous spectrum and $a^{(1)}$ is the area of the B8 star presented to us. The observed absorption in a line of spectrum 2 referred to the observed continuous spectrum, then, is

$$A_2(\nu) = \frac{(f_c^{(2)} - f_\nu^{(2)})\, a^{(2)}}{f_c^{(1)} a^{(1)} + f_c^{(2)} a^{(2)}} = \frac{f_c^{(2)} - f_\nu^{(2)}}{f_c^{(2)}} \left[1 - \frac{f_c^{(1)} a^{(1)}}{f_c^{(1)} a^{(1)} + f_c^{(2)} a^{(2)}}\right]. \tag{19}$$

Hence the observed absorption is a fraction $[1 - F_c^{(1)}/(F_c^{(1)} + F_c^{(2)})]$ of the absorption,

$$A^{(2)}(\nu) = \frac{f_c^{(2)} - f_\nu^{(2)}}{f_c^{(2)}}, \tag{20}$$

produced by the shell acting as a stellar atmosphere. The measured equivalent width of a line in spectrum 2 is

$$W_2 = \int_0^\infty A_2(\nu)\, d\nu = W^{(2)} \left(1 - \frac{F_c^{(1)}}{F_c^{(1)} + F_c^{(2)}}\right), \tag{21}$$

where we have written

$$W^{(2)} = \int_0^\infty A^{(2)}(\nu)\, d\nu. \tag{22}$$

That is, $W^{(2)}$ is the true equivalent width of the line formed in the shell. The correction factor $[1 - F_c^{(1)}/(F_c^{(1)} + F_c^{(2)})]$ is practically constant over the wave-length region that we have studied and affects the curve of growth by altering the vertical shift. Hence this shift cannot be used to determine the relative velocity of the particles in the shell with respect to those in the sun, for the unknown factor $[1 - F_c^{(1)}/(F_c^{(1)} + F_c^{(2)})]$ is included. However, this correction factor does not affect the horizontal displacements necessary to form a curve of growth. Consequently, the analysis based on these shifts and carried through above is correct. Any exact treatment of the problem of radiative transfer in the shell must take account of the dependence of the emitted flux per unit area, $f_\nu^{(2)}$, on the incident flux from the underlying star, on the shape of the shell (edge-effects), and on the distance of the shell from the exciting star (dilution effects).

VI. THE CONTRACTING SHELL

If, as a first approximation, we consider the motion of this shell to be uniform, we can analyze the contracting shell in the same way that we have analyzed the rotating shell,

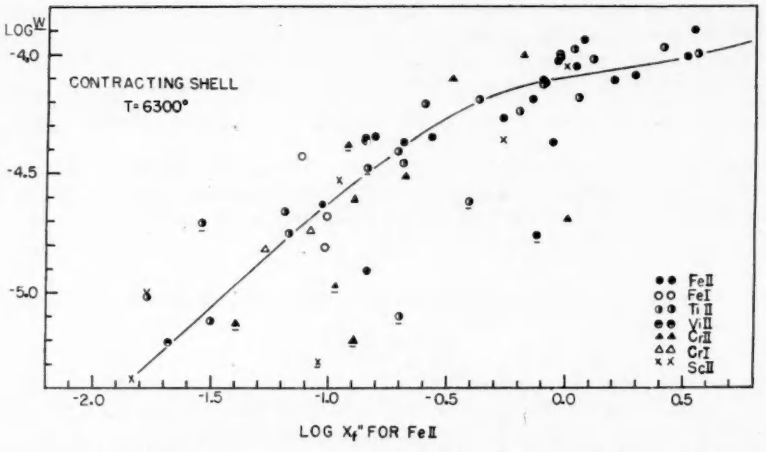

FIG. 5.—The curve of growth for the collapsing shell. A dash under a symbol indicates that log X_f for that point is uncertain.

for uniform motion in the line of sight does not affect the curve of growth.[8] However, the assumption of uniform motion is a very rough approximation; for the known variations in the radial velocity of the shell suggest that sometimes this shell is contracting and sometimes it is expanding. The accuracy of the results that we obtain will not be high because of the questionable validity of our assumption of uniform motion, but we should get a rough idea of the conditions in this shell from a curve-of-growth analysis.

Figure 5 gives the curve of growth for the contracting shell. It was formed in the same way as that for the rotating shell and is plotted for an excitation temperature of 6300°. The curve drawn is Wright's solar curve of growth displaced to fit the data. The horizontal displacements between *Fe* I and *Fe* II and between *Cr* I and *Cr* II can be used to determine the electron pressure in this shell. Table 5 gives the resulting pressure, density, electron pressure, and electron density for a number of values of the ionization temperature. These values are calculated for the dilution factor $W = 1$. If $W \neq 1$, the P_e and n_e must be reduced by the factor W. The density is, on the average, about 0.6 that

in the rotating shell. This lower density is consistent with the idea that this shell lies outside the rotating shell.

With the densities found, we can calculate the optical depth of a path length of 10^{10} cm in this shell. The values obtained are given in Table 6. Since the lines formed in this shell are saturated (if the observed curvature in the curve of growth can be so interpreted), we can argue from the strength of the lines that the thickness of this shell must be of the order of $R_\odot$. Under these circumstances the shell is certainly optically thick for radiation in the Lyman continuum, and possibly so for radiation in other regions of the spectrum. The ionization in this shell is likely controlled by a local temperature of the order of 8000° and an electron density of the order of 10^{12}–10^{13}.

TABLE 5

THE DENSITY IN THE CONTRACTING SHELL

T_{ion}	12,600°	10,080°	8400°	7200°
log P_e *Fe*	2.80	1.77	0.79	−0.15
Cr	3.50	2.58	1.71	+0.87
Mean log P_e	3.15	2.18	1.25	+0.36
n_e	8.0×10^{14}	1.1×10^{14}	1.6×10^{13}	2.3×10^{12}
log P	3.47	2.54	1.75	+1.19
n	1.7×10^{15}	2.5×10^{14}	5.0×10^{13}	1.6×10^{13}

TABLE 6

THE OPTICAL THICKNESS, $\tau\lambda$, FOR A PATH LENGTH OF 10^{10} CM IN THE CONTRACTING SHELL

T_{ion}	λ 763	λ 1570	λ 4500
12,600°	5.05×10^{6}	4.47×10^{2}	9.20×10^{2}
10,080°	2.67×10^{6}	21.7	27.4
8,400°	1.21×10^{6}	0.101	0.749
7,200°	6.22×10^{5}	4.83×10^{-2}	2.21×10^{-2}

VII. DISCUSSION

The separation of the shell of Pleione into two distinct parts, one rotating and lying inside the other, which is contracting, is a rough way of analyzing a complex situation, but it brings out the main features of the shell. There is little doubt that the shell undergoes two motions, rotation and motion in the line of sight. In February, 1946, the latter motion was toward the star; however, at other epochs this motion may be different. We may ask if there can be local thermodynamic equilibrium in such a system which is not in a state of secular equilibrium. Unless the changes are very rapid, there seems no reason why there might not be local thermodynamic equilibrium. We have little compunction in applying the concepts of local thermodynamic equilibrium to the atmospheres of cepheid variables, and the changes in velocity of the shell of Pleione are less rapid than those of cepheids. The data of Tables 4 and 6 show that the shell is optically thick for radiation from a B8 star (T_{ion} = 12,600°). Consequently, the incident radiation from the B8 star will be redistributed in the shell, and we shall have a state close to thermodynamic equilibrium at a lower temperature. The excitation and ionization of the metals in the shell will depend on the opacity of the shell in each wave length at any epoch and will approach the values for thermodynamic equilibrium as the shell becomes more dense.

The history of the relative ionization of the metals in the shell of Pleione and the fact that the relative strengths of the lines from the ionized metals are now similar to those observed in α Cygni suggest that at first the shell was not optically thick in all wave lengths but that in 1946 it was more nearly so. The present evidence indicates that in February, 1946, the electron density, n_e, in the shell of Pleione was of the order of 10^{12}–10^{13}; that the density of particles, n, was of the order of 10^{13}–10^{14}; and that the geometric dilution factor had little to do with the excitation of the lines. A pure hydrogen atmosphere at the densities given above will be opaque to radiation of temperatures of the order of 12,000° if the path length is close to 10^{10} cm. Such a path length is a conservative estimate for the extent of the shell of Pleione.

Struve[27] has shown that the *Mg* II line, λ 4481, and the *Si* II doublet λ 4128, λ 4130 are greatly weakened if the radiation field is dilute; for the lower levels of these lines will then be depopulated. When we compare our values of $-\log W/\lambda$ for λ 4481 (Table 2) with those given by Greenstein[20] for some F stars, we see that λ 4481 is indeed weak in the shell of Pleione. This observation can be explained by postulating that the radiation field in the shell is dilute and that the temperature of the exciting radiation is about 12,600°. However, such a conclusion is in direct contradiction to the results that we have deduced from our study of the metallic lines of low excitation, and we must consider whether another explanation can be found for the weakness of λ 4481.

We have two limiting cases: (1) the shell is optically thin, hence the excitation to the lower level of λ 4481, 3^2D of E.P. 8.8 volts, is governed by equation (6) with $T = 12{,}600°$ and $W = 0.061$; and (2), the shell is in near thermodynamic equilibrium at a lower temperature than that of the exciting star. Then the excitation to the level 3^2D of *Mg* II is governed by equation (6) with $T = 8{,}400°$ (say) and $W = 1.0$. In the first case $\log n_{r,s}/n_r = -4.03$; in the second case $\log n_{r,s}/n_r = -4.58$. The second case gives a weaker *Mg* II line than the first. Hence we cannot say that the observed weakness of λ 4481 in comparison to the strength of the metallic lines in any way contradicts our conclusion that the shell is optically thick and that the geometric dilution factor has little direct effect on the excitation of the atoms to upper levels. From this analysis we might rather ask, Why is the line λ 4481 so strong in F stars? The strength of the lines of high-excitation potential in stars of comparatively low effective temperature is connected with the transparency of the stellar atmosphere to continuous radiation of the appropriate wave lengths for the excitation of these lines. In transparent regions we look through the stellar atmosphere to layers of high temperature. However, in a shell we can look through only to layers of a temperature equal to the effective temperature of the underlying star. There is no undiluted source of radiation of higher temperature than this, as there is when we look deep into a stellar atmosphere. Consequently, in a shell which is in a state of near thermodynamic equilibrium, necessarily at a lower effective temperature than that of the exciting star, we do not get the enhanced excitation of lines of high-excitation potential that is observed in ordinary stars. The observed weakness of the *Mg* II line λ 4481 in the shell should be taken as a confirmation of the conclusion reached from other evidence that the shell is in a state near to thermodynamic equilibrium rather than as a contradiction to this conclusion. It would be difficult to explain strong lines of λ 4481 and λ 4128 or λ 4130 in the shell of Pleione.

The visibility of the B8 spectrum cannot be taken as direct evidence that the shell is optically thin, for the shell may be concentrated in an equatorial ring. If this is so and the shell is optically thick, the width of the *Mg* II line λ 4481 does not give the equatorial velocity of rotation of the B8 star, but a value somewhat less than this. (The axis of rotation is assumed to be perpendicular to the line of sight in all this discussion.) Consequently, it is probable that the geometric dilution factor is less than the estimate, 0.061, given, and the radius of the shell, r, is greater than $2.08R$.

[27] *Physica*, **12**, 739, 1946.

The effective reduction of gravity in the shell due to rotation is

$$g_{\text{rot}} = \frac{v_s^2}{r} = 4.5 \times 10^2 \text{ cm/sec}^2 , \tag{23}$$

where v_s is the velocity of rotation of the shell, 140 km/sec, and if we put $R = 3R_\odot$. Since the gravitational attraction at the distance r is $0.23g$, or 2.3×10^3 if $g = 10^4$ for the B8 star, the net acceleration of gravity acting on the material in the shell is about 2.0×10^3 cm/sec^2.

In deriving the dilution factor, we have assumed that the lobes of the shell are invisible. However, our conclusion that the shell is optically thick suggests that this may not be so. We know that the lobes of the shell are visible in the hydrogen emission lines. A measurement of the width of these lines should indicate whether the true velocity of rotation of the inner shell, v_s, is 140 km/sec or whether it is 67 km/sec, the value we obtain from the width of the shell absorption lines. If the latter value is correct, then

$$W = \frac{1}{2}\left\{1 - \sqrt{1 - \frac{v_s^2}{v_0^2}}\right\} = 0.014 . \tag{24}$$

With this value of W we find that the radius of the shell is $4.37R$.

I am grateful to Dr. Jesse L. Greenstein for lending me the coudé plates and for calling my attention to the interesting shapes of the absorption lines of the shell of Pleione in February, 1946. I am also indebted to Dr. Bengt Strömgren for many fruitful discussions of the problems of the shell of Pleione.

LUMINOSITY DISTRIBUTION AND PROPER MOTIONS OF TENTH-MAGNITUDE K STARS

F. K. EDMONDSON, A. N. VYSSOTSKY, AND EDITH M. JANSSEN
Goethe Link and Leander McCormick Observatories
Received May 31, 1949

ABSTRACT

Absolute luminosities and proper motions have been determined for 681 K stars between 10.0 and 11.0 photovisual magnitude in a sampling of the entire sky north of −25°. It is found that some 85 per cent of these stars in low latitudes are giants, and approximately 75 per cent in higher latitudes. Thus the galactic concentration of the K giants is very low.

Since the dispersions in the motions of the higher-latitude giants and their group motion with respect to the sun appear to be considerably larger than average, it is inferred that they are characterized by larger-than-average eccentricities in their orbits around the galactic center.

I. INTRODUCTION

This paper deals with part of the results of an observational program[1] to survey the distribution, radial velocities, proper motions, and luminosities of more than 1000 faint A and K stars. The program stars were chosen from the two McCormick proper-motion catalogues,[2,3] and in most cases slit spectrograms were obtained with the McDonald 82-inch reflector. For the rest, spectrograms secured with the Mount Wilson 60-inch were kindly put at our disposal by Professor S. A. Mitchell. The observational material will be presented in detail in the *Publications of the Goethe Link Observatory*.

In all, 732 faint K stars were selected for observation. In general, the McCormick photovisual magnitude was between 10.0 and 11.0, and the McCormick spectral type either K0 or K2. The stars were selected without regard to the size of the proper motion. As far as possible, these 732 stars are uniformly distributed from the North Pole to declination −25°; in other words, a given area in high latitudes contains as many program stars as an equal area in low latitudes.

Of the 732 stars, 23 were subsequently found to be either earlier than G8 or later than K3. In addition, there were 28 stars for which the luminosity class could not be determined with confidence because of inferior plate quality. Thus luminosity classes have been assigned to 681 G8–K3 stars of average photovisual magnitude 10.4. These constitute the material of the present discussion.

The observational program was initiated by Edmondson and carried through under his supervision; Vyssotsky contributed some spadework in the early phases of the project and the discussion of the proper motions and luminosities; Miss Janssen has estimated the absolute luminosities and spectral types.

II. DETERMINATION OF LUMINOSITY AND SPECTRAL CLASS

The Yerkes system of classification[4] was followed after a careful study of numerous spectrograms of 23 bright standard stars; these were obtained with the same equipment as that used for the program stars. However, it was necessary to modify the Yerkes criteria somewhat, since the dispersion was small (152 A/mm) and the quality of the spectrograms of the program stars was not always high because of the long exposures re-

[1] Edmondson, *A.J.*, **51**, 19, 1944.

[2] *Pub. McCormick Obs.*, Vol. **7**, 1937. [3] *Pub. McCormick Obs.*, Vol. **10**, 1948.

[4] Morgan, Keenan, and Kellman, *An Atlas of Stellar Spectra* (Chicago: University of Chicago Press, 1943).

quired. The following pairs of lines were used: for absolute luminosity, λλ 4077 and 4072, 4077 and 4063, 4077 and 4132, 4215 and 4260, and, finally, the strength of the *CN* band head at λ 4215; for spectral class, λλ 4030–4034 and 4300, 4096 and 4100, 4144 and 4100, 4290 and 4300, 4290 and 4340, 4406 and 4340, 4325 and 4340, and, finally, 4045 and 4227.

Numerical estimates of intensity ratios for each pair of lines were recorded as well as intensity estimates of the *CN* band. However, the adopted classification depended also to some extent on the general impression of the continuum of the spectrum. Since, in general, only one spectrogram was available for each star, obviously no great refinement was possible in the determination of luminosity. Consequently, the only stars assigned to the "in-between" classes such as III+ (i.e., III–IV in the Yerkes notation) were those which appeared to be precisely halfway between the integral classes. Throughout the entire period during which Miss Janssen was working with the spectrograms, she had no knowledge of the proper motion of any particular star or of its position in the sky. This was to insure freedom from bias.

TABLE 1

INTERNAL PROBABLE ERRORS

	Luminosity Class						
	I, I+, II	II+	III	III+	IV	IV+	V
Probable error of one plate	$\pm 0^m.5$:	$\pm 0^m.4$:	$\pm 0^m.42$	$\pm 0^m.44$	$\pm 0^m.46$	$\pm 0^m.4$:	$\pm 0^m.29$
No. of stars	14	7	57	34	40	15	41

TABLE 2

PROBABLE ERRORS FROM DUPLICATE SPECTROGRAMS

Two spectra estimated in succession	$\pm 0^m.52$
Two spectra estimated at different times	$\pm .73$
Three spectra	± 0.75

An alternate, purely numerical luminosity classification was later computed from the recorded line and band estimates. These alternate classifications seldom differ by more than half a spectral class from the original classification; their purpose will appear in various subsequent sections, where they will be referred to as "computed" classifications. They are not the adopted classifications, however.

III. ACCIDENTAL ERRORS OF CLASSIFICATION

An evaluation of the accidental errors in the luminosity classification is important for a determination of the true luminosity distribution from the observed distribution. We have approached this in two ways. Using random samples of the material, we have derived internal probable errors (Table 1) from the interagreement of the various line estimates for a given spectrogram. These must be regarded as minimum values, since in making an estimate the observer is inevitably influenced by other estimates from the same spectrogram. A second method is afforded by the cases in which more than one spectrogram were available for one star. Thus there were 79 stars with two spectrograms and 9 additional stars with three spectrograms. For 39 stars of the first group, line-intensity estimates from the two spectrograms were made within a short time interval. For the other 40 stars the line intensities from the second spectrogram were estimated after an interval of many days. The interagreement of the "computed" classifications yields the probable errors in Table 2. Since in several cases a duplicate spectrogram was

obtained because of the inferiority of the first one, we regard the values in the last two lines of Table 2 as possibly slightly excessive and consequently have adopted ± 0.7 mag. as the probable error of a luminosity assigned from one plate.

IV. OBSERVED LUMINOSITY DISTRIBUTION

The frequency distribution of the adopted luminosities is shown in Table 3. Because of the relatively large error of classification and since the frequency is greatest in class III, it is obvious that most of the stars classified as II+ and III+ really belong to class

TABLE 3

OBSERVED NUMBERS OF K STARS

ADOPTED LUMINOSITY CLASS	LATITUDE ZONE		
	0°–30°	31°–90°	0°–90°
I	3	.....	3
I+	2	.....	2
II	6	4	10
II+	4	4	8
III	251	189	440
III+	21	25	46
IV	46	48	94
IV+	6	14	20
V	20	38	58
Total	359	322	681

TABLE 4

OBSERVED NUMBERS OF K STARS REDUCED TO 10 SQUARE DEGREES

LUMINOSITY CLASS	LATITUDE ZONE		RATIO LOW : HIGH
	0°–30°	31°–90°	
I, I+, II	1.6	0.3	5:
II+, III, III+	41	17	2.4
IV, IV+	8	5	1.6
V	3	3	1:

III. Consequently, to reduce the number of subdivisions in the further discussion, we have grouped the classes as indicated in Table 4.

By means of the spectral statistics of the Second McCormick Catalogue[3] corrected for incompleteness, the average number of K0 and K2 stars between 10th and 11th magnitudes for an area of 10 square degrees was found to be 53 in latitudes 0°–30° and 25 in latitudes 31°–90°. When these values are combined with the figures in Table 3, we obtain Table 4. Here we see from the last column that the apparent galactic concentration increases from the dwarfs to the supergiants, as is to be expected. That the proportion of giants in higher latitudes is so large was not expected, however.

It is interesting to compare this observed luminosity distribution in low latitudes with

the distribution found in a discussion[5] of Stenquist's spectrophotometric investigation of the Cambridge proper-motion stars. In Table 5 the limiting absolute magnitudes for the arbitrary luminosity groupings of Stenquist's material have been chosen so that the percentages may be about the same as those in our own low-latitude material. It is seen that these arbitrary limiting magnitudes are in good agreement with those usually assigned to delimit supergiants, giants, subgiants, and dwarfs. It should be noted that Stenquist based his determination of absolute magnitude on spectrophotometric tracings of the continuous spectrum,[6] and thus his results are from an independent approach.

TABLE 5

COMPARISON WITH STENQUIST'S LUMINOSITY DISTRIBUTION FOR K STARS BETWEEN 10.0 AND 11.0 MAG.

PRESENT MATERIAL		STENQUIST	
Luminosity Class	0°–30° (Per Cent)	M_{pv}	0°–20° (Per Cent)
I, I+, II	3	<-0.5	4
II+, III, III+	77	-0.5 to $+1.9$	78
IV, IV+	14	$+2.0$ to $+4.4$	13
V	6	$>+4.4$	5

TABLE 6

SECULAR PARALLAXES (CENTENNIAL MOTIONS)

LUMINOSITY CLASS	0°–30°		31°–90°		0°–90°	
	R.A.	Decl.	R.A.	Decl.	R.A.	Decl.
I, I+, II	.....	.....	.....	.....	$+0''.2\pm0''.4$	$-0''.2\pm0''.4$
II+, III, III+	$+0''.8\pm0''.2$	$+0''.6\pm0''.1$	$+1''.3\pm0''.2$	$+1''.4\pm0''.2$	.....	.....
IV, IV+	$+2.3\pm0.4$	$+1.5\pm0.4$	$+2.3\pm0.4$	$+1.7\pm0.4$	$+2.3\pm0.3$	$+1.6\pm0.3$
V	.....	.....	.....	.....	$+3.9\pm0.7$	$+4.2\pm0.7$

V. SECULAR PARALLAXES AND DISPERSIONS

Using the conditioned motions described in section 1.5 of the Second McCormick Catalogue,[3] we have derived secular parallaxes for stars in each of the four luminosity groups. In the case of the larger groups, the material was subdivided according to galactic latitude. In every case parallaxes were derived from the motions in right ascension separately from those in declination. In Table 6 the agreement between the two values for any particular group of stars is seen to be satisfactory. This would appear to indicate that the proper motions are fairly free from systematic errors. Consequently, the two sets of values have been combined in Table 7. The unexpectedly large value of the parallax for the giants in high latitudes appears in both hemispheres; from $+31°$ to $+90°$ it is $1''.15$ and from $-31°$ to $-90°$ it is $1''.64$, the difference being no larger than is to be expected

[5] Vyssotsky and Williams, *A.J.*, **53**, 83, Table 8.IX, 1948.

[6] Stenquist, *Medd. Upsala*, No. 72, 1937.

from the probable errors. This feature will be discussed later. In other respects the general run of the values is quite satisfactory.

Parallaxes may also be obtained from the dispersions in the peculiar motions. These give reliable values when the average peculiar motion is large with respect to the observational errors. In the case of the stars of highest luminosity, however, the motions are so small that the corrected dispersions are extremely sensitive to the value adopted for the observational errors. In Table 8 the first column in each latitude grouping contains the average residual motion after the parallactic motion has been removed. Here n is equal to twice the number of stars given in Table 7, since we have residual motions both in right ascension and in declination. The second column in each grouping contains the value of the error of observation; these are taken from Tables 1.VII and 1.VIII of the

TABLE 7

COMBINED SECULAR PARALLAXES (CENTENNIAL MOTIONS)

Luminosity Class	0°–30°			31°–90°			0°–90°		
	$\overline{k/r}$	$\overline{m_{pv}}$	No.	$\overline{k/r}$	$\overline{m_{pv}}$	No.	$\overline{k/r}$	$\overline{m_{pv}}$	No.
I, I+, II	.....	.....	.....	.....	.....	.....	0".0±0".3	10.4	15
II+, III, III+	0".66±0".11	10.4	276	1".34±0".13	10.5	218	.....	10.4	494
IV, IV+	1.8±0.3	10.4	52	2.1±0.3	10.5	62	2.0±0.2	10.5	114
V	.....	.....	.....	.....	.....	.....	4.0±0.5	10.6	58

TABLE 8

DISPERSIONS OF PECULIAR MOTIONS (CENTENNIAL MOTIONS)

Luminosity Class	0°–30			31°–90°			0°–90°		
	$\Sigma\|v\|/n$	ϵ	σ	$\Sigma\|v\|/n$	ϵ	σ	$\Sigma\|v\|/n$	ϵ	σ
I, I+, II	.....	.....	.....	.....	.....	.....	0".77	0".63	0".1::
II+, III, III+	1".00	0".58	0".92	1".40	0".78	1".31	.....	.....	.....
IV, IV+	1.64	0.58	1.85	2.13	0.78	2.40	.....	.....	2.14
V	.....	.....	.....	.....	.....	.....	3.84	0.73	4.68

Second McCormick Catalogue. For the errors of the brightest luminosity group, allowance was made for the fact that most of the observed stars are in low latitudes, whereas for the faintest luminosity group they are mostly in high latitudes. The last column in each grouping contains the dispersions in the peculiar motions (centennial) as computed from the items in the other two columns. We have combined the dispersions in the two latitude zones for the subgiants into a mean value for the whole sky; this has not been done for the giant group, however, since in this case the difference between the value in the low zone and that in the high zone is large with respect to its probable error. The larger value in higher latitudes appears in both hemsipheres, the two values being nearly identical. This will receive further attention in the last section.

VI. ABSOLUTE MAGNITUDES OF THE LUMINOSITY CLASSES

There are several ways of evaluating the mean absolute magnitude of our luminosity classes. Since the classification rests on the spectra of 23 bright standard stars, we have

derived mean absolute magnitudes from their individual values taken from the Mount Wilson catalogue[7] and the Yerkes *Atlas*. These mean values are given in the third column of Table 9. In the fourth column are contained mean absolute magnitudes derived from the luminosity distribution of Stenquist's K0 and K2 stars between the arbitrary luminosity limits adopted in Table 5 (cf. Table 8.IX of Second McCormick Catalogue). The secular parallaxes in Table 7 also yield determinations of $\bar{M}_v$; the values listed in the fifth column are computed with no allowance for interstellar absorption and with an assumed solar velocity of 20 km/sec. Finally, the dispersions in Table 8 have been used to obtain the values in the last column; these were also derived without any allowance for interstellar absorption. The dispersions in kilometers per second (mean value for three axes) for the giants and subgiants have been assumed as 32 and 28, respectively, from the preliminary discussion of the radial velocities of these stars;[8] for the dwarfs the dispersion of 24 km/sec has been taken from Table 10.I of the Second McCormick Catalogue.

Very good agreement is found in Table 9 for the mean absolute magnitude of the dwarfs, and it is fairly good for the subgiants; from this we infer mean distances of 110 and 240 parsecs, respectively. In the giant group, however, we encounter inconsistencies. The relatively faint absolute magnitudes found from the motions in low latitudes may

TABLE 9

MEAN ABSOLUTE MAGNITUDES, M_v

Luminosity Class	Latitude	Standard Stars	Stenquist	Secular Parallax	Dispersion
I, I+, II	0°–90°	-2^m:	-0^m8	.....	0^m::
II+, III, III+	0 –30	+0.6	+0.6	+1.4	+1.1
	31 –90		.....	+3.0	+1.9
IV, IV+	0 –90	+3.:	+3.1	+3.9	+3.3
V	0 –90	+5.5	+5.9	+5.4	+5.4

be attributed, at least in part, to the effects of interstellar absorption. In higher latitudes the disagreement is much worse, and we must look to something other than absorption for the explanation. This will be considered in the last section.

VII. TRUE DISTRIBUTION OF LUMINOSITIES

The figures of the observed distribution of luminosities given in Table 3 are somewhat misleading, in that they tend to give the impression of a separate maximum corresponding to luminosity group IV. However, the distribution of the stars when grouped according to the "computed" classification described in the second section shows no such maximum (Table 10); for, whereas in Table 3 the limits for the group III+ are approximately III.4–III.6, those in Table 10 are III.25–III.75.

It is of interest to attempt an estimate of the true numbers of subgiants. Combining the probable error of an assigned luminosity, ± 0.7 mag., with the very careful determination by Russell and Moore[9] of the true dispersion among giants of a given spectral type, ± 1.0 mag., we find that probably at least half the stars classified as subgiants are really giants. This means that giants constitute about 85 per cent of all the K stars of apparent magnitude 10.4 in low latitudes and approximately 75 per cent of those in higher latitudes

[7] Adams, Joy, Humason, and Brayton, *Mt. W. Contr.*, No. 511, 1935; *Ap. J.*, **81**, 187, 1935.

[8] Edmondson, *A.J.*, **54**, 35, 1948.

[9] *Mt. Contr.*, No. 636, 1940; *Ap. J.*, **92**, 354, 1940.

and that among these K stars the true number of subgiants is probably no greater than the true number of dwarfs. In this connection we may note that the number of bright stars individually known to be subgiants is small and their absolute magnitudes are rather poorly determined.

Since the question is of considerable interest, we have examined the distribution of total motions in each luminosity group in the hope that it would shed light on the problem (Table 11). From the fact that five of the stars in the subgiant group have motions greater than 0".100, we may infer that there is a liberal admixture of dwarfs as well as of giants in this group. In fact, it is possible to reproduce the frequency distribution among the subgiants fairly closely by assuming that the motions of three-quarters of the stars

TABLE 10

NUMBER OF K STARS ("COMPUTED" CLASSIFICATION)

LUMINOSITY CLASS	LATITUDE ZONE		
	0°–30°	31°–90°	0°–90°
I	2	.....	2
I+	4	.....	4
II	8	6	14
II+	23	28	51
III	197	135	332
III+	58	53	111
IV	42	43	85
IV+	13	34	47
V	12	23	35
Total	359	322	681

TABLE 11

DISTRIBUTION OF TOTAL PROPER MOTIONS*

TOTAL PROPER MOTION	I, I+, II	II+, III, III+		IV, IV+		V	
	0°–90°	0°–30°	31°–90°	0°–30°	31°–90°	0°–30°	31°–90°
0".000–0".003	1	12	6	.....	2	1	.....
.004– .006	1	31	14	2	7	.....	.....
.007– .009	5	37	18	10	2	.....	1
.010– .015	5	69	35	10	13	.....	5
.016– .025	1	82	74	12	16	6	.....
.026– .039	2	33	45	12	8	4	9
.040– .063	.....	9	19	2	9	5	4
.064– .099	.....	3	7	2	2	2	8
.100– .158	.....	.....	.....	1	.....	2	8
.159– .252	.....	.....	.....	1	2	.....	3
0.253–0.398	.....	.....	.....	.....	1	.....	.....
Total	15	276	218	52	62	20	38

* It should be borne in mind that this is the observed distribution; for the true distribution the figures must be corrected for the effect of the observational errors.

follow the observed distribution among the giants and that the motions of one-quarter follow the observed distribution among the dwarfs.

The viewpoint underlying this program has been that it is preferable to have a single spectrogram for each of 700 K stars than two each for 350 K stars because of the great dispersion in their motions. This viewpoint is now justified, since it is apparent from this discussion that a negligible number of giants have been classified as dwarfs, and conversely. Furthermore, to make sure of the subgiant character of any particular star would certainly require more than two spectrograms each.

We must consider also the difference between the true luminosity distribution of the giants in low latitudes and that in higher latitudes. Both Table 3 and Table 10 show a somewhat greater proportion of giants classified as III+ in high latitudes, as would be expected. However, at most, the mean luminosity of the giant group in high latitudes would exceed that of the same group in low latitudes by only 0.2 or 0.3 mag.; and this is not nearly sufficient to account for the absolute magnitudes derived from the secular parallaxes and dispersions in high latitudes (Table 9). Moreover, since the secular parallax derived from the motions in right ascension is in good agreement with that from the motions in declination and since the northern and southern zones are in agreement as to its large value, it appears inadmissible to attribute the difficulty to systematic errors in the proper motions.

This leaves us as the only alternative the supposition that 20 km/sec is not the appropriate solar velocity for the high-latitude giants and that the dispersion in the space motions at large distances from the plane of the Milky Way is greater than that assumed. This explanation, indeed, appears to be the correct one; it agrees with the previous finding[10] that stars having higher-than-average orbital inclinations tend to have larger-than-average orbital eccentricities, and, as a consequence, the solar velocity with respect to these stars will be relatively large, as will also be the dispersions in their motions. In other words, the high-latitude K giants at distances of some 600 or 700 parsecs from the galactic plane must have larger-than-average inclinations, and consequently we expect larger dispersions in their motions and a greater value of the solar velocity. Another indication that this is the correct interpretation lies in the fact that the dispersions found from the preliminary discussion of these faint K stars in all latitudes[8] are considerably larger than those found from bright K stars, which, on the average, are much closer to the galactic plane and hence, on the average, have smaller orbital inclinations. More light will be thrown on this subject when the final discussion of the radial velocities has been completed.

The authors are indebted to Dr. E. T. R. Williams for valuable discussion of various aspects of this project and also to all those who took part in the observing program with the McDonald telescope.

The work of classifying the spectra was carried through at the University of Virginia; it was supported in part by a grant from the Draper Fund of the National Academy of Sciences and a similar grant from the Indiana University Graduate School Research Fund.

We also acknowledge appreciatively the substantial financial help from the Research Fund of the Indiana University Graduate School, without which the observing program would not have been possible.

[10] Williams and Vyssotsky, *A.J.*, **53**, 101, 1948.

COLOR EXCESS, TOTAL PHOTOGRAPHIC ABSORPTION, AND THE DISTANCE OF THE DARK CLOUD IN THE AQUILA REGION OF THE MILKY WAY*

HAROLD F. WEAVER
Lick Observatory
Received June 20, 1949

ABSTRACT

In an area of nearly 15 square degrees centered at $\alpha(1900) = 19^h01^m6$, $\delta(1900) = 8°19'$, magnitudes, colors, and spectral classes were determined for all stars (388 in number) brighter than $m_{pg} = 12.0$. Star counts, both pg and pv, also were made in the area for all stars brighter than $m_{pg} = m_{pv} = 14.0$. Approximately 1900 stars were included in the pg counts, 3400 in the pv counts.

The magnitudes, colors, and spectral classes were used for the derivation of the color-excess–distance-modulus relationship, $\gamma(y)$, in the area.

The function $\gamma(y)$, combined with the van Rhijn luminosity functions and the star counts, was used to evaluate χ, the ratio of total photographic absorption to selective absorption, both on the International System. In an area as heavily obscured as the dark rift in the Milky Way in Aquila, χ is relatively insensitive to variations in the luminosity function or in the density law. A final value of $\chi = 3.4 \pm 0.2$ was derived.

With the value $\chi = 3.4$ and the observed function $\gamma(y)$, the distance, extent, and opacity of the dark cloud in Aquila were determined. The very dark front edge of the cloud is only 110 parsecs distant; over the distance range 110–260 parsecs, the cloud has the very large absorption coefficient 7.4 mag/kpc. Within the distance range 260–350 parsecs the absorption coefficient of the cloud is 0.75 mag/kpc. Beyond the distance 350 parsecs the cloud, of at least a kiloparsec total extent, has an absorption coefficient of 3.2 mag/kpc. The cloud has a total extent of at least 1 kiloparsec.

I. INTRODUCTION

The present investigation is concerned with a portion of the dark rift in the Milky Way in the constellation Aquila. The region studied[1] (hereafter denoted by "R"), of irregular outline to avoid obvious large-scale inhomogeneities in the interstellar material and to stay within a circle of prescribed radius on the Schmidt films, covers an area of 14.98 square degrees centered at $\alpha_{1900} = 19^h01^m6$, $l = 9°.9$; $\delta_{1900} = 8°19'$, $b = -0°.9$.

The principal purposes of this investigation are: (i) the determination of the relationship between color excess and distance modulus in the direction of R; (ii) the evaluation of the dimensionless constant χ, the ratio of photographic absorption to color excess; and (iii) the transformation of the color-excess–distance-modulus relationship found in (i) to a total photographic-absorption–distance relationship, and a determination of the distance, extent, and opacity of the obscuring cloud or clouds in R.

II. THE OBSERVATIONAL DATA

The observational data upon which this investigation is based consist of (i) photographic magnitudes, colors, and spectral classes for all stars located within R and brighter than $m_{pg} = 12.0$ and (ii) photographic and photovisual counts of stars brighter than magnitude 14.0. All magnitudes are on the International System.

THE MAGNITUDES

The magnitudes were determined with the 18-inch Schmidt telescope at Palomar. For photometric comparisons only half the film was exposed at one time. The polar sequence

* *Contributions from the Lick Observatory*, Ser. II, No. 24.

[1] See Fig. 1.

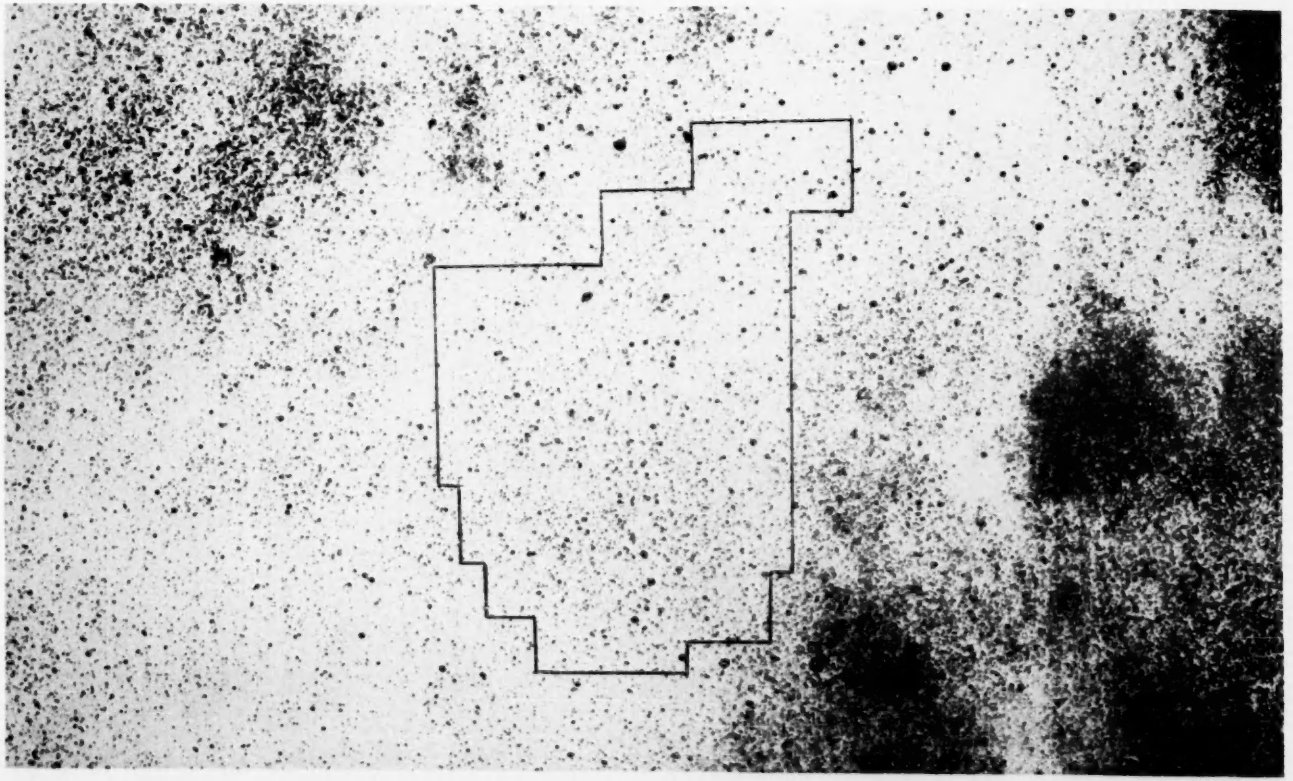

FIG. 1.—The region studied outlined on a copy of a portion of Plate 13 of the Ross-Calvert *Atlas of the Milky Way*. North is at the top; west at the left

was photographed on one half of the film, the area under study on the other half. The center of each area photographed was thus a short distance from the center of the film. Unpublished investigations made at Mount Wilson indicate that this procedure does not introduce systematic distance-from-center errors in the magnitudes; it does eliminate appreciable errors produced by the superposition of two fields, with consequent post-fogging of one field, pre-fogging of the other.[2]

For the determination of photographic magnitudes Eastman 103-O films were used. Five polar comparisons were made; exposure times ranged from 30 seconds to 5 minutes. For the determination of photovisual magnitudes Agfa Triple S Ortho films were exposed behind a Wratten No. 5 filter. Exposure times for the five photovisual polar comparisons ranged from 1 to 7 minutes.

From these polar comparisons photographic and photovisual magnitudes were derived for a sequence of approximately 100 stars ranging in brightness from 6.4 to 14.5 mag. On the average, each sequence star was observed on three of the five polar comparisons, in each color.

Magnitudes of the field stars in R were determined from films showing only R; the photographic and photovisual magnitudes of the sequence stars served to establish the necessary magnitude scales. The magnitude of each field star was measured on at least two films.

Measurements of both the sequence stars and the field stars were made with an image-scale taken with the Schmidt telescope. The reductions of these photometric measurements were made in the customary manner. For each polar comparison, for example, the known magnitude of each polar-sequence star was plotted as a function of the image estimate of that star. The smooth curve best representing these plotted points was drawn, and the residuals (known magnitude *minus* magnitude read from the curve for the value of the image estimate) were determined.

Analysis of these residuals yielded the following color equations:

$$\begin{aligned} m_{pg,\,IS} &= m_{pg,\,Schmidt} + 0.020\, c_{IS}\,, \\ m_{pv,\,IS} &= m_{pv,\,Schmidt} - 0.029\, c_{IS}\,, \end{aligned} \tag{1}$$

where the subscript IS indicates that the quantity is on the International System.

In the derivation of equation (1) the assumption was made that Purkinje effect and distance-from-center errors were not present. This assumption was found to be fulfilled.

For the analysis of residuals, the stars were divided into several magnitude groups, in each of which all colors were represented. The color equations for these various groups do not differ significantly from the final color equation for the stars as a whole. The slight correlation between color and magnitude in the polar sequence has thus not influenced our final results for color equation.

The color equations (1) were used to transform the NPS magnitudes to the Schmidt system. These transformed magnitudes were replotted as functions of the NPS image estimates, and the reduction-curves were redrawn. From these corrected reduction-curves the magnitudes of the stars n the area sequence were determined from their image estimates. Where necessary, differential extinction was applied to the area stars.

The accuracy of this simple procedure can be judged from the sizes of the probable errors of a single measurement of a sequence star as determined from internal agreement:

$$\text{p.e.} = 0^{m}.058 \text{ (photographic)}\,,$$

$$\text{p.e.} = 0^{m}.061 \text{ (photovisual)}\,.$$

[2] Alter, Barber, and Edwards, *M.N.*, **100**, 529, 1940.

For a final mean magnitude of a sequence star the probable errors are

$$\text{p.e.} = 0^{m}.032 \text{ (photographic)},$$

$$\text{p.e.} = 0^{m}.034 \text{ (photovisual)}.$$

The probable error of the final mean magnitude of a field star is

$$\text{p.e.} = 0^{m}.045 \text{ (photographic)},$$

$$\text{p.e.} = 0^{m}.042 \text{ (photovisual)}. \quad (2)$$

SPECTRAL CLASSIFICATION

The spectral classes of all stars in R brighter than $m_{pg} = 12.0$ were derived from objective-prism spectra kindly taken by Dr. F. Zwicky. It is a pleasure to thank Dr. Zwicky for obtaining these excellent films.

The linear dispersion obtained with the objective prism on the 18-inch Schmidt telescope is such that the distance from $H\beta$ to the K line is very nearly 2.25 mm. The focus is good for the entire wave-length range recorded—from $H\beta$ to far beyond K in the ultraviolet. The cyanogen band at λ 3883 thus forms an easily visible criterion for separation of giants and dwarfs among the later-type stars.[3]

The stars were classified on the Victoria system[4] by the use of the line-intensity ratios given in Table 1. The various classification criteria were calibrated on the basis of spectra of stars for which Victoria classes were available.

TABLE 1

LINE-INTENSITY RATIOS USED IN SPECTRAL CLASSIFICATION

Stellar Type	Line Ratio	Stellar Type	Line Ratio
B	4026/$H\delta$	F, early G	$H\gamma$/4226
B8, B9	4471/4481	Late G, K	4045/4226
A	K/$H\delta$, K/H + $H\epsilon$	M	Intensity *TiO*

To judge from internal consistency, the probable error of an estimated spectral type is less than 0.1 class.[5]

THE STAR COUNTS

For all stars brighter than (i) $m_{pg} = 13.0$, and (ii) $m_{pv} = 12.0$, individual magnitudes are available for the whole of R, 14.98 square degrees in area. The number of these brighter stars per magnitude interval per square degree is thus easily established. For the fainter stars, $13.0 \leq m_{pg} \leq 14.0$, $12.0 \leq m_{pv} \leq 14.0$, the star numbers were interpolated from star counts made on Schmidt films of intermediate exposures on which the magnitude

[3] For the separation of stars into luminosity classes the method described by Smith, *Lick Obs. Bull.*, **18**, 39, 1937 (No. 484), was also found useful in some instances. In this procedure, which is particularly applicable to supergiants, the star in question is assigned to the luminosity class that will make its color excess and distance consistent with the general color-excess–distance-modulus relationship found from the stars as a whole in the area under investigation.

[4] *Pub. Dom. Ap. Obs. Victoria*, Vol. **3**, No. 1; *Trans I.A.U.*, **5**, 180, 1935.

[5] This means, however, only that the class assignments are consistent with the calibration-curves; it tells little about the consistency of the assigned types and the Victoria types. Because of the relatively small number of stars classified at Victoria, a direct comparison between the present system and the Victoria system is difficult. On the basis of indirect tests it appears that these two systems differ by no more than a fraction of a tenth of a class, except perhaps at G0. Here the systematic differences between the systems may be as great as 0.25 class. This latter value, however, rests upon a comparison of only seven stars, and is therefore quite uncertain.

sequence served to establish the magnitude scale. These star counts of fainter stars referred to a somewhat smaller area of 14.0 square degrees.

Transformation of the counts of the fainter stars to values on the International System was made with the aid of the color equations (1), and the mean color index of the stars in R as a function of magnitude.

Inasmuch as the photovisual counts must be used in connection with data based on the Harvard visual system (HV) they were transformed to HV by means of the average color equation derived by Seares:[6]

$$\mathrm{IPv} = \mathrm{HV} - 0.14\, c_{\mathrm{IS}} . \tag{3}$$

The final star counts, $A(m)$, the number of stars per magnitude (at the stated value of m) per square degree, are given in Table 2.

TABLE 2

NUMBER OF STARS PER MAGNITUDE INTERVAL PER SQUARE DEGREE IN AREA R

m	$A_{pg}(m)$	$A_v(m)$	m	$A_{pg}(m)$	$A_v(m)$
8.0	0.7	1.3	11.5	12.8	21.6
8.5	1.3	2.9	12.5	28.9	64.3
9.5	4.7	5.3	13.5	78.9	131
10.5	6.6	11.8			

III. THE COLOR-EXCESS–DISTANCE-MODULUS RELATIONSHIP

The color excess, E, of a star is the difference between the star's observed color, c, and intrinsic or absolute color, C,

$$E = c - C . \tag{4}$$

The apparent photographic distance modulus, y, of a star is the difference between the star's apparent photographic magnitude, m, and absolute photographic magnitude, M,

$$y = m - M . \tag{5}$$

The intrinsic color, C, and absolute magnitude, M, are assumed to be known for a star when the star's spectral and luminosity classes are known. Those stars in R for which magnitudes, color indices, and spectral classes are available thus furnish data from which the color-excess–distance-modulus relationship can be determined.

The apparent distance modulus, y, defined by equation (5), is related to true linear distance, r, by the equation

$$y = 5 \log \frac{r}{10} + a\,(r) . \tag{6}$$

Here r is measured in parsecs, and $a(r)$ represents the decrease in the star's photographic brightness (measured in magnitudes) caused by the absorption and scattering of the star's light by the interstellar medium.

For the determination of E for the stars in R the absolute color indices, C_s, derived by Seares and Miss Joyner,[7] were employed.

[6] *Ap. J.*, **41**, 284, 1925; *Mt. W. Contr.*, No. 288.

[7] *Ap. J.*, **98**, 261, 1943; *Mt. W. Contr.*, No. 684. I wish to thank Dr. Seares and Miss Joyner for communicating their color values in advance of publication.

For use in the present work the values of C_s tabulated by Dr. Seares and Miss Joyner as a function of HD spectral class have been transformed to the system of spectral classification used in this investigation.

The absolute magnitudes used in the calculation of the distance moduli of the stars were derived from a number of sources.[8] The spectral types from each of these sources were reduced to the Victoria system; the values of M were weighted on the basis of their independence and estimated accuracy. An abbreviated tabulation of the absolute magnitudes and colors adopted for the Victoria spectral system is given in Table 3.

With the M and C values from Table 3, color excesses and distance moduli were computed for all stars in R for which the necessary data were available. These individual values were then grouped according to y, and the normal points given in Table 4 were computed.

The values of $\bar{y}$ and $\bar{E}$ given in Table 4 are plotted in Figure 2. Mean errors of the $\bar{E}$-values are indicated by the lengths of the vertical lines through the plotted points. A

TABLE 3

ADOPTED ABSOLUTE PHOTOGRAPHIC MAGNITUDES AND COLORS (INTERNATIONAL SYSTEM) FOR THE VICTORIA SYSTEM OF SPECTRAL CLASSIFICATION

Sp.	Dwarfs		Giants	
	M_{pg}	C_s	M_{pg}	C_s
B3	−2.1	−0.53		
B5	−1.2	−0.43		
B8	−0.2	−0.28		
A0	+0.4	−0.15		
A2	+1.0	−0.05		
A5	+1.7	0.00		
A8	+2.2	+0.04		
F0	+2.7	+0.08		
F2	+3.0	+0.14		
F5	+3.6	+0.23		
F8	+4.2	+0.33	+1.2	+0.39
G0	+4.5	+0.40	+1.3	+0.47
G2	+4.9	+0.47	+1.3	+0.55
G5	+5.4	+0.58	+1.4	+0.69
G8	+6.0	+0.72	+1.5	+0.85
K0	+6.4	+0.82	+1.5	+0.98
K2	+6.9	+0.92	+1.5	+1.12
K5	+7.8	+1.08	+1.6	+1.33
M0			+1.4	+1.50

smooth curve representing the probable relationship of color excess and distance modulus is indicated in the diagram.

This curve of color absorption, which we shall denote by $\gamma(y)$, begins to rise, we note, at a value of $y = 6.0$, levels off between $y = 8.0$ and 9.0, and then begins to rise once more for $y > 9.0$. Physically, this behavior of $\gamma(y)$ may be interpreted to mean that a dense cloud of absorbing material begins at a distance modulus of 6.0, thins out very considerably within the distance modulus range 8.0–9.0, and then again increases in density beyond $y = 9.0$.

[8] Lundmark, *Hdb. d. Ap.*, **5**, No. 1, 539 (adopted values); Trumpler, *Lick Obs. Bull.*, **14**, 154, 1930; R. E. Wilson, *A.J.*, **41**, 169, 1932; Gyllenberg, *Lund Medd.*, Ser. II, No. 68; Strömberg, *Ap. J.*, **72**, 117, 1930; *Mt. W. Contr.*, No. 411, *Ap. J.*, **73**, 40, 1931; *Mt. W. Contr.*, No. 418, *Ap. J.*, **74**, 110, 1931; *Mt. W. Contr.*, No. 430. *Ap. J.*, **74**, 342, 1931; *Mt. W. Contr.*, No. 440; Stebbins, Huffer, and Whitford, *Ap. J.*, **90**, 209, 1939; *Mt. W. Contr.*, No. 617; Merrill and Sanford, *Ap. J.*, **87**, 118, 1938; *Mt. W. Contr.*, No. 585; R. E. Wilson, *Ap. J.*, **94**, 12, 1941; *Mt. W. Contr.*, No. 646; Russell and Moore, *Ap. J.*, **87**, 389, 1938; *Mt. W. Contr.*, No. 589.

The reality of the relatively flat portion of $\gamma(y)$ between $y = 8.0$ and $y = 9.0$ appears to be well established. This characteristic persists if we subdivide the data upon which Table 3 is based and consider separately (*a*) each spectral class or (*b*) intervals of apparent magnitude. These subdivided data show that, within the uncertainties of the measurements, the systems of magnitudes, color indices, and spectral types appear to be mutually consistent.

It is of considerable interest to compare the $\gamma(y)$-curve found here with the $\gamma(y)$-curves found by two other investigators for essentially the same region of the Milky Way.

C. E. Smith[9] has examined the stars in five small areas located within R. The agreement between the $\gamma(y)$ relationship found here and the one deduced by Smith by a method identical with that used in the present investigation may be considered satisfactory.

TABLE 4

MEAN VALUES OF COLOR EXCESS AND DISTANCE MODULUS

Interval in y	$\bar{y}$	$\bar{E}$	No. of Stars	Interval in y	$\bar{y}$	$\bar{E}$	No. of Stars
1.9–5.8	4.49	−0.004	24	9.0– 9.4	9.18	+0.358	31
6.0–6.4	6.28	+0.095	10	9.5– 9.9	9.68	+0.448	45
6.5–6.9	6.68	+0.118	17	10.0–10.4	10.23	+0.513	46
7.0–7.4	7.22	+0.180	16	10.5–10.9	10.70	+0.541	38
7.5–7.9	7.68	+0.267	28	11.0–11.4	11.17	+0.652	40
8.0–8.4	8.24	+0.340	23	11.5–13.0	12.01	+0.745	20
8.5–8.9	8.70	+0.329	20	13.6	13.6	+1.0	2

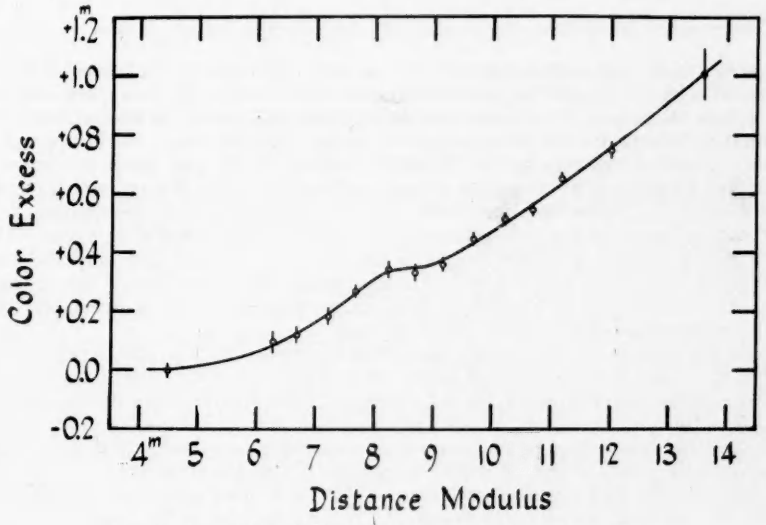

FIG. 2.—The observed color-excess–distance-modulus relationship

[9] *Lick Obs. Bull.*, **18**, 39, 1937 (No. 484).

However, the number of stars observed by Smith is small and permits the determination of only five normal points[10] on the $\gamma(y)$-curve over the interval $y = 6.0$ to $y = 12.5$.

Comparison of Smith's observations with those reported here requires the reduction of Smith's color system to the one used in this investigation. The necessary conversion factors can be determined (i) by comparing Smith's spectral-class–absolute-color relationship with that of Table 3 and (ii) by comparing the colors of 32 stars observed in common.

The differences between Smith's absolute colors and those of Table 3 are shown in Table 5.

Smith's absolute colors of stars earlier than F5 are represented by the equation

$$C_{\text{Smith}} = 1.8\, C_{\text{Table 3}} + 0.27\,. \tag{7}$$

Stars of types later than F5 depart from this relationship very considerably.

From the 32 stars in common with Smith's list we find

$$c_{\text{Smith}} = 1.9\, c_{\text{Weaver}} + 0.04\,. \tag{8}$$

The p.e. of the zero point of this relationship is approximately ± 0.03.

TABLE 5

COMPARISON OF ABSOLUTE COLORS

Sp. Class	C_{Smith}	$C_{\text{Table 3}}$	Difference	Sp. Class	C_{Smith}	$C_{\text{Table 3}}$	Difference
A0	0.00	−0.15	0.15	gG0	0.98	+0.47	0.41
A5	.24	− .01	.25	gK0	1.45	+1.05	.40
F0	.49	+ .04	.45	gK5	1.68	+1.22	0.44
F5	0.74	+0.20	0.54				

The G and K stars observed in common do not depart from the relationship defined by equation (8). However, the colors of the G and K stars do depart from the relationship of absolute colors (eq. [7]). An examination of the G and K stars in all Smith's regions shows that these later stars have consistently higher color excesses than the appropriate mean $\gamma(y)$-curve indicates for the distance modulus of the star under investigation. Since Smith's mean $\gamma(y)$-curve was strongly influenced by the A stars, which received double weight in his final solution, it seems that in his calibration of color indices Smith observed the late stars too blue relative to the A stars. Smith observed only four stars of types gG4, gG7, gK0, and gK4 in making his calibration of later-type color indices; it is therefore impossible to state whether the discrepancy mentioned here is due to chance or to errors introduced by Smith's method of observing the bright standard stars with small diaphragms and very short exposure times

With the mean of the two conversion factors determined from (i) and (ii) above, 1.85, we find in Table 6 Smith's values of E reduced to the system of the present investigation.

The systematic differences in the last column of Table 6 arise primarily from systematic departures in the absolute color systems of the two investigations. The constant term of +0.04 in equation (8) shows that the observed color systems differ very little in zero point; the constant term of +0.27 in equation (7), on the other hand, indicates that a significant difference exists between the two systems of absolute colors. The differences in Table 6, we note, are all equal essentially to the difference of the constant terms of equations (7) and (8), or more precisely, of expressions similar to equations (7) and (8)

[10] On the average, each normal point is based on fifteen values.

but referring specifically to early A stars. The A stars had high weights in the determination of Smith's $\gamma(y)$-curve.

The main effect of the differences in the fifth column of Table 6 will appear in the estimated distance of the dark cloud in R. The distance obtained by Smith must necessarily be greater than that derived in the present investigation.

Mrs. P. Th. Shajn[11] has studied the selective absorption in a region of Aquila partially overlapping R. Two comparisons of her work may be made with the results of the present investigation. From Mrs. Shajn's color equations for m_{pg} and m_{pv} we find

$$c_{IS} = 1.19\, c_{Shajn}\,. \tag{9}$$

A comparison of her results for the Pleiades shows that her absolute color values require a correction of -0.08 mag. to make them consistent with the values of Table 2. Thus

$$\begin{aligned} E_{IS} &= 1.19\, c_{Shajn} - C_{Shajn} + 0.08 \\ &= E_{Shajn} + 0.19\, c_{Shajn} + 0.08\,. \end{aligned} \tag{10}$$

TABLE 6

COMPARISON OF COLOR EXCESSES

Smith			$\bar{E}_{\text{Fig. 2}}$	Diff.	Smith			$\bar{E}_{\text{Fig. 2}}$	Diff.
Mean y	No. of Stars	$\bar{E}_{\text{reduced}}$			Mean y	No. of Stars	$\bar{E}_{\text{reduced}}$		
6.84.....	12	+0.02	+0.14	−0.12	10.43.....	13	+0.34	+0.54	−0.20
8.44.....	17	+ .15	+ .34	− .21	12.47.....	16	+0.61	+0.84	−0.23
9.49.....	17	+0.21	+0.41	−0.20					

Inasmuch as Mrs. Shajn does not give c_{Shajn} for individual stars, we cannot rigorously convert E_{Shajn} to E_{IS}. We can, at best, assume that $c_{Shajn} = E_{Shajn}$ (the relationship implies that all the stars observed are of absolute color zero) and hence that

$$E_{IS} \backsim 1.19 E_{Shajn} + 0.08\,. \tag{11}$$

Since no data are given on the values of M_{Shajn}, we can only assume that M_{Shajn} and M_{pg} as given in Table 3 are consistent.

In her diagram (Fig. 1), Mrs. Shajn exhibits the relationship between color excess, $\gamma(y)$, and distance modulus, y, as determined from all the stars (B5–F5) within apparent magnitude limits 10.0–11.0. Values of y and E_{Shajn} read from this figure are given in Table 7. The values E_{IS} are obtained by applying equation (11) to E_{Shajn}.

The adjusted values, E_{IS}, are plotted as dots in Figure 3, in which the solid line, representing $\gamma(y)$, is repeated from Figure 2. The two sets of data agree very well for the larger values of y, but only moderately well for the smaller values. This disagreement is not surprising; it is of the type to be expected from the approximate adjustment afforded by equation (11). The values of E_{IS} for the smaller values of y are derived from the stars of later spectral type. For these stars $\bar{c}_{Shajn} > \bar{E}_{Shajn}$, and therefore the values $\bar{E}_{IS}$ are too small. The values of $\bar{E}_{IS}$ for the larger values of y, on the other hand, are derived from stars of earlier spectral type, for which $\bar{c}_{Shajn} \backsim \bar{E}_{Shajn}$. For these objects the adjustment afforded by equation (11) is substantially correct.

[11] *Bull. Abastumani Ap. Obs.*, **7**, 189, 1943. We shall consider only what Mrs. Shajn terms her region "B," which covers the area 19^h06^m to 19^h25^m, $+10°$ to $+19°.5$.

Probably the most important feature of the E_{IS} values exhibited in Figure 3 is their supporting evidence for the existence of the plateau in $\gamma(y)$ in the range $y = 8.0$–9.0, as found in the present investigation.

If we reduce the data of Mrs. Shajn's Table I, area 8, which is based on all the stars that she observed, we find the values of E_{IS} shown in Figure 3 by open circles. In this case the values of E_{IS} are generally smaller than the values of $\gamma(y)$ exhibited by the solid curve. This discrepancy, like the previous one, is explained by the fact that, for the stars as a whole, $c_{Shajn} > E_{Shajn}$, and therefore the approximate transformation equation (11) underestimates the value of E_{IS}.

Under these circumstances the agreement between E_{IS} and $\gamma(y)$ may be considered quite satisfactory.

IV. THE EVALUATION OF χ

An interstellar cloud as dense, as near by, and as extensive as the one forming the dark rift in Aquila exercises a profound influence on the number of stars seen against it and

TABLE 7

COLOR-EXCESS–DISTANCE-MODULUS RELATIONSHIP FOR ALL SPECTRAL TYPES
($10.0 \leq m \leq 11.0$)

y	E_{Shajn}	E_{IS}	y	E_{Shajn}	E_{IS}
6.40	−0.031	+0.04	8.84	+0.183	+0.30
6.90	− .024	+ .05	9.35	+ .223	+ .35
7.35	+ .040	+ .13	9.84	+ .290	+ .43
7.89	+ .152	+ .26	10.33	+ .350	+ .50
8.39	+0.175	+0.29	10.77	+0.320	+0.46

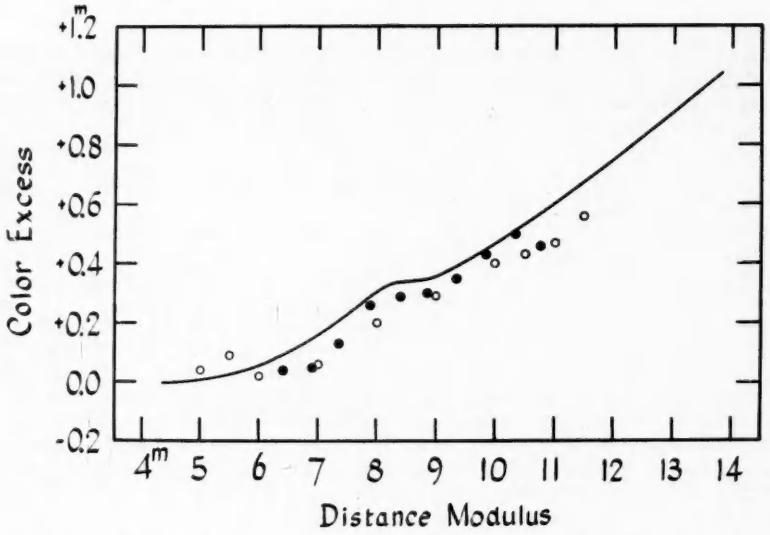

FIG. 3.—Comparison of the color excess–distance modulus found in the present study with that found for the same region by other investigators.

through it. The absorption and scattering of light by such a cloud is, in fact, the controlling factor in the integral equation relating the true density and luminosity functions to the apparent luminosity function of stars seen in the direction of the cloud. Variations in the coefficient of absorption and scattering in the Aquila region produce a much greater influence upon the observed numbers of stars than do comparable variations in the density or luminosity functions. The dark cloud in Aquila therefore affords a rather powerful means of evaluating the dimensionless parameter χ by which we transform our observed color-absorption function, $\gamma(y)$, to the function expressing total photographic absorption, $a(y)$, as a function of apparent distance modulus, y.

If space is perfectly transparent, the total number of stars, $A(m)$, per square degree per unit magnitude interval, is given by the integral equation,

$$A(m) = b\omega 10^3 \int_{-\infty}^{+\infty} 10^{0.6y} \Delta(y) F(m-y)\, dy\,, \tag{12}$$

in which

$b = 0.2 \log_e 10$;

$\omega = \dfrac{4\pi}{41{,}253}$;

y = Apparent distance modulus, $m - M$;

$\Delta(y)$ = Relative space density of stars at distance y, that is, the ratio of the total number of stars per cubic parsec at distance y to the total number of stars per cubic parsec in the vicinity of the sun;

$F(m-y) = F(M)$, the luminosity function, represents the number of stars of magnitude M per unit magnitude interval per cubic parsec in the vicinity of the sun.

In equation (12) the assumption is implicit that $F(M)$ is not correlated with y. We assume that the mixture of stars is everywhere the same as it is in the solar neighborhood. This is, of course, only a crude approximation to reality even in the vicinity of the galactic plane. We shall, in a later section, discuss the effect of this approximation on the value of χ that we derive from the material at hand.

In equation (12) we have also assumed that space is perfectly transparent. If this is not the case, we must modify equation (12) to allow for absorption. If we again let y represent the apparent distance modulus $m-M$, then y is related to r through the equation

$$5 \log \frac{r}{10} = y - a(y)\,, \tag{13}$$

where $a(y)$ represents the total amount of photographic absorption suffered by the starlight. With this definition of y, the total number of stars, $A(m)$, per square degree per unit magnitude interval, is given by the modified integral equation,

$$A(m) = b\omega 10^3 \int_{-\infty}^{+\infty} 10^{0.6y} P(y) \Delta(y) F(m-y)\, dy\,, \tag{14}$$

where $P(y)$ is given by the expression

$$P(y) = 10^{-0.6a(y)} \left(1 - \frac{da(y)}{dy}\right). \tag{15}$$

If we place

$$\Delta'(y) = P(y)\Delta(y), \tag{16}$$

we may write

$$A(m) = b\omega 10^3 \int_{-\infty}^{+\infty} 10^{0.6y}\Delta'(y)F(m-y)\,dy. \tag{17}$$

Equation (17) is identical in form with equation (12). In place of the true space density of stars, $\Delta(y)$, in equation (12), however, we must consider the apparent space density of stars, $\Delta'(y)$ in equation (17). The relationship between the true and apparent space densities is given by equation (16).

For an area in which there is a near-by dense accumulation of interstellar material—as in this Aquila region—the function $\Delta'(y)$, or, more particularly, $P(y)$, dominates equation (17). Variations in $\Delta(y)$ or $F(m-y)$ have, relatively speaking, a much smaller effect upon $A(m)$ than have comparable changes in $\alpha(y)$.

TABLE 8

CALCULATED AND OBSERVED VALUES OF $A(M)$
THE INTERPOLATED VALUES OF χ

m	$\chi=3.1$	$\chi=3.3$	$\chi=3.5$	Observed	Interpolated χ
≤ 10.5*	12.3	10.7	9.7	13.0±0.96	3.04±0.09
11.5	16.9	14.1	12.2	12.5±0.94	3.46± .11
12.5	38.3	31.0	25.9	29.5±1.45	3.35±0.05
Σ	67.8	55.8	47.8	55.0± 2.0	3.32±0.05

* The observed values of $A(m)$ for m = 6.5, 7.5, 8.5, 9.5, and 10.5 are small and therefore subject to large percentage uncertainties. Rather than give these individual values, we tabulate $\sum_{m=6.5}^{10.5} A(m)$ under the entry ≤ 10.5.

For the dark cloud in Aquila we have established the function $\gamma(y)$. If we make use of the fact that

$$\alpha(y) = \chi\gamma(y), \tag{18}$$

we can write the equation for the star counts in Aquila as

$$A(m) = b\omega 10^3 \int_{-\infty}^{+\infty} 10^{0.6y} 10^{-0.6\chi\gamma(y)} \left(1 - \chi \frac{d}{dy}\gamma[y]\right)\Delta(y)F(m-y)\,dy. \tag{19}$$

From this equation we can determine the value of χ.

We consider, first, the photographic star counts. If we assume (i) that $\Delta(r)$ is constant and equal to the density of stars in the solar region, that is, that $\Delta(r) = 1$, and (ii) that $F(M)$ is given by van Rhijn's[12] luminosity function, then for the Aquila region the only unknown in equation (19) is χ. We may thus assign various values to χ, compute the corresponding values of $A(m)$ from equation (19), and then, by interpolation, find the value of χ that produces the best fit between the observed and the computed values of $A(m)$.

In Table 8 are tabulated the values of $A(m)$ computed for $\Delta(r) = 1$, van Rhijn's luminosity function, and three values of χ = 3.1, 3.3, and 3.5.

The interpolated values of χ necessary to produce a fit between calculation and observation for each value of m are given in the last column of Table 8. The weighted mean

[12] *Groningen Pub.*, No. 47, 1936.

of the three determinations gives $\chi = 3.30$. An equally reliable mean value of χ can be obtained from the sums $\sum_{m=6.5}^{12.5} A(m)$. From these sums we find $\chi = 3.32 \pm 0.05$.

The photovisual star counts (transformed to the Harvard Visual System) treated[13] in the same manner as the photographic counts just discussed, yield, on the International System, the value $\chi = 3.43 \pm 0.04$.

Thus, if we adopt the assumption of constant space density of stars in the direction of the dark cloud in Aquila and of the universality of van Rhijn's photographic and visual luminosity functions, we find

$$\chi = 3.38 \pm 0.03 .$$

Both these assumptions, however, are subject to considerable doubt. We must therefore investigate the variations that can be produced in χ by variations in $\Delta(r)$ and $F(M)$.

VARIATIONS IN $\Delta(r)$

We shall here continue to use van Rhijn's luminosity function. If we assume that the true space density of stars is not constant but that it doubles in a distance of 2000 parsecs, as shown in Figure 4, *a*, we find

$$\chi = 3.55 \pm 0.04 .$$

If we assume that the true space density of stars decreases to half its normal value in a distance of 2000 parsecs, as shown in Figure 4, *b*, we find

$$\chi = 3.14 \pm 0.04 .$$

If we assume that the true space density of stars varies in an irregular manner, as illustrated in Figure 4, *c*, we find

$$\chi = 3.20 \pm 0.04 .$$

Clearly, any reasonable variation in the true space density of stars does not produce a very great variation in the values of χ.

VARIATIONS IN THE LUMINOSITY FUNCTION

We shall here assume that $\Delta(r)$ is constant and equal to unity. McCuskey and Seyfert[14] have examined the variations in the luminosity function in an area of the Milky Way only six degrees from R and have found indications of a variation of the stellar mixture with distance. Specifically, they found (i) an excess of early-type stars, particularly at distances greater than 600 parsecs, and (ii) a deficiency of faint stars ($M > +4$), particularly at distances less than 600 parsecs.

If we adopt the mean mixture of stars given by McCuskey and Seyfert in their Table 15 and adjust this varied luminosity function so that it predicts the same number of stars per cubic parsec as does van Rhijn's, we find the values of $F(M)$ given in Table 9.

On the basis of uniform star density and the varied luminosity function of Table 9 we find

$$\chi = 3.46 \pm 0.03 .$$

The parameter χ is thus seen to be relatively insensitive to variations in either the density law or the luminosity function. The dominating factor in equation (17) is $P(y)$, which is controlled by the value of $\alpha(y)$ or of χ if we place $\alpha(y) = \chi\gamma(y)$.

[13] We represent these transformed pv counts with $\Delta(r) = 1$, van Rhijn's HV luminosity function, and the $\gamma(y)$-curve transformed to HV.

[14] *Ap. J.*, **106**, 1, 1947.

We may thus adopt for the final value of χ as determined from the dark cloud in Aquila

$$\chi = 3.4 \pm 0.2 ,$$

where the rather conservative figure of uncertainty, ± 0.2, seems justified on the basis of the foregoing calculations.

We may compare this value of χ with some of the other recent determinations of the same constant. The value of χ varies with the temperature of the star under consideration. The value found in the present investigation is a mean value referring to the particular group of stars observed. In making comparisons with the values found by other in-

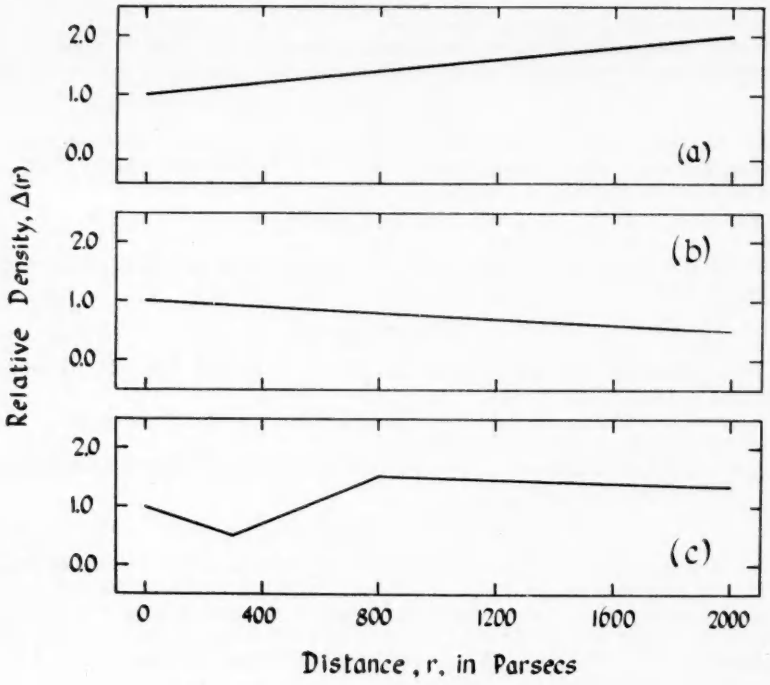

FIG. 4.—Hypothetical relative density functions

vestigators, we shall assume that the "average star" in the Aquila region is of early A type; its effective wave lengths[15] may then be taken as

$$\bar{\lambda}_{pg} = 4270 ,$$

$$\bar{\lambda}_{pv} = 5430 .$$

For these wave lengths the theoretical curve derived by Oort and van de Hulst[16] gives $\chi = 3.35$; the interstellar absorption and scattering curve derived observationally by Whitford,[17] on the other hand, gives $\chi = 4.0$, with an estimated uncertainty of 0.2 or

[15] Seares and Joyner, *Ap. J.*, **98**, 302, 1943; *Mt. W. Contr.*, No. 685.

[16] *B.A.N.*, **10**, 187, 1946.

[17] *Ap. J.*, **107**, 102, 1948.

0.3. Unfortunately, the critical point at $\lambda = 2.1\mu$ in Whitford's curve depends upon only a few observations; further observations may change its value by several hundredths of a magnitude and thus change by an appreciable amount the value of χ derived from his curve.

V. THE DISTANCE, EXTENT, AND OPACITY OF THE ABSORBING CLOUD

With the value of χ derived in Section IV we may convert $\gamma(y)$ to $a(r)$, the total photographic absorption at distance r. The color-excess-curve in Figure 2, transformed to $a(r)$ with the value $\chi = 3.4$, is shown in Figure 5. The absorbing cloud forming the dark rift is, in the Aquila region at least, relatively near by; its distance is only 110 parsecs, a value that appears to be rather well determined. The near edge of the cloud is very dense; its coefficient of absorption and scattering is 7.4 mag. per kiloparsec. This very dense portion of the cloud extends to a distance of 260 parsecs. In the distance range

TABLE 9

COMPARISON OF VAN RHIJN'S LUMINOSITY FUNCTION AND THE AVERAGED LUMINOSITY FUNCTION OF MCCUSKEY AND SEYFERT*

M	No. of Stars per Cubic Parsec		M	No. of Stars per Cubic Parsec	
	Van Rhijn	McCuskey and Seyfert		Van Rhijn	McCuskey and Seyfert
−6	1.26×10^{-8}	2.37×10^{-8}	+2	5.89×10^{-4}	4.72×10^{-4}
−5	1.17×10^{-7}	2.20×10^{-7}	+3	7.24×10^{-4}	7.49×10^{-4}
−4	4.47×10^{-7}	8.41×10^{-7}	+4	1.55×10^{-3}	1.19×10^{-3}
−3	1.78×10^{-6}	2.65×10^{-6}	+5	2.24×10^{-3}	1.68×10^{-3}
−2	5.62×10^{-6}	7.49×10^{-6}	+6	3.09×10^{-3}	2.37×10^{-3}
−1	1.17×10^{-5}	2.37×10^{-5}	+7	3.39×10^{-3}	2.97×10^{-3}
0	4.79×10^{-5}	1.01×10^{-4}	+8	2.88×10^{-3}	4.22×10^{-3}
+1	2.19×10^{-4}	2.79×10^{-4}			

* The two luminosity functions as given refer to slightly different standards. Van Rhijn's luminosity function as tabulated gives the number of stars in the interval $M \pm \frac{1}{2}$, that is, it gives the average value of $F(M)$ in the interval $M \pm \frac{1}{2}$. The varied luminosity function, on the other hand, gives the value of $F(M)$ at the value of M in the table.

260–350 parsecs the cloud is very much less dense than in the region of its forward edge. In this second distance range the coefficient of absorption and scattering is only 0.75 mag. per kiloparsec, a value normal for our region of the galaxy in general. Beyond 350 parsecs the coefficient of the cloud increases to the value 3.2 mag. per kiloparsec. This second dense portion of the cloud extends to 1000 parsecs and possibly beyond.

The distance of the absorbing cloud determined from the present observational data is in satisfactory agreement with the determinations of other investigators. Smith[18] found a distance of about 250 parsecs. If allowance is made for the zero-point difference between Smith's absolute colors and those of Table 2, however, Smith's distance to the cloud becomes approximately 100 parsecs. The conspicuousness of the cloud argues somewhat in favor of the smaller of these two distances. If the cloud were as distant as 250 parsecs, probably it would be much less prominent than it actually is.

Mrs. Shajn[19] found the dark cloud in Aquila to be approximately 130 parsecs distant.

[18] *Op. cit.*

[19] *Op. cit.* The quoted value has been interpolated from Mrs. Shajn's Table 1 and Fig. 1. The zero-point difference of 0.08 mag. between Mrs. Shajn's absolute color system and that of Table 2 was applied before this interpolation was made.

McCuskey and Seyfert,[20] who studied an area of the Milky Way less than 6° distant from R, found that a dark cloud starts at a distance of approximately 100 parsecs. It is likely that the cloud examined by McCuskey and Seyfert is an extension of the same general mass of interstellar material causing the conspicuous darkening in the area examined in this study. Baker,[21] using the principle of absorbing clouds in interpreting his star counts in an area about 10° from R, postulated a dark cloud at a distance of about 500 parsecs, with an absorption of 2.3 mag.

The average absorption coefficient found in the present study is somewhat larger than that found by either Smith or Mrs. Shajn. From Smith's data we can deduce a minimum absorption coefficient of 2.8 mag. per kiloparsec; from Mrs. Shajn's work, about 3.0

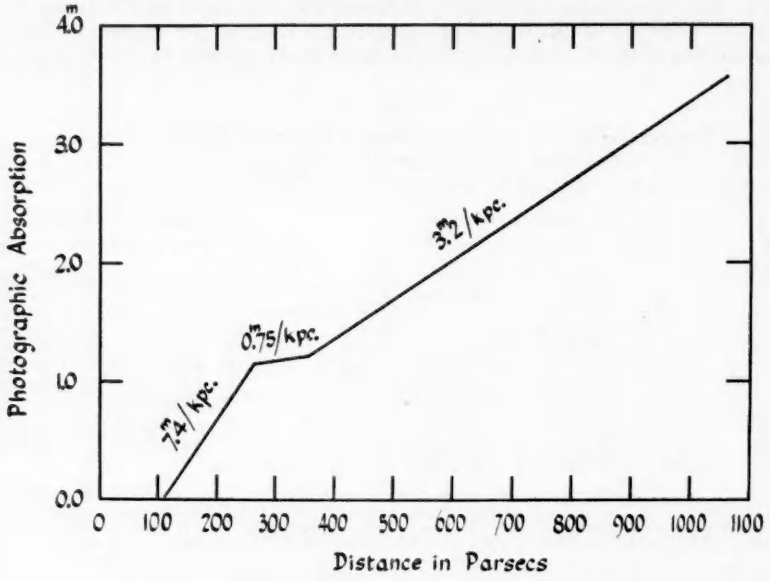

FIG. 5.—The photographic absorption–distance relationship

mag. per kiloparsec. From the results of the present investigation we find an average absorption coefficient of 3.7 mag. per kiloparsec. The differences among these three values are caused primarily by the differences in the color systems used by the different investigators and by the differences and uncertainties[22] in the values of χ used to convert color excess to total photographic absorption.

It is a pleasure to acknowledge my indebtedness to Dr. W. S. Adams and the members of the staff of the Mount Wilson Observatory for their hospitality during the summers of 1940, 1941, and 1942. It is likewise a pleasure to thank Dr. W. Baade and Dr. F. Zwicky for making arrangements for me to use the 18-inch Schmidt telescope. Finally, and especially, my thanks go to Dr. Baade and to Dr. R. J. Trumpler for many discussions on problems of photometry and galactic structure during the period 1940–1942.

[20] *Op. cit.* [21] *Ap. J.*, **94**, 493, 1941.

[22] Caused by uncertainties in the effective wave lengths of the color systems used.

THE URSA MAJOR GROUP

NANCY GRACE ROMAN
Yerkes Observatory
Received May 18, 1949

ABSTRACT

The Ursa Major group is investigated in detail. It is shown that a small, compact cluster can be distinguished from the large, ill-defined stream. An introduction to the problem is given in Section I. Section II contains a summary of the previous work on the group, together with a bibliography. In Section III the position of the convergent point is determined from the proper motions of the nucleus stars. It is shown that these proper motions determine the position of this point quite accurately. New measurements of the radial velocities of the brighter nucleus stars are discussed in Section IV and are used to determine the space velocity of the cluster. The results indicate that a velocity may be found which agrees with the individual parallaxes and radial velocities within their expected uncertainty, but the systematic differences between the results from these two sets of data cannot be completely removed. In SectionV, the results of a search for new members within 20 parsecs of the center of the nucleus are described. A list of members and a description of the cluster are given. Section VI contains a list of all stars which have been assigned to the Ursa Major stream and compares the observed and the computed data for these stars. New spectral types and spectroscopic absolute magnitudes are given for those stars for which the agreement between the observed and the computed data is best and which are north of declination $-30°$. Section VII summarizes the results of the investigation.

I. INTRODUCTION

Information gained from the study of moving clusters has played an important role in both stellar astronomy and astrophysics, by furnishing fairly accurate data on the absolute magnitudes of stars too distant to be reached effectively by trigonometric methods. As a result, the nearest open clusters have been studied extensively. Unfortunately, in spite of numerous investigations, the status of the Ursa Major cluster is far from satisfactory. The long lists of members of the cluster are strikingly discordant; the space velocity of the group and thus the parallaxes of the cluster members have been uncertain by as much as 20 per cent; and even the existence of the group has been doubted. In the present investigation some of the causes of these problems are examined, the uncertainty in the space velocity of the cluster is diminished, and the current state of knowledge about the cluster is presented.

The Ursa Major group can be considered as composed of two subgroups: a moderately compact cluster of stars sharing *accurately* the same space motion and an extended stream of stars possessing *approximately* the same space motion. It is well known that the five central stars in the Big Dipper and five fainter ones in the same region of the sky are moving with velocities which are equal within the errors of observation. Moreover, these stars are collected in a volume of space less than 10 parsecs across. On the other hand, the stars of the extended Ursa Major group seem to fill a volume of space which is limited only by the effects of observational selection, a volume which contains not only the sun but also the Hyades, the Pleiades, and the Coma clusters. In this paper we shall refer to the compact group in Ursa Major as the "nucleus" or "cluster" and to the extended group as the "Ursa Major stream." However, the gravitational interactions between the members of the cluster are much smaller than between members of such compact groups as the Pleiades or the Hyades clusters.

The following is a list of some of the symbols and abbreviations used in this paper:

A, D = Right ascension and declination of the convergent point

L, B = Galactic longitude and latitude of the convergent point or of the solar apex

R = Difference in velocity between the space motion of a star or group of stars and that of the cluster

V = Velocity of the cluster

X, Y, Z = Rectangular galactic co-ordinates of the star referred to the center of the nucleus. X points to galactic longitude 0°; Y, to galactic longitude 90°; and Z, to the north galactic pole.

GC = *General Catalogue*

FK3 = *Dritter Fundamentalkatalog des Berliner Astronomischen Jahrbuchs*

NFK = *Neue Fundamentalkatalog*

PGC = *Preliminary General Catalogue*

λ = Angular distance between a star and the convergent point

ρ = Radial velocity of a star in kilometers per second

μ_α, μ_δ = Components of proper motion in right ascension and declination, respectively

π_{tr} = Trigonometric parallax of a star

π_{sp} = Spectroscopic parallax of a star

π_{cl} = Parallax of a star computed on the assumption that it shares the motion of the cluster

II. DISCUSSION OF THE LITERATURE

In 1869 Proctor called attention to the fact that the available proper motions were not distributed at random but that rather, in many regions of the sky, several stars seemed to share a common motion (45).* Among others, he pointed out the remarkable group in Ursa Major of stars moving toward the solar apex. Three years later, Huggins published radial velocities for the seven stars of the Big Dipper which confirmed the hypothesis that the five central stars share a common space motion not shared by the other two (29). Moreover, he remarked that these five stars, which are of approximately equal brightness, also have similar spectra.

Since that time, numerous attempts have been made to determine more accurately the position of the convergent point and the amount of the cluster motion. Two basic methods have been used for most of these determinations. One is attributed to Bohlin, although it was used by Klinkerfues thirty years earlier (30). The essential reasoning on which Bohlin's method is based is the following: The proper motion of each cluster member defines a great circle through the radiant and convergent points. Therefore, the poles of these circles must lie on another great circle, every point of which is 90° distant from the convergent point. In turn, the poles of this latter circle must be the convergent and the radiant points. Unfortunately, the five bright stars in the Ursa Major nucleus lie approximately on the great circle defined by their motions. This means that the poles of the proper-motion circles are badly clustered, and a position for the convergent point determined by this method is necessarily uncertain. This method has not been used extensively for the nucleus stars alone.

The method of differential corrections—the standard method of treating nonlinear equations by least squares—has proved to be more fruitful. In this method the equations expressing the observed quantities as functions of the elements of the motions are dif-

* Numbers in parentheses refer to numbered entries in the bibliography on p. 240.

ferentiated. Then the differences between the observed and the predicted amounts of the proper motions, the radial velocities, or the tangential motions are used to compute small corrections to the preliminary cluster elements. Besides its simplicity, this method has the important advantage of minimizing the residuals in the observed quantities rather than in functions of these quantities. Moreover, the constants in the equations of condition contain only the position of the star and the assumed preliminary position of the convergent point and are thus known exactly, while in Bohlin's and Charlier's methods the constants contain errors in the proper motions which are reflected in the final position of the convergent point.

Haas assumed that the space velocity and parallax of each cluster member was the same and computed the three components of the space velocity from the observed radial velocities and proper motions (21). This method is equivalent to determining the position of the convergent point from the change in the radial velocities and proper motions as a function of position in the sky. In theory the method is open to no objections, but in practice it seems unwise to disregard the most accurate data available, the position angles of the proper motions. The method also involves the unnecessary assumption that all the members considered are at the same distance from the sun.

Hertzsprung has published several short notes suggesting faint stars which may be members of the nucleus (24, 25), but Haas seems to have been the only person to search for such stars systematically. By consulting the catalogues from the Cincinnati Observatory, the Yale proper motions determined for the A.G. stars and the difference (Vatican catalogue — Helsingfors A.G. catalogues), he extended the list of nucleus stars to include 26 members. These stars defined the main sequence as far as M0, but there were radial velocities only for the brighter ones. As we shall see in Section V, the radial velocities rule out all but two others.

In 1909 Hertzsprung noticed that two stars, in widely separated regions of the sky, 37 UMa and α CrB, also possessed proper motions directed toward the convergent point of the Ursa Major motions (23). This discovery led him to make a systematic search for members of the group outside the region of the Big Dipper. From the stars which then had the best proper motions, he selected eight new members. He determined the position of the convergent point in two ways, both based on the proper motion of Sirius. The velocity of the group was computed in the usual way and checked by the observed tangential velocity of Sirius.

Shortly later, Ludendorff criticized the high weight given to Sirius in determining the position of the convergent point, arguing that the motions of the members of the group might not be strictly parallel (35). He redetermined this position from the directions of the proper motions of all group members but did not obtain an appreciably different result.

During the next decade, Hertzsprung and Oppenheim compiled new lists of cluster members which were discussed by Bottlinger (7) and Ledersteger (32), respectively. The latter used a new method, introduced by Oppenheim (40), to determine the position of the convergent point, but this is essentially a mathematical modification of Bohlin's method.

With the accumulation of observational data, it became possible to distinguish stream members on the basis of common space motion. As early as 1915, Plummer noted four F-type members of the stream in this way, as a by-product of his discussion of the space motions of F-type stars using hypothetical parallaxes[1] (44), and Dziewulski used the space motions of individual members with known parallaxes to compute the cluster elements (14). By 1930, radial velocities and parallaxes were available for most of the bright stars and a new interest arose in compiling lists of members of the Ursa Major and other streams. In that year Mohr investigated all A- and F-type stars with complete

[1] These were computed on the assumption that the true space motion of each star is parallel to the galactic plane.

proper motion, radial velocity, and parallax data (37). Using R, the difference between the space motion of the star and that of the cluster, as a criterion, he concluded that 35 per cent of the A-type stars and 8 per cent of the F-type stars which he examined belonged to the Ursa Major stream. This result increased the membership of the group to 96 stars. In a similar way, Bertaud found 94 stars with R less than 10 km/sec (3). Nassau and Henyey used the criterion that R is less than 9.5 km/sec to pick stream members from among the stars in the *Yale Catalogue of Bright Stars* (38). One out of every 24 stars examined satisfied this test. These authors did not claim that field stars had been eliminated from their list or that the group of stars thus distinguished had any physical significance, but they treated these stars as a cluster in their further discussion. Later, Nassau decided that there were few, if any, field stars present among the stars with R less than 7.5 km/sec (39). Furthermore, he concluded that both the distribution of spectral types and a large percentage of binaries served to distinguish the stream stars from the field stars.

By 1939 the list of stream members had grown greatly, and many stars were included for which the status in the group was doubtful. In that year Smart published two papers in which he examined more critically the stars from Bottlinger's and Plummer's lists (47) and those from Henyey and Nassau's lists (49). He subjected each star in these lists to three tests: (*a*) agreement between the observed and the computed position angles of the proper motion, (*b*) agreement between the computed and observed radial velocities, and (*c*) agreement between the computed and both the spectroscopic and the trigonometric parallaxes. Of the 135 stars examined, 42 were retained as definite members of the group, and 52 additional stars were retained as possible members. The definite members from the first paper were used to compute the position of the convergent point by Bohlin's method. Since Smart found that the velocity of the cluster as computed from the radial velocities of the members was somewhat uncertain, he determined the velocity of the group from the trigonometric parallax and proper motion of Sirius. He also determined this velocity by using all stars with large trigonometric parallaxes, but, as the result was not appreciably different (Sirius still received 40 per cent of the weight), he adopted the value which he had determined from Sirius alone.

About the same time, Bartholeyns treated both a new list of members which he had found from space motions (1) and a number of stars from older lists in much the same way (2). He also included three small tables of stars which appeared to be members on the basis of new or incomplete data.

In 1941 Gliese examined the space motions of all stars in the FK3 for which radial velocities and parallaxes were available (17). After attempting to allow for galactic rotation and for any systematic errors present in the observational data, he considered the distribution of the velocity vectors of these stars. He studied each of the moving clusters, determining its boundary as the edge of the region in which there was a higher concentration of velocities than normal. Although he did not define what constituted a significant deviation from the normal concentration of velocity vectors, he distinguished 80 stars as members of the Ursa Major stream. However, even after excluding these stars and a similar set of members of the Taurus stream, he found traces of the two streams in his further discussions.

Each investigator has recomputed the cluster elements, using different lists of members, different data, and different methods. However, all reliable determinations have given values near $A = 306°$, $D = -37°$, and $V = 18$ km/sec.

Several attempts have been made to find a change in the motion of the stream stars with their space positions (2, 9, 11, 16). In each case, the investigator believed that such a systematic variation existed. Mlles Canavaggia and Fribourg, and Bartholeyns each found that the motion of the stream stars is consistent with a rotation of the group about its center but not with differential galactic rotation. However, the problem is a difficult one, and the results are not conclusive.

In a short note published in 1911, Turner called attention to the fact that the members of the Ursa Major group listed by Hertzsprung lay approximately in a plane which is nearly perpendicular to the plane of the galaxy and to the direction of the motion of the cluster (51). Guthnick and Prager (18) and Nassau and Henyey have confirmed this suggestion, while Oppenheim, Ledersteger, and Horn-d'Arturo (28) found that the stars were distributed in three planes which contained their motions. A description of the space distribution of the stream members depends largely on the list of members chosen and is of little worth unless the effects of observational selection are eliminated or at least recognized.

Recently, Delhaye has studied the dispersion of the velocities among the members of the Ursa Major stream on the basis of the space motions of about 2000 stars brighter than 6.5 mag. (13). A plot of all velocities for the A- and F-type stars (exclusive of the stars in the nuclei of the Ursa Major and Taurus clusters) showed that there were more velocities near the Ursa Major velocity than in the diametrically opposite portion of the diagram. Allowing for field stars, the distributions of both the radial velocities and the proper motions of the stars with velocities within 10 km/sec of that of the Ursa Major group "indicate that there is a real concentration of velocities toward the motion of the Ursa Major nucleus. At the same time, they show that the space motions of the members of the extended Ursa Major stream are not identical, but have a real dispersion, the amount of which may be estimated as between 2 and 3 km/sec in one coordinate."

In addition to the papers which treat the Ursa Major stream as an exact concept, many have been written on the appearance of this stream as a velocity maximum in studies of the distribution of space velocities. Early in the study of stellar motions Kapteyn noticed an apparent tendency for stars to move in nearly opposite directions. The stars moving in these preferred directions, which were known as Kapteyn's streams I and II, became identified with the Taurus and the Ursa Major streams, respectively. Three-quarters of the stars which B. Boss assigned to stream II (6) have appeared among the lists of members of the Ursa Major group.

With the development of the theory of galactic rotation, Kapteyn's streams were recognized as a natural consequence of this rotation. Thus it has become important to decide whether the Ursa Major stream can be distinguished from stream II. Opinion on this question varies. In a recent investigation of the space motions of early A-type stars, Bourgeois and Coutrez found that there is no trace of either the Ursa Major or the Taurus streams in their results (8). On the other hand, Wilson and Raymond (52) and Gliese have found that it is impossible to represent the observed distribution of space velocities by a single velocity ellipsoid because of the presence of the Ursa Major and Taurus streams. Lindblad suggested that the deviation of the vertex of star-streaming from its expected direction of about 325° to a direction of about 345° is a result of the existence of the Ursa Major stream (33).

Various authors have attempted to decide whether the condensations of velocities in the regions of the scattered moving clusters are significant or mere chance deviations from a uniform distribution. Allowing for the effects of star-streaming but not for those of solar motion, Dziewulski concluded that the stars whose proper-motion circles pass near the convergent point belong to a physically significant group but that the number of spurious members increases rapidly as larger residuals are allowed (15). Had he been able to consider the distances of the stars as well as the proper motions, his argument would have been still stronger.

In 1932 Bertaud conducted a similar investigation using space motions (3). His results are given in Table 1. He, too, concluded that the group is real, with a definite concentration of motions toward the motion of the nucleus stars. However, as the allowed tolerance in the velocity residuals is increased, the space motion found for the group deviates somewhat from that of the central stars toward the direction of star-streaming.

In a personal communication Dr. J. H. Oort stated that, among the stars brighter than

6.5 mag. with known space motions, 22 stars of types A–G are within a cube 10 km/sec on a side and centered on the motion of the Ursa Major nucleus. The ellipsoidal distribution of velocities predicts that 5.6 stars will be found in such a cube.

The evidence seems to favor the existence of the Ursa Major stream. There is a real concentration of velocities near the velocity of the nucleus group, but the limits of the stream are ill defined.

III. THE DETERMINATION OF THE POSITION OF THE CONVERGENT POINT

The position of the convergent point of the Ursa Major group has been computed many times, but, since 1910, only one determination has been based on the nucleus stars alone. In view of the finite dispersion among the space velocities of the stream members, it seems essential to determine this quantity from the motions of the nucleus stars.

The data from which the position of the convergent point can be found are the proper motions, the radial velocities, and the parallaxes of the individual stars. Bohlin's and Charlier's methods depend only on the proper motions; the method of differential corrections can be based on any or all of the three types of data; a determination from the

TABLE 1

THE CONCENTRATION OF SPACE VELOCITIES TOWARD THAT OF THE NUCLEUS STARS

Maximum Residual in Space Velocity (Km/Sec)	No. of Stars*	Observed No. / Expected No.	Maximum Residual in Space Velocity (Km/Sec)	No. of Stars*	Observed No. / Expected No.
10	109	1.3	4	36	2.6
8	87	1.5	2	15	3.7
6	59	1.9			

* The nucleus stars and the stars α CMa, α CrB, and ξ Eri have been excluded in compiling this table.

space motions depends on a combination of the three types. Since the intrinsic accuracies of the proper motions, radial velocities, and tangential velocities are quite different, it seems advisable to treat the three sets of data separately, as far as possible. For this reason and for the reasons discussed in Section II, it was decided that the method of differential corrections was the most satisfactory one to use for a new determination of the position of the convergent point.

Equations were written relating each of the observed quantities cot θ, ρ, and $4.74\,\mu/\pi$, with the elements of the cluster motion. When differentiated, these yielded the equations of condition:

$$\Delta \cot \theta = l\Delta A + m\Delta D\,,$$

$$\Delta \rho = g\Delta A + h\Delta D + \cos\lambda\Delta V\,,$$

$$\Delta\left(\frac{4.74\mu}{\pi}\right) = g\cot\lambda\Delta A + h\cot\lambda\Delta D + \sin\lambda\Delta V + \frac{4.74\mu}{\pi}P\,,$$

where

P = A correction to the system of the parallaxes such that $\pi_{\text{true}} = \pi_{\text{sp}}(1 + P)$;

$l \sin(\alpha - A) = \csc(\alpha - A)\sin\delta - \cos\delta\cot(\alpha - A)\tan D$;

$m \sin(\alpha - A) = \cos\delta\sec^2 D$;

$g = V\cos\delta\cos D\sin(\alpha - A)$;

$h = V\sin\delta\cos D - V\cos\delta\sin D\cos(\alpha - A)$

The work was so arranged that the set of equations of condition for each type of data could be treated separately or combined with the others.

Oort and his co-workers have investigated the systematic errors of the GC and the FK3 proper motions and have compared these errors with the systematic differences between the two catalogues.[2] Their results indicate that the GC proper motions in right ascension are to be preferred over those in the FK3; for the proper motions in declination, the FK3 system is preferable. In addition, a correction should be applied to each system to allow for errors in the precession constants used. In this paper the proper motions used are those from the GC,[3] to which the following corrections have been applied: (*a*) a correction for the errors in the precession constants and a correction for the effect of galactic rotation taken from tables given by Smart[4] and (*b*) the corrections $\Delta\mu_\alpha'$ and

TABLE 2

THE WEIGHTS USED IN THE LEAST-SQUARES SOLUTIONS

Star	Weights			Star	Weights		
	cot θ	ρ	$4.74\mu/\pi$		cot θ	ρ	$4.74\mu/\pi$
37 UMa	1600	6	9	78 UMa	1600	6	9
β UMa	2500	24	9	HD 115043	900	12	9
γ UMa	2500	3	9	ζ UMa A	2500	24	9
δ UMa	2500	3	9	ζ UMa B	0	24	0
HR 4867	900	1.5	9	80 UMa	1600	3	9
ϵ UMa	2500	1.5	0				

TABLE 3

THE SOLUTIONS FOR THE POSITION OF THE CONVERGENT POINT

Solution	*A*	*D*	*V*	*P*
Smart's	306°.7±1°.3	−39°.5±0°.7	19.1 km/sec	.....
Proper motions	306.2±0.5	−37.1±1.2	.....	.....
Combined solution	306.4±1.9	−37.4±4.6	17.9±0.5	0.05±0.14

$\Delta\mu_\delta'$ necessary to reduce the proper motions in declination to the FK3 system. These have been taken from tables given by Kopff of the systematic differences between the GC and the FK3 motions.[5] The radial velocities will be discussed in Section IV. In computing the tangential motions, the spectroscopic parallaxes have been employed in this section. They are more concordant than are the trigonometric parallaxes, and the term *P* allows for any systematic error arising from the uncertainty in the zero point of the absolute-magnitude scale. The position of the convergent point and the value of the stream velocity found by Smart have been used as preliminary values.

The amount and mean errors of the observed quantities will be found in Table 15. Table 2 lists the weights assigned to each quantity for each star. It will be noticed that the proper motions are given much more weight than are the other types of data. Table 3

[2] See, e.g., *B.A.N.*, **9**, 417, 424, 1943.

[3] The proper motion for the stars near the nucleus which are too faint to be included in the GC have been taken from *Trans. Yale U. Obs.*, **4**, 1925, **7**, 1937.

[4] *M.N.*, **101**, 37, 1941. [5] *A.N.*, **269**, 160, 1939.

gives the stream elements found by Smart and those obtained in the present investigation from the proper motions alone and from the solution combining the three sets of data. Solutions were also made from the radial velocities and from the tangential motions separately. In these cases the position of the convergent point is determined only by the variations in the observed quantities across the nucleus region. The uncertainty in these solutions is so large that they are of no interest.

At first sight, it seems surprising that the probable errors of A and D are less in the solution from the proper motions alone than in the combined solution. This happens because the additional data contribute little weight, while two additional unknowns are introduced. Further, the uncertainties in the radial and tangential velocities are forced on the determination of A and D in the combined solution, as well as on the determination of V. As a result of these effects and of the high accuracy of the proper-motion data, the solution from the position angles alone is to be preferred, although the results are not appreciably different. Table 4 indicates how well the position angles of the proper motions of the nucleus stars are satisfied by this position; the agreement in the case of the radial velocities and parallaxes will be discussed in Section IV (see Table 12).

TABLE 4

RESIDUALS FROM THE ADOPTED POSITION OF THE CONVERGENT POINT

Star	$\Delta\theta$	Star	$\Delta\theta$	Star	$\Delta\theta$
37 UMa	+1°.5	HR 4867	+2°.2	ζ UMa A	−1°.9
β UMa	−0.1	ϵ UMa	−2.5	ζ UMa B	+2°.3
γ UMa	−0.1	78 UMa	−0.8	80 UMa	−2°.4
δ UMa	+0.5	HD 115043	+2.3		

IV. THE RADIAL AND SPACE VELOCITIES OF THE NUCLEUS STARS

Although the point of convergence of the motions of the Ursa Major nucleus stars can be found quite accurately from the large proper motions of these stars, a determination of the space velocity of the cluster must depend on either the radial velocities or the parallaxes. The parallaxes are about 0".040, and the individual trigonometric determinations may be uncertain by 20 per cent or more. Since the stars are mainly early A-type stars and many have poor lines, there are discordances among the numerous measurements of their radial velocities. Some of the determinations were based on only a few plates; others indicated that the velocities of several of the stars were variable, without further confirmation or disproof. For these reasons it was considered worth while to remeasure these radial velocities in an attempt to strengthen the value of the speed of the cluster. Table 5 gives the radial velocities available for these stars in Moore's catalogue.[6]

Dr. W. P. Bidelman kindly agreed to obtain the plates for this purpose. These were taken with the Cassegrain glass spectrograph of the McDonald Observatory, which gives a dispersion of 26 A/mm at $H\gamma$. The dispersion is such that the kilometers per second per millimeter is reasonably large but the star lines, while broadened by rotation, are not widened to the extent that they are particularly difficult to measure. The spectra are wide and well exposed, and the cores of the hydrogen lines can be measured with reasonable ease. Plates of other stars in the same region of the sky were taken at the same time as those of the nucleus stars, in order to afford a check on the system of the velocities. Table 6 contains a summary of the plates obtained. The spectral type, line quality, and the measured radial velocity are given for each of the nucleus stars.

[6] *Lick Obs. Bull.*, Vol. **18**, 1932.

TABLE 5*

PREVIOUSLY PUBLISHED RADIAL VELOCITIES FOR THE NUCLEUS STARS

Star	Measures (Km/Sec)	Mean (Km/Sec)
37 UMa	W −9.9±2.2 L −13.0±1.3	−12.4±1.2
β UMa	Pot −15.5±0.6 var? L −11.4±0.1 Y −10.6±1.3	−12.1±0.1
γ UMa	L −12.9±3.0 M −13.4±1.8 P +30.3 Y −5.8±2.7	−11.1±1.3
δ UMa	L −15.8±3.0 Y −9±15 Vn −10 ±7	−12 ±6
HR 4867	W −9.5±3.1 L −10.2±3.3	−9.7±2.2
ε UMa	Pot −11.9	SB O Ludendorff
78 UMa	L −9.2±1.5 W −3.1±1.6	−7.2±1.2
HD 115043	L −7.9±1.3	
ζ UMa A	M −9.6 O Hadley Pot −12.0 O Ludendorff Vn −8 O Hnatek	−9.9
ζ UMa B	Y −7.4±0.7 var L −10.8±1.3 Pot −12.5±0.7 O −23.6±1.2	−9.2±0.1*
80 UMa	Y +0.1±2.5 L −12.5±0.4	−2.0±2.1*

* The notation used in this table is that of Moore's catalogue of radial velocities.

TABLE 6

SUMMARY OF THE MCDONALD VELOCITIES FOR THE BRIGHT NUCLEUS STARS

Name	Sp. Type	Line Quality	No. of Plates	Measured Velocity	Corrected Velocity
37 UMa	F1 V	Fair	10	−17.3±0.7	−14.6
β UMa	A0 V	Fair	10	−13.3±0.7	−10.6
γ UMa	A0 V	Poor	15	−16.6±0.9	−13.9
δ UMa	A3 V	Poor	14	−20.6±1.5	−17.9
HR 4867	F6 V	Good	10	−20.0±0.4	−17.3
ε UMa	A0 p	Good	10	−8.1±0.3	−5.4
78 UMa	F2 V	Fairly poor	10	−17.7±0.9	−15.0
HD 115043	G2 V	Good	5	−11.8±0.3	−9.1
ζ UMa A	A2 V	Fair	14	−8.0±1.0	−5.3
ζ UMa B	A2 m	Fair	10	−15.4±0.7	−12.7
80 UMa	A5 V	Poor	14	−10.3±1.2	−7.6

Each plate was measured in the direct and reverse direction at the same sitting, as the systematic error in setting on the broad lines characteristic of many of the stars changed perceptibly from time to time. Care was taken to choose comparison lines of nearly the same strength, since the strong ones were broadened asymmetrically. An investigation showed that the asymmetrical broadening is not sufficient to affect the measures noticeably in the range of line strengths used; it may account, at least partly, for the systematic difference between the McDonald and the Lick velocities.

Table 7 gives the wave lengths used for the star lines. For the lines in the A- and early F-type stars, which are essentially unblended, they have been taken from the *Revised Multiplet Table*;[7] for the later-type stars measured, the wave lengths are from the list recommended by the I.A.U.[8] except that the *RMT* wave lengths have been retained for the strong lines also measured in the earlier-type stars. For each star the velocity was also determined from each line separately. The results are given in Table 8, where the velocity from each line has been compared with the velocity from $H\gamma$, in order to make the results from the various stars comparable. ζ UMa A has not been included because

TABLE 7

ADOPTED WAVE LENGTHS

Wave Length	Identification	Wave Length	Identification
3933.664	*Ca* II K	4260.479	*Fe* I
3970.076	*He*	4271.545	*Fe* I blend
4005.256	*Fe* I	4307.927	*Fe* I
4045.818	*Fe* I	4320.816	*Sc* II, *Ti* II
4063.621	*Fe* I	4340.468	$H\gamma$
4067.979	*Fe* I	4351.770	*Cr* I
4071.742	*Fe* I	4383.555	*Fe* I
4101.737	$H\delta$	4385.381	*Fe* II
4130.884	*Si* II	4404.752	*Fe* I
4143.722	*Fe* I blend	4427.258	*Ti* I, *Fe* I
4202.054	*Fe* I	4443.802	*Ti* II
4226.742	*Ca* I	4468.493	*Ti* II
4233.167	*Fe* II	4481.228	*Mg* II
4254.350	*Cr* I		

the plates of this star were taken at random phases and the lines measured differed according to whether the star lines appeared sharp, diffuse, or widely double. A correction was applied to the velocities of this star to allow for the small difference in amplitude between the two components.

The difference between the velocity measured for each plate and the mean velocity of the star was computed for each of the stars with moderately good lines. These were then grouped according to the date on which the plates were taken and the hour angle at the middle of the exposure. Table 9 summarizes the results, together with the mean error of the mean, computed from the range of the residuals, and the number of plates included in the mean (in parentheses). A systematic hour-angle effect is apparently absent, as is to be expected for a well-built instrument used near the meridian.

The measured velocities for the six standard stars are collected in Table 10, together with the Lick velocity, the difference McDonald minus Lick, and the number of plates measured. The McDonald velocities are definitely more negative than those from Lick. From the six stars the mean correction to the McDonald system is $+2.7 \pm 0.6$ km/sec, and a correction of this amount has been applied to the measured velocities in Table 6.

[7] *Contr. Princeton U. Obs.*, No. 20.

[8] *Trans. I.A.U.*, **5**, 193, 1935.

The differences McD − Lick for the corrected velocities of the nucleus stars show a large scatter, but the mean amount is McD − Lick = -0.8 ± 1.5 km/sec. Because of the meager data, a single correction was applied independently of spectral type.

While this investigation was in progress, R. M. Petrie, at Victoria, was conducting a similar investigation into the velocities of the cluster stars, using a dispersion of 11 A/mm. He obtained a number of plates of each star and took great care to reduce his measures to the Lick system. Table 11 compares the Victoria (Petrie) velocities, the velocities from Moore's catalogue, the Lick velocities, and the McDonald velocities. For most of the stars the agreement is good. ϵ UMa is a spectrum variable for which a velocity variation has been announced by several observers. There is no evidence of

TABLE 8

MEAN RESIDUALS: LINE − 4340

Line	γ UMa	δ UMa	80 UMa	ϵ UMa	β UMa	λ UMa	84 UMa	ζ UMa B
3933	+9.5	−0.5	−1.9	+1.4	+ 1.5	− 2.1	+0.4	+0.4
3970	.....	.....	.....	.....	.....	.....	−1.1	.....
4005	.....	.....	.....	.....	.....	.....	.....	+1.5
4045	.....	.....	.....	+1.6	− 2.4	− 5.3	−0.4	−3.9
4063	.....	.....	.....	+0.5	+ 0.1	− 8.8	−7.0	−7.9
4067	.....	.....	.....	.....	+10.2	+ 7.4	.....	−6.7
4101	+1.6	−4.3	−5.6	−2.2	− 4.2	− 6.3	−1.4	−2.7
4130	.....	.....	.....	.....	+ 2.1	− 2.5	.....	.....
4233	.....	.....	.....	+5.9	− 3.4	+ 4.0	+3.2	.....
4254	.....	.....	.....	+4.7	.....	.....	+5.5	−1.2
4260	.....	.....	.....	.....	.....	.....	.....	−8.3
4340	0	0	0	0	0	0	0	0
4351	.....	.....	.....	+8.0	+ 1.9	+ 6.7	+4.5	.....
4383	.....	.....	.....	.....	.....	+ 2.0	.....	−1.1
4385	.....	.....	.....	.....	.....	.....	.....	−7.9
4404	.....	.....	.....	.....	.....	.....	.....	−1.2
4443	.....	.....	.....	.....	+ 6.1	− 1.7	.....	.....
4468	.....	.....	.....	.....	+ 4.3	+13.2	.....	.....
4481	+5.4	.....	+9.6	−1.9	+ 6.6	+ 0.6	−1.9	.....
4340−mean	−3.4	+1.6	+0.1	−1.8	− 1.2	+ 0.6	−2.1	+3.2

Line	78 UMa	37 UMa	15 UMa	HR 4867	θ Boo	47 UMa	HD 115043	Sun
3933	.....	.....	+ 0.3	.....	.....	.....	.....	.....
4005	.....	− 8.3	− 4.8	−4.8	−6.8	−6.1	−8.9	− 3.5
4045	−20.1	− 2.8	− 5.4	+1.1	−3.3	−4.1	−3.5	+ 2.0
4063	−15.7	− 7.0	−10.7	−0.6	−3.5	−2.8	−3.6	+ 2.7
4071	−11.1	− 6.8	−11.6	−1.1	−0.5	0	−0.3	+ 3.2
4101	− 7.4	− 4.1	− 1.5	−2.4	−3.8	−4.2	−7.1	0
4143	.....	.....	.....	.....	.....	−3.3	+0.6	+ 7.6
4202	.....	.....	.....	.....	.....	+1.0	+1.6	+ 4.5
4226	.....	.....	.....	.....	.....	+4.8	+7.1	+11.5
4254	+ 0.1	− 7.4	.....	+3.9	−0.4	−6.2	−2.4	− 6.3
4260	− 7.6	−14.7	−12.2	−4.1	−6.9	−7.4	−8.6	.....
4307	.....	.....	.....	.....	.....	−1.4	−6.2	+ 1.0
4320	.....	.....	.....	.....	.....	−1.2	−4.6	+ 2.4
4340	0	0	0	0	0	0	0	0
4383	.....	− 4.7	.....	−4.0	−8.3	−7.2	−8.8	− 7.7
4404	− 8.5	− 5.4	.....	+1.7	−0.1	−0.6	−2.5	+ 2.1
4427	.....	.....	.....	.....	.....	+3.8	−1.2	+ 0.9
4340−mean	+ 9.2	+ 6.3	+ 6.0	+1.0	+3.4	+1.6	+2.9	− 1.8

TABLE 9

THE VELOCITY RESIDUALS AS A FUNCTION OF THE DATE AND THE HOUR ANGLE

DATE	EAST				WEST			MEAN
	1½ Hours	1 Hour	½ Hour	0 Hour	½ Hour	1 Hour	1½ Hours	
Apr. 3	0.0 ±1.8 (2)	−1.6 ±0.5 (3)	−1.6 ±0.3 (2)	−1.2 ±0.7 (4)	+1.4 ..... (1)	0.0 ..... (1)	....	−0.88 ±0.27 (13)
Apr. 4	....	....	+0.4 ±1.3 (4)	−0.3 ±0.8 (10)	+1.6 ±1.6 (2)	−0.1 ±1.8 (4)	....	+0.08 ±0.15 (20)
Apr. 8	....	....	....	....	−1.5 ±0.7 (4)	+0.3 ±1.0 (9)	−0.8 ±1.2 (4)	−0.37 ±0.22 (17)
Apr. 9	....	....	−0.2 ±1.2 (5)	−1.1 ±0.8 (3)	+2.1 ±0.4 (2)	....	....	−0.01 ±0.35 (10)
Apr. 15	....	....	+1.6 ±0.4 (2)	....	−0.8 ±0.9 (4)	+0.1 ±1.0 (7)	+0.2 ±0.9 (5)	+0.09 ±0.12 (18)
Apr. 16	....	....	+0.7 ..... (1)	+0.4 ±0.9 (3)	0.0 ±1.4 (2)	+1.2 ±0.9 (4)	....	+0.67 ±0.18 (10)
Apr. 17	....	+0.6 ±0.9 (2)	−0.8 ±0.8 (2)	+0.2 ..... (1)	+0.1 ±1.1 (2)	+0.5 ±1.2 (4)	+1.0 ±0.4 (2)	+0.31 ±0.15 (13)
Mean	0.0 ±1.8 (2)	−0.7 ±0.7 (5)	−0.02 ±0.23 (16)	−0.45 ±0.13 (21)	−0.01 ±0.34 (17)	+0.34 ±0.07 (29)	−0.02 ±0.11 (11)	....

TABLE 10

RADIAL VELOCITIES OF THE STANDARD STARS

Star	Lick Velocity	McD Velocity	McD−L	No. of Plates
15 UMa	− 1.0±0.4	− 5.6±0.7	−4.6	4
λ UMa	+17.5±1.2	+17.2±0.7	−0.3	8
47 UMa	+13.0±0.9	+ 8.2±0.6	−4.8	8
84 UMa	− 4.8±1.3*	− 2.7±1.6	+2.1	5
θ Boo	−11.2±0.4	−15.5±0.4	−4.3	14
Sun	+0.5†	− 1.0±0.6	−1.5	3

* No Lick velocity is available for this star. This is a mean of the velocities from Victoria, Yerkes, and Mount Wilson.

† Computed.

variation in the measures of the McDonald plates, but, as these were taken within an interval of 2 weeks, a long period or irregular variation is not excluded. The velocity of ζ UMa A from the McDonald plates is somewhat more uncertain than that of other observers because of the scatter in the phase at which the plates were taken; Petrie's measures were made at the time of gamma-velocity. It is possible that HR 4867 is a spectroscopic binary, with a long period. The McDonald plates show no appreciable variation, but the disagreement between them and the Lick and Mount Wilson velocities, as well as the probable errors of these determinations, are larger than would be expected for a late F-type star.

In order to reduce the scatter among the individual velocities and, at the same time, to keep the system as uniform as possible, the Lick, Victoria, and McDonald velocities were combined to form the means also given in Table 11. These mean velocities were then used, together with the convergent point derived in Section III, to determine the speed of the cluster as 15.7 ± 0.8 km/sec. Allegheny Observatory has published trigonometric parallaxes for eight of the ten nucleus stars. There is also another determination of the

TABLE 11

RADIAL VELOCITIES OF THE NUCLEUS STARS

Star	Lick	Petrie	McD	Adopted Mean
37 UMa	−13.0	− 9.8	−14.6	−12.5
β UMa	−11.4	−12.5	−10.6	−11.5
γ UMa	−12.9	−13.6	−13.9	−13.5
δ UMa	−15.8	−14.6	−17.9	−16.1
HR 4867	−10.2	.....	−17.3	−13.8
ϵ UMa	− 8.0	.....	− 5.4	− 6.7
78 UMa	− 9.2	− 8.7	−15.0	−11.0
HD 115043	− 7.9	.....	− 9.1	− 8.5
ζ UMa A	− 9.9*	− 7.4	− 5.3	− 9.3
ζ UMa B	−10.8	−10.2	−12.7	−11.2
80 UMa	−12.5	− 9.1	− 7.6	− 9.2

* Mean of the Potsdam, Michigan, and Vienna orbits.

parallax available for several of these stars, but, as these add little weight to the Allegheny values, they were omitted in order to keep the observational data uniform. A combination of these parallaxes and the corrected proper motions yields the value 18.4 ± 1.3 km/sec for the speed of the cluster and $0''.040 \pm 0''.004$ for the mean parallax of the nucleus. An unweighted mean of the two determinations, 17.0 km/sec, appears to be the best value available. Table 12 shows the agreement between the observed radial velocities and parallaxes and those computed from this mean. Although the difference between the results of the two determinations is somewhat larger than might have been expected from their mean errors, the individual residuals are satisfactorily small. Table 13 summarizes the elements of the cluster motion.

V. THE NUCLEUS

The ten stars which we have called the nucleus stars form a condensation in a stream which extends as far as observations permit us to reach. The question naturally arises as to whether there are any other stars which are more closely associated with the nucleus than with the remainder of the stream. In order to investigate this question, the volume of space within 20 parsecs of the center of the nucleus has been considered more carefully. The choice of this region was governed by three considerations: the proper motions are fairly large throughout most of this area; the stars all have parallaxes greater than

0".020; and, since this region extends to four times the radius of the nucleus itself, it is possible to estimate the boundary of the condensation.

Among the brighter stars, only the ones already distinguished as nucleus members exhibit any concentration. Only four of the stars discussed in Section VI lie within the region considered and have space velocities accurately parallel to those of the nucleus stars. Since the discovery probability for such stars would be high, there are probably only nine nucleus members brighter than 6.5 mag.

To ascertain whether there are any members of the cluster among the fainter stars, two searches were made. The first, among the stars in the GC, covered all areas containing stars within 20 parsecs of the center of the nucleus, with the exceptions of a belt within 10° of the line on which the proper motions of the cluster stars are indistinguishable from those of stars moving toward the solar antapex, and of the region within 25° of the radiant of the cluster. The second search, in the *Transactions of the Yale University Observatory*, Volumes **4** and **7**, covered the area between the declinations +50° and +60° and between the right ascensions of 10^h and 14^h. However, the latter search revealed only one star not previously listed by Haas, and this was later ruled out by its radial velocity.

TABLE 12

RESIDUALS FROM THE ADOPTED CLUSTER VELOCITY

STAR	VELOCITIES		PARALLAXES	
	Comp.	Obs.	Comp.	Trigonometric
37 UMa	−14.9	−12.5	0".043	0".033±0".018
β UMa	−14.4	−11.5	.046	.047± .009
γ UMa	−13.3	−13.5	.042	.027± .011
δ UMa	−12.7	−16.1	.044	.050± .009
HR 4867	−11.8	−13.8	.041	.038± .016
ε UMa	−11.6	− 6.7	.043	.....
78 UMa	−11.4	−11.0	.043	.030± .016
HD 115043	−11.0	− 8.5	.041	.....
ζ UMa A	−10.6	− 9.3	.045	.041± .011
ζ UMa B	−10.6	−11.2	.043	
80 UMa	−10.5	− 9.2	0.043	0.039±0.015

TABLE 13

THE ADOPTED CLUSTER ELEMENTS

1900 Equatorial Elements	1900 Galactic Elements	Motion in Local Centroid	Assumed Solar Motion
$A=306°.2$ $D=-37°.1$ $V=17.0$ km/sec	$L=332°.8$ $B=-36°.4$ $V=17.0$ km/sec	$L=2°$ $B=-6°$ $V=29$ km/sec	$L=23°.5$ $B=+21°.6$ $V=19.6$ km/sec

Both searches were conducted similarly. Among the stars with proper motions greater than 0".030/year, those were selected for which the position angle of the proper motions agreed approximately with the direction of motion of a cluster star in the same position. If the star's radial velocity was available, it was used as a second criterion. For each star selected in this way, the GC proper motion was corrected and the direction compared

with that computed for the star from the elements of the cluster motion. If the position-angle residual was less than 20° and could be eliminated by a change of less than five times the published probable error in the proper motion, the cluster parallax was used to compute the galactic rectangular co-ordinates of the star. In this way, 35 stars were selected which lay within 20 parsecs of the center of the nucleus and which might be members of the cluster on the basis of existing data. For each of these stars spectroscopic parallaxes and/or radial velocities were obtained. These ruled out the majority of the stars selected.

A one-prism spectrograph attached to the 40-inch refractor was used to obtain the plates for the spectroscopic parallaxes in this section and in Section VI. This is the spectrograph used for the Yerkes spectral atlas[9] and all spectral types are on the system of that atlas unless otherwise noted. The radial-velocity plates were taken with the $f/2$ glass spectrograph of the McDonald Observatory by Messrs. Hiltner, Code, and Braun, and have a dispersion of 75 A/mm at $H\gamma$.

Figure 1 shows all stars within 20 parsecs of the center of the nucleus which apparently share the cluster motion accurately, including the five stars found in the present investigation. It appears that thirteen of the stars form a compact group, $10 \times 6 \times 4$ parsecs across. The remaining stars are probably members of the stream. It is interesting to note that the dimensions of this cluster are about average for a poor cluster showing little contrast with the background,[10] although the total membership of thirteen stars (fifteen, if the components of ζ UMa are counted separately) makes it a very poor cluster indeed. Raab lists only two clusters with less than twenty members.[11] Moreover, since his figures are based on counts on the Franklin Adams charts, his estimates probably include only the brighter stars and are minimum values.

Table 14 gives for each cluster star the name, the HD number, the position, the apparent magnitude, the HD spectral type, and the rectangular galactic co-ordinates referred to the center of the nucleus. Stars 5 and 6 were included in Haas's list[12] and 6 was also suggested as a possible member by Hertzsprung.[13] Table 15 contains the relevant observational data and compares this with the computed data. For the stars brighter than 7.5 mag. the spectral types in this table have been given by W. W. Morgan. The three K-type stars have been added as a result of the present investigation; the remaining stars were used in the above discussion of the motion of the nucleus stars. The two members from Haas's list are included here rather than in Section VI.

Figure 2 illustrates the H-R diagram of the cluster. There are no giants, although the peculiar star ϵ UMa lies above the main sequence. There is no indication that the ending of the main sequence at K3 is not the result of incomplete observational data. The faintest star in the cluster is 9.2 mag. pg, and it is improbable that the Yale catalogues are complete even to this limit.

It is interesting to note that, of the four stars later than G0, three show emission at H and K.[14] The emission in HD 115043 is weak and would be missed except on fairly high dispersion, but that in the two K-type stars is quite strong. Thus 75 per cent of the stars in this cluster later than G0 show emission at H and K as compared with 70 per cent of the stars G5 and later in the Hyades[14] and with 6 per cent of the stars of spectral types G0–K4 among the proper-motion stars.[15] The latter two percentages are minimum

[9] Morgan, Keenan, and Kellman, *An Atlas of Stellar Spectra* (Chicago: University of Chicago Press, 1943).

[10] Trumpler, *Lick Obs. Bull.*, **14**, 154, 1930.

[11] *Lund Medd.*, Ser. II, No. 28, 1922.

[12] *A.N.*, **241**, 233, 1931. [13] *B.A.N.*, **9**, 286, 1942.

[14] HD 115043 and 110463 are included in the list of stars with emission at H and K by Joy and Wilson, *Ap. J.*, **109**, 231, 1949. The discovery of H and K emission in HD 109011 is apparently new.

[15] Joy, *Ap. J.*, **105**, 96, 1947.

values, since some plates may not be sufficiently exposed in the region of the K line to show the emission; but the difference between 6 per cent for stars in general and 70 per cent for members of the two open clusters must indicate a real difference. However, HD 124752 shows no strong emission lines.

Table 16 contains a list of the remaining stars for which radial velocities were measured. The spectral types of the three standard-velocity stars are from the I.A.U. list;[16] those marked by an asterisk were estimated from the radial-velocity plates rather than from plates taken specifically for spectral classification. The five plates of standard stars are not sufficient to secure the system of these velocities. The discrepancy for HD 107328 is much larger than would be expected from the run of the mean errors for the other stars. The velocities from the two plates of this star agree within 1 km/sec, and no combina-

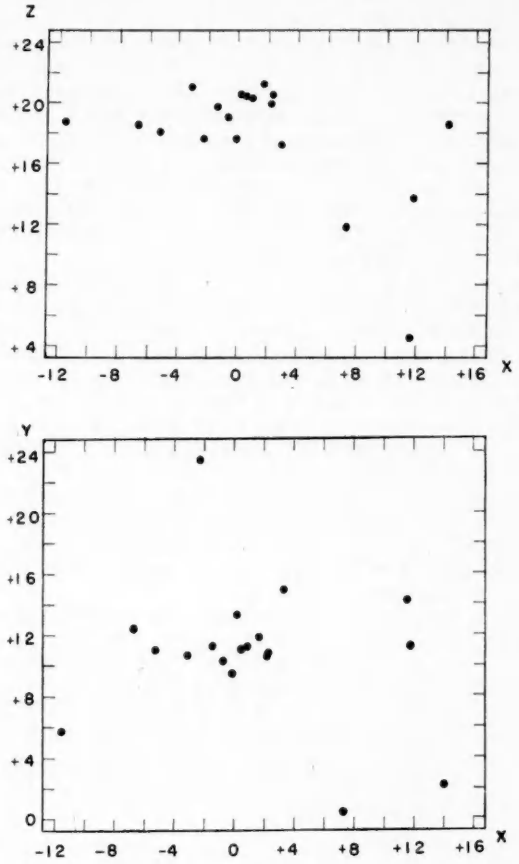

FIG. 1.—The space distribution of the nucleus and stream members within 20 parsecs of the center of the nucleus. The scale is in parsecs, measured from the sun.

[16] *Trans. I.A.U.*, 5, 191, 1935.

tion of lines measured will give a velocity as low as the catalogue velocity for the star. Since the other two standard-velocity stars yielded satisfactory residuals, no attempt has been made to correct the system. Also, the velocity found by R. E. Wilson for HD 110463 is in excellent agreement with that found from the McDonald plates (53). The agreement of the velocities from different plates of the same star indicates an average mean error per plate of 5 km/sec.

It is usually thought that a loose cluster, such as the Ursa Major cluster, is unstable, since there can be no important gravitational interaction between members. The shearing effects of galactic rotation will disrupt such a cluster if all members have the same linear velocity. Also, since the density of the nucleus is barely that of the field of stars through which the cluster moves, encounters with field stars will tend to disintegrate it further.

TABLE 14

THE MEMBERS OF THE URSA MAJOR NUCLEUS

No.	Name	HD No.	α_{1900}	δ_{1900}	m_v	Sp.	X	Y	Z
1	37 UMa	91480	$10^h28^m.7$	+57° 36′	5.16	F0	−6.2	+0.9	−1.0
2	β UMa	95418	10 55.8	56 55	2.44	A0	−4.8	−0.5	−1.5
3	γ UMa	103287	11 48.6	54 15	2.54	A0	−2.6	−0.8	+1.5
4	δ UMa	106591	12 10.5	57 35	3.44	A2	−0.9	−0.2	+0.2
5	.....	109011	12 26.5	55 40	8.1	K0	−0.2	−1.2	−0.4
6	.....	110463	12 37.2	56 17	8.4	K0	+0.4	−2.0	−1.9
7	HR 4867	111456	12 44.3	60 52	5.87	F5	+0.7	+1.8	+1.0
8	ϵ UMa	112185	12 49.6	56 30	1.68	A0p	+0.9	−0.4	+0.9
9	78 UMa	113139	12 56.4	56 54	4.89	F0	+1.4	−0.3	+0.8
10	.....	115043	13 9.5	57 14	6.74	G0	+2.2	+0.4	+1.7
11	ζ UMa A	116656	13 19.9	55 27	2.40	A2p	+2.7	−0.9	+0.5
	ζ UMa B	116657			3.96	A2			
12	80 UMa	116842	13 21.2	55 30	4.02	A5	+2.8	−0.7	+1.0
13	.....	124752	14 10.3	68 03	8.2	K0	+3.8	+3.8	−2.3

TABLE 15

DATA CONCERNING THE NUCLEUS MEMBERS

No.	μ	θ_o	θ_c	ρ_o	ρ_c	π_{tr}	π_c	Sp.	M_c
1	0″.074±0″.002	60°.0	58°.5	−12.5±1.0	−14.9	0″.033±0″.018	0″.043	F1 V	+3.2
2	.087± .001	67.8	67.9	−11.5±0.6	−14.4	.047± .009	.046	A0 V	+0.5
3	.094± .001	84.5	84.6	−13.5±1.0	−13.3	.027± .011	.042	A0 V	+0.5
4	.106± .001	85.1	85.6	−16.1±1.5	−12.7	.050± .009	.044	A3 V	+1.7
5*	.111± .021	93.1	90.8	−12.4±1.7	−12.3	.....	.045	K2 V	+6.4
6†	.127± .021	90.0	90.8	− 5.8±1.5	−12.0	.....	.050	K3 V	+6.9
7	.107± .005	91.1	88.9	−13.8±1.0	−11.8	.038± .016	.041	F6 V	+3.9
8‡	.113± .001	92.5	95.0	− 6.7±1.0	−11.6	.....	.043	A0 p	−0.2
9	.114± .003	95.0	95.8	−11.0±1.0	−11.4	.030± .016	.043	F0 V	+3.3
10§	.115± .006	104.6	102.3	− 8.5±0.6	−11.0	.....	.041	G2 V	+4.8
11A	.126± .001	99.6	101.5	− 9.3±0.5	−10.6	.041± .011	.044	A2 V	+1.3
11B‖	.122± .003	103.8	.....	−11.2±0.8	.....	.....	.....	A2 m	+2.1
12	.120± .002	98.1	101.5	− 9.2±1.5	−10.5	0.039±0.015	.043	A5 V	+2.2
13	0.149±0.016	129.0	126.2	− 5.6±2.0	− 9.8	.....	0.043	K0 V	+6.4

* H and K emission; the emission lines give the velocity −4 km/sec.

† H and K emission; the emission lines give the velocity −4 km/sec.

‡ A spectrum variable (see *An Atlas of Stellar Spectra*, p. 18).

§ H and K emission. ‖ A metallic-line star. The K line type is A2, but the type obtained from the metallic lines is A7.

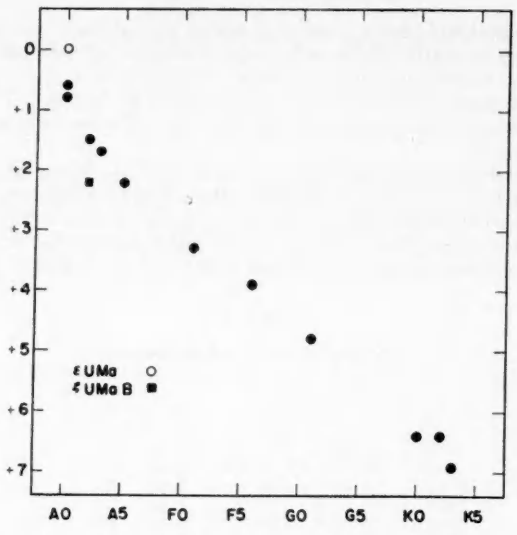

FIG. 2.—The H-R diagram for the Ursa Major nucleus

TABLE 16

NONCLUSTER STARS MEASURED FOR RADIAL VELOCITY

Star	ρ_c	ρ_o	No. of Plates	M_c	Sp.	Remarks
HD 77624	−15.2	−36.5	3	+8.3	G8 III*	
84703	−13.6	+30.4	3	+7.2	F8 V*	
86987	−13.2	−11.8	3	+6.6	F5 V*	
88009	−15.0	−12.3	3	+5.6	K2 III	
88270	−15.1	+ 1.9	5	+8.0	F2 VI	
89449	+ 6.2	+10.4	2	.....	F5	Standard-velocity star
90915	−14.7	− 1.2	5	+6.2	G0 V*	
94426	−14.8	+ 9.4	4	+5.0	F8 V	
94686	−12.0	−21.7	4	+4.9	F8 V	Stream member
98618	−14.2	+12.8	4	+5.1	G5 V	
107328	+35.4	+53.4	2	.....	K1	Standard-velocity star
114762	+49.6	+50.3	1	.....	F9	Standard-velocity star
115349	− 9.5	−45.7	2	+8.4	G2 V	
140625	− 6.7	−30.0	2	+6.3	K0 V	
149907	+ 2.6	− 7.8	3	+5.4	K0 III*	
151044	− 3.0	− 0.1	1	+5.0	F8 V	Stream member
160291	+ 0.2	−24.1	2	+5.6	F6 V*	
238179	−11.4	−34.4	3	+6.8	G8 V	(21)
238208	−11.0	−41.9	3	+6.3	K2 V	(21)
BD+8°2658	− 6.7	+11.3	1	+9.1	K0 V*	

Shearing effects will play no role if the stars in the cluster have the same angular momentum in their revolution about the galactic center rather than the same linear velocity. Instead, the stars will move together in epicycles about the same circular orbit.[17] The investigations of Mlles Canavaggia and Fribourg and of Bartholeyns indicate that the latter may be the case, although their results are highly uncertain. The high velocity of the cluster with respect to the local standard of rest leaves little chance for strong gravitational interactions between cluster members and field stars. Following the method of analysis developed by Chandrasekhar,[18] it is found that a member of the cluster will probably change its kinetic energy with respect to the center of the nucleus by less than 20 per cent in a time of 3×10^9 years. This means that the lifetime of the cluster is of the same order as the galactic time scale.

These arguments also apply to the extended stream, but, in this case, any dispersion in velocities already existing among the members will disrupt the group much more rapidly.

VI. STREAM STARS

That the overlap among the numerous lists of members of the Ursa Major stream is surprisingly small has been mentioned earlier. Since most of the authors possessed similar observational data, the differences must be laid to varying treatments of these data. The method which has been used most frequently to pick up stream members has been to calculate space velocities for all stars and to include as stream members all stars with velocities agreeing with the cluster velocity within a given tolerance. This is by far the simplest method of finding stream members and has the added advantage that the resulting space velocities are useful in other studies. However, the effects of observational errors, which are different in the different components of the velocity, are badly confused. Thus, in order to allow for a large observational uncertainty in the tangential velocities computed from small parallaxes, a large tolerance is necessary, while this tolerance may be completely unallowable when applied to the direction of a large proper motion. Thus this method tends to pick up most stars which might be stream members, but it is uncritical. Some of the differences between the various lists made in this manner can be attributed to different choices of the cluster velocity; others arise from the different tolerances permitted in the velocity residuals. Among the recent investigators, only Smart, Bartholeyns, and Delhaye have treated the proper motions, radial velocities, and parallaxes separately.

To facilitate statistical studies of the Ursa Major stream, the numerous lists of members have been combined and are repeated in this section. Dr. J. H. Oort has kindly sent me an unpublished list of stars brighter than 6.5 mag. with space motions differing from that of the cluster by less than 10 km/sec in each co-ordinate. This list is also included in this section, although many of the stars are probably not members of the stream. It is improbable that more than a very few stream stars brighter than 6.5 mag. with known space motions have been omitted from this combined list of stream members; the list is very incomplete among the fainter stars. Table 17 gives for each star the name, another identification, the 1900 position, the apparent magnitude, the HD spectral type, and a reference to the paper listing the star. These references are indicated by the number of the paper in the bibliography. The two stream stars discovered as a result of the investigation discussed in Section V are marked by an asterisk in the references, while the stars included on Oort's list but not on any list of stream members are designated by O. If four or more authors have listed the same star independently, it is considered to be generally recognized as a stream member, and no individual reference is given. The 69 stars north of declination $-30°$ which are most likely to be stream members are marked by an asterisk following the number of the star. Star No. 91 is also probably a stream member.

[17] See S. Chandrasekhar, *Principles of Stellar Dynamics* (Chicago: University of Chicago Press, 1942), sec. 4.3.

[18] *Ap. J.*, **93**, 285, 1941.

TABLE 17

Stars Listed by Various Authors as Members of the Ursa Major Stream

No.	Name	HR No.	α(1900)	δ(1900)	m	Sp.	Reference
14	36 Psc	59	$0^h11^m.4$	+ 7°41'	6.19	G5	0
15		60	0 11.6	+60 59	5.80	G5	0
16	θ And	63	0 11.9	+38 8	4.44	A2	2, 16, 37
17*	σ And	68	0 13.1	+36 14	4.51	A2	17, 38
18	44 Psc	97	0 20.3	+ 1 23	5.99	G5	17
19		157	0 32.0	+34 51	5.62	G5	0
20	32 And	175	0 35.7	+38 55	5.42	G5	0
21	μ Phe	180	0 36.6	-46 38	4.65	K0	17, 38
22		196	0 39.6	+54 40	5.47	A0	2, 16, 38
23	φ^2 Cet	235	0 45.1	-11 11	5.24	F5	
24*	η And	271	0 51.9	+22 53	4.62	G5	0
25		276	0 52.7	+13 9	6.44	G5	0
26	39 And	290	0 57.3	+40 48	5.86	A2	
27	27 Cet	315	1 0.6	-10 31	6.41	G5	0
28	β Phe	322	1 1.6	-47 15	3.35	K0	32
29	80 Psc	330	1 3.2	+ 5 7	5.67	F0	7, 16
30	44 And	340	1 4.6	+41 33	5.74	G0	0
31	33 Cet	347	1 5.4	+ 1 55	6.20	K0	0
32*	89 Psc	378	1 12.6	+ 3 5	5.28	A2	
33	ρ Psc	413	1 20.9	+18 39	5.32	F0	16, 37
34	ω And	417	1 21.7	+44 53	4.96	F5	
35	40 Cas	456	1 30.5	+72 32	5.50	K0	37
36*		461	1 31.6	+57 28	5.74	K0	0
37		485	1 36.0	+29 32	6.02	K0	0
38	γ Psc	489	1 36.2	+ 4 59	4.68	K0	0
39	π Scl	497	1 37.6	-32 49	5.28	K0	2, 38
40		498	1 37.6	-37 20	5.64	A0	32
41		501	1 37.7	-50 33	6.72	A2	32
42		513	1 41.0	- 6 14	5.53	G5	0
43	1 Ari	530	1 44.6	+21 47	6.2, 7.6	F5, A2	0
44	χ Cet	531	1 44.7	-11 11	4.77	F0	17, 38, 44
45		534	1 45.6	+10 33	5.94	F0	
46		541	1 47.1	-50 42	6.05	A0	2, 7, 32
47	55 And	543	1 47.3	+40 14	5.63	K0	0
48	λ Ari	569	1 52.4	+23 7	4.83	A5	2, 3, 38
49	48 Cas	575	1 53.8	+70 25	4.61	A3	
50	50 Cas	580	1 54.9	+71 56	4.06	A2	17
51	49 Cas	592	1 56.0	+75 38	5.30	G5	0
52	HD 12350		1 56.0	+70 43	7.64	F0	2
53	ϵ Tri	599	1 57.1	+32 48	5.44	A2	37
54	γ And	603-4	1 57.8	+41 51	2.28	K0	3
55	55 Cas	640	2 6.6	+66 3	6.15	F5+A2	17
56*		647	2 7.6	+47 1	6.03	F0	13, 38
57	65 f' Cet	649	2 7.7	+ 8 23	4.54	G5	2, 17
58	7 Tri	655	2 10.0	+32 54	5.26	A0	3, 16, 37
59	7 Per	662	2 11.0	+57 3	6.15	K0	2
60*		710	2 21.2	-15 47	5.84	A2	
61	HD 15929		2 28.5	-46 19	7.01	G5	32
62	χ' For	744	2 28.9	-35 5	5.88	K0	32
63*	γ Cet	754	2 30.6	+ 5 9	5.02	G5	17
64*		797	2 37.1	+10 19	6.27	A0	
65	κ_1 Cet	804	2 38.1	+ 2 49	3.58	A2	16, 37
66	η For	835	2 43.5	-35 58	6.51	K0	32
67	γ Hyi	872	2 51.1	-75 29	4.70	K2	38
68*		875	2 51.6	- 4 7	5.27	A2	16, 17, 37
69	ϵ Ari	887-8	2 53.5	+20 56	5.25	A2	13
70		892	2 53.7	- 3 11	5.20	A2	3, 38
71*		906	2 56.2	+81 5	5.95	A2	3
72	τ^3 Eri	919	2 58.0	-24 1	4.16	A3	17
73		958	$3^h7^m.1$	+ 6°17'	5.84	G5+A2	0

TABLE 17 (continued)

No.	Name	HR No.	α(1900)	δ(1900)	m	Sp.	Reference
74	32 Per	1002	$3^h14.^m7$	+42°58'	4.98	A2	
75		1016	3 17.0	-24 0	5.67	G5	0
76*		1046	3 22.4	+55 6	4.98	A2	16, 37
77		1112	3 34.5	+59 39	5.98	K0	0
78	η Per	1135	3 38.4	+42 16	3.93	F5	
79		1143	3 39.1	-37 38	4.64	K2	38
80		1195	3 45.7	-36 30	4.24	K0	2, 17, 38
81*		1327	4 11.3	+64 54	5.40	G0	38
82	54 Per	1343	4 13.9	+34 19	5.10	G5	17
83	66 Tau	1381	4 18.4	+ 9 14	5.06	A2	2, 3, 38
84*	$\mathfrak{f}$ Eri	1383	4 18.7	- 3 58	5.23	A2	
85*		1448	4 28.8	+ 5 21	5.78	A0	
86		1483	4 34.2	-12 19	5.02	A2	0
87	R Dor	1492	4 35.6	-62 16	4.8-6.8	Mc	32
88*	2 Aur	1551	4 45.9	+36 32	5.04	K2	0
89	7 Cam	1568	4 49.3	+53 35	4.44	A2	16, 37
90	ϵ Lep	1654	5 1.2	-22 30	3.29	K5	0
91	β Eri	1666	5 2.9	- 5 13	2.92	A3	
92		1686	5 6.1	+79 7	5.16	F8	2, 17, 37
93	14 Aur	1706	5 8.9	+32 34	5.14	A2	13
94	18 Ori	1718	5 10.5	+11 14	5.50	A0	2,3
95	HD 34496		5 12.7	-33 39	7.02	G5	32
96		1752	5 14.8	+29 28	5.72	A0	16, 37
97	σ Aur	1773	5 17.8	+37 18	5.22	K5	0
98	29 Ori	1784	5 19.1	- 7 54	4.21	K0	0
99	17 Cam	1802	5 20.7	+62 59	5.75	K5	0
100	β Lep	1829	5 23.9	-20 50	2.96	G0	17
101	HD 36094		5 24.1	-32 30	6.88	G5	32
102		1866	5 28.4	+54 22	5.96	K5	0
103*	38 Ori	1872	5 29.0	+ 3 42	5.32	A2	2, 3, 38
104	23 Cam	1943	5 34.9	+61 26	6.39	G5	0
105*	θ Aur	1971	5 38.2	+49 47	5.52	A0	3, 17
106*	γ Lep	1982-3	5 40.3	-22 29	3.83	F8	
107*	τ Aur	1995	5 42.2	+39 9	4.64	K0	38
108	ι Aur	2029	5 46.5	+55 41	4.92	A2	
109	136 Tau	2034	5 47.0	+27 35	4.54	A0	17
110*	χ' Ori	2047	5 48.5	+20 16	4.62	F8	
111*	β Aur	2088	5 52.2	+44 56	2.07	A0p	
112		2174	6 3.8	+ 2 31	5.58	A0	32
113	γ Mon	2227	6 10.0	- 6 15	4.09	K0	0
114*	42 Aur	2228	6 10.1	+46 27	6.46	F0	13
115*	8 Gem	2230	6 10.2	+24 0	6.11	G5	0
116		2233	6 10.5	- 0 28	5.68	F5	32
117	2 Lyn	2238	6 10.8	+59 3	4.42	A0	16, 37
118*	RR Lyn	2291	6 18.0	+56 20	5.50	A3	2, 16, 37
119	ζ Col	2296	6 18.5	-33 23	3.98	G5	2, 38
120		2395	6 28.6	- 1 9	5.02	B3	32
121	γ Gem	2421	6 31.9	+16 29	1.93	A0	17
122	ν^3 CMa	2443	6 33.5	-18 9	4.65	K0	0
123	ψ^5 Aur	2483	6 39.5	+43 41	5.34	G0	37
124	ψ^6 Aur	2487	6 40.0	+48 54	5.28	K0	17, 38
125*	α CMa	2491	6 40.8	-16 35	-1.58	A0	
126		2514	6 43.2	- 1 12	5.66	A5	32
127		2551	6 47.4	+ 8 30	5.76	A5	32
128	37 Gem	2569	6 49.2	+25 30	5.77	G0	0
129*	16 Lyn	2585	6 50.3	+45 13	4.80	A2	3, 23
130	ω Gem	2630	6 56.3	+24 21	5.21	K0	17
131	64 Aur	2753	7 11.1	+41 4	5.75	A3	3, 38
132*	λ Gem	2763	7 12.3	+16 43	3.65	A2	
133	65 Aur	2793	$7^h15.^m4$	+36°57'	5.21	K0	32

TABLE 17 (continued)

No.	Name	HR No.	α(1900)	δ(1900)	m	Sp.	Reference
134	59 Gem	2816	$7^h18^m.3$	+27°50'	5.71	F0	16, 37
135	ε CMi	2828	7 20.2	+ 9 28	5.07	G5	0
136	δ CMi	2864	7 24.2	+12 13	4.85	K0	16, 17
137	α Gem	2890,1	7 28.2	+32 6	1.99	A0	32
138		2967	7 36.4	+14 27	5.81	Mb	0
139		2998	7 39.9	-44 55	5.22	G5	32
140	9 Pup	3064	7 47.1	-13 38	5.34	G0	32
141*		3131	7 55.4	-18 7	4.64	A2	
142	4 Cnc	3132	7 55.7	+25 22	6.20	A0	38
143		3182	8 2.8	+68 46	5.48	G5	17
144	12 Cnc	3184	8 3.1	+13 56	6.26	F5	13
145	ε Cnc	3208-10	8 6.5	+17 57	5.56	G0	0
146		3212	8 6.7	- 7 28	5.36	G5	0
147		3221	8 7.4	+60 41	6.36	F0	
148	29 Lyn	3235	8 9.5	+59 53	5.52	A5	3
149	30 Lyn	3254	8 12.4	+58 3	5.94	F2	13
150		3263	8 14.3	+60 57	6.48	G5	0
151		3279	8 16.9	-19 46	5.56	G0+A3	0
152	π^1 UMa	3391	8 30.3	+65 22	5.69	G0	2, 38
153	9 Hya	3441	8 37.1	-15 35	4.98	K0	38
154	45 Cnc	3450	8 37.7	+13 3	5.67	A3+G	
155	46 Cnc	3464	8 39.2	+31 4	6.14	K0	0
156	ε Hya	3482	8 41.5	+ 6 47	3.48	F8	0
157	ζ Vel	3485	8 41.9	-54 21	2.10	A0	2, 3, 38
158		3512	8 45.8	-32 25	5.23	G5	2, 38
159		3570	8 52.4	-54 35	5.72	F5	2
160	α Cnc	3572	8 53.0	+12 15	4.27	A3	
161	66 Cnc	3587	8 55.3	+32 39	5.83	A2	2, 3, 38
162	ν Cnc	3595	8 56.9	+24 51	5.45	A0	2, 3, 38
163	α Vol	3615	9 0.9	-66 0	4.18	A5	
164	τ Cnc	3621	9 2.0	+30 3	5.38	G5	0
165	ξ Cnc	3627	9 3.6	+22 27	5.22	G5	0
166		3636	9 4.4	-11 57	5.81	K0	0
167	79 Cnc	3640	9 4.6	+22 24	6.09	G5	0
168	16 UMa	3648	9 6.4	+61 50	5.23	F8	13
169	18 UMa	3662	9 9.0	+54 26	4.89	A5	37
170		3676	9 10.8	+47 14	5.70	A0	
171	ω Leo	3754	9 23.1	+ 9 30	5.52	G0	0
172	23 UMa	3757	9 23.6	+63 30	3.75	F0	16, 17, 37
173	10 LMi	3800	9 28.1	+36 51	4.62	G5	17, 38
174		3809	9 28.8	+40 4	4.99	K0	0
175	42 Lyn	3829	9 32.1	+40 41	5.24	A5	16, 37
176		3850	9 35.7	+31 43	6.08	K5	2
177	φ UMa	3894	9 45.3	+54 32	4.54	A2	
178*	ν^1 Hya	3903	9 46.7	-14 23	4.29	K0	38
179		3954	9 58.0	+54 23	5.74	F5	0
180*	21 LMi	3974	10 1.5	+35 44	4.47	A5	2, 3, 38
181*	34 Leo	3998	10 6.3	+13 51	6.41	F5	2, 3, 38
182*	ε Leo	4031	10 11.1	+23 55	3.65	F0	
183	HD 89882		10 17.2	+58 19	9.0	G5	21
184	27 LMi	4075	10 17.3	+34 25	5.83	A3	17
185	45 Leo	4101	10 22.4	+10 16	5.87	A0	3, 38
186	HD 91347		10 27.7	+49 42	7.57	F8	
187	35 LMi	4150	10 30.6	+36 51	6.27	F2	0
188	HDE 237917		10 32.2	+58 13	8.8	K0	21
189	37 LMi	4166	10 33.1	+32 30	4.77	G0	0
190	50 Leo		10 33.5	+16 38	6.62	F2	32
191	μ Vel	4216	10 42.5	-48 54	2.84	G5	38
192	ω UMa	4248	10 48.2	+43 43	4.84	A0	3
193*	HD 94686		$10^h50^m.7$	+80°13'	7.23	F8	*

TABLE 17 (continued)

No.	Name	HR No.	α(1900)	δ(1900)	m	Sp.	Reference
194	61 Leo	4299	$10^h56.^m7$	- 1°57'	4.97	Ma	2, 38
195	δ Leo	4357	11 8.8	+21 4	2.58	A3	
196	ι Leo	4399	11 18.7	+11 5	4.03	F5	
197	τ Leo	4418	11 22.8	+ 3 24	5.18	K0	
198		4465	11 31.0	+28 20	5.82	A3	32
199*	ε Crt	4514	11 39.7	-17 48	4.90	G5	
200	HD 104620		11 57.7	+58 0	9.1	G	21
201	α Crv	4623	12 3.3	-24 10	4.18	F2	16, 37
202	5 CVn	4716	12 19.2	+52 7	4.97	K0	38
203		4725	12 20.2	+24 29	6.08	K0	32
204	HD 108134		12 20.3	+61 14	7.41	G0	25
205	20 Com	4756	12 24.7	+21 27	5.72	A2	32
206	HD 108875		12 25.5	+10 16	7.9	F2	32
207*		4803	12 32.4	-26 35	5.44	F0	13
208		4837	12 38.5	- 1 2	6.08	G0	0
209	ι Cru	4842	12 39.8	-60 26	4.68	K0	2, 38
210	34 Vir	4855	12 42.2	+12 30	6.05	A3	32
211		4859	12 43.1	+63 20	5.83	A5	
212*	29 Com	4865	12 43.9	+14 40	5.64	A0	
213*	41 Vir	4900	12 48.8	+12 58	6.34	A3	
214	HD 112394		12 51.3	+57 39	9.0	K0	21
215	HDE 238179		12 55.3	+55 12	8.9	K0	21
216	HDE 234006		13 1.1	+51 31	9.0	F8	21
217	BD+51°1808		13 1.2	+51 33	9.4		21
218	49 Vir	4955	13 2.6	-10 12	5.26	K0	38
219		4960	13 4.2	+10 33	5.95	K0	32
220		4998	13 9.5	+11 52	5.81	K5	32
221	HDE 238208		13 10.7	+57 32	9.0	K0	21
222		5009	13 11.5	+81 1	6.32	G5	38
223*	ν Hyd	5020	13 13.5	-22 39	3.33	G5	16, 17
224	HDE 238224		13 19.5	+58 25	9.0	M0	21
225*	78 Vir	5105	13 29.1	+ 4 10	4.93	A2p	
226		5110	13 30.3	+37 42	4.96	F0	16, 37
227		5162	13 38.4	+65 20	5.70	A0	32
228		5164	13 39.0	+23 12	6.41	K2	32
229*	83 Vir	5165	13 39.1	-15 41	5.71	G0	17
230	HD 120528		13 44.9	+53 44	8.8	G5	21
231*		5214	13 46.7	+35 16	6.57	A2	
232		5220	13 47.4	+12 40	5.99	A2	16, 32, 37
233*	τ Vir	5264	13 56.6	+ 2 2	4.34	A2	
234	κ Boo	5328-9	14 9.9	+52 15	4.60	A5	
235		5343	14 11.4	+19 23	5.84	A5	
236	18 Boo	5365	14 14.4	+13 28	5.31	F0	
237*		5373	14 15.7	+39 15	5.98	A2	
238		5467	14 35.1	+54 27	5.52	A0	2, 16, 37
239		5473	14 35.9	+13 58	5.98	A5	32
240*	ε Boo	5477-8	14 36.4	+14 9	4.43	A2	13
241		5492	14 39.6	+61 41	6.17	F2	13, 31, 32
242	38 Boo	5533	14 45.7	+46 32	5.76	F5	0
243	ξ Boo	5544	14 46.8	+19 31	4.64	G5	7, 16
244		5573	14 52.4	+ 0 14	5.71	K0	32
245		5575	14 52.5	+16 47	5.78	K0	32
246*	45 Boo	5634	15 2.9	+25 16	5.03	F0	
247	δ Boo	5681	15 11.5	+33 41	3.54	K0	0
248*	8 Ser	5721	15 18.6	- 0 40	6.10	F0	
249	η CrB	5727-8	15 19.1	+30 39	5.58	G0	
250	34 Lib	5750	15 25.0	-16 16	5.86	K0	0
251	ν Boo	5763	15 27.3	+41 10	5.15	K5	0
252*	α CrB	5793	15 30.5	+27 3	2.31	A0	
253	τ^2 Ser	5804	$15^h31.^m9$	+16°27'	5.88	F0	0

TABLE 17 (continued)

No.	Name	HR No.	α(1900)	δ(1900)	m	Sp.	Reference
254	41 Lib	5814	$15^h33^m.1$	-18°58'	5.53	G5	32
255		5815-6	15 33.3	- 8 28	6.54	F8	0
256		5830	15 35.1	+47 8	5.78	F0	2, 17, 37
257*	τ^6 Ser	5840	15 36.4	+16 21	5.97	G5	
258	χ Ser	5843	15 37.1	+13 10	5.26	A0p	
259	α Ser	5854	15 39.3	+ 6 44	2.75	K0	17
260		5859	15 40.4	+ 5 46	5.56	A0	16, 32, 37
261*	β Ser	5867	15 41.6	+15 44	3.74	A2	
262		5886	15 45.1	+62 55	5.13	A2	
263		5887	15 45.2	+55 41	5.79	A2	16, 37
264	ω Ser	5888	15 45.2	+ 2 30	5.33	K0	38
265	Ψ Sco	6031	16 6.5	- 9 48	4.91	A2	37
266	16 Sco	6033	16 6.7	- 8 17	5.49	A3	2, 16, 37
267		6035	16 6.9	+16 55	5.90	A0	37
268	ν CrB	6074	16 12.7	+29 24	5.73	A0	2, 16, 37
269*		6076	16 13.3	-19 58	6.38	K0	0
270		6094	16 17.3	-38 58	5.40	G0	2
271	ξ TrA	6098	16 17.7	-69 52	4.93	G0	2, 16
272	(23 Her)	6110	16 19.1	+32 34	6.20	A2	3, 37
273	ω Her	6117	16 20.8	+14 16	4.53	A0p	
274	30 Her	6146	16 25.3	+42 6	5.02	Mb	
275	η Her	6220	16 39.5	+39 7	3.61	K0	16, 17
276*	HD 151044		16 39.8	+50 9	6.64	F5	*
277	18 Dra	6223	16 40.2	+64 47	5.00	K0	0
278		6227	16 40.8	+15 56	5.78	Mb	32
279	20 Oph	6243	16 44.3	-10 36	4.73	F5	16, 17, 37
280*	52 Her	6254	16 46.3	+46 10	4.86	A2p	2, 3, 38
281*	56 Her	6292	16 50.9	+25 54	6.33	K0	2, 38
282	ϵ^1 Ara	6295	16 51.6	-53 0	4.15	K2	17
283	ϵ UMi	6322	16 56.2	+82 12	4.40	G5	0
284	61 Her	6346	16 59.9	+35 33	6.75	Mb	32
285	γ Ser	6446	17 15.2	-12 45	4.35	A0	16, 37
286		6474	17 19.0	-24 9	6.26	K0	0
287		6481	17 20.0	+16 24	5.69	A2	
288	θ Sco	6553	17 30.1	-42 56	2.04	F0	0
289	α Oph	6556	17 30.3	+12 38	2.14	A5	17
290	26 Dra	6573	17 33.9	+61 57	5.31	F8	32
291		6575	17 34.1	+ 2 5	6.35	K0	0
292		6618	17 41.9	+53 51	5.70	A0	
293	Ψ Dra	6636-7	17 43.7	+72 12	4.90	F5	17
294		6666	17 47.5	-10 52	6.34	G5	32
295	1 Sgr	6801	18 5.6	-23 43	5.13	K0	0
296	ξ Pav	6855	18 14.0	-61 32	4.25	K2	17
297		6861	18 15.4	-24 58	6.36	Mb	0
298		6917	18 22.1	+29 46	5.71	A2	
299*		6993	18 32.5	- 0 24	5.80	A0	
300	ϵ^1 Lyr	7051-2	18 41.0	+39 34	5.06	A3	37
301	5 Aql	7059	18 41.3	- 1 4	5.68	A0	3, 13
302	110 Her	7061	18 41.4	+20 27	4.26	F5	37
303	8 Aql	7101	18 46.1	- 3 26	6.04	A3	2, 13
304		7137	18 50.7	+50 35	4.97	G5	0
305	10 Aql	7167	18 54.2	+13 46	5.94	A3p	2, 3,
306	11 Aql	7172	18 54.5	+13 29	5.37	F5	0
307		7186	18 55.8	-15 25	6.38	G5	0
308*	16 Lyr	7215	18 58.6	+46 48	5.06	A5	2
309		7267	19 4.2	+16 42	6.46	F5	2,38
310		7278	19 7.1	-66 50	5.57	A5	2
311	1 Sge	7301	19 11.0	+21 3	5.62	A3	
312	43 Sgr	7304	19 11.8	-19 8	5.03	K0	17
313		7311	$19^h12^m.7$	+49°54'	6.34	G5	0

TABLE 17 (continued)

No.	Name	HR No.	α(1900)	δ(1900)	m	Sp.	Reference
314*	59 Dra	7312	19h12m.8	+76°24'	5.06	F0	2, 38
315	ρ' Sgr	7340	19 15.9	-18 2	3.95	A5	16, 37
316	2 Sge	7369	19 19.9	+16 45	6.03	A0	16, 37
317		7382	19 20.8	+43 12	5.95	G5	0
318	35 Aql	7400	19 24.0	+ 1 45	5.77	A0	
319*		7451	19 31.7	+51 1	5.65	F5	
320	π Aql	7544	19 44.0	+11 34	5.70	F2	0
321		7545	19 44.5	+69 6	5.90	A0	3, 38
322		7555	19 45.9	+38 28	6.21	G5	38
323*	18 Sge	7746	20 11.9	+21 17	6.16	K0	0
324	24 Vul	7753	20 12.5	+24 22	5.45	K0	16
325		7781	20 15.9	+55 5	5.97	A0	
326		7784	20 16.6	+39 5	6.24	A0	2, 16, 37
327	ρ Cap	7822	20 23.1	-18 9	4.96	F0	
328	40 Cyg	7826	20 23.9	+38 7	5.45	A0	2, 3, 38
329	41 Cyg	7834	20 25.3	+30 2	4.09	F5p	0
330	δ Del	7928	20 38.8	+14 43	4.53	A5	
331	ψ Cap	7936	20 40.2	-25 38	4.26	F8	16
332	ω Cap	7980	20 45.8	-27 18	4.24	Ma	17
333	32 Vul	8008	20 50.3	+27 41	5.24	K5	0
334	γ Mic	8039	20 55.2	-32 39	4.71	G5	17, 38
335	ν Cap	8060	20 58.7	-20 15	4.93	A3	16, 37
336		8071	21 0.1	+41 14	6.33	F2	7, 16
337	ε Cyg	8115	21 8.7	+29 49	3.40	K0	17
338	ε Eql	8123	21 9.6	+ 9 36	4.61	F5	37
339	ι Cap	8167	21 16.7	-17 16	4.30	K0	0
340		8170	21 17.1	+39 55	6.46	F8	2, 38
341	35 Cap	8207	21 21.6	-21 38	6.03	K0	38
342	7 Cep	8227	21 25.8	+66 22	5.42	B5	2
343	6 PsA	8230	21 26.2	-34 23	5.99	A2	32
344*	ρ Cyg	8252	21 30.2	+45 9	4.22	K0	
345*		8263	21 32.4	- 0 50	6.27	A2	
346	26 Aqr	8287	21 37.1	+ 0 50	5.80	K5	38
347*	76 Cyg	8291	21 37.5	+40 21	6.05	A0	7
348	HD 206874		21 39.9	+28 19	6.90	A5	3
349	15 Peg	8354	21 48.0	+28 20	5.62	F5	0
350	28 Aqr	8390	21 56.0	+ 0 7	5.75	K0	0
351*		8407	21 58.9	+44 10	5.52	A0	
352*	32 Aqr	8410	21 59.6	- 1 23	5.23	A3	
353*	π Peg	8454	22 5.5	+32 41	4.38	F5	
354*		8461	22 7.0	+15 33	6.06	K0	2
355*		8473	22 8.3	+71 37	6.36	B9	2
356	μ^2 Gru	8488	22 10.4	-42 8	5.19	G5	38
357	HD 212005		22 16.1	+24 26	8.3	K0	2
358	σ Aqr	8573	22 25.3	-11 11	4.89	A0	
359	ο Peg	8641	22 37.1	+28 47	4.85	A0	
360	66 Aqr	8649	22 38.2	-19 21	4.88	K5	38
361	η Peg	8650	22 38.3	+29 42	3.10	G0	0
362	HD 215812		22 42.7	- 4 45	6.75	G0	32
363	τ Aqr	8679	22 44.3	-14 7	4.21	K5	0
364	ι Cep	8694	22 46.1	+65 40	3.68	K0	
365	γ PsA	8695	22 47.0	-33 24	4.52	A0	3, 38
366		8708	22 49.2	+44 13	5.62	A0	0
367	ε Aqr	8709	22 49.4	-16 21	3.51	A2	
368		8726	22 52.0	+49 12	5.10	K0	0
369*	4 And	8804	23 3.1	+45 51	5.56	K5	0
370	58 Peg	8821	23 5.0	+ 9 17	5.34	B8	38
371	γ Tuc	8848	23 11.6	-58 47	4.10	F2	17
372	9 And	8864	23 13.6	+41 14	5.90	A3	16, 37, 38
373	99 Aqr	8906	23h20m.8	-21°11'	4.52	K5	2, 38

TABLE 17 (continued)

No.	Name	HR No.	α(1900)	δ(1900)	m	Sp.	Reference
374*	15 And	8947	$23^h29^m.7$	+39°41'	5.50	A0	3
375	μ Scl	8975	23 35.4	-32 38	5.33	K0	2, 32
376*	λ Psc	8984	23 36.9	+ 1 14	4.61	A5	7, 16
377	21 Psc	9022	23 44.3	+ 0 31	5.77	A2	3, 16, 37
378		9057	23 52.0	+42 6	6.04	F5	16, 37
379	ψ Peg	9064	$23^h52^m.6$	+24°35'	4.75	Ma	17, 38

TABLE 18

Probable Members of the Ursa Major Stream

No.	μ		θ_o	$\Delta\theta$	ρ_o	$\Delta\rho$	π_{tr}		π_{cl}	Sp.	M_{sp}	M_{cl}
17	".069	± ".003	239°3	+17°1	- 9.9 ± 3.0	- 9.8	".015	± ".013	".019	A2 V	+1.2	+0.9
20	.011	.004	240.9	+15.3	- 5.1 0.4	- 3.6			.003	G5 III	+0.3	-2.2
23	.319	.003	225.3	- 8.8	+ 7.7 0.4	- 0.1	.063	.010	.100	F8 IV	+2.7	+5.2
24	.051	.003	218.7	- 8.4	- 8.8 1.3	- 9.9	.001	.009	.014	G5 III	+0.3	+1.1
25	.013	.004	228.0	0.0	+15.2 2.7	+12.2			.004	G5 III	+0.3	-0.6
26	.021	.004	247.2	-18.5	+ 3.3 1.0	+ 6.5			.006	A7 V	+2.4	-0.3
27	.045	.004	228.6	- 5.6	+12.8 1.8	+ 6.0			.014	K0 III	+0.2	+2.1
29	.316	.002	235.9	+ 5.4	+ 6 9	+ 2.4	.020	.016	.090	F0 V	+3.0	+5.4
32	.051	.002	250.5	+19.4	+ 4.8 2.8	+ 1.2	.011	.006	.015	A3 V	+1.6	+1.2
36	.011	.006	225.0	-12.9	- 8.1 2.1	- 1.3			.003	G5 II	-1.6	-1.9
37	.013	.004	251.6	+19.7	+ 5.2 0.7	+ 7.6			.004	K0 III	+0.2	-1.0
43	.016	.004	243.5	+11.5	+ 3.6 2.1	+ 5.0	.017	.009	.004	G0 III + A	+1.0	-0.5
44	.174	.002	240.3	+ 5.9	- 0.9 1.2	+ 1.6			.050	F2 III	+1.1	+3.3
45	.072	.003	250.6	+18.7	+10.6 1.3	+10.0			.020	F0 V	+3.0	+2.4
53	.018	.004	222.3	+12.3	+ 2.6 2.7	+ 6.6			.005	A2	+1.2	-1.1
56	.085	.006	246.9	+ 6.4	- 8.3 1.2	- 1.5	.047	.011	.026	F5 V	+3.7	+3.5
60n	.073	.006	231.1	- 3.2	+ 7.0	+ 4.0	.011	.013	.021	A7p		+2.5
63	.037	.002	227.2	- 6.0	+ 5.0 0.6	+ 6.1	.004	.013	.010	G5 III	+0.3	0.0
64	.029	.003	231.8	- 2.1	+ 4.7 3.3	+ 7.3			.008	A1	+0.8	+0.8
65	.211	.002	223.1	- 9.9	- 9.2 2.2	- 7.9	.040	.006	.059	A3 V	+1.6	+2.5
68	.051	.007	213.1	-19.7	- 8.6 3.9	- 7.9			.014	A3 V	+1.6	+1.0
69	.014	.002	252.9	+16.6	- 6.9 1.3	- 1.8	.011	.018	.004	A2 V	+1.2	-1.5
71n	.050	.003	258.5	-10.7	- 2.5 1.6	+ 7.8	.017	.013	.018	A7m		+2.2
72	.169	.003	251.1	+17.9	- 9.7 2.2	-12.2	.043	.013	.048	A5 V	+2.2	+2.6
75	.036	.006	212.4	-19.3	+11	+ 9.5			.010	G5 II	-1.6	+0.7
76	.043	.003	256.6	+ 0.3	+ 0.7 3.0	+10.9	.018	.007	.015	A3 V	+1.6	+0.8
81	.028	.004	255.5	- 9.0	-18.5 0.6	- 6.7			.011	G2 III	+0.7	+0.6
83	.014	.003	245.2	+12.3	- 1.5 1.6	+ 6.5			.006	A2	+1.2	-1.8
84	.075	.003	218.6	- 9.7	-10.7 4.2	- 4.9	.009	.006	.022	A2	+1.2	+1.9
85	.020	.006	239.5	+ 8.7	- 7.2 1.6	+ 0.7			.006	A2	+1.2	+0.3
88	.025	.004	248.6	- 3.4	-16.5 0.3	- 4.3			.010	K3 III	-0.2	0.0
89	.020	.003	281.3	+12.7	- 7.9 SB0	+ 5.0			.009	A0 V	+0.5	-0.8
91	.124	.002	228.4	+ 4.7	- 7 4	+ 0.7	.050	.010	.039	A3 III	-0.4	+0.8
103	.034	.004	238.2	+13.5	- 9 6	+ 1.4	.010	.013	.012	A2	+1.2	+0.9
105n	.011	.003	259.7	-16.8	- 8.4 2.4	+ 5.9	.015	.013	.009	A0p		-0.6
106	.470	.004	221.0	+ 2.6	- 9.7 0.4	- 5.3	.122	.006	.135	F6 V	+3.9	+4.5
			217.2	- 1.2	- 9.7 1.2					K2 V	+6.3	+6.9
107	.034	.003	222.6	-18.4	-19.5 0.6	- 5.1	.003	.009	.018	G8 III	+0.3	+0.9
110	.203	.003	245.0	+ 9.6	-13.6 0.3	- 0.3	.104	.009	.092	G0 V	+4.5	+4.4
111	.052	.002	265.6	- 1.9	-18.1 SB	- 3.3	.037	.006	.029	A2 IV	+0.1	+0.1
114	.044	.004	291.3	+13.7	- 7.6 4.0	+ 7.5			.027	F0 V	+3.0	+3.6
115	.014	.004	225.0	-13.2	-20.9 1.9	- 6.5			.007	G5 III	+0.3	+0.3
118n	.028	.006	317.9	+20.0	-12.7 SB	+ 2.2			.016	A5m		+2.2
122	.012	.003	221.6	+15.7	- 1.5 ± 0.4	+ 6.7	.008	.015	.004	G5 III	+0.3	-2.4
125	".325	± ".002	203°8	- 0°6	- 7.5 St.vel.	+ 1.3	".373	± ".003	".426	A1 V	+0.8	+1.6

TABLE 18 (continued)

No.	μ		θ_o	$\Delta\theta$	μ_o	$\Delta\mu$	π_{tr}		π_{cl}	Sp.	M_{sp}	M_{cl}
129	".021	± ".003	264°6	+13°1	- 9.1	± 3.4	+ 6.9		".017	A2 V	+1.2	+1.0
132	.057	.002	225.7	+10.8	-13.8	2.8	+ 1.5	'040	± '010	.037	A3	+1.6	+1.5
135	.012	.003	194.1	-12.3	- 7.6	0.7	+ 6.9	.001	.013	.006	G5 III	+0.3	-1.0
138	.009	.006	192.5	-12.3	-16.4	1.8	- 1.0	.002	.013	.006	M2 III	-0.2	-0.3
140	.346	.002	189.1	- 0.5	-19.6	0.6	- 9.0	.060	.006	.123	G0 V	+4.5	+6.3
141	.050	.004	183.4	- 4.6	-12	4	- 2.4			.017	A3 V	+1.6	+0.8
151	.025	.007	173.2	- 9.5						.008	G2 III + A	+0.7	+0.8
152	.090	.003	342.6	-19.7	-11.2	0.4	+ 3.7			.053	G0 V	+4.5	+4.3
153	.097	.004	178.2	+ 1.3	- 2.1	0.9	+11.5	.023	.010	.034	G8 III	+0.3	+2.6
155	.005	.003	168.7	+ 9.6	-12.9	1.8	+ 4.0	.003	.013	.013	G5 III	+0.3	+1.7
162	.006	.003	161.6	+ 9.3	-16.3	1.5	+ 0.2			.007	A0	+0.5	-0.3
169	.080	.002	43.4	+14.8	-16.9	3.4	- 0.8			.069	A5	+2.2	+4.1
178	.040	.003	143.1	-16.9	-14.5	0.4	- 4.7	.018	.010	.014	G5 III	+0.3	0.0
180	.053	.003	88.9	-10.9	-16.8	2.5	- 0.8			.044	A5	+2.2	+2.7
181	.057	.003	130.7	- 9.6	-16.5	1.0	- 2.1			.030	F6 V	+3.9	+4.2
182	.024	.002	112.2	-11.9	-18.7	2.2	- 3.5	.010	.009	.015	F0 II-III	-0.8	-0.5
193	.086	.013	38.0	- 4.3	-21.7	2.8	- 9.7			.052	F8 V	+4.3	+4.9
195	.200	.001	132.0	+ 8.5	-23.2	2.2	-10.0	.050	.007	.089	A4 V	+1.8	+2.3
196	.189	.002	113.7	-17.5	- 9.7	0.6	+ 1.9			.072	F2 V	+3.3	+3.4
197	.027	.002	121.3	-17.2	- 9.1	0.3	0.0	.032	.007	.019	G8 II	-1.9	+1.6
199	.055	.002	133.5	+ 2.8	- 4.6	0.6	+ 0.8	.025	.013	.016	G5 III	+0.3	+0.9
201	.099	.003	115.8	-15.3	+ 4.4	0.6	+ 7.5	.056	.015	.028	F2 V	+3.2	+1.4
203	.073	.004	122.2	+ 3.3	- 5.4	0.6	+ 5.2	.003	.018	.026	K0 III	+0.2	+3.2
207	.122	.004	140.7	+ 6.1	- 0.8	0.9	+ 0.5	.033	.013	.034	F2 V	+3.2	+3.1
208n	.102	.004	146.3	+15.8	+ 0.2	0.6	+ 6.3			.030	G8 IIIp		+3.5
212	.045	.003	128.7	+ 4.3	- 7.0	2.1	- 1.0			.013	A2	+1.3	+1.2
213n	.060	.003	114.9	-10.4	- 3.8	3.1	+ 3.8			.019	A7p		+2.7
214	.105	.012	108.4	+10.6						.040	G5 IV-V	+4.3	+7.0
215	.096	.019	112.0	+14.6	-34.4	2.2	-23.0			.036	G8 V	+5.7	+6.7
218	.022	.002	114.2	-13.9	- 9.1	0.6	- 8.4	.022	.009	.006	K2 III	+0.1	-0.9
221	.108	.019	111.8	+14.4	-41.9	6.0	-30.9			.040	K2 V	+6.3	+7.0
223	.088	.002	122.4	- 8.4	- 5.4	0.3	- 5.3	.026	.010	.025	G5 III	+0.3	+0.3
224	.088	.019	99.2	+ 0.7						.032	M0 V		+6.5
225n	.050	.003	121.2	+19.5	-10.9	0.7	- 0.5	.018	.007	.018	A2p		+1.2
229	.015	.003	118.3	-10.3	+ 0.5	1.9	+ 0.5			.004	G0 II	-1.7	-1.3
230	.137	.022	114.1	+ 7.7						.047	G5 V	+5.2	+7.2
231	.034	.004	112.8	- 4.9	-12.3	2.4	- 4.6			.011	A3	+1.7	+1.8
233	.028	.002	140.7	+17.7	- 2.1	1.8	+ 3.5	.015	.007	.008	A5 III	0.0	-1.1
234	.064	.003	91.8	- 3.2	-14.9	0.3	- 6.3	.010	.010	.018	F0 V	+3.0	+0.9
235n	.055	.003	123.1	- 1.1	+ 6.3	2.1	+10.6			.016	A6m		+1.8
236	.111	.003	105.7	-20.0	- 1.9	0.9	+ 1.0			.031	F2 V	+3.2	+2.8
237	.027	.004	121.3	+ 2.0	-12.6	2.2	- 5.8			.008	A2	+1.3	+0.5
240	.057	.002	109.4	-15.3	- 6.2	1.8	- 0.9	.008	.018	.017	A2	+1.3	+0.6
241	.078	.004	112.6	-12.6	- 6.8	1.6	+ 1.9	.018	.009	.025	F2 III	+1.1	+3.2
243	.169	.002	126.3	- 0.3	+ 4.2	0.2	+ 6.4	.147	.009	.048	G8 V	+5.7	+3.2
246	.251	.003	132.4	+ 5.2	- 7.0	0.6	- 4.7	.063	.012	.071	F5 V	+3.7	+4.3
248	.078	.003	112.6	-14.9	- 2.7	2.5	- 5.8			.022	F0 V	+3.0	+2.8
249	.235	.002	144.3	+16.1	- 6.5	SB	- 4.1	.068	.012	.066	G2 V	+4.8	+4.7
251	.013	.002	116.5	-10.7	- 9.4	0.7	- 5.3	.021	.010	.004	K5 III	-0.2	-1.9
252	.151	.001	126.9	- 2.7	+ 1.0	SB0	+ 2.3	.053	.015	.042	A0 V	+0.5	+0.4
256	.151	.003	144.4	+17.4	- 2.3	2.7	+ 2.5	.010	.016	.044	F2 V	+3.2	+4.0
257	.031	.003	114.9	-15.4	+ 3.3	1.0	+ 2.2			.009	G5 III	+0.3	+0.8
260	.028	.006	113.0	-16.3	- 7.3	0.6	-10.6			.008	A2 V	+1.3	+0.1
261	.083	.002	124.6	- 5.0	- 1.5	2.8	- 8.7	.034	.010	.026	A2 IV	+0.3	+0.8
264	.055	.003	148.3	+19.1	- 3.5	0.6	- 7.7	.031	.015	.016	G8 III	+0.3	+1.3
268	.026	.003	133.4	- 0.7	+ 6.4	3.1	+ 6.4			.007	A3 V	+1.7	0.0
269	.014	.004	126.0	- 1.2	+ 8.0	1.8	+ 0.5			.004	K5 III	-0.2	-0.6
273n	.071	.002	143.0	+ 8.9	- 5.3	0.7	- 9.2	.033	.009	.020	A0p		+1.0
276	'164	'009	131.8	- 6.1	- 0.1		+ 2.9	.035	.009	.047	F8 V	+4.3	+5.0
280n	'059	± '003	152°6	+13°6	- 1.4	± 0.6	+ 0.5	'004	± '012	'017	A2p		+1.0

TABLE 18 (continued)

No.	μ		θ_o	$\Delta\theta$	ρ_o		$\Delta\rho$	π_{tr}		π_{cl}	Sp.	M_{sp}	M_{cl}
281	″023	± ″003	142°2	+ 2°9	- 0.4	± 1.2	- 3.2			″007	G5 III	+0.3	+0.5
289	.257	.001	151.4	+ 9.6	+15	3	+ 7.7	″047	± ″007	.079	A5 III	0.0	+1.6
298	.025	.006	139.7	-15.0	+ 8.5	SB	+ 3.4			.007	A2 V	+1.3	-0.1
299	.023	.004	156.8	+ 9.9	+13.3	2.7	+ 1.2			.009	A2	+1.3	+0.6
301n	.023	.003	151.2	+ 2.7	+18	4	+ 5.7			.009	A2m		+0.5
306	.121	.003	173.8	+16.6	+16.0	0.6	+ 6.2	.035	.012	.041	F8 V	+4.3	+3.6
308	.081	.004	166.3	+ 4.1	+ 8.1	3.1	+ 7.0	.031	.009	.023	A7	+2.4	+1.9
314	.127	.003	155.2	- 9.1	- 3.9	0.7	+ 3.0	.046	.009	.039	F2 V	+3.2	+3.0
319	.188	.003	170.5	+ 1.1	+ 1.0	1.6	+ 0.6	.035	.010	.052	F8 V	+4.3	+4.2
323	.021	.004	174.6	- 1.5	- 4.1	1.6	-13.7			.007	K1 III	+0.2	+0.4
325	.021	.003	185.4	+ 7.2	- 2.8	1.0	+ 3.2	.000	.009	.006	A2	+1.3	-0.2
326	.018	.003	180.0	+ 2.4	0.0	3.0	- 4.1			.005	A3 V	+1.7	-0.3
332	.007	.003	206.5	+ 6.4	+ 9.0	0.4	- 7.7	.004	.015	.011	K5 III	-0.2	-0.6
340	.205	.013	184.5	-12.7	+ 1.2	SB0	-13.8			.014	F8 V	+4.3	+2.2
341	.038	.003	221.8	+ 6.1	+23.4	3.7	+ 7.4			.032	K5 III	-0.2	+3.6
344	.088	.003	191.2	- 1.9	+ 6.9	0.3	+ 4.9	.004	.010	.025	G5 III	+0.3	+1.2
345	.025	.004	220.6	+19.1	+16.9	2.5	+ 3.8			.011	A2	+1.3	+1.5
347	.042	.003	191.0	- 3.2	var			.008	.018	.012	A2	+1.3	+1.4
351	.030	.004	202.2	+ 7.4	- 1.2	2.7	- 3.3			.008	A0	+0.5	+0.2
352n	.050	.003	198.8	-18.0	+20.4	SB	+ 5.0	.010	.006	.033	A5m		+2.8
353	.020	.002	204.0	+ 3.2	+ 2.2	2.5	- 2.6	.003	.010	.006	F5 II	-2.0	-1.7
354	.015	.003	203.2	- 0.3	+10.9	1.9	+ 1.8			.005	K1 III	+0.2	-0.5
355	.021	.004	198.1	- 3.1	- 2.8	1.6	+ 3.0			.006	A0	+0.5	+0.2
360	.037	.004	226.1	- 6.4	+21.6	0.3	+ 7.5	.010	.015	.019	K3 III	-0.2	+1.3
367	.045	.001	239.5	+10.1	+18.0	1.0	+ 4.7	.042	.010	.020	A3 V	+1.7	0.0
369	.029	.003	200.3	- 9.8	- 6.5	1.3	- 6.1			.008	K5 III	-0.2	+0.1
373	.077	.003	222.4	-15.4	+15.6	0.4	+ 2.8	.003	.010	.033	K5 III	-0.2	+2.1
374	.042	.003	199.3	-15.9	+12.8	2.8	+10.0	.011	.009	.012	A1 V	+0.8	+0.9
376	.195	.002	221.9	+ 0.1	+12.1	0.6	+ 0.8	″024	± ″012	.050	A5	+2.2	+3.1
379	″041	± ″003	232°0	+12°0	- 4.3	± 0.7	- 7.6			″012	M3 III	-0.2	+2.8

Notes to Table 18

60. A strontium star. The Sr II lines λ 4077 and λ 4215 are very strong. The blends near λλ 4172, 4130, and just to the red of Hδ are also well marked. There is no evidence of spectral variability.

71. A metallic-line star. The K line and the hydrogen lines indicate a type of A7 but the metallic-line spectrum is that of an F2 star.

105. This star is spectroscopically similar to ε UMa. The K line is sharp and weak; the blend at λ 4171 is strong.

118. The type from the metallic lines is F0; the hydrogen lines are about as strong as in an A7 star.

208. This star appears to be a high-velocity giant.

213. The hydrogen lines are too weak for the weakness of the K line.

225. See An Atlas of Stellar Spectra, p. 18.

235. The metallic-line type is F2; the hydrogen-line type, F0.

273. This star is also similar to ε UMa, although the normal metallic spectrum is slightly stronger. The K line is very weak; λ 4171 and λ 4077 are strong.

280. A strontium star. λ 4077 of Sr II is very strong and the blends at λ 4171 and λ 4130 are well marked.

301. 5 Aql A is a metallic-line star. The type from the metallic lines is A7 while that from the hydrogen lines is A5. The K line is also somewhat weak in 5 Aql B, an F0 star.

352. The metallic-line type is F0; that from the hydrogen lines is A7.

TABLE 19

Stars Probably Not Members of the Ursa Major Stream

No.	μ		θ_o	θ_c	ρ_o		ρ_c	π_{tr}		π_{cl}	M_{cl}
14	″027	± ″003	250°2	225°3	+ 0.8	± 0.9	+ 6.2			″008	+ 0.7
15	.004	.004	75.9	224.1	- 4.6	2.4	- 5.2			.001	- 4.2
16	.052	.003	250.8	221.5	+ 0.7	1.5	- 0.3			.015	+ 0.3
18	.018	.002	231.8	228.0	- 3.3	0.7	+ 6.9			.006	+ 2.6
19	.015	.003	258.7	224.4	- 0.7	0.7	- 0.4			.004	- 1.4
21	.026	.003	283.5	254.7	+16.5	0.2	+11.5	″001	± ″015	.010	- 0.4
22	.022	.004	280.3	228.3	- 8.3	1.6	+ 4.9			.006	- 0.6
28	.035	.003	283.2	254.9	- 1.2	0.2	+10.8	.018	.015	.013	+ 1.0
30	.140	.004	253.4	229.5	-10.7	0.6	- 3.1			.040	+ 3.7
31	.011	.003	180.0	230.8	- 2.6	1.9	+ 4.5			.003	- 1.4
33	.025	.003	297.3	230.0	- 8.5	1.6	+ 0.5			.007	- 0.4
34	.352	.002	103.4	232.5	+10.4	0.6	- 4.5	.024	.009	.102	+ 5.1
35	.016	.002	194.1	242.9	- 4.0	0.6	- 8.4			.005	- 1.0
38	.021	.002	280.8	190.4	+ 0.4	0.3	+ 1.1	.032	.009	.006	- 1.4
39	.058	.004	254.1	241.8	+10.4	1.3	+ 7.9			.018	+ 1.0
40	.049	.004	243.4	244.1	+20	6	+ 8.4			.016	+ 1.9
41	.034	.006	244.2	251.8			+ 9.7			.012	+ 2.3
42	.032	.004	201.8	233.5	+11.3	1.3	+ 3.9			.009	+ 0.1
46	.060	.006	266.2	250.3			+ 9.0			.020	+ 2.6
47	.004	.003	236.3	235.0	- 6.9	1.2	- 4.7	.002	.018	.001	- 4.4
48	.089	.002	262.9	233.0	+ 0.1	1.6	- 2.3	.026	.013	.026	+ 2.4
49	.062	.003	274.6	248.4	- 4.2	1.8	- 8.9	.026	.007	.020	+ 1.1
50	.046	.001	299.9	249.5	-12.5	1.9	- 9.1			.015	- 0.1
51	.023	.004	219.8	252.0	0.0	0.9	- 9.4	.021	.013	.007	- 0.5
52	.038	.003	256.9	249.0	- 9.1	4.2	- 9.0			.012	- 3.0
54	.067	.001	139.9	236.9	-11.7	0.2	- 5.5	.005	.006	.020	- 1.2
55	.006	.002	225.0	248.6	-12.3	2.8	- 8.8			.002	- 2.4
57	.021	.001	259.2	232.8	- 4.9	1.2	- 0.3	.018	.012	.006	- 1.6
58	.038	.003	189.2	236.0	- 1.3	1.8	- 4.6			.011	+ 1.4
59	.017	.003	290.6	244.7	-10.8	1.6	- 8.0			.005	- 0.4
61	.048	.004	246.7	241.9			+ 7.3			.015	+ 2.9
62	.028	.004	225.0	237.8			+ 5.7			.008	+ 0.4
66	.057	.006	230.7	236.5			+ 5.1			.017	+ 2.7
67	.033	.006	244.2	252.2	+ 4.7	0.6	+ 9.5	.004	.013	.011	- 0.1
70	.062	.007	207.0	232.6	- 7.2	0.6	- 1.4	.013	.013	.017	+ 1.4
73	.005	.004	270.0	233.6	+ 3.6	2.8	- 3.4			.001	- 4.2
74	.055	.003	277.9	247.8	- 6.6	2.4	- 9.1	.021	.009	.018	+ 1.4
77	.001	.004	315.0	262.0	-10.4	1.8	-10.8			.004	- 1.0
78	.009	.002	276.3	249.7	-13.0	0.7	- 9.9	.016	.010	.003	- 3.7
79	.116	.004	231.0	230.0	+ 9.9	0.5	+ 2.8	.024	.013	.033	+ 2.2
80	.070	.003	223.3	229.1	+ 2.0	0.7	+ 2.3	.021	.015	.020	+ 0.7
82	.021	.003	244.6	247.6	-27.4	0.5	-10.8			.008	- 0.4
86	.053	.004	258.0	225.2	+ 7.4	1.0	+12.1	.037	.015	.015	+ 1.0
87	.108	.007	217.5	225.4	+26.1	1.5	+ 5.7			.032	var
90	.081	.002	160.5	220.1	+ 1.0	0.3	- 3.9	.009	.009	.023	+ 0.1
92	.172	.002	332.7	302.0	- 9.9	0.3	-11.7	.054	.007	.066	+ 4.3
93	.022	.003	310.6	249.6	- 9.7	SB	-12.9			.009	- 0.1
94	.008	.004	194.0	231.2	- 8.0	1.2	-10.7			.003	- 2.1
95	.023	.006	223.3	216.6			- 1.9			.006	+ 1.2
96	.008	.004	76.0	246.5	-18.7	SB	-13.0			.003	- 1.3
97	.011	.003	158.2	255.7	-19.2	0.9	-13.5	.004	.009	.005	- 1.3
98	.048	.004	195.8	221.2	-18.2	0.4	- 7.7	.007	.006	.015	+ 0.1
99	.006	.002	188.2	290.2	-18.8	0.7	-13.3			.003	- 0.9
100	.094	.002	178.2	215.2	-13.5	± 0.2	- 1.0	″009	± .009	.026	+ 0.1
101	″036	± ″006	210°4	214°9			- 2.5			″010	+ 1.9

TABLE 19 (continued)

No.	μ		θ_o	θ_c	ρ_o		ρ_c	τ_{tr}		τ_{cl}	M_{cl}
102	₹002	± ₹004	333?5	281?2	+ 0.6	± 0.6	-13.9			₹001	- 4.0
104	.002	.004	296.5	292.0	- 3.6	1.3	-13.7			.001	- 3.6
108	.020	.003	329.1	288.1	-12.5	1.0	-14.3			.010	- 0.1
109	.017	.002	151.9	244.0	-16.1	SB	-13.9	₹019	± ₹010	.008	0.0
112	.021	.003	166.0	218.7			-11.5			.008	+ 0.1
113	.019	.002	183.0	214?1	- 4.8	0.4	-10.0	.012	.006	.007	- 1.7
116	.273	.006	215.6	215.9	-35.8	3.7	-11.2	.039	.015	.101	+ 5.8
117	.023	.002	342.4	299.7	- 3.8	0.7	-14.5	.032	.016	.012	- 0.2
119	.069	.004	204.2	205.6	- 2.4	SB	- 4.0	.015	.012	.018	+ 0.2
120	.019	.004	191.9	212.1	+25	6	-11.7			.007	- 0.8
121	.066	.001	132.0	225.8	-11.3	SB0	-14.3	.040	.009	.034	- 0.4
123	.161	.002	0.4	279.0	-23.7	0.7	-15.8	.065	.009	.122	+ 5.7
124	.006	.003	329.0	292.1	- 9.0	0.9	-15.7			.006	- 1.7
126	.057	.007	222.9	205.9			-12.0			.023	+ 2.5
127	.058	.007	235.5	214.0			-13.7			.027	+ 3.0
128	.042	.003	298.4	235.5	-11.5	1.0	-15.5			.030	+ 3.2
130	.003	.003	251.6	232.1	- 8.8	0.6	-15.6	.013	.007	.002	- 3.3
131	.019	.002	308.7	280.5	-15.0	3.1	-16.4			.021	+ 2.4
133	.090	.003	253.2	265.0	+23.2	0.6	-16.5	.022	.009	.105	+ 5.4
134	.022	.003	46.8	235.7	- 5.0	1.9	-16.2			.021	+ 2.3
136	.016	.002	172.9	207.4	-15.4	0.4	-14.9	.027	.010	.009	- 0.4
137	.197	.001	236.8	242.9	- 1.2	SB0	-16.6	.073	.004	.250	+ 7.2
139	.565	.007	186.7	189.0	+22.5	0.4	- 2.1	.051	.015	.159	+ 6.3
142	.024	.004	131.6	206.2			-16.5			.029	+ 3.5
143	.009	.002	353.7	350.5	- 8.5	0.6	-10.9			.071	+ 4.7
144	.018	.003	170.5	192.4	-14.1	2.8	-15.6			.013	+ 1.8
145	.154	.002	137.2	193.0	- 8.1	0.3	-16.0	.039	.006	.127	+ 6.1
146	.044	.007	237.0	186.0	-11.3	0.6	-12.1			.017	+ 1.5
147	.016	.004	291.8	351.3	-16.2	1.5	-15.6			.011	+ 1.6
148	.002	.003	270.0	350.6	-19.6	1.8	-15.6			.001	- 4.5
149	.060	.003	76.4	351.4	-15.9	0.9	-15.8			.046	+ 4.3
150	.009	.003	116.6	353.4	- 5.9	0.6	-15.5			.006	+ 0.4
154	.004	.003	56.4	173.8	-18.8	1.8	-15.5			.003	- 2.0
156	.195	.001	252.9	176.5	+36.8	SB0	-10.9	.012	.009	.071	+ 2.7
157	.083	.003	163.1	176.6	+ 2.2	2.2	+ 0.1			.023	- 1.1
158	.050	.006	168.3	176.6	- 7.8	1.0	- 5.9			.015	+ 1.1
159	.091	.006	154.0	175.6	- 1.5		+ 0.3			.025	+ 2.7
160	.051	.001	130.2	166.9	-13.5	0.7	-15.3			.033	+ 1.9
161	.002	.003	270.0	171.9	-12.8	2.0	-12.0			.001	- 4.2
163	.102	.003	177.2	172.8	+ 8	4	+ 0.7	.047	.016	.028	+ 1.4
164	.027	.003	273.7	136.5	-13.1	0.6	-16.7			.044	+ 3.6
165	.008	.002	60.3	154.0	- 7.4	1.2	-16.3			.008	- 1.2
166	.028	.006	117.5	170.4			-11.0			.010	+ 0.8
167	.011	.003	68.2	153.3	- 7.1	2.5	-16.3			.011	+ 1.3
168	.032	.002	180.0	18.0	-14.0	SB	-15.3	.042	.007	.021	+ 1.8
170	.022	.003	64.4	27.9	-12.1	SB	-16.0			.018	+ 2.0
171	.057	.003	95.0	157.6	- 5.4	0.7	-14.7	.028	.015	.032	+ 3.0
172	.111	.001	76.0	24.2	- 8.2	1.9	-15.0	.037	.009	.066	+ 2.8
173	.026	.002	155.4	96.7	-11.7	0.4	-16.6			.033	+ 2.2
174	.026	.004	300.6	100.6	-11.9	0.5	-16.6			.034	+ 2.6
175	.016	.004	277.1	77.6	- 2.0	1.8	-16.6			.020	+ 1.7
176	.032	.006	97.1	65.1	-12.2	3.4	-16.4			.035	+ 3.8
177	.018	.002	333.6	46.8	-12.2	0.9	-15.7	.018	.019	.013	+ 0.1
179	.025	.004	251.6	41.6	-16.6	0.4	-15.8			.019	+ 2.1
183	.086	.021	88.7	50.2			-14.9			.050	+ 7.5
184	.017	.003	205.0	104.5	-12.7	3.1	-15.7			.013	+ 1.4
185n	.010	.003	84.3	139.8	-10.0	2.7	-13.4			.005	- 0.6
186	.292	.006	63.3	70.7	-25.9	1.2	-15.4	₹032	± ₹007	.192	+ 9.0
187	.055	.004	137.9	99.9	-24.2	± 2.1	-15.5			.037	+ 4.2
188	₹050	± ₹022	87?7	57?2			-14.8			₹028	+ 6.1

TABLE 19 (continued)

No.	μ	θ_o	θ_c	ρ_o	ρ_c	π_{tr}	π_{cl}	M_{cl}
189	?006 ± ?003	59?0	109?9	- 6.8 ± 0.6	-16.2	?015 ± ?010	?005	- 1.7
190	.064 .003	70.7	132.2		-13.6		.031	+ 4.2
191	.087 .003	125.7	153.4	+ 6.9 0.2	+ 0.4		.024	- 0.3
192	.054 .002	119.0	87.6	-17.4 SB	-15.1		.033	+ 2.4
194	.045 .003	153.4	131.6	-13.1 0.9	-10.3	.028 .015	.016	+ 1.0
198	.025 .003	87.7	113.9		-13.1		.011	+ 1.0
200	.090 .021	112.3	59.0		-11.4		.034	+ 6.8
202	.017 .003	40.2	95.6	-13.0 0.4	-12.4	.036 .010	.007	- 0.8
204n	.138 .015	87.9	95.7	-39.6 0.9	-12.4		.053	+ 6.0
205	.043 .002	138.8	121.1		-10.1		.015	+ 1.6
206	.077 .004	133.4	127.0		- 8.5		.025	+ 4.9
209	.122 .007	120.5	139.8	+ 8.9 0.4	+ 6.0	.032 .012	.036	+ 2.5
210	.049 .003	112.9	126.0		- 8.7		.016	+ 2.1
211	.017 .004	100.0	95.8	-18.0 0.4	-10.7		.006	- 0.3
216	.018 .022	306.9	100.8		-11.1		.004	+ 2.0
217	.024 .012	125.0	101.0		-11.1		.009	+ 4.2
219	.018 .007	99.5	125.7	- 0.4 1.0	- 6.7		.005	+ 6.1
220	.091 .004	124.7	120.9		- 8.1		.029	+ 3.1
222	.016 .003	317.2	78.6	-10.5 2.8	-10.8		.006	+ 0.2
226	.090 .003	95.7	112.6	+ 6.6 SBO	- 8.9	.019 .009	.030	+ 2.4
227	.054 .003	106.1	97.7		-10.5		.019	+ 2.1
228	.063 .003	126.0	120.3	+ 9.1 0.4	- 6.5		.019	+ 2.8
232	.027 .004	107.1	125.2	-17.1 0.7	- 4.6		.008	+ 0.5
238	.022 .003	136.8	114.8	+ 1.9 3.0	- 8.1		.007	- 0.2
239	.061 .004	116.1	126.8		- 1.8		.017	+ 2.1
242	.074 .003	181.5	127.6	- 5.4 2.5	- 0.2		.021	+ 2.4
244	.071 .003	110.7	127.3	+19.6 0.4	+ 1.6	.034 .012	.020	+ 2.3
245	.005 .003	101.3	127.4	-16.0 0.4	- 1.4		.001	- 4.2
247	.143 .002	147.6	126.5	-12.7 0.4	- 3.6	.026 .010	.041	+ 1.7
250	.019 .003	96.0	123.9	- 1.7 2.2	+ 6.1		.009	- 0.3
253	.076 .004	97.6	129.7	- 0.4 3.9	- 0.7		.021	+ 2.6
254	.117 .003	133.0	122.9		+ 7.1		.036	+ 3.4
255	.036 .004	139.6	127.6	+ 3.0 1.5	+ 5.3		.010	+ 1.5
258	.042 .003	106.7	130.2	+ 1.4 1.3	+ 1.8		.012	+ 0.7
259	.145 .001	70.2	129.6	+ 3.0 0.2	+ 2.9	.045 .010	.041	+ 0.8
262	.067 .002	144.7	124.6	- 5.6 2.4	- 7.0	.013 .007	.020	+ 1.2
263	.016 .004	47.5	126.4	- 2.5 1.3	- 5.9		.005	- 0.7
265	.018 .003	206.6	126.3	- 6.1 1.2	+ 7.3		.006	- 1.2
266	.039 .003	90.0	126.9	+ 5.5 3.6	+ 7.1	.017 .012	.012	+ 0.9
267	.006 .003	51.3	132.8	-12.6 3.1	+ 2.5		.002	- 2.6
270	.078 .006	92.9	108.4	+10.1 0.6	+11.3	.052 .013	.029	+ 2.7
271	.226 .006	61.5	78.9	+ 8.5 SBO	+11.7	.086 .012	.087	+ 4.6
272	.017 .006	110.6	135.4	- 6.3 3.3	0.0		.005	- 0.3
274	.028 .003	92.0	136.0	+ 3.3 0.7	- 1.7		.008	- 0.4
275	.090 .001	155.2	137.8	+ 7.9 0.3	- 0.7	.053 .009	.025	+ 0.7
277	.013 .003	161.6	134.1	+ 0.3 0.3	- 6.1	.021 .015	.004	- 2.0
278	.050 .004	146.3	136.7	-18.8 2.1	+ 4.5	.019 .010	.014	+ 1.6
279	.132 .001	135.9	127.5	- 0.5 0.4	+ 9.4		.044	+ 3.0
282	.021 .003	357.3	91.4	+23.1 0.7	+13.0	.001 .012	.009	- 1.1
283	.018 .001	67.6	141.2	-11.4 SB	- 9.0	.015 .015	.006	- 1.7
284	.047 .004	134.1	141.5	-12.2 2.8	+ 0.9	.005 .012	.013	+ 2.5
285	.042 .015	83.2	128.6	+ 4.7 1.9	+11.1	.022 .010	.015	+ 0.2
286	.017 .003	61.9	119.0	+20.0 2.5	+12.6		.007	+ 0.6
287	.028 .004	161.6	142.2	+10.8 1.0	+ 5.0		.008	+ 0.2
288	.010 .003	90.0	95.8	+ 1.4 2.2	+13.9		.005	- 4.5
290	.567 .003	153.0	147.3	-12.8 0.6	- 0.1	.066 .007	.016	+ 6.4
291	.043 .006	121.1	138.0	- 1.2 0.9	+ 9.7		.015	+ 2.2
292	.027 .004	116.6	146.8	+ 1.8 3.6	- 2.3		.008	+ 0.2
293	.260 .002	175.2	145.3	-10.2 ± 0.6	- 6.6	?048 ± ?006	.079	+ 3.4
294	?063 ± ?004	123?9	133?1		+12.2		?025	+ 3.3

TABLE 19 (continued)

No.	μ	θ_o	θ_c	ρ_o	ρ_c	π_{tr}	π_{cl}	M_{cl}
295	⁰024 ± ⁰004	145°2	121°8	+ 4.4 ± 0.4	+14.2	⁰010 ± ⁰012	⁰012	+ 0.5
296	.010 .006	330.9	55.8	+12.2 SB	+14.4		.005	- 2.3
297	.008 .006	50.2	120.8	+ 3.1 3.0	+14.6		.004	- 0.6
300	.065 .002	14.3	158.5	-33.5 1.5	+ 2.8	.015 .006	.018	+ 1.3
302	.331 .002	181.5	156.2	+23 0.4	+ 7.8	.051 .010	.104	+ 4.4
303	.025 .003	182.3	148.3	+12 3	+12.9		.011	+ 1.2
304	.022 .003	185.2	160.8	+ 8.2 0.6	+ 0.4		.006	- 1.2
305	.049 .003	183.5	157.5	+14.6 0.9	+ 9.7		.016	+ 2.1
307	.002 .003	270	140.7	+20.8 1.5	+14.8		.001	- 3.6
309	.097 .010	196.2	160.8	+ 9.8 SB	+ 9.3	.041 .015	.032	+ 4.1
310	.018 .007	160.6	31.3	+11.5 2.2	+14.4		.009	+ 0.4
311	.042 .003	67.7	17.6	-22.8 2.4	+ 8.3		.013	+ 1.2
312	.022 .002	212.3	140.9	+15.3 1.0	+15.5	.002 .012	.015	+ 0.9
313	.006 .006	99.4	165.1	+ 6.0 1.2	+ 0.5		.002	- 2.2
315	.034 .003	310.2	143.7	+ 1.8 1.9	+15.5	.044 .012	.023	+ 0.8
316	.009 .003	212.0	163.6	+12.0 SB	+ 9.5		.003	+ 1.6
317	.028 .004	142.3	166.6	- 0.3 0.9	+ 1.4		.008	+ 0.5
318	.030 .003	187.6	161.4	+16.8 1.3	+12.8		.013	+ 1.3
320	.018 .003	93.2	168.4	+12.1 2.1	+11.0		.007	- 0.1
321	.025 .004	130.1	171.6	0.0 0.7	- 4.8		.007	+ 0.1
322	.011 .003	131.2	172.0	+10.1 0.7	+ 4.1		.003	- 1.4
324	.021 .003	127.4	186.4	+15.2 0.7	+ 8.1	-.004 .009	.007	- 0.3
327	.030 .001	209.2	179.0	+19.5 1.6	+16.1	.046 .009	.026	+ 2.1
328	.069 .003	197.7	179.8	- 0.2 1.5	+ 4.4	.019 .010	.020	+ 2.0
329	.012 .003	85.2	179.4	-18.8 0.5	+ 6.7	.004 .007	.004	- 2.9
330n	.047 .002	203.8	183.6	+ 9.9 0.4	+10.5	.008 .009	.017	+ 0.7
331	.163 .003	195.9	192.0	+25.8 0.7	+16.7	.093 .015	.023	+ 6.1
333	.002 .002	63.5	184.9	+ 8.1 1.3	+ 7.2	.002 .010	.001	- 7.2
334	.012 .003	59.0	218.0	+17.6 0.2	+16.8	.029 .015	.025	+ 1.7
335	.050 .002	223.3	187.3	+23.8 1.5	+ 9.1	.047 .012	.017	+ 1.1
336	.049 .004	174.2	191.1	-10.5 1.6	+ 3.3		.014	+ 2.1
337	.054 .001	175.8	188.7	+16.9 0.6	+ 6.5	.021 .010	.016	- 0.4
338	.304 .003	176.5	191.3	-15.4 0.4	+11.5	.060 .006	.115	+ 5.0
339	.035 .002	81.9	206.4	+11.5 0.3	+15.7	.027 .013	.026	+ 1.4
342	.016 .003	217.6	191.8	+ 1.2 3.0	- 4.1	.006 .016	.005	+ 1.1
343	.011 .006	236.3	251.9		+16.7		.016	+ 2.0
346	.003 .003	161.6	202.0	+ 9.9 2.5	+12.7		.001	- 4.2
348	.049 .003	173.0	195.2	+ 4.2 SB0	+ 6.5		.015	+ 2.8
349	.084 .003	222.1	197.7	+16.3 1.9	+ 7.4		.026	+ 2.7
350	.012 .003	128.7	206.5	+ 6.7 2.1	+12.6		.005	- 0.8
356	.015 .006	222.3	267.7	+12.5 1.0	+15.6	.006 .013	.011	+ 0.4
357	.018 .007	19.4	203.4	+ 2 2	+ 6.8		.005	+ 1.8
358	.029 .001	195.3	221.5	+13.5 0.9	+13.5	.017 .009	.013	+ 0.6
359	.024 .002	182.4	207.2	+ 6.6 0.7	+ 5.0		.007	+ 0.9
361	.029 .001	143.5	206.7	+ 4.4 SB	+ 4.9	-.002 .010	.008	- 2.4
362	.243 .003	304.1	219.6	-22.8 2.7	+12.0	.028 .007	.096	+ 5.8
363	.038 .002	199.9	220.4	+ 1.0 0.6	+12.3	.010 .012	.015	+ 0.2
364	.135 .001	206.9	220.7	-12.4 0.3	+ 0.3	.038 .009	.038	+ 1.6
365	.041 .003	234.0	256.1	+16.5 1.8	+14.9	.040 .016	.024	+ 1.4
366	.015 .004	233.1	208.6	+ 7.9 2.5	+ 3.6	.016 .013	.004	+ 1.4
368	.006 .004	80.6	208.1	- 9.5 0.4	- 0.5	.000 .012	.002	- 0.5
370	.013 .003	243.5	216.6	+ 8.8 2.4	+ 8.6		.004	- 1.7
371	.094 .003	330.0	291.5	+18.4 0.4	+ 4.6	.038 .012	.047	+ 2.5
372	.009 .004	192.5	212.0	- 3.9 SB	+ 9.3		.003	- 1.7
375	.111 .004	241.6	250.2	+14.1 0.6	+13.3	⁰024 ± ⁰012	.050	+ 3.8
377	.023 .003	185.0	217.7	+ 9.4 2.4	+ 8.8		.007	+ 0.3
378	⁰009 ± ⁰004	120°5	218°4	- 7.4 ± 1.3	- 6.9		⁰003	- 1.6

For each star in this list, the position angle of the proper motion, the radial velocity, and the parallax were computed on the assumption that the star shares the velocity of the cluster. These are given in Tables 18 and 19, together with the corrected GC proper motion, its observed position angle, the observed radial velocity, and the trigonometric parallax if this is contained in Schlesinger's catalogue.[19] Table 18 contains those stars north of declination $-30°$ which might be stream members according to the agreement of these data, while Table 19 contains the remaining stars. Spectral types on the system of the Yerkes atlas and spectroscopic absolute magnitudes are also given in Table 18 for comparison with the cluster absolute magnitudes. An "n" following the number of the star indicates a remark at the end of the table.

In considering the tables in this section, it is important to keep in mind the dispersion in space velocities found by Delhaye. Thus, for example, the proper motion and parallax of Sirius are known accurately enough to exclude the possibility that this star has exactly

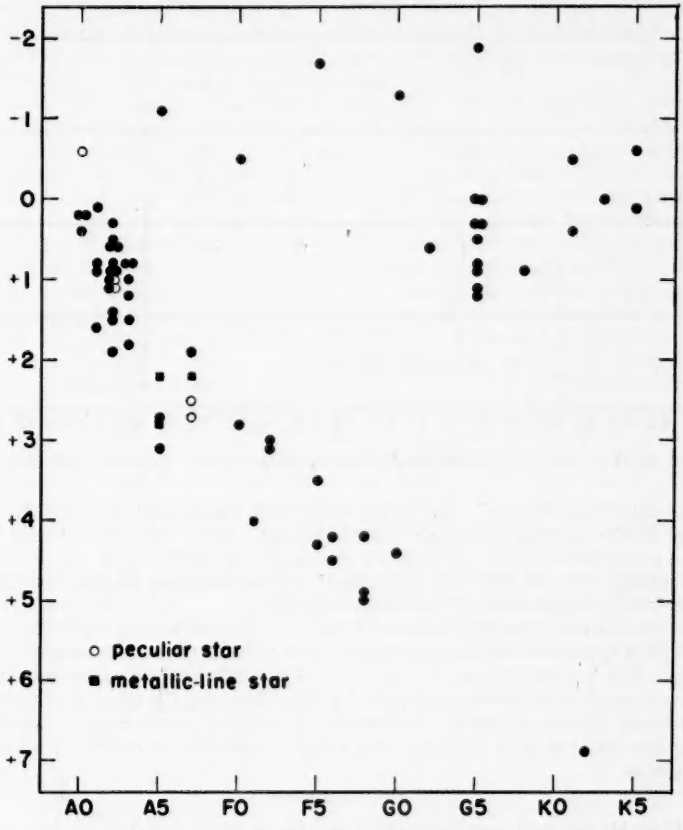

FIG. 3.—The H-R diagram for the Ursa Major stream

[19] *General Catalogue of Stellar Parallaxes* (New Haven: compiled at the Yale University Observatory, 1935).

the same motion as the nucleus stars, but the difference of 1½ km/sec is well within a dispersion of 2 or 3 km/sec. If the adopted speed of the cluster were changed to agree with the tangential motion of this star, as suggested by Hertzsprung and Smart, the radial velocity would no longer agree. The latter is also well determined, as Sirius is a standard-velocity star with good lines.

As a check on the hypothesis that there is a stream of stars having approximately the same space motion as the nucleus stars, the space velocity of the stream was determined from the radial velocities of 87 stars, chosen primarily on the basis of the agreement of their tangential motions with the space motion of the cluster. These stars gave 16.7 km/sec as the velocity of the stream. The agreement of this value with the determination, $V = 17.0$ km/sec, for the nucleus is well within the observational uncertainty.

Figure 3 shows the H-R diagram for the stream. Both observational errors and the dispersion in tangential velocities contribute to the scatter in the diagram. On the other hand, only stars for which the cluster absolute magnitudes agree with the spectroscopic

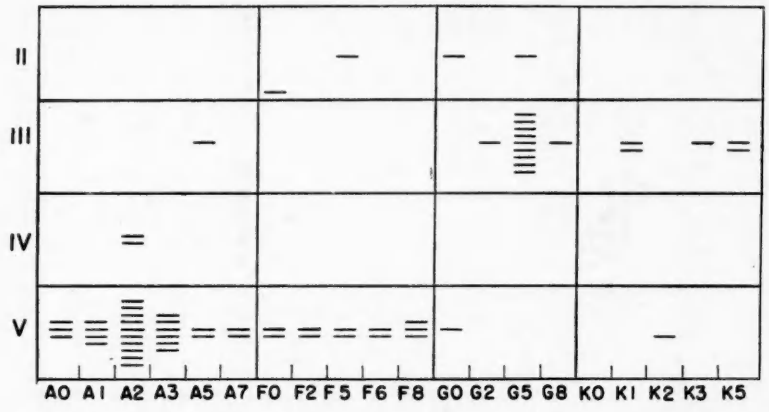

FIG. 4.—The observed distribution of stream members among the various spectral types

absolute magnitudes within 1 mag. were selected as stream members. That this criterion probably did not introduce a serious selection effect is shown by the fact that the main sequence is nowhere as wide as 2 mag. and has less than half this width in most portions of the diagram. Some of the width in the early A-type stars may be due to the failure to separate the various luminosity classes in this region.

Figure 4 illustrates the distribution of stream members among the various spectral types. The A-type stars for which no luminosity classes were determined have been plotted as class V stars. The scatter in Figure 3 has little effect on this figure, since the data have been obtained purely spectroscopically. However, the effect of incompleteness below 6.5 mag. is very evident in the presence of only one main-sequence star later than G0. The five peculiar stars and the three metallic-line stars have not been included in this diagram.

VII. SUMMARY

The Ursa Major group can be divided into two parts, a compact nucleus, similar in size to an ordinary loose galactic cluster, and an extended stream, limited primarily by incomplete observational data for distant stars.

The nucleus, which is located about 23 parsecs from the sun, occupies a roughly ellipsoidal region, $4 \times 6 \times 10$ parsecs in diameter. The shortest diameter is perpendicular to the galactic plane, the longest, in the direction of motion of the cluster. The nucleus consists of a peculiar A star, a metallic-line star, and twelve stars which define the main sequence from A0 to K3. The limit at the faint end is probably set by the lack of observational data for faint stars, but there are no early-type stars or giants in the cluster.

The proper motions of these stars are large and define the position of the convergent point accurately, but the speed of the cluster is less satisfactorily known. The results from the tangential and radial velocities differ by more than would be expected from the mean errors of the two determinations, although the average of the results agrees with the individual observations.

The density of the nucleus, about 0.1 solar mass/psc^3, is comparable to the density of the average star field through which it moves. However, because of the high velocity of the cluster with respect to the local centroid, the effects of encounters with field stars will be small and the cluster can have remained in essentially its present condition for the duration of the galactic time scale, 3×10^9 years. A more slowly moving aggregation of this type would have been disrupted much more quickly.

The stream stars show no concentration toward the nucleus. Therefore, the stream has probably not resulted from the disruption of a compact group of which the nucleus is now the only remnant. Instead, the stream stars are scattered throughout the region, about 100 parsecs in radius, in which we have good observational data for the bright stars. An appreciable dispersion may exist among the velocities of the stream stars, but it is fairly small, and the mean velocity of the group is close to that of the nucleus stars.

The existence of relatively large observational errors, together with the dispersion in velocities, makes it impossible to segregate the stream stars definitively. Sixty-nine stars which are likely to be stream members have been distinguished. Although the membership of the stream is probably larger than this list would indicate, these stars are representative of the group. Like the nucleus, the stream contains no B-type stars, but it differs from the nucleus by having a number of giant stars.

The motion of the Ursa Major stream is directed toward a point 30° distant from the vertex of star-streaming or of Kapteyn's stream II. The number of stars moving with the velocity of the Ursa Major group exceeds the number predicted on the basis of the ellipsoidal distribution by a factor of 4. Moreover, the dispersion about the mean velocity is small. Thus the Ursa Major stream is real, but it is often difficult to decide whether a particular star belongs to the stream. If numerous spurious members are to be avoided, care must be taken to choose only stars with velocities close to that of the group.

In conclusion, I wish to thank Dr. W. W. Morgan, particularly, for his kind advice throughout the investigation; Dr. J. H. Oort both for the use of unpublished data and for many helpful suggestions; Drs. R. M. Petrie and J. Delhaye for the use of their papers before publication; and the other members of the Yerkes Observatory for their discussions of various phases of the problem.

BIBLIOGRAPHY

1. BARTHOLEYNS, R. "Nouvelle liste d'étoiles appartenant au courant de la Grande Ourse," *C.R.*, **208**, 259, 1939.
2. ———. "Le Courant de la Grande Ourse," *A.N.*, **269**, 149, 1939.
3. BERTAUD, CH. "Les Étoiles *A* dans le courant de la Grande Ourse," *B.A.*, **8**, 109, 1932.
4. ———. "Les Amas d'étoiles en mouvement," *B.A.S.F.*, **47**, 216, 1933.
5. BOK, B. "The Stability of Moving Clusters," *Harvard Circ.*, No. 384, 1934.
6. BOSS, B. "Systematic Motions of the Stars Arranged According to Type," *A.J.*, **27**, 83, 1912.
7. BOTTLINGER, K. "Die Eigenbewegung der Bärengruppe," *A.N.*, **198**, 153, 1914.
8. BOURGEOIS, P., and COUTREZ, R. "Étude statistique intrinsèque des étoiles de type spectral *A* à mouvement spatial connu," *Ann. Obs. R. de Belgique*, Ser. 3, **3**, 193, 1948.
9. CANAVAGGIA, R., and FRIBOURG, M. "Recherches sur les mouvements internes dans les courant du Taureau, de la Grande Ourse, et du Scorpion-Centaure," *B.A.*, **9**, 259, 1935.
10. COLLINDER, P. "On Structural Properties of Open Galactic Clusters and Their Spatial Distribution," *Lund Obs. Ann.*, **2**, 1931. (This paper merely quotes Rasmuson's data for the Ursa Major cluster, but it does contain a good bibliography of papers written before 1931.)
11. COURVOISIER, L. "Über die Bahnkrümmung des Sternsystems Ursa Major," *A.N.*, **202**, 121, 1915.
12. DARO, S. "La Question des courants stellaire," *Ciel et terre*, **58**, 240, 1942.
13. DELHAYE, J. "The Concentration of the Motions of A- and F-Type Stars around the Velocity of the Ursa Major Cluster," *B.A.N.*, **10**, 409, 1948.
14. DZIEWULSKI, W. "Über die Bewegung einiger Sterngruppen im Raume," *Bull. Internat. Acad. Sci. Cracovie, A*, p. 185, 1915.
15. ———. "Kritische Bemerkung über Sterngruppen mit Berücksichtigung der Stern der Gruppe β, γ, δ, ϵ, and ζ UMa," *ibid.*, p. 251, 1916.
16. FILIPPOV, J. "On the Curvature of the Movement of the Ursa Major Stream" (in Russian with an English abstract), *Russ. A.J.*, **12**, 117, 1935.
17. GLIESE, W. "Die Untersuchungen der Raumgeschwindigkeiten des FK3," *A.N.*, **272**, 97, 1941.
18. GUTHNICK, P., and PRAGER, R. "Über eine Gesetzmässigkeit im System Ursa major." In: *Arbeiten aus den Gebeiten der Physik, Mathematik, Chemie; Festschrift Julius Elster und Hans Geitel*, p. 652. Braunschweig: Friedrick Vieweg und Sohn, 1915.
19. GYLLENBERG, W. "Stars with Large Proper Motions in the A.G. Zone of Lund (0^h–12^h)," *Lund. Medd.*, Ser. II, No. 56, 1930.
20. ———. "Streams among Stars with Large Proper Motions," *ibid.*, No. 57, 1931.
21. HAAS, J. "Über die Ursa-Gruppe," *A.N.*, **241**, 233, 1931.
22. VAN HERK, G. "Note on GC 17919, a Probable Member of the Ursa Major Cluster," *B.A.N.*, **9**, 14, 1939.
23. HERTZSPRUNG, E. "On New Members of the System of the Stars β, γ, δ, ϵ, and ζ Ursae Majoris," *Ap. J.*, **30**, 135, 1909.
24. ———. "A New Probable Member of the Ursa Major Group," *B.A.N.*, **6**, 60, 1930.
25. ———. "BD+56°1618 and +61°1294 as Possible Members of the Ursa Major Group," *ibid.*, **9**, 286, 1942.
26. HÖFFLER, F. "Versuch einer Ermittelung der Parallaxe des Systems Ursa Major," *A.N.*, **144**, 369, 1897.
27. HOPMAN, J. "Bemerkungen über den Ursa Major-Strom," *A.N.*, **269**, 90, 1939.
28. HORN-D'ARTURO, G. "La Corrente dell'Orsa maggiore e le stratificazioni nell'universo stellare," *Pub. dell'Osserv. astron. della R. U. di Bologna*, **2**, 97, 1931.
29. HUGGINS, W. "On the Spectrum of the Great Nebula in Orion, and on the Motions of Some Stars towards or from the Earth," *Proc. R. Soc., London* **20**, 379, 1872.
30. KLINKERFUES, W. "Über Fixstern-Systeme, Parallaxen, und Bewegungen," *Göttingen Nachr.*, June, 1873.
31. KOBOLD, H. *Der Bau des Fixsternsystems*, p. 145. Braunschweig: Friedrick Vieweg und Sohn, 1906.
32. LEDERSTEGER, K. "Das System der Bärensterne," *A.N.*, **224**, 153, 1925.
33. LINDBLAD, B. "On the Cause of the Ellipsoidal Distribution of Stellar Velocities," *Upsala Medd.*, No. 26, 1927.

34. LUDENDORFF, H. "Über die Radialgeschwindigkeiten von β, ϵ, ζ, Ursae majoris und über die Bewegung und Parallaxe der sieben Haupsterne des Grossen Bären," *A.N.*, **180**, 265, 1909.
35. ———. "Über die Bewegung des spektroskopischen Doppelsterns β Aurigae nebst Bemerkungen über das erweiterte System Ursa major," *ibid.*, **183**, 113, 1909.
36. ———. "Die Bahn des spektroskopischen Doppelsterns ϵ Ursae majoris," *ibid.*, **195**, 369, 1913.
37. MOHR, J. "Sur le courant d'étoiles Ursa Major," *B.A.*, **6**, 147, 1930.
38. NASSAU, J., and HENYEY, L. "The Ursa Major Group," *Ap. J.*, **80**, 282, 1934.
39. NASSAU, J. "On the Ursa Major Group," *A.J.*, **45**, 25, 1935.
40. OPPENHEIM, S. "Über die Bahnbene der Sonne und ihr Verhältnis zur Ebene der Milchstrasse," *A.N.*, **204**, 417, 1917.
41. PETRIE, R. "New Radial Velocities of Nineteen Bright Members of the *Ursa Major* Cluster and the Space Motion of the Nucleus Stars," *Pub. Dom. Ap. Obs. Victoria*, Vol. **8**, No. 2, 1949.
42. PLUMMER, H. "On the Motions of the Brighter Stars of Class A in Relation to the Milky Way," *Lick Obs. Bull.*, **7**, 30, 1912.
43. ———. "Preliminary Discussion of the Galactic Motions of the Bright Stars of Type I, with Some Additional Material," *M.N.*, **73**, 450, 1913.
44. ———. "On the Motions and Distances of the Bright Stars of Type F," *ibid.*, **76**, 121, 1916.
45. PROCTOR, R. "Preliminary Paper on Certain Drifting Motions of Stars," *Proc. R. Soc., London*, **18**, 169, 1869.
46. RASMUSON, N. "A Research on Moving Clusters," *Lund Medd.*, Ser. II, No. 26, 1921.
47. SMART, W. "The Ursa Major Cluster," *M.N.*, **99**, 441, 1939.
48. ———. "A New Member of the Ursa Major Cluster," *ibid.*, p. 700.
49. ———. "The Ursa Major Cluster [2d paper]" *ibid.*, p. 710.
50. STROMBERG, G. "Distribution of the Velocities of Stars of Spectral Type A," *Ap. J.*, **57**, 77, 1923.
51. TURNER, H. "Notes from an Oxford Notebook," *Observatory*, **34**, 246, 1911.
52. WILSON, R., and RAYMOND, H. "The Space Motions of 4233 Stars," *A.J.*, **40**, 121, 1930.
53. WILSON, R. "Radial Velocities of Two Suggested Members of the Ursa Major Cluster," *Pub. A.S.P.*, **57**, 311, 1945.

THE FREQUENCY AND POSITIONS OF FLARES WITHIN THREE ACTIVE SUNSPOT AREAS

HELEN W. DODSON AND E. RUTH HEDEMAN
McMath-Hulbert Observatory, University of Michigan
Received April 16, 1949

ABSTRACT

Continuous spectroheliographic records of three active sunspot groups secured during 105 hours of observation include 83 flares for which the intensity was at least four times the intensity of the undisturbed disk of the spectroheliograms. Composite maps of these flares indicate that they occurred repeatedly in the same location and with a certain continuity or chainlike nature in position. Although they appeared most often in the region between spots, or close to and over the penumbrae of spots, upon occasion, they seemed to occur exactly over the umbrae of the spots. Many flares appeared to follow, in part, channels already established by dark filaments (prominences seen in projection on the disk); the filaments persisted even though they were adjacent to, or apparently over, the bright flares.

Spectroheliograms of spot group II carry the record of a hitherto unreported, postflare phenomenon. Flare 1 of July 29, 1947, and flares 2, 3, and 4 of July 31, 1947, occurred in the same position and were followed by the ejection of a long bright streamer. In each case the streamer was at first brighter than the undisturbed disk of the hydrogen spectroheliogram and then became dark or bordered by a region of dark absorption.

The 50-foot tower telescope and the Stone spectroheliograph of the McMath-Hulbert Observatory were used during the recent sunspot maximum to secure continuous photographic records of active areas moving across the solar disk. These spectroheliograms, taken day after day of the same spot group, provide material ideally suited to the study

TABLE 1

GENERAL DATA FOR SUNSPOT GROUPS INCLUDED IN STUDY

	Spot Group		
	I	II	III
Mount Wilson No.	8129	8745	8767–8769
Date of central meridian passage	1946, July 26.9	1947 Aug. 3.9	1947 Aug. 13–14
Heliographic latitude	23° N.	18° S.	10° N., 11° N., 18° N.
Magnetic classification*	$\beta\gamma$	$\beta\gamma$	γ, α, βp
Magnetic field strength in 100 gausses*	36	24	23, 26, 36

* Data from the Mount Wilson Observatory, *Pub. A.S.P.*, **58**, 316, 1946; **59**, 274, 1947.

of the short-lived, but intensely bright, solar phenomenon known as a bright chromospheric eruption or flare. Some of the spectroheliograms were made in the light of $H\alpha$; others in the K_{2v2} line of ionized calcium. Film from the Stone instrument provides not only spectroheliograms of the disk but also a series of short sections of the spectrum centered on $H\alpha$[1].

Three especially active areas have been selected for analysis. Table 1 identifies the re-

[1] For a detailed description of the work of the Stone spectroheliograph see *Pub. Michigan U. Obs.*, **8**, 141–149, 1941.

gions and gives the pertinent magnetic data. It should be noted that spot group III, according to the Mount Wilson classification, actually consisted of three separate spot groups. This paper presents the first part of the analysis and is concerned primarily with the positions and frequency of the bright flares within each of these active areas. The study is based on more than twelve thousand spectroheliograms secured during 105 hours of observation. The dates and times of observation are summarized in Table 2.

TABLE 2

SUMMARY OF OBSERVING TIMES AND NUMBERS OF FLARES RECORDED

Date	Camera		Actual Running Time	No. of Frames	No. of Flares
	Start (U.T.)	Stop (U.T.)			
	Spot Group I				
1946					
July 23	13h02m	21h36m	5h44m	669	5
July 24	14 49	19 47	2 27	208	4
July 25	18 45	21 29	2 06	400	1
July 26	12 46	21 19	6 02	503	5
July 27	13 02	20 47	6 49	593	5
July 28	15 13	20 11	4 26	271	3
July 29	13 44	21 26	5 29	400	1
July 31	13 41	22 29	3 10	233	0
Aug. 1	14 46	19 37	3 02	382	2
Total	.....	.....	39h15m	3659	26
	Spot Group II				
1947					
July 29	15h39m	21h27m	4h01m	597	1
July 30	13 00	17 32	2 53	342	4
July 31	12 59	22 08	3 32	430	4
Aug. 1	12 44	20 36	6 30	820	2
Aug. 2	15 56	16 30	0 34	67	0
Aug. 6	19 18	22 28	2 31	268	1
Total	.....	.....	20h01m	2524	12
	Spot Group III				
1947					
Aug. 10	13h26m	22h37m	8h03m	1016	3
Aug. 11	14 14	22 25	6 49	938	10
Aug. 12	12 47	22 16	6 31	783	9
Aug. 13	13 39	22 23	6 14	728	9
Aug. 14	13 38	20 31	4 49	587	6
Aug. 15	16 22	18 03	0 59	118	2
Aug. 17	13 51	22 35	6 12	704	5
Aug. 18	14 05	22 24	6 28	985	1
Total	.....	.....	46h05m	5859	45
Total for Groups I, II, III	.....	.....	105h21m	12,042	83

I. INTENSITY AND FREQUENCY OF FLARES INCLUDED IN THIS STUDY

Examination of the spectroheliograms revealed the occurrence of so many fluctuations in brightness that it was necessary to limit the study only to the most intense flare phenomena. The maximum intensity of each flare was estimated in terms both of the intensity of the surrounding plage area and of that of the undisturbed disk, as recorded on the spectroheliograms. For this purpose a photographic strip was used which was divided into ten steps, graduated from white to black. Since the solar films had been standardized for photometric work, it was possible, by means of the calibrated strip, to estimate the intensity ratios of solar features recorded on the film. On the average, the bright plage areas were two to two and a half times as bright as the undisturbed solar disk. Some of the flares reached maximum intensities which were four to six times that of the surrounding bright plage. This study includes only those flares which became at least twice as bright as the surrounding plage and had at maximum at least four to five times the intensity of the undisturbed disk. Fluctuations with less intense maxima, even though they appeared suddenly and had a short lifetime, as is characteristic of flares, have been excluded from this investigation. Table 2 shows that a total of 83 flares, brighter than this limiting intensity, were recorded on the films. During the days of greatest activity for each of the areas, there was, on the average, slightly more than one flare per hour of observation.

It should be pointed out that a number of the flares that have been included in this study covered only a very small area of the solar disk. Those who observe and report flares for possible correlation with terrestrial phenomena would probably have excluded from their list some of these small, but relatively intense, outbursts. Since this investigation attempts to study flares in relation to the sun, rather than to the earth, it was felt that it should include all cases of sudden, short-lived increases in brightness that reached a certain intensity. The smaller outbursts appear to differ in degree rather than in kind from those phenomena that have terrestrial consequences.

II. DETERMINATION OF THE POSITIONS OF RECORDED FLARES

The large-scale spectroheliograms taken with the tower telescope are well suited to the detailed study of the positions of flares with respect to plage areas, dark filaments (prominences seen in projection on the disk), and other solar features visible in these monochromatic photographs. For a determination of flare positions with respect to underlying sunspots, it is necessary to compare the spectroheliograms with studies of the disk made in integrated light. It must be borne in mind that many sunspots do not show at all on hydrogen and calcium spectroheliograms; furthermore, certain round, relatively dark regions in the large-scale spectroheliograms do not correspond in any way to underlying spots. For this study, spectroheliograms showing flares were projected against sunspot maps drawn on the same linear scale. In this way the position of each flare was determined, not only with respect to other features of the spectroheliograms, but also with respect to the underlying spots.

All the flares that occurred on any one day were plotted on the same map. Figures 1, 2, and 3 show these maps and photographs of typical flares for the most active days for each of the spot groups under investigation. The position of each flare is indicated on the maps by diagonal shading against the fainter background of the spots. The small numbers give the serial order of occurrence of the flares. Regions having simultaneous flares carry similar shading and the same serial numbers. When flares recur in the same position on the same day, the slanting lines overlap. To assist in description of the flares and in comparison of data for successive days, two of the underlying spots have been marked *A* and *B* throughout each series. Table 3 gives the time, intensity, and pertinent comments for each of the recorded outbursts of flares.

Finally, all the observations have been brought together in composite maps which depict the flare activity during the sunlit hours of the entire disk passage of each group.

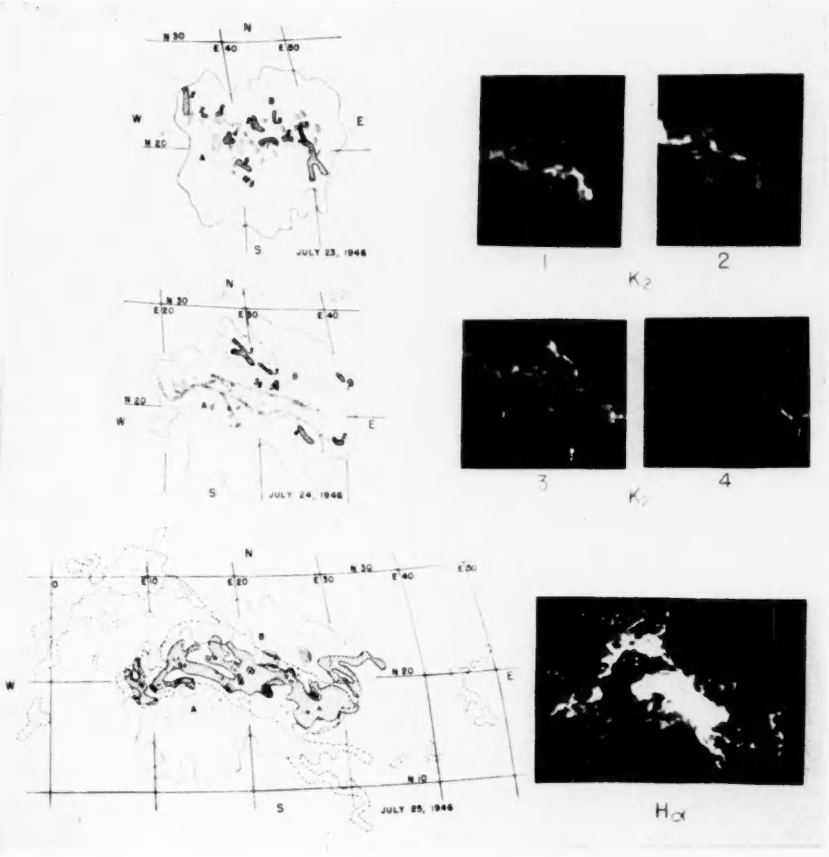
N 30
E 40
E 50
N
W
E
N 20
A
B
S
JULY 23, 1946
N 30
E 20
E 30
E 40
N 20
W
E
A
B
S
JULY 24, 1946
N
E 10
E 20
E 30
N 30
E 40
E 50
N 20
W
E
A
B
N 10
S
JULY 25, 1946
1
2
K_2
3
4
K_2
H_α

FIG. 1.—PART 1

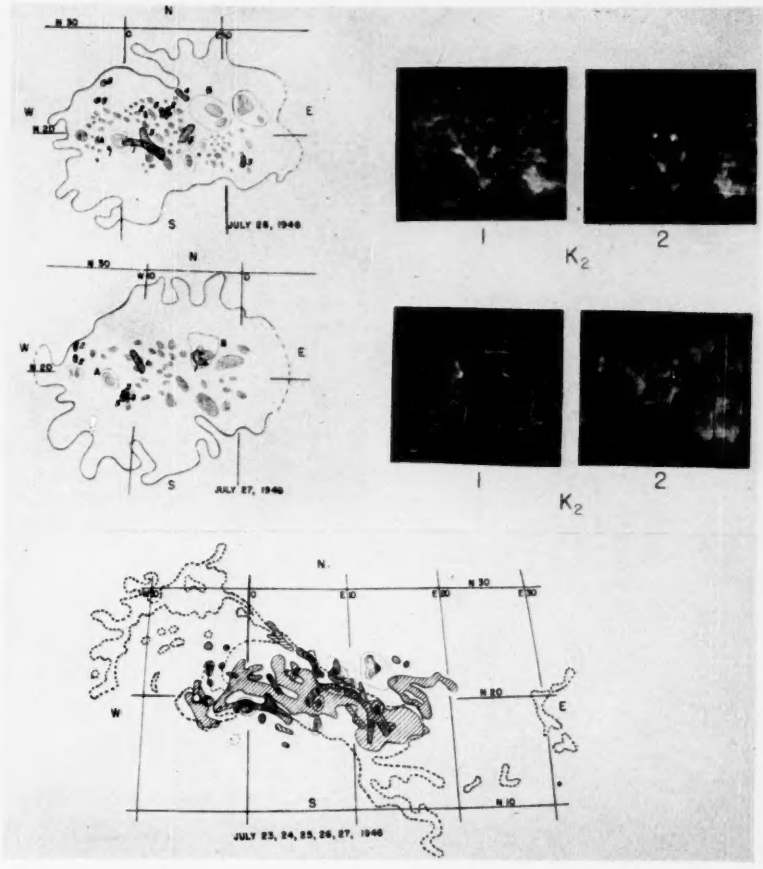

FIG. 1.—PART 2

FIG. 1.—Location of flares within spot group I, with $H\alpha$ and K_2 spectroheliograms of several bright flares, July 23–July 27, 1946. The scale of the photographs is approximately 0.75 that of the accompanying drawings. For July 25 the scale is approximately 0.50.

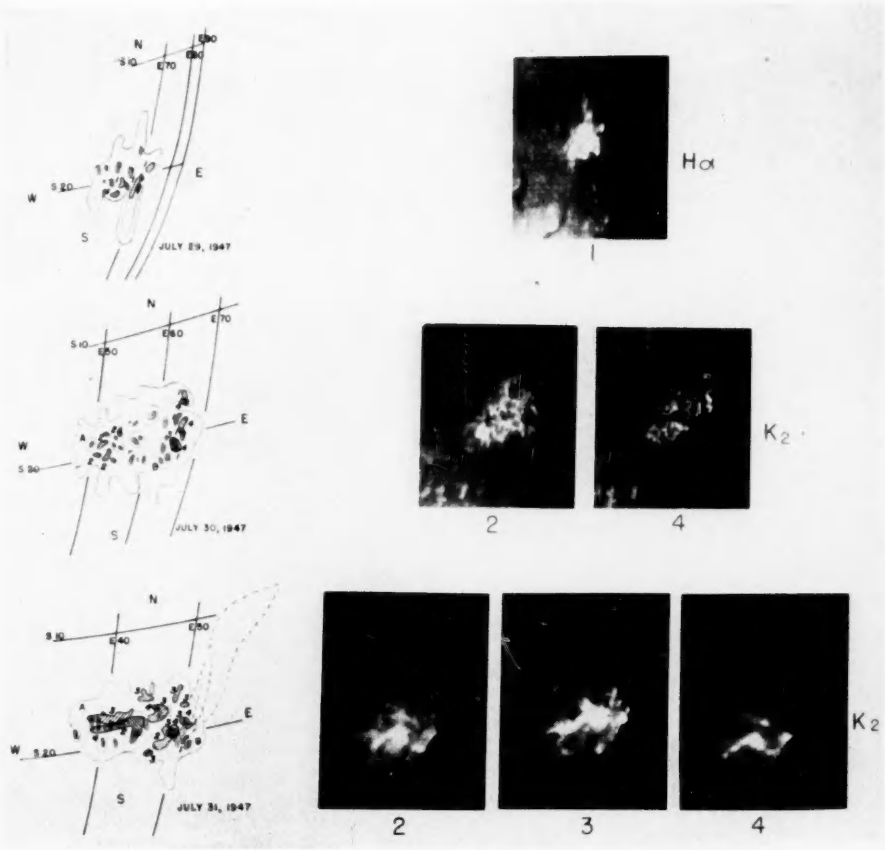
N
S10
E70
E60
E
W
S20
S
JULY 29, 1947
Hα
1
N
S10
E70
E60
E50
E
W
S20
S
JULY 30, 1947
K2
2
4
N
S10
E50
E40
E
W
S20
S
JULY 31, 1947
K2
2
3
4

FIG. 2.—PART 1

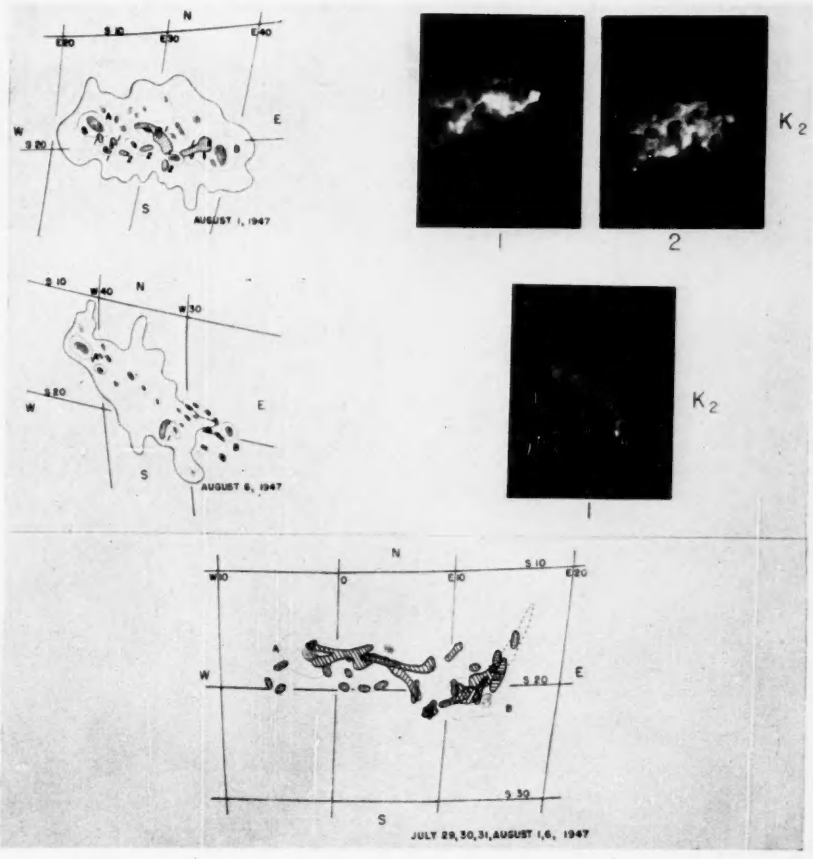

FIG. 2.—PART 2

FIG. 2.—Location of flares within spot group II, with *Hα* and K_2 spectroheliograms of several bright flares, July 29–August 6, 1947. The scale of the photographs is approximately 0.8 that of the accompanying drawings.

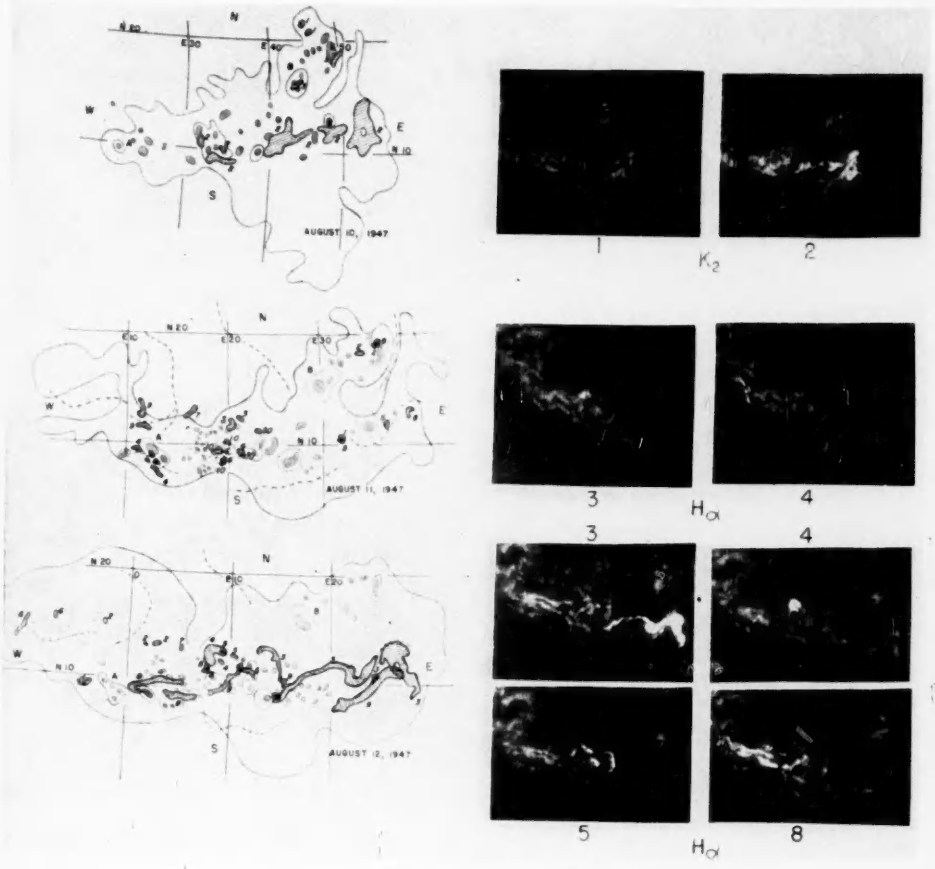
N
N 20
E 30
E 40
E 50
W
E
N 10
S
AUGUST 10, 1947
N
N 20
E 10
E 20
E 30
W
E
N 10
S
AUGUST 11, 1947
N
N 20
E 10
E 20
W
N 10
E
S
AUGUST 12, 1947
1
K2
2
3
Hα
4
3
4
5
Hα
8

FIG. 3.—PART 1

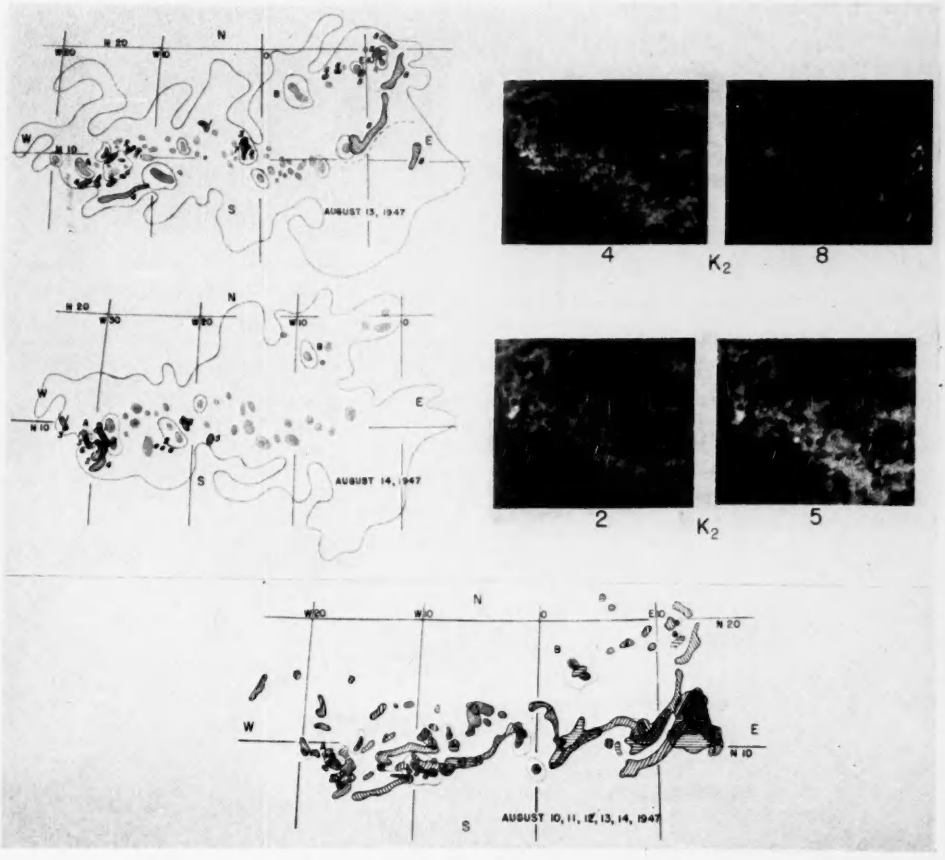

FIG. 3.—PART 2

FIG. 3.—Location of flares within spot group III, with *Hα* and K_2 spectroheliograms of several bright flares, August 10–August 14, 1947. The scale of the photographs is approximately 0.6 that of the accompanying drawings.

TABLE 3

TIME, INTENSITY, AND LOCATION FOR INDIVIDUAL FLARES

DATE	SERIAL NO. OF FLARE	U.T. OF MAXIMUM INTENSITY	INTENSITY RATIO OF FLARE TO PLAGE	REMARKS
	Spot Group I			
1946				
July 23	1	14^h45^m	6	Very bright and extensive
	2	17 18	6	Flares 1 and 2 form a chain extending from northwest to southeast across the plage
	3	17 56	4	One part of flare occurs directly over the umbra of spot B
	4	17 59	3	Three bright points near spot A
	5	20 24	2.5	
July 24	1	14 56	2.5	In addition to the four flares, the spectroheliograms exhibited very bright veins that fluctuated in intensity; these regions are indicated in the map in Fig. 1 by diagonal lines
	2	15 28	2.5	
	3	16 37	6	
	4	19 38	2.5	
July 25	1	(18 45)	>6	The region crossed by diagonal lines gives the extent and position of the flare at 16^h24^m, which is close to time of maximum intensity; dotted lines indicate the position of the flare at 17^h57^m when it extended over a much greater area
	Because of clouds, record starts at 18^h45^m, which is after the maximum of this great flare; map and spectroheliogram in Fig. 1 are based on data from the Observatory of Meudon			
July 26	1	13 45	4	Two flares near spot A, one extending into umbra of spot
	2	14 48	6	Two small but very intense flares
	3	15 58	2.5	Extensive eruptions in three different places; the flare near spot A coincides in part with flare 1
	4	17 45	2.5	
	5	18 09	2	Three small outbreaks, one of which coincides in position with part of flare 2
July 27	1	14 01	5	Two very bright flares which occur simultaneously; one is crescent-shaped and extends over the umbra of spot B
	2	16 38	2.5	
	3	17 51	2.5	Flares 3, 4, and 5 are separate phenomena which recur in the same location
	4	19 16	2.5	
	5	20 10	2–	
July 28*	1	15 14	4	
	2	16 35	3	
	3	17 14	4	Simultaneous outbreak in six different places in the vicinity of spots A and B; one portion of flare lies directly over the umbra of spot B
July 29*	1	14 46	4	Bright flare near spot A; fluctuations in intensity of plage region extending from northwest to southeast occurred frequently during period of observation
July 31				No flares recorded in the 2.5 observing hours
Aug. 1*	1	15 15	3	Two bright points; no flare previously observed in this position
	2	16 00	4	Very bright flare near spot A; prominence material is later recorded beyond the limb of the sun, with this bright flare apparently at its base

* Flares observed on this date have not been included in the composite maps of Fig. 4 because of the uncertainty in position when the region is close to the limb.

TABLE 3—*Continued*

Date	Serial No. of Flare	U.T. of Maximum Intensity	Intensity Ratio of Flare to Plage	Remarks
	Spot Group II			
1947				
July 29	1	19^h54^m	3	Four bright points; one of these, at head of U-shaped filament, ejects an elongated, bright streamer
July 30	1	(13 00)	2	Four flares were occurring when camera was started at 13^h00^m
	2	13 17	3	Four bright regions near spot A
	3	13 30	2	Coincides with part of flare 1
	4	16 12	3	Extensive flares north of spot B, overlapping parts of flares 1 and 3
July 31	1	13 40	2	Two flares in penumbra of spot B
	2	14 58	2.5	Large area covered by flare; portion near spot B ejects bright streamer or plume, which is bordered by dark absorbing material
	3	18 55	3	Several very intense flares; bright plume is again ejected from region near spot B
	4	20 21	3	Coincides in position with flare 2; bright plume, in same position, is again ejected from region near spot B
Aug. 1	1	15 20	4	Intense flare in region between spots A and B
	2	20 17	2.5	Three flares in heretofore inactive part of plage
Aug. 2	.....	.....	.....	No flares recorded in the half-hour of observing time
Aug. 6	1	19 35	2.5	Small bright point
	Spot Group III			
Aug. 10	1	13^h49^m	2.5	Two small bright points
	2	16 15	2.5	Flares extended over a large area
	3	19 55	2	Two flares in northeastern portion of plage; one of these lies directly over the umbra of spot B
Aug. 11	1	14 33	2	Small bright point
	2	15 28	2	Two bright points in northeastern portion of plage
	3	16 38	2	Two small points near center
	4	17 10	2.5	Four bright flares which border filament near spot A
	5	17 38	2	Coincides in position with flare 1
	6	18 04	2	Three flares near center of plage
	7	20 30	2	
	8	20 45	2	Three flares in eastern portion of plage; one of these coincides with one of the bright points of flare 2
	9	22 14	2	Two elongated flares in western portion of plage, with part of a long filament lying between them
	10	22 25	2.5	Five bright areas in center of plage, three of which coincide with parts of flare 6
Aug. 12	1	12 56	2	One bright point near spot A
	2	13 55	2	Three bright points

TABLE 3—*Continued*

Date	Serial No. of Flare	U.T. of Maximum Intensity	Intensity Ratio of Flare to Plage	Remarks
	Spot Group III (Continued)			
1947				
Aug. 12	3	14^{h}06^m	5	A large spectacular flare in eastern portion of plage; an S-shaped filament appears to cross over the flare
	4	16 12	4	Large bright flare in central portion of plage; coincides in position with flare 3 of August 11
	5	17 23	3	Four regions that brighten simultaneously; one of these coincides with part of flare 4
	6	18 18	2.5	
	7	18 39	2.5	
	8	20 23	4	Long bright flares that lie apparently on either side of a dark filament
	9	21 47	3	Long bright flare in eastern part of plage and lies along southern border of S-shaped filament
Aug. 13	1	13 48	2	
	2	13 55	2	
	3	14 59	2	
	4	15 07	2.5	
	5	15 37	2	Coincides with flare 3
	6	16 12	2	
	7	16 24	2	Coincides with flares 3 and 5
	8	17 41	2	Extensive flares in eastern portion of plage; one part lies on northern border of S-shaped filament
	9	21 13	2	Two small flares in western part of plage; one coincides with flare 2
Aug. 14	1	14 30	2	Three flares near spot A
	2	14 44	2	Flare near spot A, with three very small bright points farther east
	3	15 04	2	Two small bright points near spot A, coinciding with parts of flare 1
	4	17 46	3	Large bright flare near spot A
	5	17 54	2.5	Small bright flare in central portion of plage; flare 4 still visible near spot A
	6	18 51	2	Recurrence of flares near spot A
Aug. 15*	1	16 39	3	
	2	18 03	2.5	
Aug. 17*	1	15 08	2	On penumbra of spot A
	2	16 53	4	Three bright flares in western portion of plage; one of these coincides with flare 1
	3	19 38	2.5	Two small bright points
	4	21 09	2	Three bright points in northeastern portion of plage
	5	21 40	3	Two bright points
Aug. 18*	1	14 31	3	Two bright points near limb; ejected surge with one of the bright points apparently at the base

* Flares observed on this date have not been included in the composite maps of Fig. 4 because of the uncertainty in position when the region is close to the limb.

The composite maps for the three active areas are shown at the bottom of Figures 1, 2, and 3, respectively. On these summarizing maps the flares are plotted with reference to spots that could be identified throughout the entire period of observation on maps drawn for the neighborhood of the central meridian. Diagonally shaded regions again represent flares, and the direction of the lines is the same for any one day's observations. Overlapping areas indicate regions in which flares were repeated on different days. The repetition of flares within any one day is not indicated on the composite maps.

III. GENERAL FEATURES OF FLARE POSITIONS

Visual observations and spectroheliograms of low magnification have shown that flares occur primarily in the immediate neighborhood of sunspots and generally in the bright plage area surrounding them. Examination of the data presented in Figures 1–3 and in Table 3, however, suggests certain further general aspects of flare positions.

a) Some flares appear as long bright ropes or filaments; others, as small bright dots. The composite map or plot of the small dots suggests, however, a certain continuity or chainlike nature in their position.

b) Although flares occur most often in the region between spots or close to and over the penumbrae of spots, upon occasion they seem to occur exactly over the umbrae of spots.

c) Flares occur repeatedly in the same location.[2] Although flares appear throughout a large area, there seem to be certain "preferred" regions for flare occurrence. Within the same day and on successive days, flares have appeared, not in *approximately* the same region but apparently in *exactly* the same small portion of the solar disk. Between these recurrences the flares disappear completely.

d) Many flares seem to follow, in part, channels already established by the dark filaments (prominences seen in projection on the disk). The relationships are not clear: some flares apparently lie along the sides of filaments; in other cases filaments apparently form limiting boundaries; at still other times the phenomena appear to be independent.

e) Although filaments have been observed to disappear shortly after the outbreak of a great flare,[3] the spectroheliograms here studied indicate that certain filaments can persist even though they are adjacent to, or apparently over, a bright flare. The well-defined, S-shaped filament in spot group III associated with certain flares on August 12 and 13, 1947, is an excellent example of this stability. This filament, which apparently lay directly over flare 3 of August 12 was visible on hydrogen spectroheliograms before, during, and for at least two days after the flare. It developed regions of high radial velocity on the thirteenth, but it was still well-defined on the fourteenth.

IV. ADDITIONAL COMMENTS ON THE OBSERVATIONS

In addition to the foregoing summary of general results, there are certain more specific observations for each of the spot groups that should be pointed out at this time.

Spot group I.—Because of clouds, the record at the McMath-Hulbert Observatory of the great flare of July 25, 1946, does not start until after the time of maximum intensity, 16^h30^m U.T.[4] However, a series of $H\alpha$ spectroheliograms, made available to us through the kindness of Dr. d'Azambuja, director of the Observatory of Meudon, shows the flare at 15^h37^m, 16^h14^m, 16^h24^m, 17^h32^m, and 17^h57^m. The third in this series, at 16^h24^m, gives the flare near maximum intensity. Comparison of this spectroheliogram with the two later ones in the series and with the film at the McMath-Hulbert Observatory indicates that, as the flare faded, there was not only the appearance of the great curved arms but also a marked lateral spread in the central portion of the flare. The extent of the spread can be estimated through comparison of the area crossed by diagonal lines with the

[2] This is in agreement with the findings of Waldmeier, as reported in "Chromosphärische Eruptionen," *Zs. f. Ap.*, **16**, 276, 1938.

[3] Spectroheliograms at the Observatory of Meudon show that a large filament disappeared shortly after the great flare of July 25, 1946.

[4] M. A. Ellison, "Visual and Spectrographic Observations of a Great Solar Flare, 1946 July 25," *M.N.*, **106**, 500, 1946.

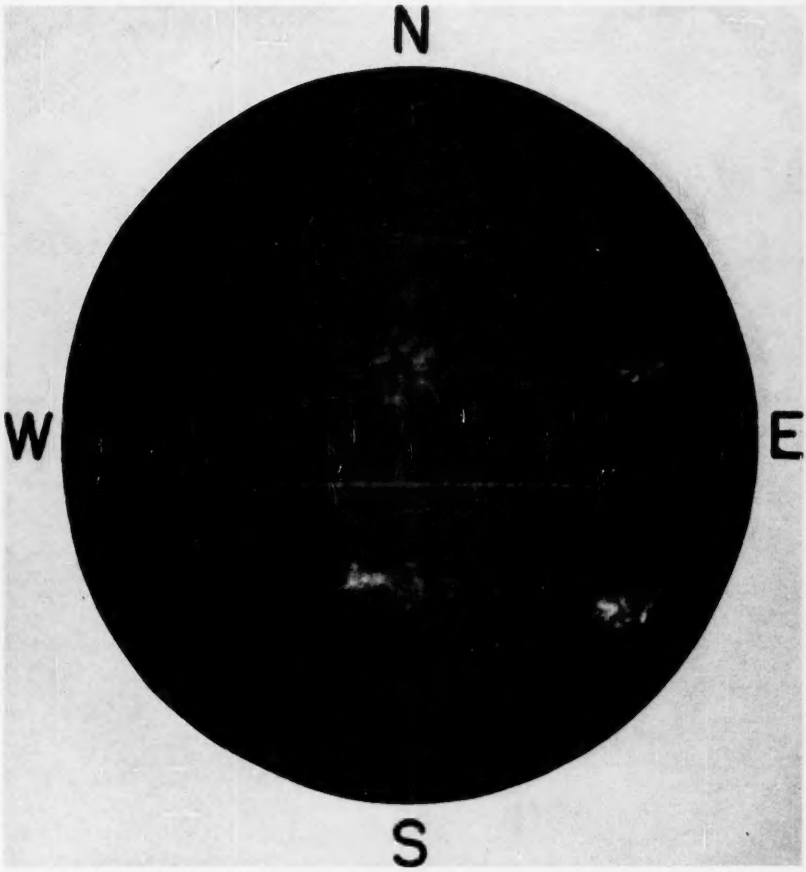

FIG. 4.—*Hα* spectroheliogram of solar disk, July 31, 1947, at 12^h00^m U.T.; spot group II, in southeast quadrant, shows bright streamer.

central portion of the figure outlined by dashes in the map for July 25, 1946, in Figure 1. The former shows the extent of the flare at 16^h24^m, the latter at 17^h57^m. The increase in width was not a mere extension of the flare; at 17^h57^m, the central section of the flare was *outlined* by two intensely bright ridges running northwest to southeast along the outer limits indicated by the dashed lines, while the very center had diminished in intensity. The composite map for this area shows that the outlining ridges coincided very closely with the locus of flares recorded on July 23, 24, and 26. This map also suggests that the great spiral arms that appeared in the flare of July 25 between 16^h24^m and 17^h32^m developed along axes or directions already indicated by the flares of July 23 and 24 (note especially flare 3 on July 24).

Spot group II.—The film for this region carries the record of another short-lived phenomenon, in addition to flares. Table 3 indicates that on July 29, 1947, flare 1, and on July 31, flares 2, 3, and 4 at 14^h58^m, 18^h55^m, and 20^h21^m, respectively, were followed by the ejection northward of a long bright streamer or plume. In each case this streamer was, at first, brighter than the undisturbed disk of the hydrogen spectroheliogram and later became dark or bordered on the northeast (limbward) side by a large region of dark absorption. The occurrence of high-velocity dark flocculi or filaments shortly after the outbreak of flares has been reported frequently by visual observers. Furthermore, the phenomenon is recorded on a number of our motion-picture films. The fact that these ejections in spot group II appeared bright gives them their special significance. Some of the films seem to indicate that certain flares are the root-points or bases of surges (see Table 3, August 1, 1946, flare 2; August 18, 1947, flare 1) and that the high-velocity dark flocculi are the surges seen in projection on the disk. It is possible that the bright streamer is the disk counterpart of one of those rarer surges which are much more brilliant, when seen at the limb, than is the usual surge.

On July 31, 1947, at 12^h00^m one of the authors observed at the spectrohelioscope still another case of a flare and subsequent bright streamer in spot group III. The small-scale *Hα* spectroheliogram of the entire disk, taken at this time and reproduced in Figure 4, shows the bright "feather" extending northward from the flare in the plage region. The bright streamer appears as bright as a plage but not so bright as a flare. The fact that the streamer followed apparently the same path at each ejection should be noted. The path of the bright ejection and the flares that occurred in it on July 29 and 30 give to the composite map of Figure 2 a curved portion suggestive of the great arcs described by the flare of July 25, 1946.

Spot group III.—The composite map for this highly complex and multiple spot group illustrates very clearly the closeness with which flare regions are duplicated on successive days. It should perhaps be noted that the greatly "preferred" region, centered at 12° N. and 12° E. in this map, lies relatively far from the direct line between any two spots. The nearest spot, 11° N., 9° E. is the principal feature of the unipolar spot group, Mount Wilson 8768.

Further analysis of these films is being undertaken. It is hoped that the work will yield more detailed intensity measures, light-curves, and certain spectral variations.

The authors wish to express their sincere appreciation to all their colleagues at the McMath-Hulbert Observatory; it is only through the co-operation of the entire staff that material such as that used in this study could have been secured and analyzed. They wish to thank Dr. Seth B. Nicholson, of the Mount Wilson Observatory, for providing detailed magnetic data for the spot groups studied, and Dr. Lucien d'Azambuja, director of the Observatory of Meudon, for making available the spectroheliograms of the great flare of July 25, 1946. Furthermore, they wish to express their gratitude to McGregor Fund of Detroit for continuing grants-in-aid in support of the work of the McMath-Hulbert Observatory.

THE DYNAMICS OF STAR STREAMING*

P. STEHLE†
Princeton University
Received March 10, 1949

ABSTRACT

The hydrodynamical model of a stellar system has had its most detailed discussion in the hands of S. Chandrasekhar. This treatment consists of smoothing out the mass distribution into one possessing no granular structure and of considering the possible states of such distributions. This can be done in a most elegant and compact way if advantage is taken of the notation and methods of the tensor calculus; for the equation of continuity in phase space can, under the assumptions made by Chandrasekhar, be broken down into four sets of equations having, in the static case at least, immediate geometrical interpretation. The object of this paper is to formulate the theory from this geometrical point of view. In a succeeding paper some further consequences of this viewpoint will be developed.

I. GEOMETRICAL PRELIMINARIES

To facilitate the writing-down of the equations describing the stellar system in a minimum of space and with a maximum of clarity, the tensor notation as used by L. Eisenhart will be adhered to throughout. The salient features of this notation will be indicated. For a detailed account see Eisenhart's work.[1]

The co-ordinates of a point in space will be denoted by x^i $(i = 1, 2, 3)$. The square of the distance between two neighboring points is given by

$$ds^2 = \sum_{i,j=1}^{3} g_{ij} dx^i dx^j \equiv g_{ij} dx^i dx^j . \tag{1.1}$$

The identity sign is used to indicate that repeated indices of opposite character (superscript or subscript) are to be summed over the range of the index, in this case from 1 to 3. (Latin indices will always have this range.) Superscripts denote contravariant indices, while subscripts denote covariant ones, the two transforming contragrediantly upon change of co-ordinates. Occasionally it will be necessary to introduce scalar indices, i.e., indices which do not indicate tensor components but which label separate vectors, tensors, etc. Greek letters will be used for these, and their range will be stated. Greek indices do not, of course, enter into the expressions for co-ordinate transformations.

Because the tensor notation used here is valid not only in any Cartesian co-ordinate system but also in any curvilinear one, the metric tensor, g_{ij}, can have components other than 1 $(i = j)$ and 0 $(i \neq j)$; the determinant of g cannot, however, vanish anywhere. Also, in curvilinear co-ordinates, ordinary derivatives must be replaced by covariant derivatives which reduce, in Cartesian co-ordinates, to ordinary derivatives. These covariant derivatives will be denoted by a comma preceding the index of differentiation. Thus

$$\lambda_{i,j} = \frac{\partial \lambda_i}{\partial x^j} - \left\{ \begin{matrix} l \\ ij \end{matrix} \right\} \lambda_l , \tag{1.2}$$

* This contains part of the substance of a thesis submitted to Princeton University in partial fulfilment of the requirements for the Ph.D. degree. Professor H. P. Robertson originated this formulation of the problem and presented it to the American Philosophical Society in the fall of 1940.

† Now at the University of Pittsburgh.

[1] L. P. Eisenhart, *Riemannian Geometry* (Princeton: Princeton University Press, 1926).

where the Christoffel symbol is defined by

$$\left\{ \begin{matrix} l \\ ij \end{matrix} \right\} = \tfrac{1}{2} g^{lm} \left(\frac{\partial g_{im}}{\partial x^j} + \frac{\partial g_{jm}}{\partial x^i} - \frac{\partial g_{ij}}{\partial x^m} \right). \tag{1.3}$$

Equations (1.2) and (1.3) will not be needed explicitly but would be needed in actually evaluating derivatives in curvilinear co-ordinates.

II. DYNAMICAL POSTULATES OF CHANDRASEKHAR

The dynamics of stellar systems proposed by Chandrasekhar rest on three postulates. These and their observational justification are discussed in detail by Chandrasekhar.[2] Here they will simply be stated as postulates.

1. At each point in space there may be defined a "local standard of rest," the centroid of the motion of the near-by stars, whose velocity in a fixed co-ordinate system is a continuous function of position. This velocity is denoted by u_0^i. Its variation with the co-ordinates gives rise to the differential motions of the system.

2. The motion of the stars relative to the local standard of rest is given by a "generalized Schwarzschild distribution," ellipsoidal in form. If dN is the number of stars in a spatial range between x^i and $x^i + dx^i$, with velocities between u^i and $u^i + du^i$, then

$$dN = \psi(x, u, t) \sqrt{g} d^3x \sqrt{g} d^3u , \tag{2.1}$$

and the distribution function is of the form

$$\psi(x, u, t) = \psi(Q + \sigma) ,$$

where

$$Q = a_{ij} (u^i - u_0^i)(u^j - u_0^j) \tag{2.2}$$

and

$$\sigma = \sigma(x, t) .$$

The Q is a quadratic form, symmetrical and positive definite, and therefore describing an ellipsoid in the residual velocities; σ is related in an unspecified way to the spatial density of stars.

3. The motion of an individual star is derivable from a potential function, V, depending only on the co-ordinates and the time, $V(x, t)$. This third postulate implies that the distribution function satisfies an equation of continuity in phase space; namely,

$$\frac{\partial \psi}{\partial t} + u^i \frac{\partial \psi}{\partial x^i} + \dot{p}_i \frac{\partial \psi}{\partial p_i} = 0 , \tag{2.3}$$

where the p_i are the momenta conjugate to the x^i. The Lagrangian per unit mass is

$$L = T - V$$

$$= \tfrac{1}{2} g_{ij} u^i u^j - V .$$

Thus

$$p_i = \frac{\partial L}{\partial u^i} = g_{ij} u^j . \tag{2.4}$$

The Hamiltonian per unit mass thus is

$$H = \tfrac{1}{2} g^{ij} p_i p_j + V ;$$

[2] *Principles of Stellar Dynamics* (Chicago: University of Chicago Press, 1942).

and the equations of motion are

$$u^i = \frac{\partial H}{\partial p_i} = g^{ij} p_j$$

$$-\dot{p}_i = \frac{\partial H}{\partial x^i} = H,_i = V,_i . \tag{2.5}$$

(This last equation holds even when g_{ij} depends on the x^i, since the covariant derivative of g_{ij} vanishes in all co-ordinate systems.) Before explicitly carrying out the differentiations in equation (2.3), it is convenient to define some new quantities. Let

$$\Delta_i = a_{ij} u_0^j ,$$

$$Q_0 = a_{ij} u_0^i u_0^j = \Delta_i u_0^i , \tag{2.6}$$

$$-\chi = Q_0 + \sigma .$$

Then

$$Q = a_{ij} u^i u^j - 2\Delta_i u^i + Q_0 .$$

With these definitions equation (2.3) becomes

$$\frac{d\psi}{d(Q+\sigma)} \left[\left(\frac{\partial a^{ij}}{\partial t} p_i p_j - 2 \frac{\partial \Delta^i}{\partial t} p_i - \frac{\partial \chi}{\partial t} \right) + (a^{ij},_k p_i p_j - 2\Delta^i,_k p_i - \chi,_k) u^k + (2a^{ik} p_i - 2\Delta^k) \dot{p}_k \right] = 0 . \tag{2.7}$$

The equations of motion allow the elimination of u^k and $\dot{p}^k$ in favor of p^k, and then the coefficients of the various powers of p's must vanish separately. This process yields the equations obtained by Chandrasekhar, namely:

$$a_{ij,k} + a_{ki,j} + a_{jk,i} = 0 , \tag{2.8}$$

$$\Delta_{i,j} + \Delta_{j,i} = \frac{\partial a_{ij}}{\partial t} , \tag{2.9}$$

$$\Delta_l V^l,_= \frac{1}{2} \frac{\partial \chi}{\partial t} , \tag{2.10}$$

$$\tfrac{1}{2} \chi,_i + a_{il} V^l,_= -\frac{\partial \Delta_i}{\partial t} . \tag{2.11}$$

Since our present concern is with the steady state, all the partial derivatives with respect to the time will be put equal to zero. The equations to be discussed are thus

$$a_{ij,k} + a_{ki,j} + a_{jk,i} = 0 , \tag{2.12}$$

$$\Delta_{i,j} + \Delta_{j,i} = 0 , \tag{2.13}$$

$$\Delta_l V,^l = 0 , \tag{2.14}$$

$$\tfrac{1}{2} \chi,_i + a_{il} V,^l = 0 . \tag{2.15}$$

III. DISCUSSION OF THE EQUATIONS

The four tensor equations, (2.12)–(2.15), are really a set of twenty partial differential equations, which lose their ease of interpretation when considered individually in that

manner. Taken together, these equations imply the existence of two integrals of the motion:

$$I_1 = \Delta_i u^i , \tag{3.1}$$

$$I_2 = a_{ij} u^i u^j - \chi . \tag{3.2}$$

These have the form of momentum and energy integrals, respectively.

Equations (2.13) are well known in geometry as Killing's equations and imply that the vector Δ_i defines a motion of the space into itself. In three-dimensional Euclidean space this means that Δ_i can be expressed as the sum of a translation and a rotation about the direction of translation. The canonical forms of Δ_i can thus be written down. Take the z-axis of a Cartesian system to be in the direction of the translation. Then

$$\Delta_1 = \beta y , \quad \Delta_2 = -\beta x , \quad \Delta_3 = k . \tag{3.3}$$

The possible cases are:

$\beta \neq 0$, $k \neq 0$, both rotation and translation;

$\beta = 0$, $k \neq 0$, translation only;

$\beta \neq 0$, $k = 0$, rotation only;

$\beta = 0$, $k = 0$, $\Delta_i = 0$.

If $\Delta_i = 0$, then, from the definition of Δ_i, it follows that either $u_0^i = 0$ or $det\ a_{ij} = 0$.

Equation (2.14) states that the motion Δ_i lies in an equipotential surface, or that V is invariant under the motion Δ_i. The four cases above thus correspond to the four forms of potential:

$$\begin{aligned} V &= V\left(x^2+y^2 , \quad z+\frac{k}{\beta}\tan^{-1}\frac{y}{x}\right), \\ V &= V(x, y) , \\ V &= V(x^2+y^2, z) , \\ V &= V(x, y, z) , \end{aligned} \tag{3.4}$$

respectively. Of these, only the third and fourth can represent systems in a steady state with a finite density of stars, for only these have closed equipotential surfaces. Equipotential surfaces extending to infinity provide energetically possible paths for diffusion of stars to infinity, thus reducing the density to zero.

The vector Δ_i can be expressed in terms of the generators of the Euclidean group of motions in an invariant way. These generators are most easily defined in Cartesian co-ordinates and obtained in other co-ordinates by means of a co-ordinate transformation. In Cartesian co-ordinates they are

$$\text{Translation: } \eta_i^a = \delta_i^a \qquad (a = 1, 2, 3) , \tag{3.5}$$

$$\text{Rotation:} \qquad \xi_i^a = -\epsilon(aij)\, x^j . \tag{3.6}$$

Here the symbol $\epsilon(aij) = \left\{\begin{matrix} +1 \\ -1 \\ 0 \end{matrix}\right\}$ when (aij) is obtained from (1 2 3) by $\left\{\begin{matrix} \text{even} \\ \text{odd} \\ \text{no} \end{matrix}\right\}$ per-

mutation. (In general co-ordinates there is a tensor, ϵ, defined by

$$\epsilon_{ijk} = \sqrt{g}\,\epsilon(ijk)\,,$$
$$\epsilon^{ijk} = \frac{1}{\sqrt{g}}\,\epsilon(ijk)\,.$$

Note, however, that the motions η_i^a and ξ_i^a are not defined in general co-ordinates by equations (3.5) and (3.6) with $\epsilon(aij)$ replaced by the tensor ϵ; for a is a scalar index and does not appear in the expression for a co-ordinate transformation. We shall make frequent use of the antisymmetric tensor ϵ, however.) Thus

$$\Delta_i = p_a \eta_i^a + q_a \xi_i^a\,. \tag{3.7}$$

Equation (2.12) is a condition on the velocity ellipsoid alone, independent of the form of the potential. The integration of this equation can be carried out. To do this, write it in the form

$$(a_{ik,\,j} + \tfrac{1}{2}\,a_{ij,\,k}) + (a_{jk,\,i} + \tfrac{1}{2}\,a_{ji,\,k}) = 0\,, \tag{3.8}$$

which is equivalent to equation (2.12) because of the symmetry of a_{ij}. Equation (3.8) shows that $a_{ik,\,j} + \frac{1}{2}a_{ij,\,k}$ is antisymmetric in i and j. Therefore, we may write

$$a_{ik,\,j} + \tfrac{1}{2}\,a_{ij,\,k} = -\tfrac{3}{2}\,b_k^a \epsilon_{aij}\,. \tag{3.9}$$

To justify this, multiply through by ϵ^{mij} and notice from the definition of ϵ that it follows that

$$\epsilon_{ijk}\epsilon^{iml} = \delta_j^m\,\delta_k^l - \delta_k^m\,\delta_j^l\,,$$
$$\epsilon_{ijk}\epsilon^{ijl} = 2\,\delta_k^l\,.$$

Then from equation (3.9) we obtain

$$\begin{aligned} -3\,b_k^m &= (a_{ik,\,j} + \tfrac{1}{2}\,a_{ij,\,k})\,\epsilon^{mij} \\ &= a_{ik,\,j}\epsilon^{mij}\,, \end{aligned} \tag{3.10}$$

which gives an explicit expression for the b's. From equation (3.10) it follows that $b_m^m = 0$.

In equation (3.9) interchange i and j, multiply by 2, and subtract the result from equation (3.9), obtaining

$$\begin{aligned} a_{ij,\,k} &= b_k^a \epsilon_{aij} = 2\,b_j^a \epsilon_{aik} \\ &= b_k^a \epsilon_{aij} - 2\,b_j^a \epsilon_{ajk}\,, \end{aligned}$$

so that, averaging the two expressions for $a_{ij,\,k}$, we get

$$a_{ij,\,k} = -\,b_j^a \epsilon_{aik} - b_i^a \epsilon_{ajk}\,. \tag{3.11}$$

Differentiate equation (3.11),

$$a_{ij,\,kl} = -\,b^a_{j,\,l}\epsilon_{aik} - b^a_{i,\,l}\epsilon_{ajk}\,.$$

Multiply by ϵ^{rkl} and sum over k and l:

$$\begin{aligned} 0 &= \epsilon^{rkl}\,(b^a_{j,\,l}\epsilon_{aik} + b^a_{i,\,l}\epsilon_{ajk}) \\ &= b^a_{j,\,a}\,\delta_i^r + b^a_{i,\,a}\,\delta_j^r - b^r_{j,\,i} - b^r_{i,\,j}\,. \end{aligned}$$

Put $r = i$ and remember that $b^r_r = 0$. Then

$$0 = b^a_{j,a}.$$

Finally, therefore,

$$b^r_{i,j} + b^r_{j,i} = 0 . \tag{3.12}$$

In Cartesian co-ordinates this means that, for each value of r, b must be a Euclidean motion. With this fact, equation (3.7) can be integrated immediately. The final result is that

$$a_{ij} = \alpha_{\sigma\rho}\eta^\sigma_i\eta^\rho_j + \beta_{\sigma\rho}(\eta^\sigma_i\xi^\rho_j + \eta^\sigma_j\xi^\rho_i) + \gamma_{\sigma\rho}\xi^\sigma_i\xi^\rho_j , \tag{3.13}$$

where the coefficients are subject to the condition that

$$\alpha_{\sigma\rho} = \alpha_{\rho\sigma} , \qquad \gamma_{\sigma\rho} = \gamma_{\rho\sigma} , \qquad \sum_\sigma \beta_{\sigma\sigma} = 0 . \tag{3.14}$$

There are twenty constants in all.

It is of interest to note that this solution of equation (2.12) also holds in the non-static case because of the identical forms of equations (2.8) and (2.12). When equation (2.9) is considered along with equation (2.8), it turns out that the $\gamma_{\sigma\rho}$ of equation (3.14) are constants but that $\alpha_{\sigma\rho}$ and $\beta_{\sigma\rho}$ are arbitrary functions of the time.

Equation (2.15) remains to be discussed. This equation is called by Chandrasekhar the "condition of compatibility." It alone connects the velocity distribution with the potential and with the spatial density of stars. If the velocity distribution is spherical, i.e., if $a_{ij} = Ag_{ij}$, then equation (2.15) puts no condition on the potential, for χ is an unspecified function. Other forms of the a_{ij} will put limitations on the possible forms of the potential.

Since the function χ is unspecified, it is better eliminated from equation (2.15). This can be done by taking the curl of both sides of the equation, since the curl of a gradient vanishes. Thus

$$\epsilon^{pij}(a_{il}V,^l)_{,j} = 0 . \tag{3.15}$$

Any further analysis must start from a restriction either on the velocity ellipsoid or on the potential, since the general theory stated here contains nothing beyond equation (3.15). Chandrasekhar has gone further in the time-dependent case by restricting the velocity ellipsoid to be a sphere.[2] The other approach, that of restricting the potential and finding the permissible forms of the coefficients of the velocity ellipsoid, is also of some interest and will be the one taken here. The program of this paper and of a following one is to consider equations (2.12) and (2.15) or (3.15) independently of equations (2.13) and (2.14), but in conjunction with additional conditions on the potential V, to see what forms of the a_{ij} are possible.

IV. THE COMPATIBILITY CONDITIONS

The compatibility conditions, equation (2.15), may be written according to equation (3.15) as

$$\epsilon^{pij}a^l_{i,j}V,_l + \epsilon^{pij}a^l_i V,_{lj} = 0 \tag{4.1}$$

This is to be considered as an equation for the a_{ij} when V is a function arbitrary except for certain restrictions explicitly applied. Suppose these conditions to be linear homogeneous equations of the first and second order, namely,

$$c^{\alpha r}V,_r = 0 \qquad (\alpha = 1, 2) , \tag{4.2}$$

$$d^{\Gamma r}V,_r + d^{\Gamma rs}V,_{rs} = 0 \qquad (\Gamma = 1, 2, \ldots) . \tag{4.3}$$

Equation (4.1) is not to restrict V in any way not already contained in equations (4.2) and (4.3). One consequence of equation (4.2) is

$$c^{ar}{}_{,s}V_{,r}+c^{ar}V_{,rs}=0\,. \tag{4.4}$$

We now assume that equations (4.2), (4.3), and (4.4) form a complete set of equations in the sense that no new relations of the second order can be obtained from them by differentiation and elimination of higher derivatives. Then equation (4.1) must be a linear combination of these equations, namely,

$$M^p_a(c^{ar}V_{,r})+N^{ps}_a(c^{ar}{}_{,s}V_{,r}+c^{ar}V_{,rs})+B^p_\Gamma(d^{\Gamma r}V_{,r}+d^{\Gamma rs}V_{,rs})=0\,. \tag{4.5}$$

Since equation (4.5) is an identity in V, coefficients of various derivatives must vanish separately. Thus we get

$$\epsilon^{pir}a^s_i+\epsilon^{pis}a^r_i=N^{ps}_a c^{ar}+N^{pr}_a c^{as}+2B^p_\Gamma d^{\Gamma rs}\,, \tag{4.6}$$

$$\epsilon^{pij}a^r_{i,j}=M^p_a c^{ar}+N^{ps}_a c^{ar}_{,s}+B^p_\Gamma d^{\Gamma r}\,. \tag{4.7}$$

TWO LEMMAS

In discussing equation (4.6), two lemmas will prove useful.

Lemma 1.—Given the quantities of c^r and A^{rs} such that

$$A^{rs}=c^rN^s+c^sN^r\,,$$

then

$$c^2A^{rs}=c^r(A^{st}c_t-\tfrac{1}{2}A^t_tc^s)+c^s(A^{rt}c_t-\tfrac{1}{2}A^t_tc^r)\,.$$

Proof:

$$A^t_t=2\,c_tN^t\,,$$

$$A^{rt}c_t=c^r(c_sN^s)+c^2N^r\,,$$

$$c^2N^r=A^{rt}c_t-\tfrac{1}{2}A^t_tc^r\,.$$

Substitute this in the definition of A^{rs}, and the lemma is proved. Note also that

$$A^{rs}c_rc_s=2\,c^2N^sc_s=c^2A^s_s\,.$$

Corollary: If

$$c^rN^s+c^sN^r=0\,,\qquad\text{and}\qquad c^2\neq 0\,,$$

then $N^s=0$.

Lemma 2.—Given the quantities c^{ar} ($a=1,2$), where a is a scalar index, such that the matrix $||c^{ar}||$ is of rank 2 and that

$$A^{rs}=c^{ar}N^s_a+c^{as}N^r_a\,,$$

then

$$A^{rs}=c^{ar}A^{st}c_{at}+c^{as}A^{rt}c_{at}-c^{ar}c^{\beta s}c_{am}c_{\beta n}A^{mn}\,.$$

Proof: Define the quantities $P^{a\beta}$ by

$$P^{a\beta}=c^{ar}c^\beta_r=P^{\beta a}\,.$$

The determinant $|P^{a\beta}|$ differs from zero, since the matrix $||c^{ar}||$ is of rank 2, as may be shown by use of Schwarz's inequality. The quantity $P^{a\beta}$ thus has a unique inverse defined by

$$P^{a\gamma}P_{\gamma\beta}=\delta^a_\beta\,.$$

The quantities $P^{\alpha\beta}$ and $P_{\alpha\beta}$ may be used to raise and lower Greek indices, except through a sign of differentiation. The $P^{\alpha\beta}$ and $P_{\alpha\beta}$ are invariant under transformations involving Latin indices. Now

$$A^{rt}c_{\alpha t} = c^{\beta r}(c_{\alpha t}N^t_\beta) + N^r_\alpha .$$

Therefore,

$$N^r_\alpha = A^{rt}c_{\alpha t} - Q_{\alpha\beta}c^{\beta r} ,$$

where

$$Q_{\alpha\beta} = c_{\alpha t}N^t_\beta ,$$

$$Q_{\alpha\beta} + Q_{\beta\alpha} = A^{rs}c_{\alpha r}c_{\beta s} .$$

Substituting the expression for N^r_α back in the definition of A^{rs} and using the above relation, the lemma follows.

Corollary: If $A^{rs} = 0$, then $Q_{\alpha\beta} = -N\epsilon_{\alpha\beta}$, and

$$N^r_\alpha = N\epsilon_{\alpha\beta}c^{\beta r} ,$$

where $\epsilon_{\alpha\beta} = \pm 1$ as α, β is an even or odd permutation of 1, 2.

V. ONE FIRST-ORDER CONDITION ON V

In Section IV it is shown that the conditions of compatibility connect the form of the a_{ij} with the restrictions which are placed on V. The general theory imposes one condition on V, namely,

$$\Delta_l V,^l = 0 . \tag{5.1}$$

This condition is already enough to show that the a_{ij} will never be restricted to the form Ag_{ij} unless the vector Δ_i vanishes.

In this section we shall consider that V is subject to the condition that

$$c^r V,_r = 0 \tag{5.2}$$

and to no other. This condition states that c^r is a vector which lies everywhere in the equipotential surfaces. We shall show that, as a result of the conditions of compatibility, the c^r must be a Euclidean motion and that the a_{ij} are given by

$$a_{ij} = A\,g_{ij} + B\,c_i c_j , \tag{5.3}$$

where A and B are constants. Since equation (5.2) is the only condition on V, if Δ_l does not vanish, it must be parallel to c_l; for, as far as equation (5.2) is concerned, c_l may be replaced by any nonvanishing vector parallel to c_l.

Suppose, then, that equation (5.2) is the only condition on V. Then from equations (4.6) and (4.7) we obtain

$$\epsilon^{pir}a^s_i + \epsilon^{pis}a^r_i = N^{ps}c^r + N^{pr}c^s , \tag{5.4}$$

$$\epsilon^{pij}a^r_{i,j} = M^p c^r + N^{ps}c^r,_s . \tag{5.5}$$

Apply lemma 1 to equation (5.4) with A^{rs} replaced by A^{prs} for each value of p, and with

$$A^{prs} = \epsilon^{pir}a^s_i + \epsilon^{pis}a^r_i . \tag{5.6}$$

From the definition of A^{prs} it follows that

$$A^{pt}_t = 0 = A^{prs}c_r c_s ,$$

so that

$$\epsilon^{pis} a_i c_s = 0 , \qquad a_i \equiv a_i^r c_r , \tag{5.7}$$

and that

$$A^{prt} c_t = \epsilon^{pit} a_i^r c_t + \epsilon^{pir} a_i . \tag{5.8}$$

This, inserted in the statement of lemma 1, yields

$$c^2 (\epsilon^{pir} a_i^s + \epsilon^{pis} a_i^r) = c^r (\epsilon^{pit} a_i^s c_t + \epsilon^{pis} a_i) + c^s (\epsilon^{pit} a_i^r c_t + \epsilon^{pir} a_i) . \tag{5.9}$$

Multiply by $\epsilon_{p'r's}$ and sum over p. This yields

$$c^2 (3 a_k^r - a_s^s \delta_k^r) = c^r (3 a_k - a_s^s c_k) + c^2 a_k^r - c^s a_s \delta_k^r . \tag{5.10}$$

Multiply by g_{jr}, sum over r, and solve for a_{jk}:

$$2 c^2 a_{jk} = (c^2 a_s^s - c^s a_s) g_{jk} - a_s^s c_j c_k + 3 c_j a_k . \tag{5.11}$$

It can be seen from this, on multiplying by c_j and summing over j, that a_k is proportional to c_k. Thus equation (5.11) reduces to

$$A_{ij} = A g_{ij} + B c_i c_j , \tag{5.12}$$

where A and B are functions of the co-ordinates. Inserting equation (5.12) in equation (5.4) yields

$$N^{ps} = B \epsilon^{pis} c_i . \tag{5.13}$$

Combining equations (5.12) and (5.13) with (5.5) shows that, since

$$a_{i,j}^r = A_{,j} \delta_i^r + B_{,j} c^r c_i + B (c^r{}_{,j} c_i + c^r c_{i,j}) , \tag{5.14}$$

it follows that

$$\begin{aligned} A_{,j} \epsilon^{prj} &= M^p c^r - B_{,j} c^r c_i \epsilon^{pij} - B \epsilon^{pij} (c^r{}_{,j} c_i + c^r c_{i,j}) + B \epsilon^{pis} c_i c^r{}_{,s} \\ &= \tilde{M}^p c^r , \end{aligned} \tag{5.15}$$

where

$$\tilde{M}^p = M^p - B_{,j} c_i \epsilon^{pij} - B \epsilon^{pij} c_{i,j} .$$

Now multiply equation (5.15) by $\epsilon_{qrs} c^s$ and sum over r:

$$c^s A_{,s} \delta_q^p - A_{,q} c^p = 0 . \tag{5.16}$$

First contract equation (5.16) with respect to p and q. Then

$$c^s A_{,s} = 0 .$$

Hence

$$A_{,q} = 0 , \qquad A = \text{Constant} . \tag{5.17}$$

The quantity B may also be chosen as a constant, by proper choice of the c^r. The c^r are important only in defining a direction in space. This direction remains unchanged if c^r is replaced by $\Lambda c^r \Lambda \neq 0$. If $B \neq 0$, Λ may be chosen equal to $1/\sqrt{B}$. The new value of B thus found is unity.

From the compatibility conditions, therefore, it has been shown that the coefficients of the velocity ellipsoid are given by

$$a_{ij} = A g_{ij} + B c_i c_j , \tag{5.18}$$

where A and B are constants, provided that the only condition on V is that given by

$$c^r V_{,r} = 0 . \tag{5.19}$$

The a_{ij} must still satisfy equation (2.12), which says that

$$a_{ij,k} + a_{ki,j} + a_{jk,i} = 0 . \tag{5.20}$$

Inserting the value of a from equation (5.18) yields

$$B [c_i (c_{j,k} + c_{k,j}) + c_j (c_{k,i} + c_{i,k}) + c_k (c_{i,j} + c_{j,i})] = 0 , \tag{5.21}$$

since, from the definition of covariant differentiation, $g_{ij,k}$ is zero. Letting $c^2\lambda_k = c^i(c_{k,i} + c_{i,k})$, equation (5.21) becomes, on multiplication by c^i,

$$B (c_{j,k} + c_{k,j} + c_j\lambda_k + c_k\lambda_j) = 0 . \tag{5.22}$$

Thus either $B = 0$ or

$$c_{j,k} + c_{k,j} = - c_j\lambda_k - c_k\lambda_j .$$

Inserting this in equation (5.21), we get

$$\lambda_i c_j c_k + \lambda_k c_i c_j + \lambda_j c_k c_i = 0 . \tag{5.23}$$

Multiply by $c^j c^k$ and sum over j and k:

$$c^4\lambda_i + 2 c^2 c^j\lambda_j c_i = 0 . \tag{5.24}$$

Multiply by c^i and sum over i:

$$c^i\lambda_i = 0 .$$

Hence, from equation (5.24),

$$\lambda_i = 0 ;$$

and then, from equation (5.22),

$$c_{j,k} + c_{k,j} = 0 . \tag{5.25}$$

Equation (5.25) shows that, unless $B = 0$, the c^r constitute a Euclidean motion and can be expressed in terms of the generators of the Euclidean group:

$$c_i = p_a\eta^a_i + q_a\xi^a_i . \tag{5.26}$$

As was noted at the beginning of this section, this result shows that c_i and Δ_i are necessarily parallel. That the Δ_i must be a motion we now see to be necessary for the consistency of the theory; for equation (2.14) must hold for all cases independently of whether there are other conditions on V and we have just seen that, if there are no other conditions, the vector Δ_i must be a motion, without recourse to equation (2.13).

If in equation (5.21) $B = 0$, then the velocity distribution is spherically symmetric and the a_{ij} satisfy equation (5.20) identically, no condition being placed on the c_i. This means simply that if the a_{ij} are given by Ag_{ij}, the compatibility equations impose no restrictions on V whatsoever, a conclusion previously noted.

From the value of a_{ij} given by equation (5.18) the expression for other quantities occurring in the theory may be obtained. From equation (2.15), which states that

$$-\tfrac{1}{2}\chi_{,i} = a_{il} V^{,l} ,$$

it follows, on integration with equation (5.18), that

$$\chi = 2 A V + \text{constant} . \tag{5.27}$$

There is an integral of the motion given by

$$J = c_i u^i , \tag{5.28}$$

since $dJ/dt = 0$. The integral of the motion I_2 given by equation (3.2) is now

$$\begin{aligned} I_2 &= a_{ij}u^i u^j - \chi \\ &= A\,(u^2 + 2\,V) + BJ^2\,. \end{aligned} \tag{5.29}$$

If $\Delta_i \not\equiv 0$, then $\Delta_i = c_i$ for a proper choice of c_i, and $J = I_1$ as given by equation (3.1).

From the definition of Δ_i the velocity of the local centroid, u_0^i, can be found to be

$$\Delta_i = c_i = a_{ij}u_0^j = (A\,g_{ij} + B\,c_i c_j)\,u_0^j\,, \tag{5.30}$$

from which

$$u_0^j = \frac{\Delta^i}{A + Bc^2}, \tag{5.31}$$

provided that $|a_{ij}| \not\equiv 0$. The motion of the local centroids is thus parallel to the direction c^i and is therefore in the equipotential surfaces.

The determinant $|a_{ij}|$ cannot vanish, for this would make the velocity distribution meaningless. At a point in space the tensor a_{ij} can be put in diagonal form by proper choice of Cartesian co-ordinates. If $|a_{ij}| = 0$, one of the diagonal elements must vanish —say, a_{33}. This means that Q is independent of u^3, and therefore so is the distribution function. But the expression for the number of stars in a volume containing this point involves the integral

$$\int_{-\infty}^{\infty} \psi\,(Q + \sigma)\,du^3\,,$$

which is not finite unless ψ vanishes. Thus the determinant $|a_{ij}|$ is different from zero.

The fact that V is invariant under a motion of the space into itself restricts V to one of two canonical forms:

(A) $$\Delta_1 = \beta y\,, \qquad \Delta_2 = -\beta x\,, \qquad \Delta_3 = k\,. \tag{5.32}$$

This means that V is invariant under a screw motion about the z-axis of a Cartesian co-ordinate system. Then

$$V = V\left(x^2 + y^2, \qquad z + \frac{k}{\beta}\tan^{-1}\frac{y}{x}\right). \tag{5.33}$$

If $k = 0$, the pitch of the screw is zero, and

$$V = V\,(x^2 + y^2,\ z)\,. \tag{5.34}$$

(B) $$\Delta_1 = 0\,, \qquad \Delta_2 = 0\,, \qquad \Delta_3 = \delta\,. \tag{5.35}$$

V is invariant under a translation in the z-direction, so that

$$V = V\,(x,\ y)\,. \tag{5.36}$$

From elementary considerations, only one of these is conceivable for a system confined to a finite volume and in a steady state. This is equation (5.34), since none of the others has closed equipotential surfaces.

REGIONS WITH VARYING MEAN MOLECULAR WEIGHT (WHITE DWARFS WITH COMPLEX STRUCTURES)*

EVRY SCHATZMAN†
Princeton University Observatory
Received May 25, 1949

ABSTRACT

The presence of metallic lines in the spectrum of certain white dwarfs seems inconsistent with the assumption of gravitational sorting of the elements in the outer, nondegenerate part of these stars. The theory of this sorting, which has been developed previously, is used to analyze this problem. For simplification, the elements other than hydrogen have been replaced by a mean element, which has been taken to be oxygen. The results indicate that, unless the metallic abundance is very high or very low, a stable equilibrium is not easily reached, since the rapid increase of the opacity with depth, due to the increase of the metallic concentration with depth, makes the radiative layer unstable against convection.

Specifically, if the density gradient is continuous at the interface between an upper convective and a lower radiative zone, it is found that, for a metallic content $1 - X$ between 0.000064 and 0.086, the radiative zone is unstable. This instability can be avoided by the introduction at the interface of a discontinuity in the density gradient, associated with a discontinuity in the gradient of molecular weight. However, the increase of opacity with depth again produces instability a short distance below the interface, resulting in another convective zone. The stratification of the star with a great number of alternatively radiative and convective zones may be possible. The number of these zones depends upon the metallic content in the Unsöld convective layer and upon the magnitude of the discontinuities in the density gradient. The value of these discontinuities seems to depend upon the history of the star.

These results do not hold if the metallic concentration $1 - X$ is so low at the surface that the critical value 0.000064 is reached in regions near degeneracy, where the density is so high that conductivity reduces the temperature gradient and produces stability.

In the case of van Maanen 2, the metallic concentration in the atmosphere is likely to exceed the upper critical value, 0.086. In this case there is only one convective zone, the Unsöld zone, which is shown to extend from the surface to the depth where the temperature is 800,000°. The central temperature is about 50×10^6 degrees, and the hydrogen concentration is about 10^{-8} at the depth where degeneracy begins. This model is compatible with the observed energy production and the presence of metallic lines in the spectrum of van Maanen 2.

I. INTRODUCTION

The apparent difficulty of reconciling the presence of strong metallic lines in van Maanen 2[1] with the theories of energy production and of gravitational sorting for that star[2] has led to the present study.

The model of white dwarfs, proposed by the author[2,3] and comprising a core of heavy elements surrounded by a pure hydrogen layer, explains the energy production of these stars on the basis of thermonuclear reactions.[2] In the particular case of van Maanen 2, the model which has been proposed has a thin hydrogen envelope at a low temperature (5,000,000°), degenerate almost everywhere; and the energy production is due to the proton-proton reaction.

The theory of gravitational sorting of the elements in an atmosphere in radiative equilibrium accounts for the assumption of a pure hydrogen layer.[4] It shows that the concen-

* A great part of this work was carried out at the Institut d'Astrophysique, Paris.

† On leave from the Institut d'Astrophysique, Paris, during 1948–49.

[1] Kuiper, *White Dwarfs* ("Actualités scientifiques et industrielles," Vol. 903 [Paris: Hermann, 1941]).

[2] *Schatzman, Ann. d'ap.*, **8**, 143, 1945.

[3] *Le Spectre des naines blanches et leur débit d'énergie* (Copenhagen [in press]); "The Spectrum of White Dwarfs," *Nature*, **161**, 61, 1948.

[4] Schatzman, *Le Triage des éléments dans une atmosphère non isotherme, C.R.*, **225**, 990, 1947.

tration of heavy elements decreases extremely quickly in regions in radiative equilibrium. For instance, in these regions of almost pure hydrogen, where the electronic gas is nondegenerate, the concentration of the positive ion of calcium, Ca^+, decreases as the temperature to the power 287.25. A slight variation in altitude in such a region produces a radical elimination of any metallic atom. This result, which explains the general absence of metallic lines in the spectrum of white drawfs,[1] appears at first sight to be quite irreconcilable with the conspicuous presence of broad metallic lines in the spectrum of van Maanen 2.[1]

This contradiction can be avoided if we suppose that convective currents transport the elements from the inside of the star toward its atmosphere.[3] It is easy to show that the weakest convective currents may be powerful enough to weaken the gravitational sorting. It is sufficient for this purpose to consider the time scale of the diffusion processes. The phenomena of diffusion over a distance ΔR reach a state of equilibrium in a time whose order of magnitude is $D^{-1}(\Delta R)^2$, where D is the diffusion coefficient. We are concerned here only with the outer parts of the star, whose geometrical dimensions are quite small; in the inner regions of the star other phenomena exhaust the hydrogen.[5] With $D = 1$,[6] $R = 3 \times 10^7$ cm, we get a time of several ten million years. It is quite clear that, whenever the speed of the streams is low, any phenomenon of convection would be more active than the gravitational field, unless we consider layers of only a few centimeters in thickness.

Consequently, wherever the source of energy production may be, we must in any case analyze the conditions under which convective zones will exist in white dwarfs. As a necessary first step, Section II gives the formulae for the gradients of temperature and of mean molecular weight as functions of the chemical composition. Section III is essentially devoted to the study of the convective zones. It is shown that, for a certain range of the metallic concentration, the density gradient must be discontinuous at the interface between an upper convective zone and a lower radiative zone in order to provide stability in the underlying radiative layer. In that range of concentration in metallic elements, a stratification of the star with a great number of alternatively convective and radiative zones may be possible. Section IV applies these results to van Maanen 2. A new atmosphere model has been calculated to determine the precise position of the bottom of the convective zone. A brief study is made of the energy production of that star. The new structure is compatible with the observed energy production and with the presence of metallic lines in the spectrum of that star. Section V summarizes the results.

II. THE SORTING IN RADIATIVE EQUILIBRIUM

1. *Relations deduced from the sorting.*—We shall assume that only two elements are present, in order to use analytical expressions and to avoid extensive numerical calculations. These two elements are hydrogen and a typical mean element, viz., oxygen. Under these conditions, the rigorous formulation given in a previous publication[3] for the sorting becomes much simpler, and a parametric representation can be obtained.

We shall always suppose that oxygen is completely ionized, without, however, making that assumption for the absorption coefficient (§2 of this section). The numbers of hydrogen nuclei, oxygen nuclei, and electrons are given by:

$$H n_H = \rho_i X_i \frac{T_i}{T} UV , \tag{1}$$

[5] Schatzman, "Reactions thermonucléaires aux grandes densités," *J. de phys. et le radium*, sér. VIII, 9, 46, 1948.

[6] This value has been obtained by a rough estimate of the cross-sections for a 90° deflection, supposed to occur when the potential energy at the distance of approach equals the mean kinetic energy.

$$AHn_A = \rho_i (1 - X_i) \frac{T_i}{T} U^A V^Z , \tag{2}$$

$$Hn_e = \rho_i \frac{1 + X_i}{2} \frac{T_i}{T} V^{-1} , \tag{3}$$

respectively, where U represents the influence of the gravitational field and V the influence of the electrostatic field. We have

$$U = \exp\left\{ - \int_{z_i}^{z} \frac{H g d z}{kT} \right\} , \tag{4}$$

where ρ_i, X_i, and T_i, at the altitude z_i, are the initial values of the density, the hydrogen concentration, and the temperature, respectively, and V is defined by the condition of electrical neutrality:

$$\rho_i X_i \frac{T_i}{T} UV + \frac{Z}{A} \rho_i (1 - X_i) \frac{T_i}{T} U^A V^Z = \rho_i \frac{1 + X_i}{2} \frac{T_i}{T} V^{-1} , \tag{5}$$

or

$$X_i UV + \frac{Z}{A} (1 - X_i) U^A V^Z = \frac{1 + X_i}{2} V^{-1} .$$

For $Z = Z_i$, $U = 1$, and, as $Z/A = \frac{1}{2}$, we also have $V = 1$. Hence we set

$$UV = y , \tag{6}$$

$$U^A V^{Z+1} = t ; \tag{7}$$

and equation (5) yields

$$X_i y + \tfrac{1}{2} (1 - X_i) t V^{-1} = \frac{1 + X_i}{2} V^{-1} . \tag{8}$$

If equations (6) and (7) are used to express V in terms of y and t, the equation finally becomes

$$y^{1 + [A/(Z-1)]} = t^{1/(Z-1)} \frac{(1 + X_i) - (1 - X_i) t}{2X_i} . \tag{9}$$

In terms of y and t, we have

$$n_H = \frac{\rho_i X_i}{H} \frac{T_i}{T} y , \tag{10}$$

$$n_A = \frac{\rho_i (1 - X_i)}{AH} \frac{T_i}{T} t^{Z/(Z-1)} y^{-A/(Z-1)} , \tag{11}$$

$$n_e = \frac{\rho_i (1 + X_i)}{2H} \frac{T_i}{T} t^{1/(Z-1)} y^{-A/(Z-1)} . \tag{12}$$

2. *The absorption coefficient.*—We now investigate, in our parametric representation, the temperature $T(t)$ and the geometric height $z(t)$ in the regions where the gravitational equilibrium is stable. For this purpose we combine the equation of transfer,

$$\frac{d}{dr}(\tfrac{1}{3}aT^4) = -\frac{\kappa\rho L}{4\pi r^2 c}, \tag{13}$$

with equations (10), (11), and (12).

The advantages of using analytical formulae have induced us to use Kramer's law for the absorption coefficient:

$$\kappa = \kappa_0 \rho T^{-3.5}. \tag{14}$$

This means, of course, that we are neglecting the "guillotine factor," even though its importance could be nonnegligible. The theory of Strömgren[7] gives[8] a value $\kappa_0 = 3.9 \times 10^{25}$ for pure Russell mixture. This value neglects completely the absorption due to the free-free transitions of the electrons in the field of the hydrogen nucleus. In addition, for the densities under consideration this absorption is greater than the scattering by the free electrons, and its value for pure hydrogen is also given by Kramer's law with $\kappa_0 = 7.41 \times 10^{22}$.[8] The total absorption, including the absorption by the free-free transition, can be written:

$$\kappa = [aX + b(1 - X)](1 + X)\rho T^{-3.5}, \tag{15}$$

where

$$\frac{b}{a} = 1000 \tag{16}$$

and

$$a = 3.7 \times 10^{22}. \tag{17}$$

These formulae mean that it is permissible to neglect the absorption due to hydrogen only if the concentration of heavy elements is much greater than one-thousandth. It is quite obvious that the use of these analytical formulae, though physically approximate, nevertheless does make it possible to determine the main features of the complex structures which we intend to study.

3. μ *gradient.*—By means of formulae (10), (11), and (12) we can calculate the quantity

$$\nabla\mu = \frac{d \log \mu}{d \log P}. \tag{18}$$

We remark immediately that, since the pressure is

$$P = (n_H + n_e + n_A)\, kT \tag{19}$$

and the mean molecular weight is

$$\mu = \frac{n_H + A n_A}{n_H + n_A + n_e}, \tag{20}$$

the quantity $\nabla\mu$ does not depend on temperature, as the temperature can be eliminated in equations (19) and (20) (n_i is inversely proportional to T) and consequently depends only on *the local chemical composition.* As this result is quite independent of the number of elements sorted by the gravitational field, $\nabla\mu$ could also be calculated as a function of X alone by adding helium to the mixture.

[7] *Zs. f. Ap.*, **4**, 118, 1932.

[8] Chandrasekhar, *An Introduction to the Study of Stellar Structure* (Chicago: University of Chicago Press, 1939), chap. vii.

By calculating $(d \log P)/dt$ and $(d \log \mu)/dt$ in the neighborhood of $t = 1$, viz., of $X = X_i$, we obtain $\nabla\mu$ directly as a function of X_i. We can also drop the subscript i. We have:

$$\left(\frac{d \log P}{dt}\right)_{t=1} = \frac{\frac{1}{Z-1} + \frac{Z-1}{Z-1+A}\left(\frac{1}{Z-1} - \frac{1-X}{2X}\right)\left(X - \frac{1-X}{Z-1} - \frac{1+X}{Z-1}\frac{A}{2}\right)}{X + \frac{1-X}{A} + \frac{1+X}{2}}, \tag{21}$$

$$\left(\frac{d \log \mu}{dt}\right)_{t=1} = \frac{(Z-1)X}{Z-1+A}\left(\frac{1}{Z-1} - \frac{1-X}{2X}\right) + (1-X) \times \left(\frac{Z}{Z-1} - \frac{A}{A+Z-1}\left[\frac{1}{Z-1} - \frac{1-X}{2X}\right]\right) - \frac{d \log P}{dt}. \tag{22}$$

After simplifications and taking $Z = 8$ and $A = 16$, we get

$$\nabla\mu = \frac{d \log \mu}{d \log P} = \frac{529}{16}\frac{X(1-X^2)}{9-5X}. \tag{23}$$

This quantity has been tabulated (Table 1). We also have

$$d \log P = -\frac{16}{23}\frac{9-5X}{X(1-X^2)}\frac{dX}{9+23X}. \tag{24}$$

TABLE 1

X	$(\nabla\mu)_{grav}$	X	$(\nabla\mu)_{grav}$
0	0	0.6	2.11600
0.1	0.38508	0.7	2.14605
0.2	0.79350	0.8	1.90440
0.3	1.20348	0.9	1.256375
0.4	1.58700	0.99	0.14470
0.5	1.90744	1	0

When X is near 1 (low concentration in heavy elements), we can integrate equation (24). If we let the starting value of X be X_0, then we find, to the first order in $1 - X$,

$$P = P_0\left(\frac{1-X}{1-X_0}\right)^{1/23} \exp\frac{111}{23.32}(X_0 - X). \tag{25}$$

This simplified relation is certainly valid up to $1 - X \cong 0.1$, for instance.

In the same way it is possible to integrate the equation of transfer (13) for small values of $(1 - X)$. According to equation (13), we have

$$\frac{\nabla T}{(\nabla T)_0} = \frac{\mu}{\mu_0}\frac{P^2}{P_0^2}\frac{T_0^{8.5}}{T^{8.5}}\frac{1+X}{1+X_0}\frac{aX + b(1-X)}{aX_0 + b(1-X_0)}. \tag{26}$$

According to equation (25) and taking into account equation (24), we now find

$$\frac{T^{7.5}dT}{T_0^{8.5}} = (\nabla T)_0\frac{\mu}{\mu_0}\frac{1+X}{1+X_0}\frac{aX + b(1-X)}{aX_0 + b(1-X_0)}\left(\frac{1-X}{1-X_0}\right)^{2/23} \times \frac{1}{23}\left(\frac{1}{1-X} + \frac{111}{32}\right)\exp\left[\frac{111}{23.64}(X_0 - X)\right]d(1-X). \tag{27}$$

After integration, we obtain ∇T as a function of ∇T_0, $(1 - X)$, and $(1 - X_0)$:

$$\frac{\nabla T}{\nabla T_0} = \frac{[aX + b(1-X)](1-X)^{2/23}\left[1 - \frac{383}{736}\{(1-X_0)-(1-X)\}\right]}{(1-X_0)^{2/23}[aX_0 + b(1-X_0)] + 4.25\nabla T_0\left[1 - \frac{383}{736}(1-X_0)\right]\mathfrak{X}}, \tag{28}$$

with

$$\mathfrak{X} = (1-X)^{2/23}\{a + 0.08079b(1-X)\} - (1-X_0)^{2/23}\{a + 0.08079b(1-X_0)\}.$$

III. THE CONVECTIVE LAYERS

1. *The hydrogen convective zone.*—To obtain a model of white dwarfs in which the metallic elements can appear in the spectrum, we must try to find the thickness of the convective zones. We begin with a study of the so-called "Unsöld layer," or hydrogen convective zone. The depths of both the top and the bottom of this convective layer are dependent on the amount of energy supposed to be transported by convection or, more precisely, on the differences between the actual temperature gradient and the adiabatic gradient. This convection layer has its smallest extension if the gradient is the radiative one (no energy being transported by convection). If the gradient is adiabatic, the top of the layer rises, and its bottom sinks considerably and reaches regions of high temperature (10^6 degrees or more).[9]

Use of the table given by Strömgren,[10] the relation of Prandtl for the energy transport in the convective zone, and the relation of Siedentopf[11] for the speed of turbulent elements makes it possible to estimate how far the actual gradient in the convective zone departs from the adiabatic gradient. It does not seem that this discrepancy differs very much from that in the sun. The study of Biermann[12] shows that the gradient becomes adiabatic very rapidly. The recent paper of De Jäger[13] confirms this point of view. In such conditions it seems that the simplest assumption, and the nearest to reality, is to suppose that the temperature gradient ∇T is adiabatic in the whole convective region.

2. *The lower limit of the convective zones.*—Certain conditions must be satisfied at the lower limit of any convective zone. As we suppose the diffusion very strong, we shall limit ourselves to models in which the chemical composition has no discontinuity. Consequently, the values of the density on both sides of the interface between a convective and a radiative zone satisfy the relation

$$(\rho)_{ad} = (\rho)_{rad}. \tag{29}$$

As we suppose that the adiabatic relation holds in the convective zone, we have

$$\nabla\rho_{ad} = \left(\frac{d\log\rho}{d\log P}\right)_{ad} = 0.6. \tag{30}[14]$$

The convective zone can stop only if in the underlying radiative zone we have

$$\nabla\rho = 1 + \nabla\mu - \nabla T \gtrsim 0.6, \tag{31}$$

[9] Rudkjøbing, *Zs. f. Ap.*, **21**, 254, 1942.

[10] "Tables of Model Stellar Atmospheres," *Pub. Copenhagen Obs.*, **138**, 35.

[11] *A.N.*, **247**, 297, 1932. [12] *Zs. f. Ap.*, **21**, 320, 1942.

[13] *Proc. Amsterdam Akad.*, **51**, 731, 1948.

[14] We write $\nabla = (d\log)/(d\log P)$. This notation is to be used through the whole paper.

where we have used the perfect gas law. The stability condition must be expressed in terms of density, because in the radiative zone the chemical composition of the matter surrounding an element in adiabatic movement is variable.

Therefore, $\nabla\rho$ can jump from 0.6 in the convective zone to any value between 0.6 and $0.6 + (\nabla\mu)_{grav}$ in the radiative zone. This range of possibilities, which does not appear in the usual case, where μ is assumed constant with depth, is illustrated in Figure 1, where A and B represent the upper and lower limits of the bottom of the convective layer.

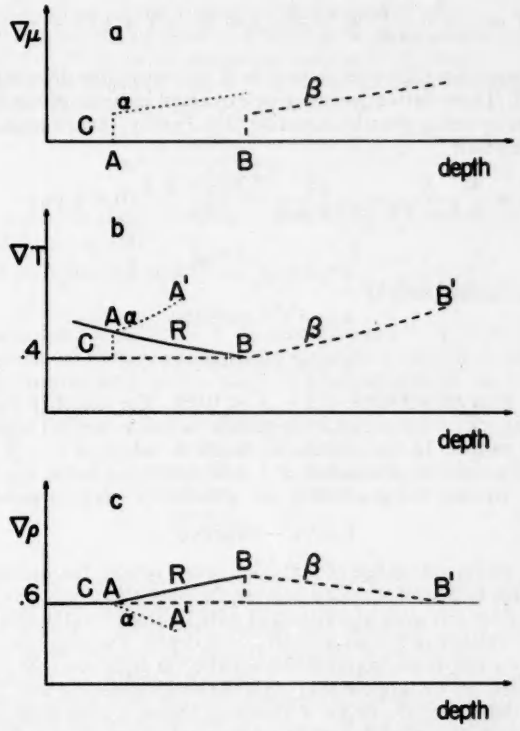

FIG. 1.—The logarithmic gradients of molecular weight, temperature and density, $d \log \mu/d \log P$, $d \log T/d \log P$, $d \log \rho/d \log P$, have been represented as functions of depth in the two extreme cases, A, ∇T discontinuous, and B, $\nabla\rho$ discontinuous. The line R on figures b and c represents the radiative gradients in the convective zone. The line C represents the actual gradients in the convective zone equal to 0, 0.4, and 0.6 for the mean molecular weight, the temperature, and the density, respectively.

The curves α and β represent for $1 - X > 0.000064$ the actual gradients in the two extreme cases A and B. The line AA' shows that $\nabla\rho$ becomes smaller than 0.6, with resulting instability immediately below the boundary of the layer, while curve BB' gives instability only at greater depth.

We shall show, first, that for a certain composition range there has to be a jump in density gradient because the hypothesis of continuity in the density gradient leads to an unstable radiative layer and, hence, to a contradiction.

Therefore, we consider what happens if the equality in equation (31) is satisfied. This equality gives

$$\nabla T = 0.4 + \nabla\mu\,, \tag{32}$$

where $\nabla\mu$ is given by equation (23). We now examine under what conditions the radiative zone remains stable with increasing depth below the convective layer. This condition is

$$\frac{d\Delta\rho}{d(1-X)} \geqslant 0 . \tag{33}$$

To evaluate $\nabla\rho$, we must know $\nabla\mu$ and ∇T. The former quantity is given in equation (23), while the latter may be found from equations (13) and (15), combined with the equation of hydrostatic equilibrium, to yield

$$\nabla T = \frac{3}{16\pi a c G}\frac{L}{M}\,\Re\,\frac{\rho^2}{\mu}\frac{1}{T^{6.5}}(1+X)\,(aX + b\,[1-X]\,) . \tag{34}$$

To differentiate equation (32) with respect to X, we must also differentiate ρ, μ, and T with respect to X. These derivatives may be expressed in terms of $\nabla\rho$, $\nabla\mu$, ∇T, and dP/dX, this last quantity being given by equation (24). Finally, then, inequality (33) gives, at the interface, the result

$$\left(\frac{1}{X}+\frac{5}{9.5\,X}\right)\nabla\mu + \frac{4}{5}\frac{X}{1-X^2} - \frac{23}{23X+9}\,\frac{7.5\nabla\mu+1.4}{\nabla\mu}\,(0.4+\nabla\mu) + \nabla\mu\left(\frac{b-a}{b-[b-a]\,X} - \frac{1}{1-X}\right) \geqslant 0 . \tag{35}$$

This condition is fulfilled only if

$$1 - X \leqslant 0.000064 \tag{36}$$

or if

$$1 - X \geqslant 0.086 . \tag{37}$$

We examine the interval $0.000064 < 1 - X < 0.086$. The quantity ∇T increases when $(1 - X)$ increases, viz., when we go from outside to inside, we find regions of increasing mean molecular weight. In the considered range of values of $1 - X$, the increase of $aX + b(1 - X)$ exceeds the decrease of $\rho^2(1+X)/\mu T^{6.5}$ just below the boundary of the convective zone, so that the gradient is not sufficiently steep to satisfy the condition

$$1 + \nabla\mu - \nabla T \geqslant 0.6 . \tag{38}$$

In other words, within this range of metallic concentration, the radiative temperature gradient is too high to permit stability because the opacity increases very abruptly with depth, changing from the weak absorption of pure hydrogen to the strong absorption of metals, as the abundance of metals increases with depth. The simplest method of avoiding this difficulty consists in dropping the equality in equation (38), keeping only the inequality. If, however, we suppose that $\nabla\rho$ is not continuous and that the bottom of the convective layer lies below the depth A shown in Figure 1, then there is no difficulty in fitting a zone in radiative equilibrium to a convective zone.

These conclusions are illustrated by the curves drawn in Figure 1. In the convective zone $\nabla\rho$ equals 0.6, and the convective currents maintain μ constant. Within the convective zone the density varies proportionally to the power $\frac{3}{2}$ of the temperature, and it follows from formula (34) that $(\nabla T)_{\text{rad}}$ decreases in this region (Fig. 1, b, curve R). As $(\nabla\mu)_{\text{grav}}$ depends only upon the chemical composition, which is the same at the top and at the bottom of the convective zone, the quantity

$$(\nabla\rho)_{\text{grav}} = 1 + (\nabla\mu)_{\text{grav}} - (\nabla T)_{\text{rad}} \tag{39}$$

increases throughout the convective zone. The convective zone can stop at any point where $(\nabla\rho)_{\text{grav}} > 0.6$ (Fig. 1, between A and B). That means that, at the interface between the convective and the radiative zones, the gradient $\nabla\rho$ jumps from 0.6 to some value between 0.6 and $0.6 + (\nabla\mu)_{\text{grav}}$. It is easily seen that the bigger the jump, the

thicker the convective zone. The assumption of continuity in $\nabla\rho$ would lead us to a vanishing thickness of the convective zone and consequently would compel us to introduce an unstable region of the kind mentioned above in this paragraph. Consequently, we are led to admit the existence of discontinuities in the gradient $\nabla\rho$.

3. *Study of the radiative zones.*—First, we consider the situation in which $\nabla\rho$ is continuous at the top of a radiative zone. We have already said that, in the case where $\nabla\rho$ is continuous and where $0.000064 < 1 - X < 0.086$, we cannot fit the convective layer of Unsöld to any layer in radiative equilibrium.

We have not studied what happens if $1 - X > 0.086$, since the other cases suggest that then we would remain in the region of radiative equilibrium.

If $1 - X_0 \leqslant 0.000064$, the increase of X may again give rise to instability. We compute the value of $1 - X$ at which convection reappears; we shall denote this critical value by $1 - X_1$. In the neighborhood of $1 - X_0 = 0.000064$ we come back to a convective zone for $1 - X_1 = (1 + \epsilon)(1 - X_0)$, in which

$$\epsilon = \frac{0.000064 - (1 - X_0)}{3.867 \times 10^{-5}}. \tag{40}$$

When $1 - X_0$ is much less than 0.000064, we come back to a convective zone for a value of $1 - X_1$ given by

$$1 - X_1 = 0.000735 - 0.000767\left(\frac{1 - X_0}{0.000735}\right)^{2/3}. \tag{41}$$

In Figure 2 the functional form of $1 - X_1$ as a function of $1 - X_0$ is shown. A convective zone may be represented by any point on the diagonal; a radiative zone is represented by a vertical line starting from such a point and terminating at the curve. It is easily

TABLE 2

$1-X_0$	$1-X_1$	$1-X_0$	$1-X_1$
0.0001	0.000108	0.0020	0.00238
.0002	.000212	.005	.0970
.0005	.000537	0.01	0.03
0.0010	0.001108		

seen from Figure 2 that in this case there is no possibility of finding any other return to a radiative layer, because the convective layer ends for a value of $(1 - X)$ inside the range $0.000064 < 1 - X < 0.086$, and within this range of $1 - X$ there is no stable radiative solution, provided that the density gradient is continuous.

Second, we consider the other extreme case, in which ∇T is continuous at the top of a radiative zone. This other case has the greatest discontinuity in $\nabla\rho$, that is to say, $\nabla\rho_{\text{grav}} = 0.6 + \nabla\mu$. At the interface, $\nabla T_{\text{rad}} = \nabla T_{\text{ad}} = 0.4$ (Fig. 1, point A), the smallest value that the radiative temperature gradient can have in the convective zone. A smaller value would mean a radiative flux greater than the total flux, which is impossible. Of course, the actual gradient must exceed the adiabatic gradient, but by only a slight margin. Starting with a metallic content $1 - X_0$ at the top of a radiative zone and a density gradient $\nabla\rho = 0.6 + \nabla\mu$, the gradient decreases with depth until it reaches the value 0.6. Then a new convective layer begins, and the value of the metallic content $1 - X_1$ at this point is given by Table 2. When $1 - X_1$ can be taken equal to $(1 - X_0)(1 + \epsilon)$, an analytical formula can be given:

$$\epsilon = \frac{\frac{529}{32}(1 - X_0)}{400(1 - X_0) - \frac{0.56}{23}}. \tag{42}$$

When $1 - X_0$ is extremely small, expression (41) can also be used. Log $(1 - X_1)$ has been plotted as a function of log $1 - X_0$ in Figure 3. Starting from a point X equal to X_0 on the diagonal of the figure, the vertical line log $(1 - X_0)$ to log $(1 - X_1)$ represents a radiative zone. A new convective zone then begins, represented by a point on the diagonal with X_0 equal to X_1. Below this we have a new radiative zone, etc. By drawing stairs in between the curve $\log (1 - X) = f[\log (1 - X_0)]$ and the diagonal of the figure, it is easily seen in Figure 3 that between $(1 - X) \cong 7 \times 10^{-5}$ and $1 - X \cong 0.03$ it is possible to find about sixty alternating convective and radiative layers and that this number may be greater, since the number of layers increases if the discontinuities in $\nabla\rho$ are smaller. In that case we are very near the case studied by Ledoux.[15] In fact, he has introduced a region with $\nabla T = 0.4$, which region is certainly stable. In the case studied here, in which the gradient $\nabla\mu$ can easily be calculated (a quantity which, in the general case of diffusion, is difficult to determine), it is easily seen that the region in which ∇T has a tendency to increase is populated with a number of layers alternately radiative and convective. It must be remarked, as a major feature, that these convective layers cannot increase in size unless $\nabla\rho_{\text{rad}}$ at their lower boundaries sinks below 0.6. It must be noticed that it is not excluded that all these thin layers might be mixed up by slow convective currents, producing a slightly unstable radiative zone with a constant mean molecular weight, that slight instability providing a continuous mixing. The bottom of such an unstable zone would be in the neighborhood of the degenerate region where, as mentioned below, the conductive transfer might overcome the radiative transfer.

4. *Effects of degeneracy.*—So far we have mentioned the case in which $(1 - X)$ increases in a nondegenerate region. If $(1 - X)$ increases in the neighborhood of a degenerate region, all these results are completely changed. In fact, in the neighborhood of the region in which the degeneracy becomes appreciable, the thermal conductivity very quickly becomes the most important feature. If the increase in ∇T produced by the increase of the concentration of heavy elements is balanced by a sufficient increase of the conductivity, then the model of white dwarfs that we have used until now is still valid.[2,3] In particular, it seems likely that the results already given for 40 Eri B[16] remain valid, as well as the conclusions connected with the proton-proton reaction.

IV. ENERGY PRODUCTION

1. *An atmosphere model for van Maanen* 2.—We do not want to make extensive calculations on the question of energy production. Approximate relations will be sufficient for the purpose that we have in mind. Nevertheless, as the depth of the hydrogen convective zone depends very sensitively upon the physical conditions at its top, it has been necessary to calculate a new atmosphere model for van Maanen 2.

The article of Rudkjøbing[17] shows that, if we wish to express the constancy of flux in that region of the atmosphere that is in radiative equilibrium, we are led to change the relation between the "ergiebigkeit" and the optical depth. By limiting himself to the linear approximation, he writes

$$T^4 = T_0^4 (1 + k\tau) , \tag{43}$$

and, in the case of the sun, he finds that $k = 2.6$ gives nearly the constancy of flux in the region of radiative equilibrium.

For this calculation, it is necessary to know the adiabatic relation between pressure and temperature in the zone of ionization of hydrogen. As Unsöld has mentioned,[18] the

[15] *Ap. J.*, **105**, 305, 1947.

[16] Schatzman, *Ap. J.*, **107**, 110, 1948. A small numerical error in that note is without any influence on the final result.

[17] *Ann. d'ap.*, **9**, 7, 1946.

[18] *Physik der Sternatmosphären* (Berlin: Julius Springer, 1938), par. 93.

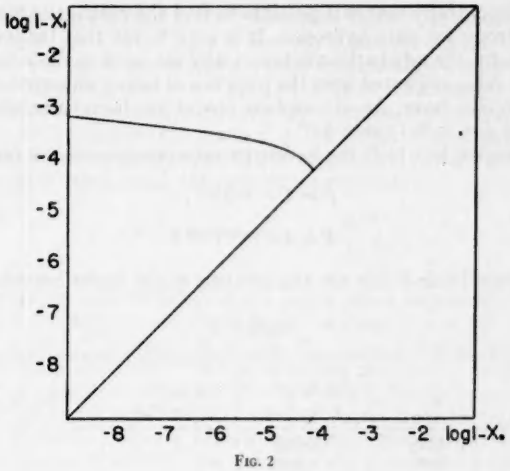

FIG. 2

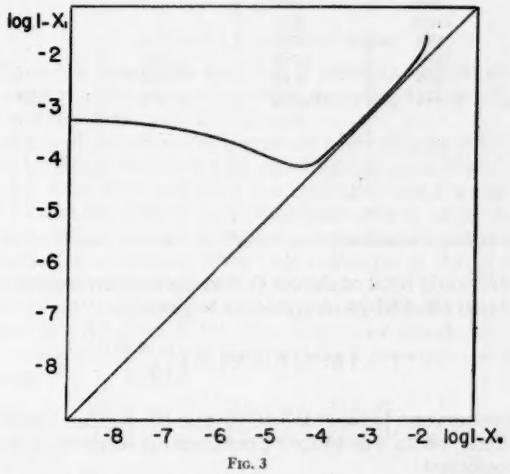

FIG. 3

FIGS. 2 and 3.—X_0 being the hydrogen concentration of a radiative zone, X_1 is the hydrogen concentration at the bottom of the radiative zone.

In Fig. 2 the top of the radiative zone is defined by the condition of continuity of $\nabla\rho$ at the interface of a convective zone above it. In Fig. 3 the top of the radiative zone is defined by the condition of the greatest possible discontinuity of $\nabla\rho$ at the interface of a convective zone above it.

A point $1 - X_0$, $1 - X_0$ on the diagonal of the figures is representative of a convective zone. A straight line going up from the diagonal to the point $1 - X_0$, $1 - X_1$ on the curve represents a radiative zone. The point $1 - X_1$, $1 - X_1$ on the diagonal represents the convective zone underlying the radiative zone. Stairs drawn between the diagonal and the curve would represent the successive radiative and convective zones.

In the case represented in Fig. 2 no stable layer can exist below a radiative zone. In the case represented in Fig. 3 a great number of alternately radiatively and convectively stable zones can exist.

computation of the entropy makes it possible to find the adiabatics easily. We have recomputed the entropy for pure hydrogen. It is easy to see that for low concentrations of the heavy elements the adiabatics are practically the same as those for pure hydrogen. Consequently, we have neglected here the presence of heavy elements in the determination of this convective layer. An atmosphere model has been calculated for $k = 2$ and with $\theta_0 = 0.5$, $\log g = 9.38$ (Table 3).[19]

Far from the region in which the hydrogen becomes ionized, we have, for this star,

$$P = 10^{-1.3} T^{5/2}, \tag{44}$$

$$P = 10^{-9.52} T^{3/2}. \tag{45}$$

It is evident from Table 3 that the temperature at the upper boundary of the Unsöld

TABLE 3

$\log P$	θ	$(d \log T / d \log P)_{\text{rad}}$	$(d \log T / d \log P)_{\text{ad}}$	$\log P_e$	τ
5	0.4995	0.001			0.001
5.2	.499	.003			0.002
5.4	.498	.005			0.004
5.6	.4965	.009			0.008
5.8	.4935	.015			0.015
6	.488	.029			0.030
6.2	.479	.059	0.085		0.063
6.4	.463	.119	.163		0.148
6.53	0.444	0.194	0.194	5.08	0.265
6.63					0.449
6.73					0.757
6.83					1.116
6.93					1.927
7.03					3.133
7.13					5.002

layer is 11,300°. The lower limit of the convective zone is determined by the value of the gradient ΔT_0 at the limit, and its temperature is given by

$$T = 10^{6.23} (1 - X)^{2/7} \left(\frac{0.4}{\nabla T_0} \right)^{2/7}, \tag{46}$$

that is to say, a temperature between 0.5×10^6 and 10^6 degrees. One of the consequences of this result is that, within this range of temperature, Kramer's law may be used for the absorption coefficient.

2. *The energy production.*—We need the temperature and the hydrogen concentration in the degenerate case in order to calculate the energy production.

The solution of equations (11), (12), (13), and (14) when the parameter t is very small (X very small) gives the approximate relation

$$\frac{T'}{T} = \left(\frac{X'}{X} \right)^{-0.1636}. \tag{47}$$

[19] It has been verified that, with this choice of k, the radiative flux is almost constant in the outer radiative part of the atmospheric model calculated. Dr. Strömgren has been kind enough to communicate to me in advance of publication tables which facilitate considerably the calculation of the flux by numerical methods.

In the atmosphere of van Maanen 2, $(1 - X)$ seems likely to be somewhat greater than 0.086.[20] Consequently, the Unsöld layer is the only convective zone. Under the convective layer the presence of regions where μ varies considerably without producing large changes in ρ shifts materially the curve $\rho(T)$ (Fig. 4) in the direction of high temperatures. Along that curve the hydrogen concentration decreases very quickly according to relation (47). The temperatures thus reached in the region of degeneracy are quite sufficient to yield a large energy production by the reactions of carbon with remaining protons. The energy production inside the degenerate region is

$$L^* = 10^{24.6} T^{1/3} \rho^2 e^{-\tau} X \frac{R^{*4}}{M^*}, \tag{48}$$

where X is the hydrogen concentration at the depth where degeneracy appears. A temperature $T = 50 \times 10^6$ degrees, corresponding to a density $\rho = 10^{4.2}$, must involve a concentration $X = 10^{-7.84}$ in order to obtain the correct energy production of van Maanen 2. This concentration $10^{-7.84}$ is reached along the curve $\rho \sim T^{3.25}$ during an increase of the temperature from 4,000,000° to 50,000,000°, this increase corresponding to the variation of T given by equation (47) when X varies from 10^{-1} to $10^{-7.84}$. Thus it seems possible to reconcile the very high temperatures involved in our new model of white dwarfs with the condition that the energy production in the degenerate region be no greater than the observed value.

V. SUMMARY AND CONCLUSION

The presence of metallic lines in the spectrum of certain white dwarfs (van Maanen 2) can be explained only by convection currents transporting the metallic elements from the inner part toward the surface of white dwarfs.

To carry out a study of the convective zones of white dwarfs, it is first necessary to undertake an investigation of radiative and gravitational equilibrium in nondegenerate regions. Formulae are given for the sorting in a nonisothermal atmosphere, and expressions are obtained for the gradient of mean molecular weight $(d \log \mu / d \log P)_{\text{grav}}$ and of the gradient of temperature $(d \log T / d \log P)_{\text{grav}}$ for a mixture of two elements (hydrogen and a mean element, that element being taken identical in charge and mass to oxygen) as a function of the hydrogen content X (Sec. II).

The study of the convective zones is based on the hypothesis that the adiabatic relation between pressure and density holds in the convective zones. It is also supposed that there is continuity in composition at the interface of a convective and a radiative zone. If the density gradient,

$$\frac{d \log \rho}{d \log P} = 1 + \frac{d \log \mu}{d \log P} - \frac{d \log T}{d \log P},$$

is also continuous at the interface for a metallic content $0.000064 < 1 - X < 0.086$, *no radiative zone can exist*. For that range of metallic concentration the radiative temperature gradient remains above the value $0.4 + (d \log \mu)/(d \log P)_{\text{grav}}$ because the opacity increases very abruptly with depth from the weak absorption by pure hydrogen to the strong absorption by metals as the abundance of metals increases. Thus the density gradient remains smaller than 0.6, which is contradictory to the assumption of a radiative zone. Thus a discontinuity in the density gradient at the interface is the only alternative. It is shown that the value of that discontinuity in density gradient very likely depends upon the whole history of the star.

[20] Schatzman. Unpublished preliminary study of the metallic content in the atmosphere of white dwarfs indicates that order of magnitude for the metallic content in the atmosphere of van Maanen 2.

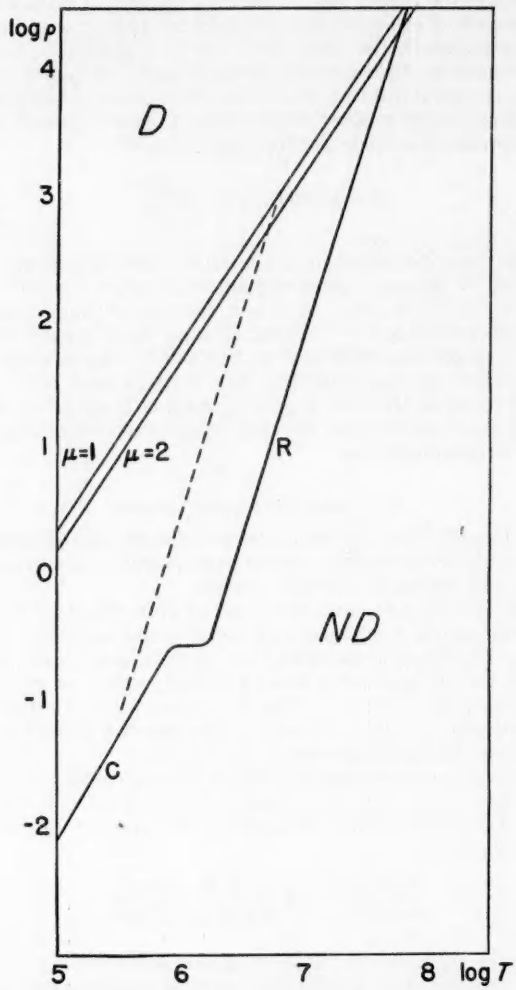

FIG. 4.—The log T, log ρ diagram for the outer layers of a white dwarf. The straight lines, $\mu_e = 1$ and $\mu_e = 2$, are the lines of apparition of degeneracy for pure hydrogen and for heavy elements. The degenerate states are indicated by D, the nondegenerate states by N and D. The representative lines are drawn for van Maanen 2. The straight line C represents the lower region of the hydrogen convective zone. The curve R represents the radiative zone of increasing mean molecular weight. S is the representative point of the surface of apparition of degeneracy. The interrupted line corresponds to the assumption of a radiatively stable envelope of pure hydrogen.

Study of the radiative zones shows that, for a metallic content $0 < 1 - X < 0.06$, these zones are of a finite thickness. They alternate with convective zones, and the number of alternately convective and radiative zones might be high.

It is possible that the convective currents might be strong enough to mix up this region of instability but not strong enough to carry energy. Thus a radiative zone with a constant chemical composition might exist, starting at the bottom of the hydrogen convective zone and ending in the region of high thermal conductivity near degeneracy, where the density becomes so high that the conductivity overcomes the opacity and forces radiative and gravitational equilibrium.

In the case of van Maanen 2 the metallic concentration in the atmosphere is very likely greater than 0.06. The structure is relatively simple. The Unsöld convective zone is shown to extend to 800,000°. The central temperature is about 50.10^6 degrees, and the hydrogen concentration is about 10^{-8} at the depth where degeneracy sets in. This model is compatible with the observed energy production and the presence of metallic lines in the spectrum of van Maanen 2.

I wish to thank Dr. Strömgren for very valuable discussions on white dwarfs, Dr. Schwarzschild for his very suggestive remarks on the regions of varying mean molecular weight, and Dr. Spitzer for his comments on diffusion processes in white dwarfs.

THE RADIATIVE EQUILIBRIUM OF A SPHERICAL PLANETARY NEBULA

HARI K. SEN
Harvard College Observatory
Received February 7, 1949

ABSTRACT

The effect of curvature of the layers of a spherical planetary nebula on the fields of ultraviolet as well as Lyman-α radiation has been investigated by the spherical harmonic method. Allowing for the dilution of the radition in the extended nebular shell, it has been found that the curvature of the nebula effects an increase in the ultraviolet flux (by a factor of the order of 2) and a corresponding decrease in the L_α flux, as compared to the plane case. The field of L_α radiation in a nebula expanding with a uniform velocity large compared with the mean velocity of molecular motion has also been investigated. The effect of curvature is not manifest in the outer parts of the nebula. But the flux decreases much more rapidly toward the interior in the plane nebula, so that the inner parts which suffer inward radiative accelerations are much more extensive in the plane than in the spherical nebula.

Chandrasekhar[1] has given an exhaustive mathematical discussion of the extension of Milne's treatment[2] of the radiative equilibrium of a planetary nebula to that required by the Zanstra-Ambarzumian theory. Both Ambarzumian[3] and Chandrasekhar, however, following Milne, have restricted themselves to the plane problem, taking account of the curvature of the shell only in the application of the Milne boundary condition.[2] The object of the present paper is to inquire what effect (if any) will be introduced by the curvature of an extended nebular shell. Spherical symmetry has been assumed, for simplicity of treatment.

I. THE FIELD OF ULTRAVIOLET RADIATION

The equation of transfer for a spherical planetary nebula consistent with Zanstra's theory is

$$\mu \frac{\partial I}{\partial r} + \frac{1-\mu^2}{r} \frac{\partial I}{\partial \mu} = -k\rho \left[I - \tfrac{1}{2} p \int_{-1}^{1} I \, d\mu - \tfrac{1}{4} pS \frac{r_1^2}{r^2} e^{-(\tau_1 - \tau)} \right], \tag{1}$$

where p is a constant factor less than unity, τ_1 is the radial optical thickness of the nebula for ultraviolet radiation (beyond the head of the Lyman series), and πS is the amount of ultraviolet radiant energy incident on each square centimeter of the inner surface (radius $= r_1$) of the nebula.

We shall use the Milne[2] boundary conditions. There is no incident radiation on the outer boundary ($\tau = 0$), and the "diffuse" flux across the inner surface vanishes. (2)

We shall employ the spherical harmonic method[4] to the solution of equation (1). We may write the expansion of $I(r_1\mu)$ in a series of Legendre polynomials, as follows:

$$I(r, \mu) = \sum_{l=0}^{l0} \tfrac{1}{2} (2l+1) I_l(r) P_l(\mu), \tag{3}$$

[1] *Zs. f. Ap.*, **9**, 266, 1935. [2] *Zs. f. Ap.*, **1**, 98, 1930.

[3] *Pulkova Obs. Bull.*, No. 13; also *M.N.*, **93**, 50, 1931.

[4] Marshak, *Phys. Rev.*, **71**, 443, 1947.

where

$$I_l(r) = \int_{-1}^{1} P_l(\mu) I(r, \mu)\, d\mu, \tag{4}$$

and l_0 is an integer determining the order of the approximation.

Multiplying both sides of equation (1) by $P_l(\mu)$ and integrating over $d\mu$, using the well-known relations between the Legendre polynomials, we get

$$\frac{1}{k\rho}\left[\frac{1}{2l+1}\left\{l I'_{l-1}(r) + (l+1) I'_{l+1}(r)\right\} + \frac{1}{r(2l+1)}\{(l+1)(l+2) I_{l-1}(r) - l(l-1) I_{l-1}(r)\}\right] + I_l(r) = \left[p I_0(r) + \tfrac{1}{2} p S \frac{r_1^2}{r^2} e^{-(\tau_1-\tau)}\right]\delta_{0l}, \tag{5}$$

where the primes denote differentiation with respect to r and δ_{0l} is the Kronecker delta-function.

In order to proceed further, we require a variation of $k\rho$ with r. We shall suppose that

$$k\rho = \frac{c}{r^n}, \tag{6}$$

where c is a constant, and $n > 1$.[5]

In the first approximation (P_1), $l_0 = 1$. From equations (5) and (6) we have the following two relations:

$$\frac{r^n}{c} I'_1(r) + 2\frac{r^{n-1}}{c} I_1(r) + I_0(r) = p I_0(r) + \tfrac{1}{2} p S \frac{r_1^2}{r^2} e^{-(\tau_1-\tau)} \tag{7}$$

and

$$\frac{r^n}{3c} I'_0(r) + I_1(r) = 0. \tag{7a}$$

The P_1 approximation is the same as the Eddingtonian one,[6] and hence the expansion by Legendre polynomials is the natural extension of the Eddingtonian method. It has the further advantage of adaptability to the geometry of the problem.

It will be interesting to consider the application of the spherical harmonic method to the case treated by Milne[2] ($p = 1$). Equation (7) in this case reduces to

$$r^2 I'_1(r) + 2r I_1(r) = \frac{c}{2} S \frac{r_1^2}{r^n} e^{-(\tau_1-\tau)},$$

which integrates to

$$\begin{aligned} r^2 I_1(r) &= \text{Constant} + \frac{c}{2} S r_1^2 \int \frac{e^{-(\tau_1-\tau)}}{r^n}\, dr \\ &= \text{Constant} - \tfrac{1}{2} S r_1^2 \int e^{-(\tau_1-\tau)}\, d\tau \\ &= \text{Constant} - \tfrac{1}{2} S r_1^2 e^{-(\tau_1-\tau)}. \end{aligned}$$

At $\tau = \tau_1$ ($r = r_1$), $F = 0$ (cf. condition [2]). Hence we have

$$2 I_1(r) = F = S \frac{r_1^2}{r^2}(1 - e^{-(\tau_1-\tau)}). \tag{8}$$

[5] The cases for $n < 1$ have presumably no astrophysical interest (see Kosirev, *M.N.*, **94**, 430, 1934).

[6] Cf. Unsöld, *Physik der Sternatmosphären* (Berlin: Julius Springer, 1938), p. 98.

Equation (8) is the flux integral. From equation (7*a*) we obtain

$$I_0'(\tau) = -\frac{3c}{\tau^n} I_1(\tau) = -\frac{3c}{2} S \frac{\tau_1^2}{\tau^{n+2}} (1 - e^{-(\tau_1 - \tau)}) ;$$

whence it follows that

$$I_0(\tau) = \frac{3}{2} S \tau_1^2 \Big[\int_0^\tau \frac{1 - e^{-(\tau_1 - \tau)}}{\tau^2} \, d\tau + K_0 \Big] . \tag{9}$$

We determine K_0 from the boundary condition (cf. condition [2]):

$$\int_{-1}^{0} \mu I(\tau_2, \mu) \, d\mu = 0 . \tag{10}$$

Now, from equations (3) and (9), we have

$$\begin{aligned} I(\tau_1, \mu) &= \tfrac{1}{2} I_0 + \frac{3}{2} I_1(\tau) \mu \\ &= \frac{3}{4} S \tau_1^2 \Big[\int_0^\tau \frac{1 - e^{-(\tau_1 - \tau)}}{\tau^2} \, d\tau + K_0 \Big] + \frac{3}{4} \mu S \frac{\tau_1^2}{\tau^2} (1 - e^{-(\tau_1 - \tau)}) . \end{aligned} \tag{11}$$

Applying equation (10), we get

$$K_0 = \frac{2}{3\tau_2^2} (1 - e^{-\tau_1}) . \tag{12}$$

Substituting K_0 in equation (9), we have, finally,

$$I_0(\tau) = \frac{3}{2} S \tau_1^2 \Big[\int_0^\tau \frac{1 - e^{-(\tau_1 - \tau)}}{\tau^2} \, d\tau + \frac{2}{3\tau_2^2} (1 - e^{-\tau_1}) \Big] . \tag{13}$$

Equation (13) checks up with the result obtained by Chandrasekhar[7] on the Eddingtonian approximation.

We shall now consider the case $0 \leq p < 1$ (Zanstra-Ambarzumian theory). From equations (7) and (7*a*) we have the following differential equation of the second order in $I_0(\tau)$:

$$\frac{1}{3c^2} [\tau^{2n} I_0''(\tau) + (n+2) \tau^{2n-1} I_0'(\tau)] - (1-p) I_0(\tau) + \tfrac{1}{2} p S \frac{\tau_1^2}{\tau^2} e^{-(\tau_1 - \tau)} = 0 . \tag{14}$$

We shall suppose[8] the nebular shell to be extensive and measure τ from the outer boundary ($\tau \to \infty$). We then have

$$\tau = \frac{c}{n-1} \frac{1}{\tau^{n-1}} = \Big(\frac{R}{\tau} \Big)^{n-1} . \tag{15}$$

Equation (15) relates the constant c to the radial distance R, where the optical depth is unity. Substituting equation (15) in equation (14), we have

$$\frac{d^2 I_0}{d\tau^2} - \frac{2}{n-1} \frac{1}{\tau} \frac{dI_0}{d\tau} - 3(1-p) I_0 = -\frac{3}{2} p S \frac{\tau_1^2}{R^2} e^{-(\tau_1 - \tau)} \tau^{2/(n-1)} . \tag{16}$$

[7] *M.N.*, **94**, 444, 1934.

[8] Cf. Chandrasekhar, *Ap. J.*, **101**, 95, 1945; and Kosirev, *M.N.*, **94**, 430, 1934.

With the following substitutions:

$$I_0 = \tau^\nu f(z), \qquad z = q\tau, \qquad q = \sqrt{3(1-p)}, \tag{17}$$

equation (16) transforms into

$$z^2 \frac{d^2 f}{dz^2} + z \frac{df}{dz} - (z^2+\nu^2) f = -\frac{3}{2} pS \frac{r_1^2}{R^2} e^{-(\tau_1 - z/q)} \left(\frac{z}{q}\right)^{\nu+1}, \tag{18}$$

where

$$\nu = \frac{n+1}{2(n-1)}. \tag{19}$$

The homogeneous part of equation (18) is Bessel's equation for a purely imaginary argument. We shall find the general solution by the method of variation of parameters[9] in terms of the fundamental solutions $I_\nu(z)$ and $K_\nu(z)$. Accordingly, we write

$$f(z) = A(z) I_\nu(z) + B(z) K_\nu(z). \tag{20}$$

Then the following equations determine $A(z)$ and $B(z)$:

$$A'(z) I_\nu(z) + B'(z) K_\nu(z) = 0, \tag{21}$$

and

$$A'(z) I'_\nu(z) + B'(z) K'_\nu(z) = -\frac{3}{2} pS \frac{r_1^2}{R^2} e^{-(\tau_1 - z/q)} \frac{z^{\nu-1}}{q^{\nu+1}}. \tag{22}$$

Using the relation[10]

$$I_\nu(z) K'_\nu(z) - I'_\nu(z) K_\nu(z) = -\frac{1}{z} \tag{23}$$

and equations (21) and (22), we have

$$A'(z) = -\frac{3}{2} pS \frac{r_1^2}{R^2} e^{-(\tau_1 - z/q)} \frac{z^\nu}{q^{\nu+1}} K_\nu(z)$$

and (24)

$$B'(z) = \frac{3}{2} pS \frac{r_1^2}{R^2} e^{-(\tau_1 - z/q)} \frac{z^\nu}{q^{\nu+1}} I_\nu(z).$$

From equations (20) and (24) we obtain

$$q^{\nu+1} e^{\tau_1} f(z) = \frac{3}{2} pS \frac{r_1^2}{R^2} \left[K_\nu(z) \int_{c_2}^{z} e^{z/q} z^\nu I_\nu(z)\, dz - I_\nu(z) \int_{c_1}^{z} e^{z/q} z^\nu K_\nu(z)\, dz \right]. \tag{25}$$

We determine the constants c_1 and c_2 as follows: Since all the quantities vanish (from physical considerations) at $z = 0 (r \to \infty)$, we have, from equation (17),

$$z^\nu f(z) \to 0. \tag{26}$$

But $K_\nu(z)$ diverges at the origin, and condition (26) can be met only by putting $c_2 = 0$.

[9] Cf. Watson, *Bessel Functions* (Cambridge University Press, 1945), p. 345, sec. 10.7.

[10] *Ibid.*, p. 80, eq. (19).

We shall determine c_1 from the vanishing of the flux at the inner surface (r_1) (cf. condition [2]). Now the flux

$$\begin{aligned} r_1 &= 2\pi \int_{-1}^{1} I(r_1, \mu)\, \mu\, d\mu \\ &= 2\pi \int_{-1}^{1} [\tfrac{1}{2} I_0(r_1) + \tfrac{3}{2} I_1(r_1)\, \mu]\, \mu\, d\mu \\ &= 2\pi I_1(r_1)\,. \end{aligned} \tag{27}$$

We see from equations (7*a*) and (27) that the flux vanishes at r_1 if

$$I_0'(r_1) = 0\,, \tag{28}$$

where the differentiation may as well be with respect to τ or z (see eq. [17]). Substituting equation (28) in equation (25), we have

$$f(z) = \frac{3}{2} \frac{pS}{q^{\nu+1}} \tau_1^{2/(1-n)} e^{-\tau_1} \Big[K_\nu(z) \int_0^z e^{z/q} z^\nu I_\nu(z)\, dz - I_\nu(z) \Big\{ \int_{z_1}^z e^{z/q} z^\nu K_\nu(z)\, dz + \phi(z_1) \Big\} \Big]\,, \tag{29}$$

where

$$\phi(z_1) = \frac{z_1 K_\nu'(z_1) + \nu K_\nu(z_1)}{z_1 I_\nu'(z_1) + \nu I_\nu(z_1)} \int_0^{z_1} e^{z/q} z^\nu I_\nu(z)\, dz\,, \tag{30}$$

and

$$z_1 = q\tau_1\,. \tag{31}$$

We have replaced r_1^2/R^2 in equation (25) by $\tau_1^{2/(1-n)}$, as

$$\tau_1 = \left(\frac{R}{r_1}\right)^{n-1}, \tag{32}$$

where r_1 is the radius of the inner surface and R the radial distance at optical depth 1 (cf. eq. [15]).

It is easy to see from equations (7*a*), (17), and (27) that at $r(\tau)$

$$F(z) = 2\pi I_1(r) = \frac{2\pi}{3}\, q\, \frac{d}{dz}\Big[\Big(\frac{z}{q}\Big)^\nu f(z)\Big] = \frac{2\pi}{3}\, q \Big(\frac{z}{q}\Big)^\nu \Big[\nu \frac{f(z)}{z} + f'(z)\Big]\,, \tag{33}$$

where $f(z)$ is given by equation (29), and

$$f'(z) = \frac{3}{2} \frac{pS}{q^{\nu+1}} \tau_1^{2/(1-n)} e^{-\tau_1} \Big[K_\nu'(z) \int_0^z e^{z/q} z^\nu I_\nu(z)\, dz - I_\nu'(z) \int_{z_1}^z e^{z/q} z^\nu K_\nu(z)\, dz - I_\nu'(z)\, \phi(z_1) \Big]\,. \tag{34}$$

Also, the radiation density

$$J(z) = \frac{1}{2} \int_{-1}^{1} I\, d\mu = \tfrac{1}{2} I_0 = \tfrac{1}{2} \tau^\nu f(z)\,, \tag{35}$$

where $f(z)$ is given by equation (29). Thus we have formally solved the problem in the first approximation.

On account of the hypothetical nature of the assumption in equation (6), we do not consider it worth while to enter into extensive numerical calculations for different values of the parameters p and n. As our primary object is to investigate the effect of curvature, we shall evaluate the radiation density, J_3, and the flux, F, for only one set of values of the parameters:

$$n = \tfrac{3}{2}\,(\nu = \tfrac{5}{2}) \qquad \text{and} \qquad p = \tfrac{2}{3}\,(q = 1)\,.$$

We have been guided in our choice for the first value by its astrophysical importance[11] and for the second by computational convenience. We shall also assume that the total radial optical depth of the nebula is $\tau_1 = 2$. Note that, for the case under consideration, $z = \tau$, as $q = 1$.

The Bessel functions $I_{5/2}(z)$ and $K_{5/2}(z)$ are known explicitly:[12]

$$I_{5/2}(z) = \sqrt{\frac{2}{\pi z}}\left[\left(1+\frac{3}{z^2}\right)\sinh z - \frac{3}{z}\cosh z\right] \tag{36}$$

and

$$K_{5/2}(z) = \sqrt{\frac{\pi}{2z}}\; e^{-z}\left(1+\frac{3}{z}+\frac{3}{z^2}\right). \tag{37}$$

Substituting equations (36) and (37) in equations (33) and (35), we obtain (after a little algebra) the following explicit expressions for the flux and the radiation density:

$$F(\tau) = \tfrac{1}{9}\,S\tau_1^{-4}\,e^{-\tau_1}\,[\tau^2(b-5\tau^2-\tau^3)\cosh\tau - \tau\,(b+5\tau^3+\tau^4(\sinh\tau] \tag{38}$$

and

$$J(\tau) = \tfrac{1}{12}\,S\tau_1^4 e^{-\tau_1}\,[\{b\,(\tau^2+3) - \tau^5\}\sinh\tau - \tau\,(\tau^4+3\,b)\cosh\tau]\,, \tag{39}$$

where

$$b = \tau_1^3 e^{\tau_1}\,\frac{\tau_1+5}{\tau_1\cosh\tau_1 - \sinh\tau_1}. \tag{40}$$

It is easy to show that[13]

$$J(\tau_1) \to \tfrac{1}{4}S\,, \qquad \text{as} \qquad \tau_1 \to \infty\,. \tag{41}$$

We tabulate in Table 1 the functions $F(\tau)$ and $J(\tau)$ in units of S from $\tau = 0$ to $\tau = 2$, for $\tau_1 = 2$.

In order to compare with Chandrasekhar's values for the plane nebula,[1] we shall have to correct our $F(\tau)$ for the dilution factor

$$\left(\frac{\tau}{\tau_1}\right)^4 = \frac{\tau^4}{16}. \tag{42}$$

Table 1 contains the corrected values as well as Chandrasekhar's corresponding values of $F(\tau)$. Figure 1 illustrates the comparison between the ultraviolet fluxes in the plane and the spherical nebula corrected for dilution of radiation.

[11] Cf. Kosirev, *op. cit.*, p. 434.

[12] Cf. Watson, *op. cit.*, p. 78.

[13] Cf. Chandrasekhar, *Zs. f. Ap.*, 9, 1935, 273, eq. (48).

II. THE FIELD OF LYMAN-α RADIATION

(a) STATIC NEBULA

Let k_α be the coefficient of absorption within the line L_α. The corresponding optical depth τ_α is

$$\tau_\alpha = \int_r^\infty k_\alpha \rho \, dr , \qquad d\tau_\alpha = -k_\alpha \rho \, dr . \tag{43}$$

Following Ambarzumian[3] and Chandrasekhar,[1] we shall assume

$$\frac{\tau_\alpha}{\tau} = \frac{k_\alpha}{\kappa} = \text{Constant} = \omega \,(\text{say}) . \tag{44}$$

We shall denote the respective quantities for the Lyman-α radiation by the suffix α and the corresponding quantities for the Milne case ($p = 1$) by the suffix 1. The equation of transfer for the Lyman-α radiation is

$$\mu \frac{\partial I_\alpha}{\partial r} + \frac{1-\mu^2}{r} \frac{\partial I_\alpha}{\partial \mu} = -k_\alpha \rho \left[I_\alpha(\tau_\alpha) - B_\alpha(\tau_\alpha) \right] . \tag{45}$$

TABLE 1

τ	$F(\tau)/S$			$J(\tau)/S$
	Original	Corrected for Dilution	Chandrasekhar's Value for Plane Nebula	
0	0	0.4480	0.134	0
0.25	0.0001	.4312	.135	0.00001
0.50	.0016	.4089	.137	.00013
0.75	.0075	.3795	.139	.00088
1.00	.0214	.3420	.137	.00344
1.25	.0446	.2925	.128	.00939
1.50	.0708	.2237	.107	.02040
1.75	0.0760	0.1297	0.068	.03501
2.00	0	0	0	0.04478

Taking into account the emission in L_α by absorption of an ultraviolet quantum, the equation of radiative equilibrium is (cf. Ambarzumian[3])

$$B_\alpha(\tau_\alpha) = J_\alpha(\tau_\alpha) + \frac{\nu_\alpha (1-p)}{\nu_c p \omega} B(\tau) . \tag{46}$$

Now $F_1(\tau)$ is the flux in the ultraviolet when there is no conversion of the ultraviolet radiation into Lyman-α ($p = 1$). The actual flux in the ultraviolet is $F(\tau)$ (for the case $0 \leq p < 1$). The difference in the two fluxes will account for the Lyman-α radiation. As each ultraviolet quantum absorbed gives rise to a Lyman-α quantum, we have the following equation of flux in Lyman-α:

$$F_\alpha(\tau) = [F_1(\tau) - F(\tau)] \frac{\nu_\alpha}{\nu_c} . \tag{47}$$

From equations (6) and (7a) we have

$$I_1 = \frac{1}{3} \frac{dI_0}{d\tau} . \tag{48}$$

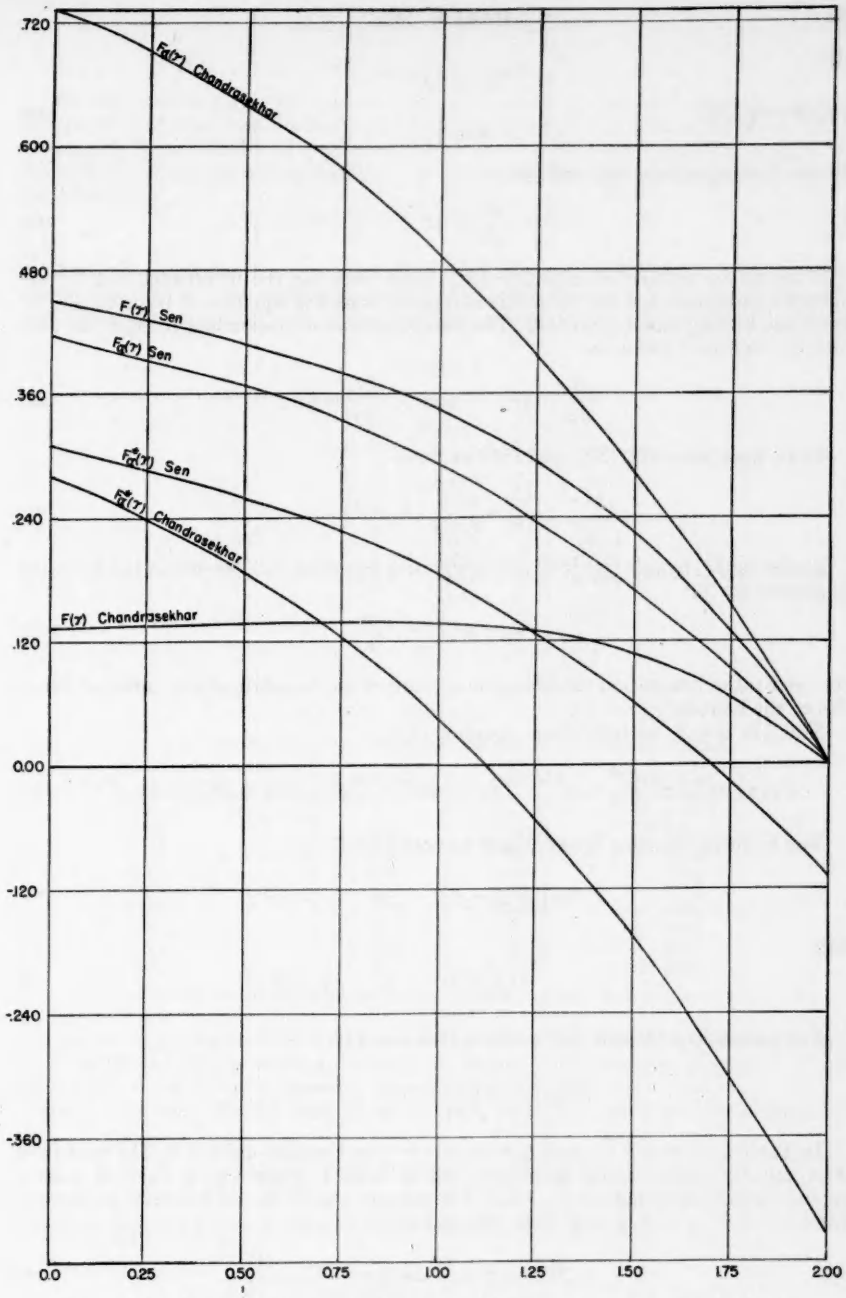

FIG. 1.—The flux of the ultraviolet and Lyman-α radiation as a function of optical depth

Also

$$I_0 = 2J$$

and (see eq. [27])

$$F = 2I_1 . \tag{49}$$

We get from equations (48) and (49)

$$\frac{dJ}{d\tau} = \tfrac{3}{4}F . \tag{50}$$

It should be noted that equation (50) holds both for the ultraviolet and for the Lyman-α radiations and can be obtained directly from the equation of transfer (45) by the usual Eddingtonian procedure. The two equations corresponding to equation (50) with the suffixes 1 and a are

$$\frac{dJ_1}{d\tau} = \tfrac{3}{4}F_1 \quad \text{and} \quad \frac{dJ_a}{d\tau} = \tfrac{3}{4}F_a . \tag{51}$$

From equations (47), (50), and (51) we have

$$\frac{dJ_a}{d\tau_a} = \frac{\nu_a}{\nu_c}\frac{d}{d\tau}(J_1 - J) . \tag{52}$$

Replacing $d\tau_a$ by $\omega d\tau$ (eq. [44]) and integrating equation (52), we obtain the following expression for J_a:

$$J_a = \omega (J_1 - J)\frac{\nu_a}{\nu_c}, \tag{53}$$

the constant of integration vanishing, on account of the vanishing of the radiation densities at the boundary ($\tau = 0$).

Now, for $n = \frac{3}{2}$, we have, from equation (13),

$$J_1(\tau) = \tfrac{3}{4}S\tau_1^{-4}\left[\frac{\tau^5}{5} - e^{-(\tau_1-\tau)}(\tau^4 - 4\tau^3 + 12\tau^2 - 24\tau + 24) + 24\, e^{-\tau_1}\right]. \tag{54}$$

The following limiting forms should be noted for $J_1(\tau_1)$:

$$J_1(\tau_1) \sim \tfrac{3}{20}\tau_1 S, \qquad \text{as} \qquad \tau_1 \to \infty ,$$

and

$$\sim \tfrac{1}{40}\tau_1^2 S, \qquad \text{as} \qquad \tau_1 \to 0 . \tag{55}$$

From equations (8) and (15) we have (for $n = \frac{3}{2}$)

$$F_1(\tau) = S\left(\frac{\tau}{\tau_1}\right)^4 (1 - e^{-(\tau_1-\tau)}) . \tag{56}$$

In Table 2 we give $F_1(\tau)$ and $J_1(\tau)$ from $\tau = 0$ to $\tau = 2$ in units of S. The quantities $F(\tau)$ and $J(\tau)$ have already been evaluated in Table 1. Table 3 gives $F_a(\tau)$ in units of $(\nu_a/\nu_c)S$ and $J_a(\tau)$ in units of $(\nu_a/\nu_c)\omega S$. The quantity $J_a(\tau_1)$ has the following asymptotic form ($\tau_1 \to \infty$, $n = \frac{3}{2}$, $p = \frac{2}{3}$) (eqs. [55] and [41]):

$$J_a(\tau_1) \sim \tfrac{1}{4}\frac{\nu_a}{\nu_c}\omega S(\tfrac{3}{5}\tau_1 - 1) . \tag{57}$$

(*b*) EXPANDING NEBULA

We shall now consider the case of a nebula expanding with a uniform velocity large compared with the mean velocity of molecular motion (see Ambarzumian[3]). For a sufficiently large velocity of expansion, we shall, in a first approximation, neglect the back-illumination (see Chandrasekhar[1]), in which case our appropriate boundary conditions will be

$$2J_a^*(\tau_1) = F_a^*(\tau_1); \qquad J_a^*(0) = F_a^*(0) = 0 . \tag{58}$$

We shall denote the corresponding physical quantities for the expanding nebula by an asterisk. We can see, as follows, that $F_a^*(\tau)$ is simply related to $F_a(\tau)$, but the relation differs from the plane case, in that the difference between the fluxes in the expanding

TABLE 2

τ	$F_1(\tau)/S$	$J_1(\tau)/S$
0	0	0
0.25	0.00020	0.00001
0.50	.00304	.00023
0.75	.01411	.00166
1.00	.03951	.00643
1.25	.08051	.01748
1.50	.12450	.03686
1.75	0.12966	.06185
2.00	0	0.07725

TABLE 3

τ	$F_a(\tau)S^{-1}\nu_c/\nu_a$	$J_a(\tau)(\omega S)^{-1}\nu_c/\nu_a$	$F_a^*(\tau)S^{-1}\nu_c/\nu_a$
0	0	0	0
0.25	0.0001	0.00000	+0.00007
0.50	.0014	.00010	+ .0010
0.75	.0066	.00077	+ .0045
1.00	.0181	.00299	+ .0113
1.25	.0359	.00809	+ .0194
1.50	.0537	.01646	+ .0195
1.75	0.0537	.02684	− .0097
2.00	0	0.03247	−0.1082

and the corresponding static cases is not a constant (cf. Chandrasekhar, *Zs. f. Ap.*, **9**, 288, eq. [1.8]). It reduces, however, to a constant (though a different one from that of the plane case), if correction is made for the dilution factor (42).

Integrating equation (45) over the solid angle, we deduce, with the help of equation (46),

$$\frac{1}{2}\frac{dF_a}{d\tau}+\frac{F_a}{\tau}= 2k_a\rho\frac{\nu_a}{\nu_c}\frac{1-p}{p\omega}B(\tau) . \tag{59}$$

Equation (59) can be transformed into (see eqs. [6], [15], and [43])

$$\frac{1}{2}\frac{dF_a}{d\tau_a}-\frac{F_a}{(n-1)\tau_a}= -2\frac{\nu_a}{\nu_c}\frac{1-p}{p\omega}B(\tau) . \tag{60}$$

The solution of equation (60) is easily seen to be

$$F_a = c\tau_a^{2/(n-1)} - 4\frac{\nu_a}{\nu_c}\frac{1-p}{p\omega}\tau_a^{2/(n-1)}\int_0^{\tau} B(\tau)\,\tau_a^{2/(1-n)}\,d\tau_a, \tag{61}$$

where c is an arbitrary constant.

The corresponding solution for the expanding nebula is

$$F_a^* = c^*\tau_a^{2/(n-1)} - 4\frac{\nu_a}{\nu_c}\frac{1-p}{p\omega}\tau_a^{2/(n-1)}\int_0^{\tau} B(\tau)\,\tau_a^{2/(1-n)}\,d\tau_a. \tag{62}$$

Since $\tau_a = \omega\tau$ (eq. [44]), we see from equations (61) and (62) that

$$F_a^*(\tau) - F_a(\tau) = a\tau^{2/(n-1)}, \tag{63}$$

where a is an arbitrary constant. It follows from equation (63) that for the plane case ($n \to \infty$) the difference between the two fluxes reduces to a constant (see Chandrasekhar[1]).

From equations (51) and (63) we have

$$J_a^* = \tfrac{3}{4}\int F_a^* d\tau_a = J_a + \tfrac{3}{4}a\omega\frac{n-1}{n+1}\tau^{(n+1)/(n-1)}, \tag{64}$$

the constant of integration vanishing on account of the vanishing of the J_a's at $\tau = 0$ (see eq. [58]).

Now applying the boundary condition (58) at τ_1, we determine

$$a = \frac{2J_a(\tau_1)}{\tau_1^{2/(n-1)} - \frac{3}{2}\frac{n-1}{n+1}\omega\tau_1^{(n+1)/(n-1)}} \sim -\frac{4}{3}\frac{n+1}{n-1}\frac{J_a(\tau_1)}{\omega}\tau_1^{(n+1)/(1-n)}, \tag{65}$$

as $\omega \sim 10^4 >> 1$ (see Ambarzumian[3]).

Hence, finally, we have the following expressions for the flux and the radiation density, respectively, for the expanding nebula:

$$F_a^*(\tau) = F_a(\tau) - \frac{4}{3}\frac{n+1}{n-1}\frac{J_a(\tau_1)}{\omega\tau_1}\left(\frac{\tau}{\tau_1}\right)^{2/(n-1)}, \tag{66}$$

$$J_a^*(\tau) = J_a(\tau) - \left(\frac{\tau}{\tau_1}\right)^{(n+1)/(n-1)} J_a(\tau_1). \tag{67}$$

We may easily verify that in the limit, as $n \to \infty$, equations (66) and (67) transform into the corresponding expressions for the plane case (eqs. [104] and [105] of Chandrasekhar[1]).

From equations (57) and (66) we deduce the following asymptotic form for the flux at the inner boundary for large τ_1:

$$F_a^*(\tau_1) \sim -\frac{\nu_a}{\nu_c}S\left(1 - \frac{5}{3\tau_1}\right). \tag{68}$$

Values of $F_a^*(\tau)$ in units of $(\nu_a/\nu_c)S$ have also been entered in Table 3.

In order to facilitate comparison with Chandrasekhar's corresponding values for the plane case,[1] we have corrected our flux values for the dilution factor (42). Table 4 contains the corrected values of the flux in L_a (in units of $(\nu_a/\nu_c)S$) and Chandrasekhar's corresponding values. Figure 1 graphically illustrates the comparison.

Allowing for the dilution factor $(\tau/\tau_1)^{2/(n-1)}$ in equation (66), we have

$$F_a^*(\tau) - F_a(\tau) = -\frac{4}{3}\frac{n+1}{n-1}\frac{J_a(\tau_1)}{\omega\tau_1}, \tag{69}$$

a constant, which is, however, different from the value obtained by Chandrasekhar[14] for the plane case. The two constants are equal only for $n \to \infty$. For the case considered by us ($n = \frac{3}{2}$), we have

$$F_a^*(\tau) - F_a(\tau) = -\frac{20}{3}\frac{J_a(\tau_1)}{\omega\tau_1}, \tag{70}$$

which differs from Chandrasekhar's value for the plane nebula by a factor of 5.

TABLE 4

τ	$F_a(\tau)\nu_c/\nu_a S^{-1}$		$F_a(\tau)\nu_c/\nu_a S^{-1}$	
	Spherical	Plane (Chandrasekhar)	Spherical	Plane (Chandrasekhar)
0	0.4167	0.730	+0.3085	+0.279
0.25	.3941	.691	+ .2859	+ .239
0.50	.3680	.639	+ .2598	+ .188
0.75	.3340	.575	+ .2258	+ .123
1.00	.2901	.495	+ .1819	+ .043
1.25	.2342	.400	+ .1260	− .052
1.50	.1697	.286	+ .0615	− .166
1.75	0.0917	0.153	− .0165	− .299
2.00	0	0	−0.1082	−0.452

From our tables and graphs we may summarize the following effects in our case of the spherical nebula, which we may attribute to the curvature of the nebular shell:

1. The ultraviolet flux monotonically increases from the inner to the outer boundary of the nebula (the plane case[1] has a maximum in the range) and is greater than that of the plane nebula by a factor of 2–3.

2. The L_a flux for the static nebula increases as in the plane nebula monotonically from the inner to the outer boundary of the nebula, but is less than that of the plane nebula by a factor of $\frac{2}{3}$.

3. The L_a fluxes for the moving plane and spherical nebulae are of the same order of magnitude toward the outer parts; the flux decreases much more rapidly toward the interior in the plane nebula, so that the inner parts, which suffer inward radiative accelerations,[15] are much more extensive in the plane than in the spherical nebula.

The author's thanks are due to Dr. Donald H. Menzel for many valuable suggestions and helpful discussions clarifying obscure points; to Dr. Harlow Shapley for opportunity to work at the Harvard Observatory; to Mr. John G. Wolbach for preparing the tables and the figure; and to Mr. David Murcray for drawing the figure.

[14] *Ibid.*, p. 288, eq. (108).

[15] Chandrasekhar, *ibid.*, p. 288.

THE TRANSFER OF RADIATION IN A SPHERICAL ATMOSPHERE OF ELECTRONS

MARSHAL H. WRUBEL
Yerkes Observatory
Received May 25, 1949

ABSTRACT

The emergent intensities in the two components of polarized light are determined for the case of an extended spherical atmosphere of electrons resting on a photosphere which emits unpolarized radiation. The problem is solved in an approximation which includes terms through $P_3(\mu)$ in an expansion in spherical harmonics and for an atmosphere extending to infinity, in which the opacity varies inversely as the square of the radius. Atmospheres are considered with total optical thicknesses, τ_1, of 0.5, 1.0, and 2.0.

It is found that the polarization of the scattered light varies from zero at the center of the star to 19, 16, and 11 per cent at the edge of the photosphere for $\tau_1 = 0.5$, 1.0, and 2.0, respectively. Beyond the discontinuity at the photosphere, the degree of polarization remains practically constant, decreasing slowly from 22 per cent for $\tau_1 = 0.5$, increasing from 19 to 20 per cent before decreasing for $\tau_1 = 1.0$, and increasing from 13 to 20 per cent and then decreasing for $\tau_1 = 2.0$. In every case the degree of polarization is approximately 20 per cent, decreasing slowly at ten radii from the center of the star.

I. INTRODUCTION

The transfer of radiation in a plane-parallel atmosphere of electrons has been extensively studied by S. Chandrasekhar,[1] with the conclusion that the emergent light is polarized a maximum of about 11 per cent at the limb. An observing program to detect this polarization in eclipsing early-type stars is now in progress at this observatory.[2]

Z. Kopal and M. B. Shapley[3] have concluded, from a study of the eclipsing system V444 Cygni, that the Wolf-Rayet component is surrounded by an extended envelope in which electrons are the main source of opacity. The dimensions of this atmosphere are so large that the curvature cannot be neglected. To determine the degree of polarization that one would expect in this case, we consider the following idealized problem: A spherically symmetrical atmosphere in radiative equilibrium rests upon a photosphere, which radiates unpolarized light in the outward direction. The problem is to derive the emergent intensities of the components of polarized light for various values of the total optical depth in terms of the darkening law of the photosphere and for a given variation of opacity with radius. Polarization should be detected if the atmosphere is subject to an eclipse.

Although the polarization recently observed by Hiltner[4] in distant stars is apparently independent of eclipse phase and may be due to interstellar matter, the connection between this phenomenon and the individual stars is not ruled out altogether, and the study of the properties of extended electron envelopes remains of more than pedantic interest.

II. THE EQUATIONS OF THE PROBLEM

In the usual notation, $I(r, \mu)$ is the specific intensity at the point r in a direction making an angle of cosine μ with the radius vector. The subscripts l and r refer to the components of the beam in which the electric vector vibrates parallel and perpendicular, respectively, to the meridian plane of a system of polar co-ordinates at the point r. The

[1] *Ap. J.*, **103**, 351, 1946; **104**, 110, 1946; **105**, 164, 1947.

[2] W. A. Hiltner, *Ap. J.*, **106**, 231, 1947.

[3] *Ap. J.*, **104**, 160, 1946.

[4] *Science*, **109**, 165, 1949.

source functions of this problem are exactly the same as those treated by Chandrasekhar in the plane-parallel atmosphere. Thus we have

$$\mu\frac{\partial I_l}{\partial r}+\frac{1-\mu^2}{r}\frac{\partial I_l}{\partial \mu}=-\kappa\rho I_l+\tfrac{3}{8}\kappa\rho\Big[2\int_{-1}^{+1}I_l(r,\mu')(1-\mu'^2)\,d\mu' +\mu^2\int_{-1}^{+1}I_l(r,\mu')(3\mu'^2-2)\,d\mu'+\mu^2\int_{-1}^{+1}I_r(r,\mu')\,d\mu'\Big] \tag{1}$$

and

$$\mu\frac{\partial I_r}{\partial r}+\frac{1-\mu^2}{r}\frac{\partial I_r}{\partial \mu}=-\kappa\rho I_r+\tfrac{3}{8}\kappa\rho\Big[\int_{-1}^{+1}I_r(r,\mu')\,d\mu'+\int_{-1}^{+1}I_l(r,\mu')\mu'^2 d\mu'\Big]. \tag{2}$$

Rewriting the integrals as Gaussian sums, we obtain two sets of equations:

$$\mu_i\frac{dI_{l,i}}{dr}+\frac{1-\mu_i^2}{r}\Big(\frac{\partial I_l}{\partial\mu}\Big)_{\mu=\mu_i}=-\kappa\rho I_{l,i}+\tfrac{3}{8}\kappa\rho\Big[2\sum_j I_{l,j}a_j(1-\mu_j^2) +\mu_i^2\sum_j a_jI_{l,j}(3\mu_j^2-2)+\mu_i^2\sum_j a_jI_{r,j}\Big] \qquad (i=0,\pm1,\ldots,\pm n) \tag{3}$$

and

$$\mu_i\frac{dI_{r,i}}{dr}+\frac{1-\mu_i^2}{r}\Big(\frac{\partial I_r}{\partial\mu}\Big)_{\mu=\mu_i}=-\kappa\rho I_{r,i}+\tfrac{3}{8}\kappa\rho\Big[\sum_j a_jI_{r,j}+\sum_j a_jI_{l,j}\mu_j^2\Big] \qquad (i=0,\pm1,\ldots,\pm n), \tag{4}$$

where $a_j=a_{-j}$ are the Gaussian weights and $\mu_j=-\mu_{-j}$ are the roots of the Legendre polynomial P_{2n+1}. (Note that in this paper we shall consider odd, as well as even, Legendre polynomials, so that the notation differs slightly from that usually employed by Chandrasekhar.) The general procedure for assigning the proper values to the partial derivatives has been discussed by Chandrasekhar.[5] Each of the above equations is multiplied by $a_i\mathcal{Q}_m(\mu_i)$ and summed over i, giving

$$\frac{d}{dr}\sum_i a_i\mu_i\mathcal{Q}_m(\mu_i)\,I_{l,i}+\frac{1}{r}\sum_i a_i(1-\mu_i^2)\Big(\frac{\partial I_l}{\partial\mu}\Big)_{\mu=\mu_i}\mathcal{Q}_m(\mu_i)=-\kappa\rho \times\sum_i a_i\mathcal{Q}_m(\mu_i)\,I_{l,i}+\tfrac{3}{8}\kappa\rho\Big[2\sum_j I_{l,j}a_j(1-\mu_j^2)\sum_i a_i\mathcal{Q}_m(\mu_i)+\sum_j a_jI_{l,j}(3\mu_j^2-2) \times\sum_i a_i\mu_i^2\mathcal{Q}_m(\mu_i)+\sum_i a_i\mu_i^2\mathcal{Q}_m(\mu_i)\sum_j a_jI_{r,j}\Big] \qquad [m=1,2,\ldots,(2n+1)] \tag{5}$$

and

$$\frac{d}{dr}\sum_i a_i\mu_i\mathcal{Q}_m(\mu_i)\,I_{r,i}+\frac{1}{r}\sum_i a_i(1-\mu_i^2)\,\mathcal{Q}_m(\mu_i)\Big(\frac{\partial I_r}{\partial\mu}\Big)_{\mu=\mu_i} =-\kappa\rho\sum_i a_i\mathcal{Q}_m(\mu_i)\,I_{r,i}+\tfrac{3}{8}\kappa\rho\Big[\sum_j a_jI_{r,j}\sum_i a_i\mathcal{Q}_m(\mu_i) +\sum_j a_jI_{l,j}\mu_j^2\sum_i a_i\mathcal{Q}_m(\mu_i)\Big] \qquad [m=1,2,\ldots,(2n+1)], \tag{6}$$

[5] *Ap. J.*, **101**, 95, 1945. Hereafter referred to as "Paper V."

where

$$\mathcal{Q}_m(\mu) = \frac{Q_m(\mu)}{1-\mu^2}, \qquad \frac{dQ_m}{d\mu} = -P_m(\mu) \tag{7}$$

and

$$Q_m = 0 \qquad \text{at} \qquad |\mu| = 1 .$$

Since (Paper V, eq. [10])

$$\sum_i a_i (1-\mu_i^2)\, \mathcal{Q}_m(\mu_i) \left(\frac{\partial I}{\partial \mu}\right)_{\mu=\mu_i} = \sum_i a_i Q_m(\mu_i) \left(\frac{\partial I}{\partial \mu}\right)_{\mu=\mu_i} = \sum_i a_i P_m(\mu_i)\, I_i , \tag{8}$$

we finally get the $2n+1$ equations of the problem

$$\frac{d}{d\tau}\sum_i a_i \mu_i \mathcal{Q}_m(\mu_i)\, I_{l,i} + \frac{1}{\tau}\sum_i a_i P_m(\mu_i)\, I_{l,i} = -\kappa\rho \sum_i a_i \mathcal{Q}_m(\mu_i)\, I_{l,i}$$

$$+ \tfrac{3}{8}\kappa\rho \left\{ 2\sum_j I_{l,j} a_j (1-\mu_j^2) \sum_i a_i \mathcal{Q}_m(\mu_i) + \sum_i a_i \mu_i^2 \mathcal{Q}_m(\mu_i) \right. \tag{9}$$

$$\left. \times \Big[\sum_j a_j I_{l,j} (3\mu_j^2 - 2) + \sum_j a_j I_{r,j} \Big] \right\} \qquad [m = 1, 2, \ldots, (2n+1)]$$

and

$$\frac{d}{d\tau}\sum_i a_i \mu_i \mathcal{Q}_m(\mu_i)\, I_{r,i} + \frac{1}{\tau}\sum_i a_i P_m(\mu_i)\, I_{r,i} = -\kappa\rho \sum_i a_i \mathcal{Q}_m(\mu_i)\, I_{r,i}$$

$$+ \tfrac{3}{8}\kappa\rho \sum_i a_i \mathcal{Q}_m(\mu_i) \left\{ \sum_j a_j I_{r,j} + \sum_j a_j \mu_j^2 I_{l,j} \right\} \qquad [m = 1, 2, \ldots, (2n+1)] . \tag{10}$$

These may be supplemented with the following relations, which are valid for both the l and the r components (Paper V, eqs. [16] and [17]). Since $\mathcal{Q}_m(\mu_i)$ is odd when m is even and the Gaussian sum of an odd power of μ_i vanishes,

$$\frac{d}{d\tau}\sum_i a_i \mu_i \mathcal{Q}_m(\mu_i)\, I_i + \frac{1}{\tau}\sum_i a_i P_m(\mu_i)\, I_i = -\kappa\rho \sum_i a_i \mathcal{Q}_m(\mu_i)\, I_i \qquad (m = 2, 4, \ldots, 2n) . \tag{11}$$

Further, since

$$P_{2n+1}(\mu_i) \equiv 0 , \tag{12}$$

it follows that

$$\frac{1}{\tau}\sum_i a_i P_m(\mu_i)\, I_{l,i} = \frac{1}{\tau}\sum_i a_i P_m(\mu_i)\, I_{r,i} = 0 \qquad (m = 2n+1) . \tag{13}$$

Because of the symmetry of the radiation field, I_l and I_r are the only Stokes intensities which we need to consider.

III. THE GENERAL P_3 APPROXIMATION

We now use Table 1, adapted from Paper V, to write the equations appropriate to the P_3 approximation. Since

$$\sum_i a_i \mu_i^m = \frac{2}{m+1} \qquad \text{for } m \text{ even}$$

$$= \quad 0 \qquad \text{for } m \text{ odd}, \tag{14}$$

we have the following six equations for $m = 1$, 2, and 3, respectively:

$$\frac{1}{2}\frac{d}{d\tau}\sum_i a_i\mu_i I_{l,i}+\frac{1}{\tau}\sum_i a_i\mu_i I_{l,i}=-\tfrac{1}{2}\kappa\rho\sum_i a_i I_{l,i}+\tfrac{3}{8}\kappa\rho\left\{2\sum_j I_{l,j}a_j(1-\mu_j^2)+\frac{1}{3}\Big[\sum_j a_j I_{l,j}(3\mu_j^2-2)+\sum_j a_j I_{r,j}\Big]\right\}, \tag{15}$$

$$\frac{1}{2}\frac{d}{d\tau}\sum_i a_i\mu_i I_{r,i}+\frac{1}{\tau}\sum_i a_i\mu_i I_{r,i} = -\tfrac{1}{2}\kappa\rho\sum_i a_i I_{r,i}+\tfrac{3}{8}\kappa\rho\left\{\sum_j a_j I_{r,j}+\sum_j a_j\mu_j^2 I_{l,j}\right\}, \tag{16}$$

$$\frac{d}{d\tau}\sum_i a_i\mu_i^2 I_{l,i}+\frac{1}{\tau}\sum_i a_i(3\mu_i^2-1)\,I_{l,i} = -\kappa\rho\sum_i a_i\mu_i I_{l,i}, \tag{17}$$

$$\frac{d}{d\tau}\sum_i a_i\mu_i^2 I_{r,i}+\frac{1}{\tau}\sum_i a_i(3\mu_i^2-1)\,I_{r,i} = -\kappa\rho\sum_i a_i\mu_i I_{r,i}, \tag{18}$$

$$\frac{d}{d\tau}\sum_i a_i\mu_i(5\mu_i^2-1)\,I_{l,i} = -\kappa\rho\sum_i a_i(5\mu_i^2-1)\,I_{l,i}+\kappa\rho\sum_j a_j(1-\mu_j^2)\,I_{l,j} +\tfrac{1}{2}\kappa\rho\Big[\sum_j a_j I_{l,j}(3\mu_j^2-2)+\sum_j a_j I_{r,j}\Big], \tag{19}$$

TABLE 1

m	$P_m(\mu)$	$Q_m(\mu)$
1	μ	$\frac{1}{2}$
2	$\frac{1}{2}(3\mu^2-1)$	$\frac{1}{2}\mu$
3	$\frac{1}{2}(5\mu^3-3\mu)$	$\frac{1}{8}(5\mu^2-1)$

and

$$\frac{d}{d\tau}\sum_i a_i\mu_i(5\mu_i^2-1)\,I_{r,i} = -\kappa\rho\sum_i a_i(5\mu_i^2-1)\,I_{r,i} +\tfrac{1}{2}\kappa\rho\Big[\sum_j a_j I_{r,j}+\sum_j a_j\mu_j^2 I_{l,j}\Big]. \tag{20}$$

The notation may be simplified by defining the following quantities

$$\begin{aligned}
&\tfrac{1}{2}\sum_i a_i I_{l,i}=J_l; && \tfrac{1}{2}\sum_i a_i I_{r,i}=J_r;\\
&\tfrac{1}{2}\sum_i a_i\mu_i I_{l,i}=H_l; && \tfrac{1}{2}\sum_i a_i\mu_i I_{r,i}=H_r;\\
&\tfrac{1}{2}\sum_i a_i\mu_i^2 I_{l,i}=K_l; && \tfrac{1}{2}\sum_i a_i\mu_i^2 I_{r,i}=K_r;\\
&\tfrac{1}{2}\sum_i a_i\mu_i^3 I_{l,i}=L_l; && \tfrac{1}{2}\sum_i a_i\mu_i^3 I_{r,i}=L_r.
\end{aligned} \tag{21}$$

By definition

$$\sum_i a_i P_3(\mu_i) I_{l,i} = 5L_l - 3H_l \equiv 0$$

and

$$\sum_i a_i P_3(\mu_i) I_{r,i} = 5L_r - 3H_r \equiv 0 . \tag{22}$$

Equations (19) and (20) may now be written as follows:

$$\frac{d}{d\tau}(5L_l - 3H_l) + 2\frac{d}{d\tau}H_l = \kappa\rho\left[J_l - \tfrac{9}{2}K_l + \tfrac{1}{2}J_r\right] \tag{23}$$

and

$$\frac{d}{d\tau}(5L_r - 3H_r) + 2\frac{d}{d\tau}H_r = \kappa\rho\left[\tfrac{3}{2}J_r - 5K_r + \tfrac{1}{2}K_l\right], \tag{24}$$

where, because of equation (22), the first term on the left side of each is identically zero.

The six equations of the P_3 approximation, therefore, are

$$\frac{dH_l}{d\tau} + \frac{2}{\tau}H_l = \tfrac{1}{4}\kappa\rho\left[J_r - 3K_l\right], \tag{25}$$

$$\frac{dH_r}{d\tau} + \frac{2}{\tau}H_r = -\tfrac{1}{4}\kappa\rho\left[J_r - 3K_l\right], \tag{26}$$

$$\frac{dK_l}{d\tau} + \frac{1}{\tau}(3K_l - J_l) = -\kappa\rho H_l , \tag{27}$$

$$\frac{dK_r}{d\tau} + \frac{1}{\tau}(3K_r - J_r) = -\kappa\rho H_r , \tag{28}$$

$$2\frac{d}{d\tau}H_l = \kappa\rho\left[J_l - \tfrac{9}{2}K_l + \tfrac{1}{2}J_r\right], \tag{29}$$

and

$$2\frac{d}{d\tau}H_r = \kappa\rho\left[\tfrac{3}{2}J_r - 5K_r + \tfrac{1}{2}K_l\right]. \tag{30}$$

IV. THE P_3 APPROXIMATION FOR $\kappa\rho \propto \tau^{-\beta}$

We shall now consider equations (25)–(30) for the case

$$\kappa\rho = \frac{c}{\tau^\beta} \qquad (\beta > 1) . \tag{31}$$

Defining

$$d\tau = -\kappa\rho\, d\tau , \tag{32}$$

we find

$$\tau = \frac{c}{\beta - 1}\frac{1}{\tau^{\beta-1}} \quad \text{and} \quad \kappa\rho\tau = (\beta - 1)\tau . \tag{33}$$

If we define

$$X_l = 3K_l - J_l \quad \text{and} \quad X_r = 3K_r - J_r , \tag{34}$$

we may write the six equations of the P_3 approximation as follows:

$$\frac{dH_l}{d\tau}-\frac{2}{(\beta-1)\tau}H_l=-\tfrac{1}{4}[J_r-3K_l], \tag{35}$$

$$\frac{dH_r}{d\tau}-\frac{2}{(\beta-1)\tau}H_r=+\tfrac{1}{4}[J_r-3K_l]; \tag{36}$$

$$\frac{dK_l}{d\tau}-\frac{1}{(\beta-1)\tau}X_l=H_l, \tag{37}$$

$$\frac{dK_r}{d\tau}-\frac{1}{(\beta-1)\tau}X_r=H_r; \tag{38}$$

$$2\frac{dH_l}{d\tau}=-J_l+\tfrac{9}{2}K_l-\tfrac{1}{2}J_r, \tag{39}$$

and

$$2\frac{dH_r}{d\tau}=-\tfrac{3}{2}J_r+5K_r-\tfrac{1}{2}K_l. \tag{40}$$

In the subsequent analysis we shall use the abbreviations

$$S=K_l-K_r, \qquad T=X_l+X_r, \qquad \text{and} \qquad R=X_l-X_r. \tag{41}$$

Adding equations (35) and (36), we obtain an analogue of the flux integral

$$H_l+H_r=\tfrac{1}{4}F_0\left[\frac{(\beta-1)\tau}{c}\right]^{2/(\beta-1)}, \tag{42}$$

where F_0 is a constant to be determined.

Subtracting equations (35) and (36), we find

$$\frac{d}{d\tau}(H_l-H_r)-\frac{2}{(\beta-1)\tau}(H_l-H_r)=\tfrac{1}{2}[-J_r+3K_l]. \tag{43}$$

Adding equations (37) and (38) and using equation (41), we obtain

$$\frac{d}{d\tau}(K_l+K_r)-\frac{T}{(\beta-1)\tau}=\tfrac{1}{4}F_0\left[\frac{(\beta-1)\tau}{c}\right]^{2/(\beta-1)}. \tag{44}$$

This is analogous to the K-integral.

Subtracting equations (37) and (38), we find

$$\frac{dS}{d\tau}-\frac{1}{(\beta-1)\tau}R=H_l-H_r, \tag{45}$$

which, when differentiated, gives

$$\frac{d^2S}{d\tau^2}-\frac{1}{(\beta-1)\tau}\frac{dR}{d\tau}+\frac{1}{(\beta-1)\tau^2}R=\frac{d}{d\tau}(H_l-H_r). \tag{46}$$

We obtain an expression for the derivative on the right by first adding and subtracting $3K_r$ inside the brackets on the right of equation (43), which gives

$$\frac{d}{d\tau}(H_l-H_r)-\frac{2}{(\beta-1)\tau}(H_l-H_r)=\tfrac{1}{2}[3K_r-J_r+3S]. \tag{47}$$

Since equation (45) is an expression for $H_l - H_r$ in terms of S and R, we can rewrite equation (47) as

$$\frac{d}{d\tau}(H_l - H_r) = \frac{X_r}{2} + \tfrac{3}{2}S + \frac{2}{(\beta-1)\,\tau}\frac{dS}{d\tau} - \frac{2}{(\beta-1)^2\tau^2}R. \tag{48}$$

Substituting this expression in equation (46), we eliminate $(H_l - H_r)$, to obtain

$$\frac{d^2S}{d\tau^2} - \frac{1}{(\beta-1)\,\tau}\frac{dR}{d\tau} + \frac{1}{(\beta-1)\,\tau^2}R = \frac{X_r}{2} + \tfrac{3}{2}S + \frac{2}{(\beta-1)\,\tau}\frac{dS}{d\tau} - \frac{2}{(\beta-1)^2\tau^2}R. \tag{49}$$

Since

$$\tfrac{1}{2}X_r = \tfrac{1}{4}(T - R), \tag{50}$$

we obtain the following second-order equation:

$$\frac{d^2S}{d\tau^2} - \frac{2}{(\beta-1)\,\tau}\frac{dS}{d\tau} - \tfrac{3}{2}S = \frac{1}{(\beta-1)\,\tau}\frac{dR}{d\tau} - \left[\frac{\beta+1}{(\beta-1)^2\tau^2} + \frac{1}{4}\right]R + \tfrac{1}{4}T. \tag{51}$$

The derivative on the left in equation (39) may be found by combining equations (35) and (37); from which it follows that

$$-\tfrac{1}{2}J_r + \tfrac{3}{2}K_r + \frac{4}{(\beta-1)\,\tau}\frac{dK_l}{d\tau} - \frac{4}{(\beta-1)^2\tau^2}X_l = -J_l + \tfrac{9}{2}K_l - \tfrac{1}{2}J_r, \tag{52}$$

which reduces to

$$\frac{4}{(\beta-1)\,\tau}\frac{dK_l}{d\tau} - \frac{4}{(\beta-1)^2\tau^2}X_l = X_l. \tag{53}$$

Similarly, the derivative in equation (40) may be found by combining equations (36) and (38), giving

$$\tfrac{1}{2}J_r - \tfrac{3}{2}K_r + \frac{4}{(\beta-1)\,\tau}\frac{dK_r}{d\tau} - \frac{4}{(\beta-1)^2\tau^2}X_r = -\tfrac{3}{2}J_r + 5K_r - \tfrac{1}{2}K_l, \tag{54}$$

which reduces to

$$\frac{4}{(\beta-1)\,\tau}\frac{dK_r}{d\tau} - \frac{4}{(\beta-1)^2\tau^2}X_r = 2X_r + S. \tag{55}$$

Finally, by adding and subtracting equations (53) and (55) and using equation (44), we obtain

$$\tfrac{3}{2}T - \tfrac{1}{2}R + S = F_0\,c^{-2/(\beta-1)}\,[(\beta-1)\,\tau]^{(3-\beta)/(\beta-1)} \tag{56}$$

and

$$\frac{4}{(\beta-1)\,\tau}\frac{dS}{d\tau} + S = \left[\frac{3}{2} + \frac{4}{(\beta-1)^2\tau^2}\right]R - \tfrac{1}{2}T. \tag{57}$$

Treating equation (56) as an equation for R and substituting in equation (57), we find

$$\left[4 + \frac{12}{(\beta-1)^2\tau^2}\right]T = \frac{4}{(\beta-1)\,\tau}\frac{dS}{d\tau} - \left[2 + \frac{8}{(\beta-1)^2\tau^2}\right]S + F_0\,c^{-2/(\beta-1)}\{3\,[(\beta-1)\,\tau]^{(3-\beta)/(\beta-1)} + 8\,[(\beta-1)\,\tau]^{(5-3\beta)/(\beta-1)}\}. \tag{58}$$

In order to write equation (51) as a function of S alone, we require the derivative of R,

which, in turn, requires the derivative of T. These can be found by differentiating equations (57) and (58), respectively; thus,

$$\frac{dR}{d\tau} = 3\frac{dT}{d\tau} + 2\frac{dS}{d\tau} - 2(3-\beta)F_0 c^{-2/(\beta-1)}[(\beta-1)\tau]^{(4-2\beta)/(\beta-1)} \tag{59}$$

and

$$\begin{aligned}[(\beta-1)^2\tau^2+3]^2\frac{dT}{d\tau} &= [(\beta-1)^3\tau^3+3(\beta-1)\tau]\frac{d^2S}{d\tau^2} \\ &\quad -\tfrac{1}{2}\{(\beta-1)^4\tau^4+[7+2(\beta-1)](\beta-1)^2\tau^2+18-16\beta\}\frac{dS}{d\tau} \\ &\quad +(\beta-1)^2\tau S+\tfrac{1}{4}F_0 c^{-2/(\beta-1)}\{[-3\beta+9][(\beta-1)\tau]^{2\beta/(\beta-1)} \\ &\quad +[-15\beta+49][(\beta-1)\tau]^{2/(\beta-1)}+24(3-\beta)[(\beta-1)\tau]^{(4-2\beta)/(\beta-1)}\}.\end{aligned} \tag{60}$$

Substituting in equation (51), we find, after some further simplification,

$$\begin{aligned}[(\beta-1)^4\tau^4+3(\beta-1)^2\tau^2]\frac{d^2S}{d\tau^2} &- \{2[(\beta-1)\tau]^3+[12-6\beta][(\beta-1)\tau]\}\frac{dS}{d\tau} \\ &-\tfrac{1}{4}\{5[(\beta-1)\tau]^4+[29-2\beta][(\beta-1)\tau]^2+(30+6\beta)\}S \\ &=\tfrac{1}{8}\{[(\beta-1)\tau]^{(3\beta-1)/(\beta-1)}+[11-4\beta][(\beta-1)\tau]^{(\beta+1)/(\beta-1)} \\ &\quad +12[(\beta-1)\tau]^{(3-\beta)/(\beta-1)}\}c^{-2/(\beta-1)}F_0 .\end{aligned} \tag{61}$$

This equation must be solved under the boundary conditions that all quantities vanish at $\tau = 0$ and that, at the lower boundary of the atmosphere (the photosphere), the outward radiation is unpolarized and obeys an assigned law of darkening.

If S is known as a function of τ, T may be found from equation (58); $K_l + K_r$ then follows from integrating equation (44). Since $K_l + K_r$ and $K_l - K_r$ are then known, we also know K_l and K_r separately.

From equation (56), we find R. Since both $X_l + X_r$ and $X_l - X_r$ are then known, X_l and X_r are known separately. Combining the appropriate K's and X's according to equations (34), we find J_l and J_r. From equations (42) and (45) H_l and H_r may be found. Finally, the source functions may be written as follows:

$$\mathfrak{J}_l = \tfrac{3}{4}[2(J_l - K_l) + \mu^2(3K_l - 2J_l + J_r)] \tag{62}$$

and

$$\mathfrak{J}_r = \tfrac{3}{4}(J_r + K_l); \tag{63}$$

and the emergent intensities may be found by properly integrating the source functions along the line of sight.

V. INTEGRATION OF THE SOURCE FUNCTIONS

Quite generally, the intensity at a point, s_0, is given by

$$I(s_0) = \int_{-\infty}^{s_0} \mathfrak{J}(s)\, e^{-\int_s^{s_0} \kappa\rho\, ds}\, \kappa\rho\, ds, \tag{64}$$

where ds is an increment of length. However, in the case under consideration the line of sight through the atmosphere may be described by the length of a perpendicular, p, from the center of the star to the line. Any point on the line may be specified by the angle,

ϕ, between the line and the center of the star measured counterclockwise from the line (Fig. 1). Since $ds = -p \operatorname{cosec}^2 \phi d\phi$, we may now write

$$I(\theta, p) = \int_{\theta}^{\theta_1} e^{-\int_{\theta}^{\phi} p\kappa\rho \operatorname{cosec}^2 \phi d\phi} \Im(\phi, p)\, p\kappa\rho \operatorname{cosec}^2 \phi d\phi$$
$$= e^{p\int_0^{\theta} \kappa\rho \operatorname{cosec}^2 \theta d\theta} \int_{\theta}^{\theta_1} e^{-p\int_0^{\phi} \kappa\rho \operatorname{cosec}^2 \phi d\phi} \Im(\phi, p)\, p\kappa\rho \operatorname{cosec}^2 \phi d\phi, \tag{65}$$

where θ_1 is the largest value of ϕ along the line of sight. It is clear that we may define two

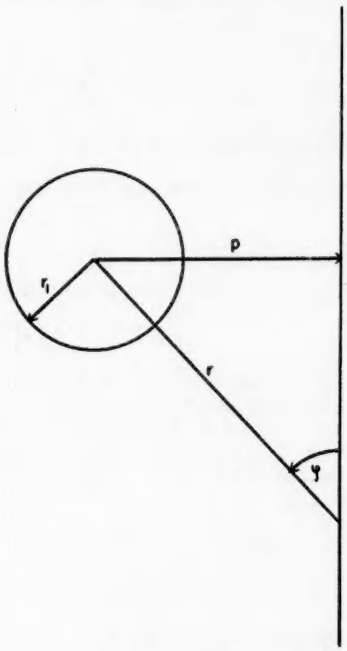

FIG. 1.—The geometry of the integration along the line of sight

integrals of this type, since, if r_1 is the radius of the photosphere, $\theta_1 = \pi$ for $p > r_1$ and $\theta_1 = \sin^{-1}(p/r)$ for $p < r_1$. For the emergent intensity, we set θ equal to zero and obtain

$$I_1(0, p) = \left[\int_0^{\pi} e^{-p\int_0^{\phi} \kappa\rho \operatorname{cosec}^2 \phi d\phi} \Im(\phi, p)\, p\kappa\rho \operatorname{cosec}^2 \phi d\phi\right]_{p>r_1} \tag{66}$$

and

$$I_2(0, p) = \left[\int_0^{\sin^{-1}(p/r_1)} e^{-p\int_0^{\phi} \kappa\rho \operatorname{cosec}^2 \phi d\phi} \Im(\phi, p)\, p\kappa\rho \operatorname{cosec}^2 \phi d\phi\right]_{p<r_1}. \tag{67}$$

The integrals I_1 and I_2 must be evaluated separately for $\Im_l$ and $\Im_r$.

There is another contribution to the intensity for $p < r_1$ due to the transmitted light

of the photosphere. If we write the law of darkening for the unpolarized photospheric radiation at $\tau = \tau_1$ as

$$I_l = I_r = \tfrac{1}{2}\,(I^{(0)} + I^{(1)} \cos\theta)\,, \tag{68}$$

this contribution is the same for the l and r components and is given by

$$I_3(0, p) = \tfrac{1}{2}\, e^{-p\int_0^{\theta_1} \kappa\rho \cos\phi^3 d\phi}\,(I^{(0)} + I^{(1)} \cos\theta_1)\,. \tag{69}$$

VI. THE P_3 APPROXIMATION FOR $\kappa\rho \propto r^{-2}$

We shall now consider the case $\beta = 2$. Equation (61) now becomes

$$(\tau^4 + 3\tau^2)\frac{d^2S}{d\tau^2} - 2\tau^3\frac{dS}{d\tau} - \tfrac{1}{4}\,(5\tau^4 + 25\tau^2 + 42)\,S = \tfrac{1}{8}\,(\tau^5 + 3\tau^3 + 12\tau)\,c^{-2}F_0\,. \tag{70}$$

This equation was solved by combining a particular solution of the equation

$$(\tau^4 + 3\tau^2)\frac{d^2S^{(A)}}{d\tau^2} - 2\tau^3\frac{dS^{(A)}}{d\tau} - \tfrac{1}{4}(5\tau^4 + 25\tau^2 + 42)\,S^{(A)} = \tfrac{1}{8}\,(\tau^5 + 3\tau^3 + 12\tau)\,, \tag{71}$$

with a solution of the homogeneous equation

$$(\tau^4 + 3\tau^2)\frac{d^2S^{(B)}}{d\tau^2} - 2\tau^3\frac{dS^{(B)}}{d\tau} - \tfrac{1}{4}\,(5\tau^4 + 25\tau^2 + 42)\,S^{(B)} = 0\,, \tag{72}$$

in the form

$$S = c^{-2}F_0 S^{(A)} + bS^{(B)}\,, \tag{73}$$

where b is an arbitrary constant and $S^{(A)}$ and $S^{(B)}$ satisfy the boundary conditions at $\tau = 0$. Both solutions were found as series from $\tau = 0$ and continued beyond $\tau = 0.8$ by numerical methods.[6]

By substituting a power series in equation (71) and equating coefficients, we find that a particular solution of the equation is given by the following series expansion for small values of τ:

$$\begin{aligned} S^{(A)} = &-0.142857\tau - 0.107143\tau^3 - 0.014610\tau^5 \\ &- 0.000685\tau^7 - 0.000016\tau^9 - \ldots\,. \end{aligned} \tag{74}$$

A series beginning with a term in τ was chosen so that $S^{(A)}$ would vanish at $\tau = 0$, as required by the boundary conditions of the problem. All coefficients of even powers of τ are zero, and the coefficient of τ^m for $m > 5$ follows the recursion formula,

$$a_m = -\frac{(4m^2 - 28m + 5)\,a_{m-2} - 5a_{m-4}}{12m^2 - 12m - 42}\,. \tag{75}$$

The solution, $S^{(B)}$, of the homogeneous equation can be found in the following manner: Writing

$$S^{(B)} = \tau^s + b_{s+2}\tau^{s+2} + b_{s+4}\tau^{s+4} + \ldots\,, \tag{76}$$

we find that the indicial equation is

$$12s^2 - 12s - 42 = 0\,, \tag{77}$$

from which it follows that $s = 2.436492$, or -1.436492. We may immediately eliminate

[6] H. Levy and E. A. Baggott, *Numerical Studies in Differential Equations* (London: Watts & Co., 1934), p. 158.

the negative solution, since one of the boundary conditions requires that $S^{(B)}$ vanish at $\tau = 0$. With $s = 2.436492$, we find the following expansion for small values of τ:

$$S^{(B)} = \tau^s + 0.216329\tau^{s+2} + 0.012949\tau^{s+4} + 0.000365\tau^{s+6} + 0.000006\tau^{s+8} + \ldots . \tag{78}$$

The higher coefficients follow a recursion formula similar to equation (75).

The $S^{(A)}$ and $S^{(B)}$ solutions may now be used to compute corresponding source functions $\mathfrak{J}_l^{(A)}$, $\mathfrak{J}_r^{(A)}$ and $\mathfrak{J}_l^{(B)}$, $\mathfrak{J}_r^{(B)}$ by the procedure following equation (61).

VII. APPLICATION OF BOUNDARY CONDITIONS

We may now apply the boundary conditions at the photosphere to determine $c^{-2}F_0$ and b. We make use of the definitions of H and K:

$$H_l = H_l^{(A)} c^{-2}F_0 + H_l^{(B)} b = \sum_i a_i \mu_i I_{l,i}$$

and

$$K_l = K_l^{(A)} c^{-2}F_0 + K_l^{(B)} b = \sum_i a_i \mu_i^2 I_{l,i} . \tag{79}$$

There is a similar set of equations for the r component. The roots of P_3 are $0, \pm(0.6)^{1/2}$. Therefore, the summations in the above equations refer to three streams: one inward, one outward, and one tangential. The tangential stream contributes nothing to the above summations because its μ is zero. The outward stream at $\tau = \tau_l$ is given by the darkening law,

$$I_l[+(0.6)^{1/2}] = \tfrac{1}{2}[I^{(0)} + (0.6)^{1/2} I^{(1)}] . \tag{80}$$

The inward stream is not known, but it may be eliminated by adding K_l and $(0.6)^{1/2}H_l$. Similarly, K_r and $(0.6)^{1/2}H_r$ may be combined to eliminate the inward stream in the r component. The resulting equations may be solved for $c^{-2}F_0$ and b. These constants contain $I^{(0)} + (0.6)^{1/2}I^{(1)}$ as a factor. As a result, the source functions and therefore I_1 and I_2 involve the same factor.

Now that $c^{-2}F_0$ and b are known, $\mathfrak{J}_l^{(A)}$, $\mathfrak{J}_l^{(B)}$ and $\mathfrak{J}_r^{(A)}$, $\mathfrak{J}_r^{(B)}$ may be combined to form $\mathfrak{J}_l$ and $\mathfrak{J}_r$.

VIII. INTEGRATIONS FOR THE CASE $\kappa\rho \propto r^{-2}$

Since

$$\kappa\rho = \frac{c}{r^2} = \frac{c}{p^2 \operatorname{cosec}^2 \phi} , \tag{81}$$

the integrations of the source functions may be written as

$$I_1 = \frac{c}{p} \int_0^{\pi} e^{-c\phi/p} \mathfrak{J}(\phi, p)\, d\phi$$

and

$$I_2 = \frac{c}{p} \int_0^{\sin^{-1}(p/r_1)} e^{-c\phi/p} \mathfrak{J}(\phi, p)\, d\phi . \tag{82}$$

Further

$$I_3 = \tfrac{1}{2} e^{-c\theta_1/p} (I^{(0)} + I^{(1)} \cos\theta_1) , \tag{83}$$

where

$$\theta_1 = \sin^{-1} \frac{p}{r_1} . \tag{84}$$

Evaluating in terms of the total optical depth of the atmosphere, τ_1, and the radius of the photosphere, r_1, we write

$$\tau_1 = \frac{c}{r_1} \quad \text{and} \quad p = \xi r_1 . \tag{85}$$

We may now write

$$I_1 = \frac{\tau_1}{\xi} \int_0^{\pi} e^{-\tau_1 \phi/\xi} \Im(\phi, \xi)\, d\phi \tag{86}$$

and

$$I_2 = \frac{\tau_1}{\xi} \int_0^{\sin^{-1}\xi} e^{-\tau_1 \phi/\xi} \Im(\phi, \xi)\, d\phi . \tag{87}$$

Further,

$$\tau = \frac{\tau_1}{\xi} \sin \phi . \tag{88}$$

If we substitute $\mu = \cos \phi$, I_1 may be written as

$$I_1(\xi) = \frac{\tau_1}{\xi} \int_{-1}^{+1} e^{-\tau_1 \phi/\xi} \operatorname{cosec} \phi \, \Im(\phi, \xi)\, d\mu . \tag{89}$$

We may evaluate this integral as a Gaussian sum

$$I_1(\xi) = \frac{\tau_1}{\xi} \sum_i a_i e^{-\tau_1 \phi i/\xi} \operatorname{cosec} \phi_i \Im(\phi_i, \xi) . \tag{90}$$

In order to bring I_2 to a similar form, we transform the co-ordinates as follows:

$$\gamma = \frac{\pi}{\sin^{-1}\xi} \phi ; \qquad \eta = \cos \gamma ; \qquad t = \tau_1 \frac{\sin^{-1}\xi}{\pi} . \tag{91}$$

Then

$$I_2 = \frac{t}{\xi} \int_{-1}^{+1} e^{-t\gamma/\xi} \Im(\gamma, \xi) \operatorname{cosec} \gamma \, d\eta , \tag{92}$$

or, writing as a Gaussian sum,

$$I_2 = \frac{t}{\xi} \sum_i a_i e^{-t\gamma i/\xi} \Im(\gamma_i, \xi) \operatorname{cosec} \gamma_i . \tag{93}$$

IX. NUMERICAL RESULTS

I_1 and I_2 were evaluated, using the roots and weights of P_5 and checking frequently with corresponding values, using P_7. In no case was the discrepancy greater than 2 per cent, and more often it was less.

Integrations were carried through for $\tau_1 = 0.5$, 1.0, and 2.0. Tables 2, 3, and 4 give I_1, I_2, and I_3 and the degree of polarization, δ, defined as

$$\delta = \frac{I_r - I_l}{I_r + I_l} \times 100 . \tag{94}$$

The table of I_2 must be used with the table of I_3 to determine observed intensities and polarization for $p < r_1$.

The results are plotted in Figures 2 and 3. Although I_3 is not plotted separately, the dashed curves represent total intensities ($I_2 + I_3$) for the special case $I^{(1)} = 0$ (no limb darkening in the photospheric radiation).

TABLE 2

COMPONENTS OF I_1 IN UNITS OF $I^{(0)}+(0.6)^{1/2}I^{(1)}$

ξ	$\tau_1=0.5$			$\tau_1=1.0$			$\tau_1=2.0$		
	r	l	δ	r	l	δ	r	l	δ
1.00..	0.3442	0.2199	22.02	0.3308	0.2244	19.17	0.2028	0.1570	12.73
1.25..	.2489	.1602	21.66	.2593	.1732	19.91	.1729	.1277	15.05
1.50..	.1881	.1219	21.37	.2083	.1383	20.22	.1488	.1065	16.58
1.75..	.1471	.09574	21.16	.1709	.1130	20.37	.1293	.09057	17.60
2.00..	.1182	.07717	20.99	.1425	.09419	20.42	.1133	.07822	18.30
2.25..	.09697	.06350	20.86	.1206	.07970	20.44	.1000	.06838	18.79
2.50..	.08099	.05315	20.75	.1034	.06830	20.44	.08890	.06035	19.13
2.75..	.06866	.04514	20.66	.08957	.05919	20.43	.07951	.05370	19.38
3.00..	.05894	.03880	20.60	.07832	.05178	20.41	.07151	.04812	19.56
3.25..	.05114	.03371	20.54	.06906	.04567	20.39	.06464	.04336	19.70
3.50..	.04479	.02956	20.49	.06134	.04058	20.37	.05870	.03930	19.80
3.75..	.03955	.02612	20.44	.05484	.03630	20.35	.05353	.03578	19.87
4.00..	.03519	.02326	20.41	.04932	.03266	20.32	.04900	.03271	19.93
4.5...	.02837	.01877	20.35	.04049	.02683	20.28	.04150	.02766	20.02
5.0...	.02335	.01547	20.31	.03385	.02244	20.27	.03558	.02369	20.07
5.5...	.01956	.01297	20.27	.02871	.01904	20.25	.03084	.02052	20.09
6.0...	.01662	.01102	20.24	.02465	.01636	20.22	.02697	.01794	20.11
6.5...	.01430	.009489	20.20	.02140	.01420	20.20	.02379	.01582	20.12
7.0...	.01243	.008253	20.19	.01875	.01245	20.19	.02113	.01405	20.13
7.5...	.01090	.007243	20.17	.01656	.01100	20.18	.01890	.01256	20.13
8.0...	.009643	.006408	20.15	.01473	.009788	20.16	.01700	.01130	20.13
8.5...	.008589	.005710	20.14	.01319	.008766	20.15	.01537	.01022	20.13
9.0...	.007698	.005118	20.13	.01188	.007897	20.15	.01396	.009280	20.14
9.5...	.006940	.004616	20.12	.01076	.007150	20.14	.01274	.008470	20.13
10.0...	0.006288	0.004182	20.11	0.009783	0.006505	20.13	0.01167	0.007760	20.12

TABLE 3

COMPONENTS OF I_2 IN UNITS OF $I^{(0)}+(0.6)^{1/2}I^{(1)}$

ξ	$\tau_1=0.5$			$\tau_1=1.0$			$\tau_1=2.0$		
	r	l	δ	r	l	δ	r	l	δ
0.1.....	0.1162	0.1160	0.11	0.1513	0.1510	0.10	0.1365	0.1363	0.08
0.2.....	.1170	.1159	0.46	.1521	.1508	0.42	.1370	.1361	0.33
0.3.....	.1183	.1159	1.05	.1536	.1506	0.96	.1379	.1358	0.76
0.4.....	.1203	.1158	1.90	.1557	.1504	1.73	.1391	.1353	1.36
0.5.....	.1231	.1159	3.04	.1586	.1501	2.75	.1408	.1348	2.15
0.6.....	.1270	.1160	4.51	.1627	.1500	4.07	.1430	.1343	3.16
0.7.....	.1324	.1165	6.39	.1683	.1500	5.74	.1461	.1338	4.41
0.8.....	.1403	.1176	8.81	.1764	.1507	7.87	.1505	.1336	5.96
0.9.....	.1537	.1205	12.12	.1898	.1530	10.71	.1573	.1342	7.92
1.0.....	0.2063	0.1395	19.33	0.2387	0.1712	16.47	0.1798	0.1433	11.29

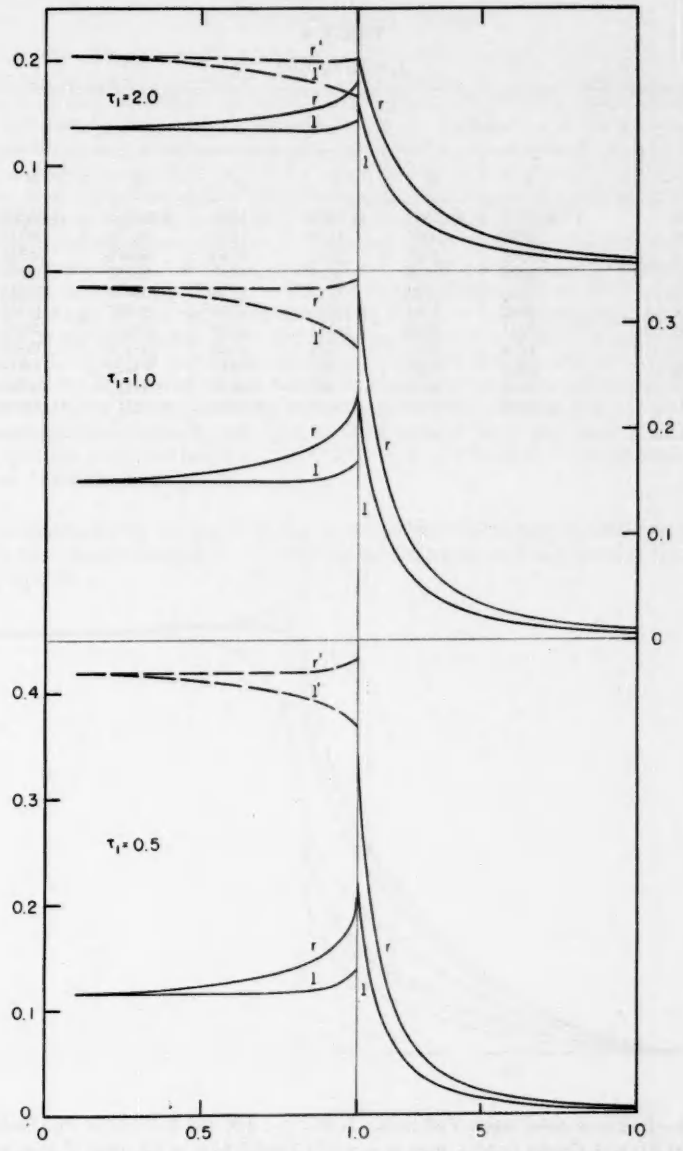

FIG. 2.—*Full curves:* I_2 $(0 < \xi < 1.0)$ and I_1 $(1 < \xi < 10)$ in units of $I^{(0)} + (0.6)^{1/2} I^{(1)}$. *Dashed curves:* $I_2 + I_3$ for $I^{(1)} = 0$. The r and l components are indicated. Note the scale changes in both co-ordinates.

TABLE 4

$I_3 = AI^{(0)} + BI^{(1)}$

ξ	$\tau_1 = 0.5$		$\tau_1 = 1.0$		$\tau_1 = 2.0$	
	A	*B*	*A*	*B*	*A*	*B*
0.0	0.3033	0.3033	0.1839	0.1839	0.06767	0.06767
0.1	.3030	.3015	.1836	.1827	.06744	.06710
0.2	.3022	.2961	.1827	.1790	.06676	.06541
0.3	.3009	.2870	.1811	.1727	.06558	.06256
0.4	.2989	.2740	.1787	.1638	.06388	.05855
0.5	.2962	.2565	.1755	.1520	.06157	.05332
0.6	.2925	.2340	.1711	.1369	.05854	.04683
0.7	.2874	.2052	.1652	.1180	.05456	.03896
0.8	.2801	.1680	.1569	.0941	.04922	.02953
0.9	.2684	.1170	.1441	.0628	.04152	.01810
1.0	0.2280	0.0000	0.1039	0.0000	0.02161	0.00000

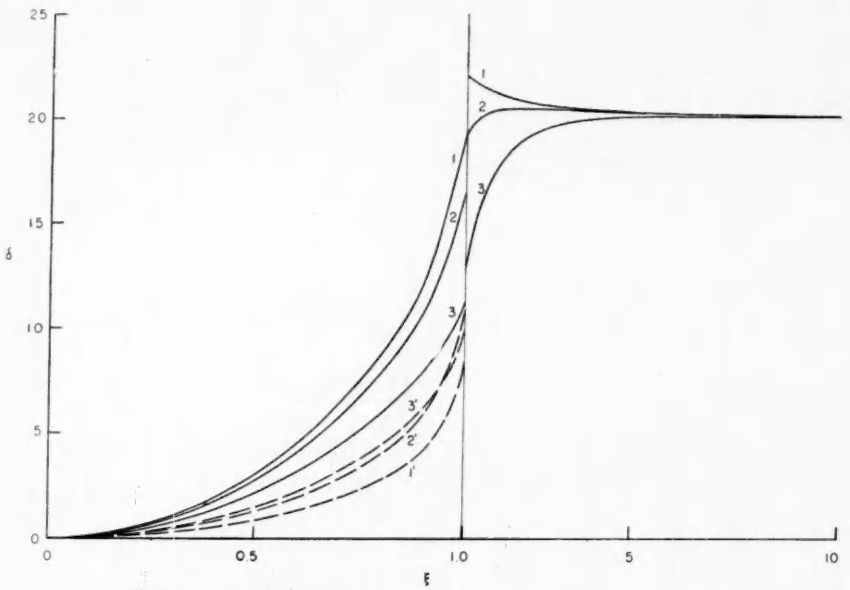

FIG. 3.—Degree of polarization. *Full curves:* I_2 $(0 < \xi < 1.0)$ and I_1 $(1 < \xi < 10)$. *Dashed curves:* $I_2 + I_3$ for $I^{(1)} = 0$. Curves *1* and *1'* refer to $\tau_1 = 0.5$; *2* and *2'* to $\tau_1 = 1.0$; *3* and *3'* to $\tau_1 = 2.0$. The meeting of curves *1* and *2* is accidental. Note the scale change at $\xi = 1.0$.

X. DISCUSSION OF THE RESULTS

In every case the degree of polarization of the scattered light (I_2) increases steadily from zero at the center toward the edge of the photosphere. The r component of I_2 has a greater variation than the l and always increases, whereas the l component decreases slightly before increasing. The degree of polarization at the edge of the photosphere is 19, 16, and 11 per cent in the scattered light for $\tau_1 = 0.5$, 1.0, and 2.0, respectively. These values are reduced when the total light is considered because of the transmitted unpolarized light, I_3. It should be recalled that 11 per cent is the degree of polarization found by Chandrasekhar at the limb in the plane-parallel semi-infinite case.

In the atmosphere observed beyond the edge of the photosphere (I_1), the r and l components decrease rapidly, the r component remaining the greater, but the degree of polarization varies only slightly. For $\tau_1 = 0.5$, the polarization falls from 22 per cent at the edge to 20 per cent at ten radii from the center. For $\tau_1 = 1.0$, the polarization increases from 19 to 20 per cent before decreasing slightly; while for $\tau_1 = 2.0$, the polarization increases from 13 to 20 per cent before decreasing. In every case the degree of polarization is approximately 20 per cent at ten radii from the center and is decreasing slowly.

It may also be noted that there is a tendency to decrease the discontinuity at the edge of the photosphere between I_1 and I_2 as the total optical depth increases. This is due to the fact that the contribution to I_1 at $\xi = 1$ for $\phi > \pi/2$ becomes unimportant, i.e., we cannot see through the envelope.

In conclusion, I wish to thank Dr. S. Chandrasekhar for suggesting this problem and for many stimulating discussions. I am also indebted to my wife for drawing the accompanying figures.

STRUCTURE OF THE CAMERON BANDS OF CARBON MONOXIDE

K. NARAHARI RAO
Yerkes Observatory
Received May 18, 1949

ABSTRACT

The Cameron bands ($^3\Pi - {}^1\Sigma$) of carbon monoxide were photographed in emission under high dispersion. From a study of their structure the following vibrational constants are derived for the ground state of the *CO* molecule: $\omega_e = 2170.21$ cm^{-1}; $\omega_e x_e = 13.461$ cm^{-1}; $\omega_e y_e = 0.0308$ cm^{-1}. The rotational constants B_v for the levels $v'' = 0$–4 can be represented by a formula of the form $B_v = B_e - \alpha(v + \frac{1}{2})$. Finally, the present knowledge regarding the molecular constants for the ground state of the *CO* molecule is summarized.

I. INTRODUCTION

A band system of *CO*, lying between λ 2100 and λ 2600, was discovered by Cameron[1] in emission in a discharge through a tube filled with high-pressure neon and traces of carbon monoxide. It was subsequently observed by Hopfield[2] in absorption. As was first suggested by Johnson[3] and later confirmed by others, this is a singlet-triplet intercombination system and is due to the transition from the lower state of the third positive group, $a^3\Pi$, to the ground state, $X^1\Sigma$, of the *CO* molecule. The (0, 0) and (1, 0) bands of this system were studied in absorption by Gerö, Herzberg, and Schmid,[4] who for the first time gave a rotational analysis of these two bands and derived more accurate values than existed at the time for the rotational constants of the ground state of the carbon monoxide molecule. Later, Gerö[5] obtained the (0, 0), (0, 1), (0, 2), (0, 3), (1, 3), (1, 4), and (2, 5) bands in emission and attempted their fine-structure analysis. More recently, Hansche[6] studied intensity variations in these bands excited in the electrodeless discharge and by electron impact.

The Cameron bands have for their lower state the ground state of the carbon monoxide molecule, and therefore the study of their fine structure gives us very valuable information regarding the rotational and vibrational constants of this state. In addition, using these results, it is possible to predict the positions of the lines in the fundamental and the overtone bands of *CO* in the infrared, which are convenient standards in infrared work and for which the data in the literature suffer from some systematic errors.[7] Finally, when the combination differences formed from the wave numbers published by Gerö[5] were examined, it was found that errors had crept into his data on account of either wrong choice of comparison lines or other causes. For these reasons it was decided to reinvestigate these bands in emission and undertake their fine-structure analysis.

II. EXPERIMENTAL

As has already been mentioned, the electronic transition involved in these bands is $^3\Pi - {}^1\Sigma$. The probability of a transition of this kind is very low. A radiative transition is possible if the *CO* in the $^3\Pi$ state has a long enough time before impact, either with the

[1] W. H. B. Cameron, *Phil. Mag.*, **1**, 405, 1926.

[2] J. J. Hopfield, *Phys. Rev.*, **29**, 356, 1927.

[3] R. C. Johnson, *Nature*, **117**, 376, 1926.

[4] L. Gerö, G. Herzberg and R. Schmid, *Phys. Rev.*, **52**, 467, 1937.

[5] L. Gerö, *Zs. f. Phys.*, **109**, 204, 1938.

[6] G. E. Hansche, *Phys. Rev.*, **57**, 289, 1940; **58**, 1075, 1940.

[7] G. Herzberg and K. N. Rao, *J. Chem. Phys.* (in press).

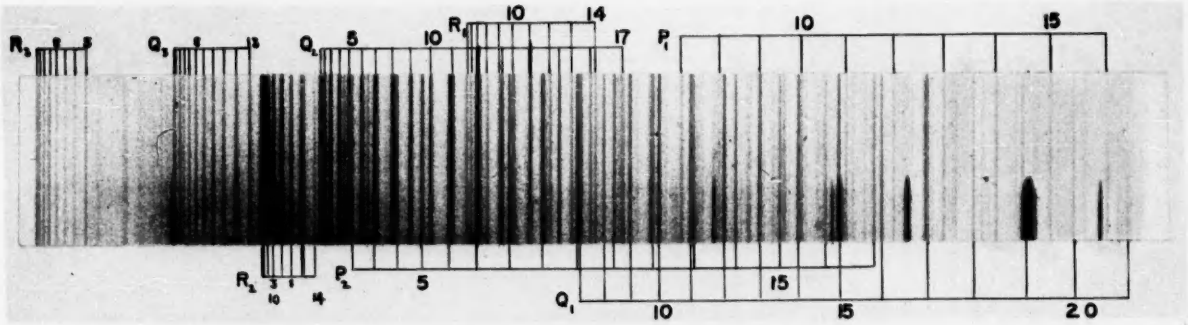

FIG. 1.—The (0, 1) Cameron band of carbon monoxide in emission

walls of the tube or with other *CO* molecules. So these bands occur only under special conditions in emission.[1,5,6]

The light-source adopted was a water-cooled Geissler tube made of Pyrex glass and provided with graphite electrodes. The tube had a diameter of 1.5 cm and a length of 70 cm between the electrodes. It was set up so that observations could be made in the "end-on" position through a quartz window. The tube was filled with pure neon at a pressure of 2–3 mm of mercury, to which a very small amount of oxygen was added. Under the action of the discharge, the oxygen combined with the carbon in the electrodes and gave the requisite amount of *CO*. The Cameron bands were obtained with a current of about 50 mA and 7000 volts, supplied by a high-voltage transformer. Final exposures were taken with the 21-foot grating spectrograph of the spectroscopic laboratory of the Yerkes Observatory. Eastman 103*a*-O UV plates were used. The (0, 0) and (0, 1) bands were obtained in the fifth order (dispersion 0.5 A/mm) and the (0, 2), (0, 3), (1, 3), and (1, 4) bands in the fourth order (dispersion 0.625 A/mm). All these bands could be photographed at one time, that is, in a single exposure. Reasonably good spectrograms were obtained with an exposure time of 26 hours. The discharge tube was refilled at the end of each hour with a fresh mixture of oxygen and neon. The bands of the fourth positive system of *CO* which lie in the same region were comparatively weak. Figure 1 gives a reproduction of the (0, 1) band. The comparison spectrum is that of an iron arc. Measurements were made with a Gaertner comparator. Their relative accuracy is estimated to be about ± 0.003 A. Averages of four measurements (two direct and two reverse) of each of the bands were used for the evaluation. For the conversion to vacuum, the index of refraction of air as given in Kayser's *Tabelle der Schwingungszahlen* from the data of Meggers and Peters was used.

III. ROTATIONAL ANALYSIS

Figure 2 illustrates the nine branches that can be expected for a $^3\Pi - {}^1\Sigma$ transition according to the selection rule $\Delta J = 0, \pm 1$. A P, Q, and R branch occurs for each component $^3\Pi_0 - {}^1\Sigma$, $^3\Pi_1 - {}^1\Sigma$, and $^3\Pi_2 - {}^1\Sigma$, and they are designated by $P_1, Q_1, R_1; P_2, Q_2, R_2$; and P_3, Q_3, R_3, respectively. The usual methods for analyzing bands[8] were adopted in obtaining the branches of the bands and their numbering. Table 1 gives the wave numbers of the branches of all the bands measured. An asterisk indicates that the line is blended. Since the $^3\Pi$ state, at least for high J values, is near Hund's case *b*, the quantum number K has a meaning for the rotational levels of both the upper and the lower states. Gerö's measurements for the (0, 1) band are completely at variance with those given here. The consistency of the new measurements with the other bands leaves no doubt that Gerö's data for this band are incorrect.

Combination differences, $R_i(K-1) - P_i(K+1) = \Delta_2 F''(K)$, were formed for all the bands measured. These depend only on the lower state, and with the use of them the rotational constants for each of the vibrational levels of the ground state were obtained by standard graphical methods.[9] The results are given in Table 2. In the same table are also given the values obtained from a study of the rotation-vibration spectrum of carbon monoxide with long absorbing paths.[7] Here the values for $v = 0$ and $v = 4$ were derived from the fine-structure study of the (4, 0) infrared band of *CO*, and the intermediate ones by using the relation

$$B_v = B_e - \alpha\,(v + \tfrac{1}{2}), \qquad (1)$$

where B_e and α are constants. The values obtained from infrared investigations are, no doubt, superior to those derived from a study of the structure of the Cameron bands.

[8] See, e.g., G. Herzberg, *Molecular Spectra and Molecular Structure*, Vol. I: *Diatomic Molecules* (New York: Prentice-Hall Book Co., Inc., 1939), pp. 206–210.

[9] *Ibid.*, p. 198.

In the latter case the fourth decimal place may be in error by several units. However, the agreement between the two sets of results presented in Table 2 within the accuracy that can be attained in the present investigation shows that the B_v values can be represented by a relation of the form given in equation (1). This result will be used in a subsequent investigation while obtaining the predicted positions of the lines in the (1, 0), (2, 0), and (3, 0) infrared bands of *CO*.

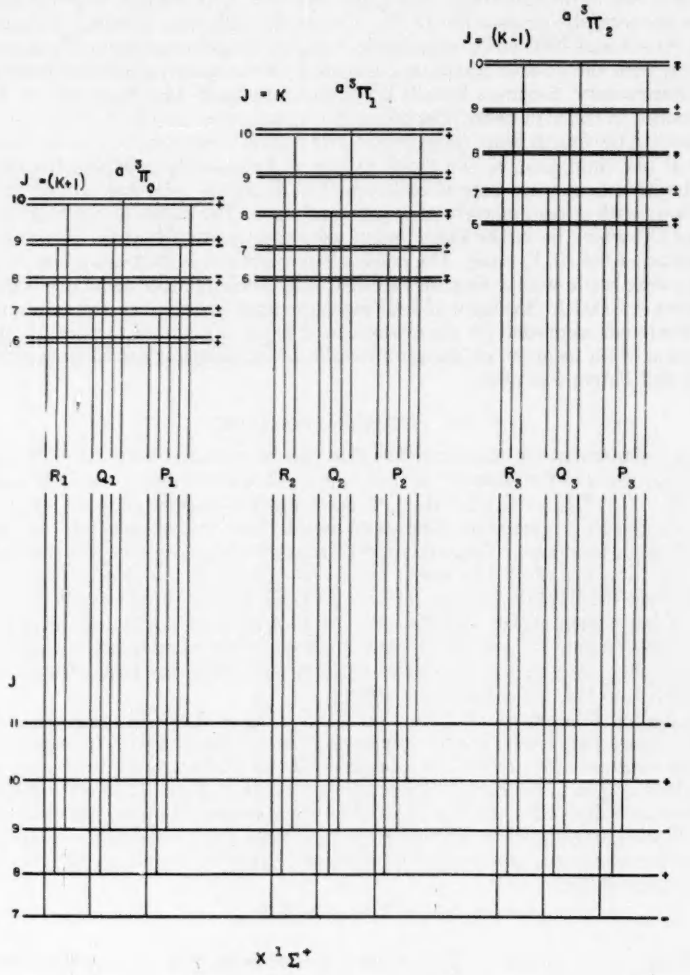

FIG. 2.—Energy-level diagram for the Cameron bands indicating the nine branches

TABLE 1

WAVE NUMBERS OF THE LINES IN THE CAMERON BANDS

K	P_1	Q_1	R_1	P_2	Q_2	R_2	P_3	Q_3	R_3
	(0, 0) Band $\nu_0 = 48473.97$ Cm^{-1}								
0	.....	.....	.....	.....	.....	48478.85*	.....	.....	.....
1	.....	.....	.....	.....	48474.57	481.36*	.....	.....	.....
2	.....	.....	.....	.....	473.59	483.60*	.....	.....	.....
3	.....	48431.68*	.....	48461.98	472.11	485.22*	.....	.....	.....
4	48415.31*	428.09*	.....	456.65*	469.94	486.40*	.....	.....	.....
5	407.63*	423.61*	.....	450.62	467.36*	.....	.....	.....	.....
6	399.40*	418.76	48439.12	444.12	464.26	.....	.....	48505.52	48530.92
7	390.36*	413.48*	437.19*	437.19*	460.76	.....	.....	503.99	532.75
8	381.35*	407.63*	434.75	429.59*	456.65	486.40*	.....	502.13	534.52
9	371.68	401.60	431.68*	421.81	452.19	485.22*	.....	500.01	535.74
10	361.62	394.67*	428.09*	413.48*	447.24	483.60*	.....	497.52	536.76
11	350.94	386.97	423.61*	404.58	441.77*	481.36*	.....	494.67	537.56*
12	339.74*	378.84	.....	395.14*	435.86	478.85*	.....	491.45	.....
13	327.76	370.14	.....	385.49	429.59*	.....	.....	.....	.....
14	.....	360.81	.....	375.17	422.72	.....	.....	.....	.....
15	.....	350.94*	.....	364.36	415.31*	.....	.....	.....	.....
16	.....	340.49	.....	353.23	407.63*	.....	.....	.....	.....
17	.....	329.37*	.....	341.66	399.40*	.....	.....	.....	.....
18	.....	318.11	.....	329.37*	390.36*	.....	.....	.....	.....
19	.....	306.42	.....	.....	.....	.....	.....	.....	.....
20	.....	293.57	.....	.....	.....	.....	.....	.....	.....
	(0, 1) Band $\nu_0 = 46330.59$ Cm^{-1}								
0	.....	.....	.....	.....	.....	46335.23	.....	.....	.....
1	.....	.....	.....	.....	46331.30	338.10*	.....	.....	.....
2	.....	.....	.....	46323.83	330.35	340.25*	.....	.....	.....
3	.....	.....	.....	318.83*	328.91	342.12*	.....	46365.13*	.....
4	.....	.....	.....	313.59	326.94	343.43*	.....	365.13*	46382.96
5	.....	.....	46297.49	307.78	324.56	344.40*	.....	363.80	385.78
6	.....	.....	296.48	301.48	321.68	.....	.....	362.94	388.38
7	46247.95*	46271.23	295.03*	295.03*	318.36	.....	.....	361.67	390.58
8	239.31*	265.83	292.71	287.61	314.60	344.40*	.....	360.12	392.56
9	229.94*	259.86	289.91	280.07*	310.42	343.43*	.....	358.32	394.19
10	220.29	253.19	286.67	271.96	305.81	342.12*	.....	356.19	395.50
11	210.01	245.91	282.88*	263.52	300.75	340.25*	.....	353.65	396.47
12	199.00	238.15	278.23	254.64*	295.03*	338.10*	.....	350.82	397.25
13	187.54	229.94*	273.24	245.25	289.33	335.66	.....	347.62	.....
14	175.42	221.10	267.80	235.52	282.88	.....	.....	.....	.....
15	162.97	211.74	.....	225.31	276.13	.....	.....	.....	.....
16	149.85	201.88	.....	214.86*	268.92	.....	.....	.....	.....
17	136.27	191.55*	.....	203.61	261.27*	.....	.....	.....	.....
18	122.16	180.71	.....	.....	.....	.....	.....	.....	.....
19	107.53	169.35	.....	.....	.....	.....	.....	.....	.....
20	092.46	157.54	.....	.....	.....	.....	.....	.....	.....
21	076.85	145.27	.....	.....	.....	.....	.....	.....	.....
22	060.74	132.50	.....	.....	.....	.....	.....	.....	.....
23	044.33	119.33	.....	.....	.....	.....	.....	.....	.....
24	027.50	105.59	.....	.....	.....	.....	.....	.....	.....

TABLE 1—*Continued*

K	P_1	Q_1	R_1	P_2	Q_2	R_2	P_3	Q_3	R_3
	(0, 2) Band $\nu_0 = 44213.85$ Cm^{-1}								
0	.....	.....	.....	.....	.....	44218.43	.....	.....	.....
1	.....	.....	.....	.....	44214.70	221.25	.....	.....	.....
2	.....	.....	.....	44207.10	213.72	223.67*	.....	.....	.....
3	.....	.....	.....	202.56*	212.37	225.69*	.....	.....	.....
4	.....	.....	.....	197.17	210.58	227.10*	.....	.....	.....
5	.....	.....	.....	191.62*	208.33	228.17*	.....	44247.68	.....
6	.....	44159.81*	.....	185.51	205.67	228.94*	.....	246.80	.....
7	.....	155.56	44179.07*	179.07*	202.56*	.....	.....	245.90	.....
8	.....	150.32	177.22*	172.03*	199.09	228.94*	.....	244.71	44277.15
9	44114.85	144.59	174.72	164.83*	195.20	228.17*	.....	243.20	279.05
10	105.62	138.34	172.03*	157.12*	190.94*	227.10*	.....	241.36	280.82
11	095.67	131.60*	168.24	149.05	186.31	225.69*	.....	239.29	.....
12	085.10	124.22	164.16*	140.58	181.26	223.67*	.....	236.82	.....
13	074.08	116.31	159.81*	131.60*	175.73	.....	.....	233.89*	.....
14	062.34*	108.00	154.71	122.37*	169.92	.....	.....	230.95	.....
15	050.44	099.22*	149.05*	112.79	163.60*	.....	.....	.....	.....
16	037.96	089.96	143.25	102.73	157.12*	.....	.....	.....	.....
17	024.90*	080.20	136.76	092.31	.....	.....	.....	.....	.....
18	.....	070.21*	129.26	081.39	.....	.....	.....	.....	.....
19	.....	059.46*	.....	.....	.....	.....	.....	.....	.....
	(0, 3) Band $\nu_0 = 42123.58$ Cm^{-1}								
0	.....	.....	.....	.....	.....	42128.07	.....	.....	.....
1	.....	.....	.....	.....	42124.44	130.93*	.....	.....	.....
2	.....	.....	.....	42116.98	123.58	133.51*	.....	.....	.....
3	.....	42080.28	.....	112.37	122.29	135.49*	.....	.....	.....
4	.....	077.57*	.....	107.27	120.64	137.13*	.....	.....	.....
5	.....	074.53	.....	101.91	118.56	138.28*	.....	.....	.....
6	.....	070.79	.....	095.99	116.15	139.88*	.....	42157.43	.....
7	.....	066.30	42089.83	089.83*	113.35	.....	.....	156.60	.....
8	.....	061.25*	088.53*	083.26*	110.14	.....	.....	155.53	.....
9	.....	056.00	086.11	076.23*	106.59	.....	.....	154.48	.....
10	.....	050.06	083.26*	068.86	102.66	.....	.....	153.01	.....
11	.....	043.61	080.28	061.25*	098.35	.....	.....	151.32	.....
12	.....	036.71	076.76*	053.12	093.73	.....	.....	149.26	.....
13	.....	029.29	072.69	044.70	088.53*	.....	.....	147.00	.....
14	.....	021.50	068.21	035.95	.....	.....	.....	144.37	.....
15	.....	013.29	063.25	026.91*	.....	.....	.....	141.37	.....
16	.....	004.42	057.98	017.27	.....	.....	.....	.....	.....
17	.....	.....	051.97	.....	.....	.....	.....	.....	.....
18	.....	.....	045.66	.....	.....	.....	.....	.....	.....
19	.....	.....	038.99	.....	.....	.....	.....	.....	.....

TABLE 1—*Continued*

K	P_1	Q_1	R_1	P_2	Q_2	R_2	P_3	Q_3	R_3
	(1, 3) Band $\nu_0 = 43838.19$ Cm^{-1}								
0						43842.80*			
1					43838.94	845.51*			
2				43831.50	838.04	847.73*			
3				826.80	836.63	849.63*			
4				821.63	834.85	851.05*			43890.49
5				816.01	832.58	852.03*			893.22*
6				810.29*	829.93	852.82*		43870.83	895.84
7				803.51	826.80			869.90	898.50*
8		43774.90		796.70	823.30	852.82*		868.54	900.68
9		769.14		789.41	819.46	852.03*		867.00	902.28*
10		762.87		781.71	815.12	851.05*		865.09	903.92
11		756.13*		773.62*	810.29*	849.63*		862.94	905.17*
12		748.68	43788.42	765.13	805.39	847.73*		860.44	906.10*
13		740.90*	783.64*	756.13*	799.83	845.51*		857.65	
14	43687.51	732.54	778.75	747.02*	793.90*	842.80*		854.40	
15	675.43	723.78*	773.62*	737.36	787.61				
16	663.07	714.41	767.18	727.01	780.79				
17	650.40	704.65	760.69	716.82*	773.62*				
18		694.47*	753.66	705.70*	766.24				
19		683.88*	747.02*	694.47*	758.28				
20			738.22		749.99				
21			728.67						
	(1, 4) Band $\nu_0 = 41774.18$ Cm^{-1}								
0						41778.72			
1					41774.95	781.58			
2				41767.50	774.15	783.98			
3				762.97	772.86	785.88			
4				757.99	771.18	787.62*			
5				752.68*	769.14	788.74*		41808.36	
6		41721.44		746.70	766.65	789.86*		807.68	
7		717.04	41740.41*	740.41*	763.80			806.82	
8		711.94*	738.87*	733.81*	760.59			805.86	
9		706.64	736.59	727.01*	757.00	789.86*		804.62	
10		700.72	733.81*	719.67	753.08*	788.74*		803.10	
11		694.28	730.61	711.94*	748.72	787.62*		801.25	
12		687.39	727.01*	703.77	744.03	786.61		799.20	
13		679.99	722.91	695.47	738.87*	784.83		796.86	
14		672.22	718.35	686.66		782.77		794.10	
15		663.89	713.18	677.43*		780.16		791.19	
16		655.11	707.97	668.09		777.25			
17				658.18					
18				647.77					

IV. VIBRATIONAL STRUCTURE

It is well known that the vibrational term values are given by

$$G(v) = \omega_e(v+\tfrac{1}{2}) - \omega_e x_e(v+\tfrac{1}{2})^2 + \omega_e y_e(v+\tfrac{1}{2})^3, \tag{2}$$

where ω_e is the vibrational frequency for infinitesimal amplitude and $\omega_e x_e \ll \omega_e$ and $\omega_e y_e \ll \omega_e x_e$. It is customary to write

$$\Delta G_{v+1/2} = G(v+1) - G(v). \tag{3}$$

The best method of obtaining the $\Delta G_{v+1/2}$ values is according to a procedure adopted by Jenkins and McKellar.[10] If, for example, vibrational transitions from $v' = 0$ of one

TABLE 2

ROTATIONAL CONSTANTS B_v (CM^{-1})

v	From Cameron Bands	From the (4, 0) Infrared Band of CO	v	From Cameron Bands	From the (4, 0) Infrared Band of CO
0	1.9226	1.92265	3	1.8695	1.87019
1	1.9053	1.90516	4	1.8531	1.85271
2	1.8872	1.88768			

electronic state to $v'' = 0$ and $v'' = 1$ of another electronic state are considered, it is easy to derive

$$\begin{aligned}&[Q^{(0,0)}(J) - Q^{(0,1)}(J)] \quad \text{or} \quad [R^{(0,0)}(J) - R^{(0,1)}(J)]\\ &\text{or} \quad [P^{(0,0)}(J) - P^{(0,1)}(J)] = \Delta G''_{1/2} + (B''_1 - B''_0)J(J+1),\end{aligned} \tag{4}$$

neglecting the contribution of the terms in D, which is very small in this case. The superscript (0, 0) or (0, 1) is used to indicate the particular vibrational transition considered. When the differences of the wave numbers of lines given on the left-hand side of equation (4) are plotted against $J(J+1)$, a straight line results. From its intercept on the ordinate axis, $\Delta G_{1/2}$ of the lower state can be derived, and from the slope a value for $(B''_1 - B''_0)$. Following a similar procedure for the (0, 1) and (0, 2) transitions, we obtain $\Delta G_{3/2}$, that is, the separation of the vibrational levels 1 and 2 of the lower state, and $(B''_2 - B''_1)$. Average values of the differences of corresponding unblended lines in the P, Q, and R branches were plotted against $J(J+1)$. On account of the fact that the observations did not reach large J values, the slopes of these plots could not be determined with the desired accuracy. But it is felt that the $\Delta G_{v+1/2}$ values are accurate within ± 0.03 cm^{-1}. Table 3 gives these vibrational quanta. If one adds these quanta, one obtains

$$\sum_{v=0}^{v=3} \Delta G''_{v+1/2} = 8414.40 \text{ cm}^{-1},$$

which should be compared to $\nu_0 = 8414.46$ cm^{-1} of the (4, 0) infrared band of CO. The difference is probably due to a constant shift of the lines in the Cameron bands relative to the comparison spectrum during the long exposure.

[10] F. A. Jenkins and A. McKellar, *Phys. Rev.*, **42**, 464, 1932.

Next, the constants ω_e, $\omega_e x_e$, and $\omega_e y_e$, in equation (2) were computed, and the following formula was derived for the vibrational term values of the ground state of *CO:*

$$G(v) = 2170.21\,(v+\tfrac{1}{2}) - 13.461\,(v+\tfrac{1}{2})^2 + 0.0308\,(v+\tfrac{1}{2})^3 + \ldots. \quad (5)$$

In determining these vibrational constants, equal weight was given to the value of

$$\sum_{v=0}^{v=3} \Delta G''_{v+1/2}$$

and the ν_0 (4, 0) (see above), that is,

$$\sum_{v=0}^{v=3} \Delta G''_{v+1/2} = 8414.43 \text{ cm}^{-1}$$

was used.

There is an alternative way of obtaining the separations of the vibrational levels,

TABLE 3

VIBRATIONAL QUANTA FOR THE GROUND STATE OF THE *CO* MOLECULE

v	$\Delta G''_{v+1/2} = G''(v+1) - G''(v)$ Cm^{-1}
0	2143.38
1	2116.74
2	2090.27
3	2064.01

TABLE 4

Ground state $^1\Sigma$:		*Upper state* $^3\Pi$:	
B_e	1.9313_9 cm^{-1}	ν_{00}	48473.97 cm^{-1}
a_e	0.01748_9 cm^{-1}	ν_e^*	48687.55 cm^{-1}
D_e	$6.4_3\times10^{-6}$ cm^{-1}	$\Delta G_{1/2}$	1714.61 cm^{-1}
β_e	$+0.0_4\times10^{-6}$ cm^{-1}		
r_e	$1.1281_9\times10^{-8}$ cm		
ω_e	2170.21 cm^{-1}		
$\omega_e x_e$	13.461 cm^{-1}		
$\omega_e y_e$	$+0.0308$ cm^{-1}		

* This was evaluated by using the ν_{00} (the origin of the [0, 0] band) and $\Delta G'_{1/2}$ values given in Table 4 and $\omega'_e x'_e = 14.47$ cm^{-1} suggested by Birge (*Phys. Rev.* **28**, 1157, 1926).

namely, from the zero lines ν_0 of the Cameron bands which can be derived by plotting $\frac{1}{3}(Q_1+Q_2+Q_3)$ against $J(J+1)$, since, according to Budó,[11]

$$\tfrac{1}{3}(Q_1+Q_2+Q_3) = \nu_0 + (B'-B'')J(J+1) - (D'-D'')J^2(J+1)^2. \quad (6)$$

Using these and the vibrational quanta given in Table 3, the most probable values for the origins of the bands studied were evaluated. These are the ones that are given in Table 1. The difference between the origins of the two bands (0, 3) and (1, 3) gives a value 1714. 61 cm^{-1} for the vibrational quantum $\Delta G_{1/2}$ of the $a^3\Pi$ state.

The rotational and vibrational constants of the *CO* molecule derived in this and the previous paper[7] are summarized in Table 4.

The predicted positions of the lines in the rotation-vibration bands of *CO*, together with a discussion of the limitations involved in using them as possible wave-length standards in the infrared, will be given in a separate paper.

The author acknowledges his sincere thanks to the government of India for the award of a fellowship and to Dr. G. Herzberg, under whose supervision this work was carried out.

[11] A. Budó, *Zs. f. Phys.*, **98**, 437, 1936.

NOTES

A NOTE ON THE SPECTROGRAPHIC ORBITS OF HD 193576

In a recent paper[1] on the Wolf-Rayet spectroscopic binary HD 190918, O. C. Wilson has taken exception to certain conclusions of mine[2] regarding a somewhat similar Wolf-Rayet star, HD 193576. The question turns on the legitimacy of using blended wave lengths for those lines of the Pickering series of *He* II which nearly coincide with the Balmer series. Dr. Wilson sees no justification for this procedure, which I adopted on the advice of Dr. J. A. Pearce, alleging that the Pickering series is too weak with respect to the Balmer lines to cause appreciable distortion. This seems very doubtful, however.

The companion of the Wolf-Rayet star in the system HD 193576 is of spectral type O5.5 or O6. Recent work by R. M. Petrie[3] at Victoria has demonstrated that in the O-type stars the intensities of *He* II increase in the spectral sequence from O9 to O5, and the maximum, if any, seems at least as early as O5. From the quantitative spectrophotometric measurements on twenty O-type stars it was found that the ratio of the mean intensity of *He* II (λ 4200 and λ 4542) to the mean intensity of $H\delta$ and $H\gamma$ (found by subtracting the mean intensity of *He* II from the measured mean intensity of the blended lines) varied fairly regularly from 1.5 for O5 to 0.2 for O9. Since the value for O6 is about 0.9, it cannot be contended that the Pickering lines are of negligible intensity.

In the 55 plates examined in my own work, the *He* II lines λ 4200 and λ 4542, and often also λ 4026, were usually measurable. I made no attempt to measure the relative intensities, except to make estimates from the microphotometer tracing. From these estimates it appears that the mean relative intensity of the blended lines and the *He* II lines was about 55/31, giving a ratio for *He* II/*H* of about 1.3, in satisfactory agreement with the value found by Petrie for a star of this type.

E. S. KEEPING

UNIVERSITY OF ALBERTA
EDMONTON, ALBERTA
April 29, 1949

THE RADIAL VELOCITY OF ALPHA-VIRGINIS

In 1945 Dr. Carlos U. Cesco, at the McDonald Observatory, obtained a series of twenty coudé spectrograms of the spectroscopic binary α Virginis. Some of the spectrophotometric results have already been reported.[1] The present note deals with the radial velocities determined from microphotometer tracings, which show the comparison lines superimposed over the record of the star's spectrum. No attempt was made to measure the fainter component. For the stronger set of star lines the precision of the measurements is about ±3 km/sec, which compares favorably to the precision obtained on diffuse absorption lines by means of micrometer measures. The linear dispersion of the coudé plates varies from 2 A/mm at λ 4026 to 4 A/mm at λ 4472. The material is not sufficient to derive a reliable velocity-curve, but the following conclusions are indicated: (1) The

[1] *Ap. J.*, **109**, 76, 1949. [2] *Pub. Dom. Ap. Obs., Victoria*, Vol. **7**, No. 23, 1947.

[3] *Pub. Dom. Ap. Obs., Victoria*, Vol. **7**, No. 21, 1947.

[1] *Ap. J.*, **108**, 154, 1948.

period of 4.014160 days, found in 1934,[2] is still satisfactory. (2) The velocity-curve in 1945 was more symmetrical than in 1934. (3) The radial velocities derived from lines of different elements agree reasonably well at maximum of the velocity-curve and near the gamma velocity but disagree at minimum; it is not certain that this effect has a physical sig-

TABLE 1

RADIAL VELOCITIES OF α VIRGINIS

Group	Plate	Date 1945	U.T.	Phase (Days)	Observed Velocity (Km/Sec)	Computed Velocity (Km/Sec)
I	622	June 29	3^h03^m	1.168	+ 8	+ 4
	601	25	3 13	1.189	+ 13	+ 8
II	667	July 16	2 43	2.097	+111	+135
	657	12	2 42	2.110	+120	+136
	668	16	3 17	2.121	+118	+136
	658	12	3 08	2.124	+121	+136
	628	June 30	3 21	2.180	+122	+136
	605	26	3 19	2.193	+129	+136
III	673	July 17	2 41	3.096	− 9	− 11
	622	13	2 47	3.104	− 8	− 14
	639	5	3 04	3.155	− 9	− 23
	610	June 27	2 51	3.171	− 13	− 27
	611	27	3 17	3.192	− 25	− 31
	634	July 1	3 49	3.200	− 24	− 32
IV	652	10	2 52	0.017	−114	−115
	653	10	3 28	0.142	−121	−115
	645	6	4 31	0.201	−124	−112
	617	June 28	3 52	0.202	−117	−112
	596	24	4 20	0.236	−115	−111
	597	24	5 17	0.275	−102	−108

nificance. The departures for the four groups of plates listed in Table 1 are summarized in the accompanying tabulation.

Group	Departures in Km/Sec from Plate Means		
	H	*He* I (Singlets) λλ 4388, 4144	*He* I (Triplets) λλ 4026, 4121, 4472
I	0	+ 5	− 7
II	+ 5	+14	−13
III	+ 6	+16	−14
IV	+20	+ 6	−17

The phases in Table 1 were computed from the epoch of minimum radial velocity determined previously,[2] viz., JD 2426038.72. The computed velocity, in the last column, was derived from the elliptical elements determined in 1934. It is quite clear that the velocity-curve has changed and was almost symmetrical in 1945. Assuming a circular

[2] *Ap. J.*, **80**, 367, 1934.

orbit, we find, for 1945, $\gamma = +0.5$ km/sec, $K_1 = 121.5$ km/sec. The corresponding values of (O − C), not listed in Table 1, would justify our previous conclusion regarding the precision of the radial velocities.

SHU-KOO KAO
O. STRUVE

YERKES AND MCDONALD OBSERVATORIES
July 4, 1949

SODIUM D IN THE SPECTRUM OF METEORS

The presence of the sodium D line in emission in meteoric spectra raises the question whether the emitting atoms may be of atmospheric origin. The present estimate of the possibility is based upon the following considerations:

1. A spectrograph with an $f/0.7$ camera will record an emission line due to 10^{11} photons/cm² column. This is based on the fact that the [O I] line 5577, whose average intensity is 2×10^8 photons/cm²·sec, gives a measurable line in 15 minutes or 900 seconds with our spectrograph. An $f/4.5$ spectrograph will therefore record an emission line resulting from 4×10^{12} photons/cm² or, if the effective exposure time is 1 second, from a luminous region emitting at the rate of 4×10^{12} photons/cm²·sec.

2. It is known from twilight observations that the density, ρ, of neutral sodium in the region of meteoric concentration (90 − 100 km) is about 200/cm³.

3. The probability of spontaneous emission, A, from the ^2P level of sodium to its ^2S level is 0.625×10^8/sec.

Let h be the thickness of the region activated by the passage of the meteor and P be the number of photons per atom produced by the meteor, or its equivalent the fraction of the sodium atoms which are excited to the ^2P level. Then the condition for recording an emission line is

$$\rho h P A = 4 \times 10^{12}$$

from which

$$Ph = 320 .$$

For various values of h the minimum value of P can be deduced, as in the accompanying tabulation.

h(cm)	P(minimum)
1	320
10	32
100	3.2
320	1.0
1000	0.32
3000	0.032

The conclusion to be drawn is that the sodium D line in meteoric spectra *may* be due to atmospheric sodium atoms if the effective thickness of the region activated by the meteor is greater than about 300 cm.

These calculations were made at the suggestion of Dr. C. T. Elvey. The study was supported by the Office of Naval Research under Project NR-082-045.

F. E. ROACH

U.S. NAVAL ORDNANCE TEST STATION
July 29, 1949

REVIEWS

Gaseous Nebulae and New Stars. By A. VORONTZOFF-VELYAMINOV. (In Russian.) Edition of the Academy of Sciences of the U.S.S.R. Moscow and Leningrad, 1948. Pp. 588+146 figs. Bound, 45 rubles.

During the night of November 8–9, 1942, Bernhard H. Dawson discovered, at La Plata, a brilliant nova in the constellation Puppis. A few nights later it reached maximum brightness at nearly zero apparent visual magnitude and then rapidly declined until it reached, in December, 1948, an apparent magnitude of 12. According to E. Pettit's light-curve,[1] it is probable that the decrease in luminosity will continue for several years and that it may ultimately reach its premaximum brightness of fainter than 17 mag. The extraordinarily large range of at least 17 mag., which exceeds by 3 mag. its nearest rivals, Nova Persei 1901 and Nova Cygni 1920, served as a welcome confirmation of a theory of stellar evolution which Professor Vorontzoff-Velyaminov had vaguely suspected before but for which he required strong observational confirmation.

The new book is essentially the basis upon which his theory rests. It contains a wealth of information on O-type stars, Wolf-Rayet stars, diffuse galactic nebulae, interstellar gas and dust, planetary nebulae, the physical mechanisms of nebular radiation, the results of observations of novae and supernovae, the physical constitution of the novae, the nova-like peculiar stars and the recurring novae, the SS Cygni and U Geminorum variables, and the P Cygni and Be stars.

Of fundamental importance is the relation, found in 1934 by Parenago and Kukarkin, between the amplitude of a recurring nova and its period. The author finds, from the entire available material,

$$\log P\,(\text{years}) = -2.716 + 0.512\,A\,(\text{mag.}).$$

Some readers will probably object to the extrapolation that he attempts on both sides of the observed interval in A. For small A he extends the formula to include the 700-day period of Z Andromedae, and he suggests that for still smaller P the variation in A becomes so small that it is lost in the irregular variations of brightness which are usually present in the novae. On the side of long P, he not only treats all normal novae as recurring phenomena—for Nova Puppis 1942 his formula gives $P = 10^6$ years—but he identifies the white dwarfs and blue dwarfs (the latter having continuous spectra without absorption or emission lines) with recurring novae of $A \backsim 20$ mag.; and he concludes that, since the corresponding $P \backsim 10^8$ years, these stars will be practically constant in light, at minimum brightness, during most of the life of our galaxy.

Unquestionably, this hypothesis is daring; but it also grips our imagination and tempts us to look deeper into its origin and its consequences. The former is very largely contained in an H-R diagram (Fig. 1), in which Vorontzoff-Velyaminov has entered (at times somewhat arbitrarily) the Wolf-Rayet stars, the novae at minimum, the nuclei of planetary nebulae, and the blue and white dwarfs. Together with main-sequence O and B stars, these groups form what he describes as the "blue-white sequence" in the H-R diagram: a vertical column running from about $M_v = -6$ to $M_v = +14$ and from O0, or continuous spectra, to about B0. Nova Puppis 1942 at $M_v \backsim +9$ or $+10$ forms a connecting link between the novae and the white dwarfs.

This sequence is regarded as representing the evolutionary path of stars which lose mass by expansion, and this is considered the predominant evolutionary process in the galaxy, leading to the formation of nebulae and interstellar matter. There is no evidence of the reverse process, the building-up of stars from interstellar matter or even from denser dust clouds; but in one part of the book the idea of a complete cycle from clouds to stars and back to clouds is regarded as possible.

It is significant that in recent years several astronomers have recognized the importance of finding an efficient evolutionary process involving a change of mass. Vorontzoff-Velyaminov's ideas are, therefore, very much in line with the general development of astronomical thought. But several points are not quite clear. He disregards the U Geminorum stars, because they have G-type spectra at minimum. The possibility that these absorption-line spectra come from a com-

[1] *Pub. A.S.P.*, **61**, 42, 1949.

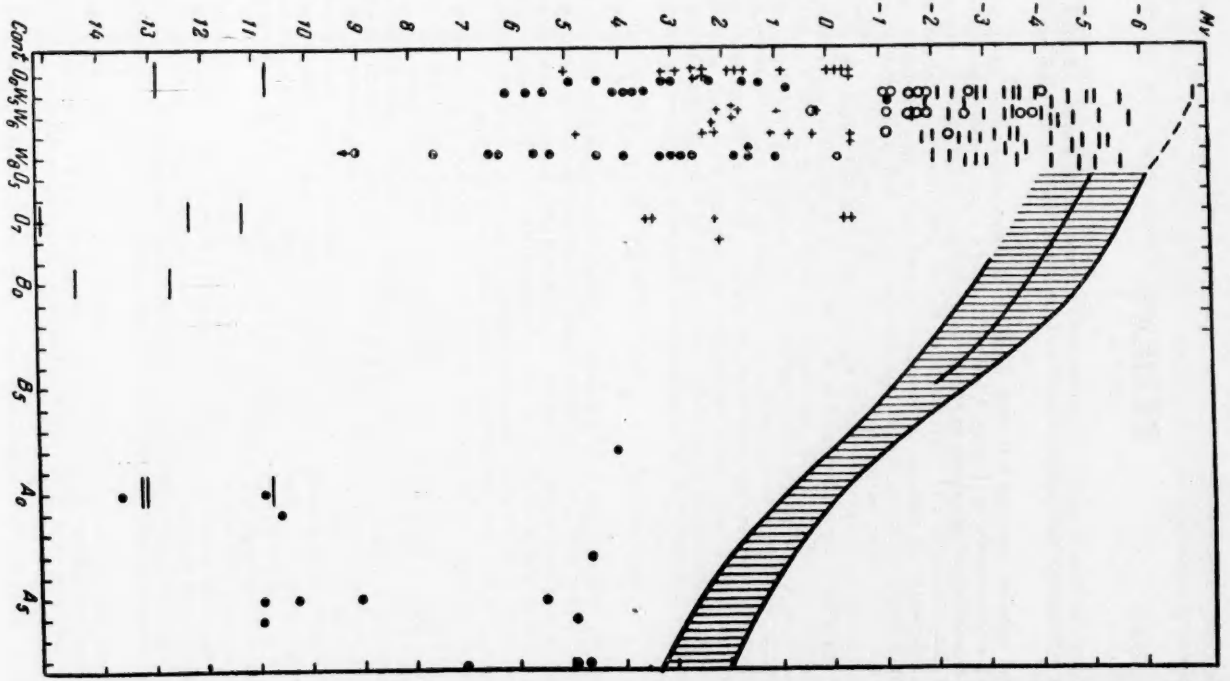

FIG. 1.—The blue-white sequence. —, Wolf-Rayet stars in the Large Magellanic Cloud; ○, galactic Wolf-Rayet stars; ●, novae at minimum light; +, nuclei of planetary nebulae; ——, blue and white dwarfs.

panion "can no longer be maintained because this type of spectrum is observed in all these stars." But perhaps they all have late-type companions. In fact, there is a large amount of information that many nova-like objects are really double stars, as are also some T Tauri variables and many Wolf-Rayet stars. At any rate, the similarity of the U Geminorum and SS Cygni stars with novae is one of their most prominent spectroscopic features. There may also be a connection between the T Tauri variables and the peculiar stars of the Z Andromedae type.

Another weakness of the proposed hypothesis is the absence of a smooth change in spectral characteristics, as well as in other properties, along the blue-white sequence. Perhaps we are here concerned with a difference in viewpoint. Vorontzoff-Velyaminov is probably not primarily a spectroscopist and looks at his sequence principally as an arrangement of stars of smoothly decreasing mass with decreasing intrinsic luminosity. But spectroscopically it is difficult to lump into one narrow sequence such objects as a Wolf-Rayet star, with its tremendously broad emission lines, all of permitted transitions; BF Cygni, with its wealth of narrow emission lines, many of them corresponding to forbidden transitions; γ Cassiopeiae, with normal Be features and occasional stages of shell-type absorption lines; 17 Leporis, with occasional nova-like outbursts of absorbing gases, which are not accompanied by appreciable changes in brightness; the nuclei of planetaries, which in intrinsic luminosity fall between the Wolf-Rayet stars and the novae at minimum but in the spectrum hardly represent a transition from one group to the other; and, finally, the white dwarfs, with no emission lines and no indication of spectroscopic changes suggestive of expansion.

It is this bewildering variety in the spectra of Vorontzoff-Velyaminov's blue-white sequence that places it in a quite distinct class from the other, generally accepted, sequences in the H-R diagram: the dwarfs, the giants, the subdwarfs, the supergiants. This does not mean that Vorontzoff-Velyaminov's hypothesis is incorrect. But it suggests caution!

But let us examine the process more closely. According to the hypothesis, a relatively young system is one having blue giants but not having either novae, nova-like objects, or white dwarfs; as the system grows older, some blue giants will become novae or nova-like objects and will begin to lose mass rapidly, because we infer, from the relative scarcity of these objects, that they last, in this stage, for a short interval of time; finally, in the oldest systems the blue giants will be absent, and the white dwarfs will take their places. Does this correspond to reality? The author does not consider the clusters, which would have given him a chance to examine the consequences of his hypothesis. But if our other theories of stellar evolution are correct—and Vorontzoff-Velyaminov apparently accepts the thermonuclear transformation of *H* into *He* along the main sequence—then it is surprising not to find in some of the older clusters (with appreciable *H*-deficiency, according to Kuiper and others) like the Pleiades, Praesepe, or the Hyades, any indication of P Cygni type or nova-like objects. Such objects abound in a relatively young cluster like NGC 6231, which also has many luminous O and B stars. But perhaps this argument is not compelling. Vorontzoff-Velyaminov would regard a globular cluster with few O and B stars, or even without any, as an extremely young object, in which the O and B stars of the main sequence had not yet come into existence. We must remember that he discards the hypothesis, frequently accepted by others, that the hot, massive, rapidly rotating, main-sequence stars are formed directly out of the interstellar dust and are the first members of any stellar population, being constantly re-formed as the older ones among them disappear from the upper-left corner of the H-R diagram. But is it not surprising that among the known globular clusters there is not one which is old enough to have passed through and beyond the blue-giant stage?

But I repeat: The main purpose of the book is to demonstrate the importance of loss of mass by stars as an evolutionary process and as a process of replenishing the interstellar gas. In this respect Vorontzoff-Velyaminov will find many sympathetic readers. The phenomena have been outlined by other workers, most recently by A. D. Thackeray.[2]

Users of the new book will find four appendices of value: a long list of references, a catalogue of planetary nebulae, a catalogue of galactic novae, and a list of supernovae.

Unfortunately, this very valuable book has been marred by a series of ungenerous and undignified attacks upon all science in what the author calls the "bourgeois, capitalistic countries." He even censures by name "the Americanized apostate Gamow," who "advances new theories only for the sake of sensation" and who "with amazing ease, sometimes even after a few months, discards them in order to propose a new, equally sensational theory." In another place the author singles out Messrs. Aller and Goldberg who "in their book *Atoms, Stars, and Nebulae* have pre-

[2] *Observatory*, **68**, 22, 1948.

sented in a distorted manner a picture of the disappearance of life on the earth in the event of a nova-like outburst in the sun." The author continues: "The purpose of such realistic descriptions in the capitalistic world is to prove the futility of life on earth, and to undermine the will of the people to rebuild their social order."

We have become used, during the last two or three years, to being showered with abuse from Soviet sources. But it is a revelation to learn that our "bourgeois science is completely incapable, in a fruitful way, of explaining the regularities which lie at the bottom of the observed phenomena, because the method of bourgeois science is sinful." Instead, the author proposes "to base himself upon the forward march of the philosophy of dialectic materialism," which will enable him to "create a really advanced theory" and to provide for the Soviet astrophysicists "the knowledge of the weak sides of bourgeois science which will enable them to carry on the fight on the solid ground of dialectic materialism." It appears that "the sum-total of all these labors demonstrates in a concrete manner the endless circulation of matter, which had been predicted, long ago, by the philosophy of materialism." The book ends with several quotations from Stalin and one from Engels, which have no bearing upon the problems of astronomy.

It would seem that we, who "are unable to form sound theories," are nevertheless sufficiently competent to furnish the raw data of world science. At least, the vast majority of the observational facts used by Vorontzoff-Velyaminov come from Western sources, and in the body of the book these results are given fairly and usually with the proper references. But the photographic illustrations are another matter. Out of the 49 halftones—many of them composite—all but two or three will be easily recognized by their intellectual fathers in the United States and Canada. But the only acknowledgements which I can find are two exceptions: both are credited to Russian astronomers in Moscow, and both are poor beyond description.

Perhaps we should not blame the author personally for the political nonsense, which adorns only the first and the last few pages of his book. But the control of thought by powerful political groups in many countries is a threat to the whole world.

OTTO STRUVE

Yerkes Observatory

Astronomischer Jahresbericht, Vol. **45**, Part I. Published by the Astronomisches Rechen-Institut, Heidelberg, Germany, and containing the literature of the years 1943–1946. Berlin: Walter de Gruyter & Co., 1948. Pp. 333. RM. 40.[1]

At the 1948 meeting of the International Astronomical Union a resolution was passed encouraging Professor A. Kopff, director of the Heidelberg section of the German Astronomisches Rechen-Institut, to continue the publication of the annual volumes which have appeared regularly since 1899. Volume **45** contains the literature from 1943 to 1946, or, perhaps more correctly, it contains reviews and summaries of those publications up to and including the year 1946 which had arrived at the Rechen-Institut before December 1, 1947. The present volume is labeled Part I because it had been decided to issue Part II as Volume **46**, covering the literature for the same years, 1943–1946, which had not arrived in Heidelberg in time for the present volume.

As was the case in the pre-war years the *Jahresbericht* is exceedingly valuable because it is as nearly complete as anyone might wish. In the forty-two introductory pages the authors have given a list of all publications which they have reviewed. It is to be hoped that the directors of all observatories and the editors of astronomical publications who have not yet made their publications available to the Rechen-Institut will do so at once, so that the next volume may contain the entire remaining literature. Authors of articles which were printed in periodicals not ordinarily accessible to the Rechen-Institut are likewise requested to send reprints to Heidelberg. Institutions which have not yet purchased the *Jahresbericht* may now do so through any established bookstore in this country.

The editor of Volume **45** was Dr. K. Heinemann, who had already been responsible for several of the earlier issues. His collaborators were A. Bohrmann, Heidelberg; H. Gollnow, Göttingen; I. Groeneveld, Heidelberg; K. O. Kiepenheuer, Freiburg; H. Klauder, Heidelberg; A. König,

[1] The price of the current volume is 40 German marks or about $13. That of the earlier volumes (1940, 1941, and 1942) is about 20 German marks. The editors have informed us that all volumes may be purchased through the following address: Carl Fr. Fleischer, Buchhandlung, Frankfurt/M, Bürgerstrasse 9–11, Germany.

Heidelberg; G. R. Miczaika, Heidelberg; E. Rabe, Heidelberg; W. Strohmeier, Göttingen. Dr. Jr. Bouska, of Prague, covered the Czechoslovak literature of 1943; Dr. F. Zagar, of Bologna, has reviewed the Italian literature for 1943–1945; and Dr. W. Lohmann, of Heidelberg, has reviewed the entire Russian literature.

The general arrangement of the book is similar to that of previous years, but a new section has been introduced for theoretical astrophysics listing separately the following topics: physical foundations; stellar atmospheres and spectra; stellar interiors; nebulae and interstellar matter; stellar evolution and cosmogony. Several new sections have been added to Part VI—the sun, namely, the photosphere and the spectrum; solar radiation; the chromosphere and the prominences; the corona; solar activity in relation to terrestrial effects.

What was formerly a single part devoted to the fixed stars has now been split into four new parts entitled, respectively, (1) "The Stars"; (2) "Double Stars"; (3) "Variable Stars and Novae"; (4) "Stellar Systems, Nebulae, and Interstellar Space." The Rechen-Institut especially records its gratitude to the Astronomer Royal, Sir Harold Spencer Jones, for his efforts in making available a large part of the literature from the allied countries.

O. STRUVE

Yerkes Observatory

Johannes Kepler. By MAX CASPAR. Stuttgart: W. Kohlhammer Verlag, 1948. Pp. 479. DM 18.

Professor Caspar is the editor of Kepler's collected works and is probably better informed concerning the life of Kepler and the times in which he lived than is any other living person. Hence his new book is an important event. It is the best and most complete biography of the great German astronomer.

Kepler was born in 1571 and as a child knew some of the great contemporaries of Martin Luther. He died in 1630, when the Thirty Years' War was at its height. His life was marked by religious persecution, financial worries, and the constant danger and turmoil of war. Born in a Protestant community of Württemberg and educated at the Protestant University of Tübingen, he was, nevertheless, excluded from communion in his own church because his religious and scientific views were regarded as radical. He dared to uphold the Copernican theory, equally denounced by both the Protestant and the Roman Catholic clergies, and he was exiled from Graz because he refused to be converted to Catholicism. And yet, despite the constant worries of his mother's trial for witchcraft, of the emperor's failure to pay him his salary, and of the scorn which he had to endure from many scientists, he became the greatest theoretical genius of his own period and one of the greatest in the history of mankind.

Caspar's biography is full of interesting details and of no less interesting generalizations. He has spiced the text with numerous quotations from Kepler's own writings—many of them from letters which have not been previously accessible. But this most interesting feature will make the book rather difficult to read for persons who are not thoroughly familiar with the German language: most of the quotations are exact not only in their wording but even in their peculiar, old-German spelling. Moreover, Kepler, following the usage among scientists of the sixteenth and seventeenth centuries, often interspersed his letters with Latin words carefully adapted in form to the structure of his German sentences.

The author has so completely entered into the mind of his subject that he has succeeded in giving a vivid, yet truthful, picture of the mental processes which gradually led Kepler to the enunciation of his first two laws of planetary motion, when he served as imperial mathematician in Prague, and, much later, of his third law, when he was living in Linz.

But Kepler was not an easy person to get along with. A few days of close contact with Tycho Brahe brought about a violent explosion between the two men; and one wonders whether the unreasonable Dane had not finally met an even more unreasonable German. But the very fact that Caspar does not attempt to idealize Kepler but presents him as he was—a small, sickly man with a brilliant mind and a difficult character; a man who was hot tempered but never completely free of his reliance upon others, who often soon regretted the outbursts of his fury; a man who, even as a student, had embraced the Copernican teaching but who remained an astrologer until his dying days—makes this book an outstanding accomplishment and an indispensable source for future studies.

OTTO STRUVE

Yerkes Observatory

Skalnate Pleso Atlas of the Heavens. By ANTONIN BECVAR. Cambridge, Mass.: Sky Pub. Corp., 1949. 16 charts. $5.00.

With the single exception of the *Bonner Durchmusterung*, this is the most useful atlas to the practicing astronomer that the reviewer knows of. The whole sky is illustrated on sixteen charts, which include the following information: all stars to magnitude 7.5, variables, novae, galactic nebulae, globular clusters, and over a thousand of the brightest extragalactic nebulae of magnitude 13 or brighter according to the Shapley-Ames catalogue. In addition, the outlines of the dark nebulae are shown, together with the Milky Way as delineated by Pannekoek.

The author, Dr. A. Becvar, director of the observatory at Skalnate Pleso, is responsible for the preparation of the charts; the work was first published in Prague in 1948 to commemorate the thirtieth anniversary of the astronomical society. The present edition is published in the United States under the sponsorship of the Sky Publishing Corporation and the Harvard College Observatory. The atlas represents a research project of major importance to astronomy, and it is certain to be an invaluable part of the astronomer's tools for many years to come.

W. W. MORGAN

Yerkes Observatory

Mappa coelestis nova. Cambridge, Mass.: Sky Pub. Corp., 1949. 1 map. $3.50.

This is an attractively printed colored chart, giving the location of all stars north of declination $-40°$ and brighter than visual magnitude 5.0. The magnitudes to two decimals are entered near the star images, and the latter are colored in accordance with their spectral types.

It would be hard to imagine a more interesting map of the brightest stars.

W. W. M.

THE OBSERVATORY

FOUNDED 1877

* * *

A Magazine presenting current developments in Astronomy by means of Articles, Correspondence, Notes on discoveries and Reviews of important astronomical books. The papers read at the Meetings (Astronomical & Geophysical) of the Royal Astronomical Society and the discussions which follow are also fully reported.

* * *

Annual subscription for 6 issues, post free, 15/- should be sent to

The Editors, ROYAL OBSERVATORY
Greenwich, London S.E., 10

The FACE of the MOON

BY RALPH B. BALDWIN

An answer, in terms of the meteorite theory, to the question of how the moon came to exist in its present form.

The study of the moon—a mirror for the study of the earth.

286 pages. 6" × 9". Illustrated. $5.00.

THE UNIVERSITY OF CHICAGO PRESS

POPULAR ASTRONOMY

A magazine now in its fifty-seventh year, devoted to the elementary aspects of Astronomy and allied sciences.

Published monthly, except July and September.

Yearly subscription rates: Domestic $4.00; Canadian $4.25; Foreign $4.50.

Address:

POPULAR ASTRONOMY
CARLETON COLLEGE
NORTHFIELD, MINNESOTA, U.S.A.

THE ATMOSPHERES OF THE EARTH AND PLANETS

Papers presented at the Fiftieth Anniversary Symposium of the Yerkes Observatory—September, 1947

Edited by GERARD P. KUIPER

CONTRIBUTORS: A. Adel, H. Brown, R. T. Chamberlin, H. E. Clearman, T. Dunham, E. Durand, J. Franck, J. L. Greenstein, G. Herzberg, L. Jacchia, Z. Kopal, G. P. Kuiper, M. V. Migeotte, C.-G. Rossby, L. Spitzer, P. Swings, H. C. van de Hulst, F. L. Whipple

366 pages 6¼×9¼ *Illustrated* $7.50

THE UNIVERSITY OF CHICAGO PRESS

PRINCIPLES OF STELLAR DYNAMICS

By S. CHANDRASEKHAR, *Yerkes Observatory*

A concise and authoritative account of current investigations by the author and others on the dynamics of the galaxy, spiral nebulae, and star clusters.

$5.00

In the *Astrophysical Monographs Series*

UNIVERSITY OF CHICAGO PRESS

"... a well-rounded book which should for many years to come be 'must' reading for every prospective student of galactic structure and dynamics."—BART J. BOK, *Science*.

"... to a specialist in the field this brilliant work should prove invaluable."—LYMAN SPITZER, JR., *Popular Astronomy*.

"The book fills an obvious gap in astronomical literature, and it should give a valuable stimulus to research."—A. S. EDDINGTON, *Nature* (England).